Synthesis, optimisation and control of crystallization systems

Ahmad Yahya Sheikh
B.Eng. (Hons)

A thesis submitted to the University of London
for the Degree of Doctor of Philosophy

Ramsay Memorial Laboratory
of Chemical Engineering
University College London
Torrinton Place
London WC1E 7JE

11-04-1418 (H)
August 1997 (G)

ABSTRACT

Process systems engineering has provided with a range of powerful tools to chemical engineers for synthesis, optimisation and control using thorough understanding of the processes enhanced with the aid of sophisticated and accurate multi-faceted mathematical models. Crystallization processes have rarely benefited from these new techniques, for they lack in models that could be used to bridge the gaps in their perception before utilising the resulting insight for the three above mentioned tasks.

In the present work, first a consistent and sufficiently complex models for unit operations including MSMPR crystallizer, hydrocyclone and fines dissolver are developed to enhance the understanding of systems comprising these units. This insight is then utilised for devising innovative techniques to synthesise, optimise and control such processes.

A constructive targeting approach is developed for innovative synthesis of stage-wise crystallization processes. The resulting solution surpasses the performance obtained from conventional design procedure not only because optimal temperature profiles are used along the crystallizers but also the distribution of feed and product removal is optimally determined through non-linear programming.

The revised Machine Learning methodology presented here for continual process improvement by analysing process data and representing the findings as zone of best average performance, has directly utilised the models to generate the data in the absence of real plant data. The methodology which is demonstrated through KNO_3 crystallization process flowsheet quickly identifies three opportunities each representing an increase of 12% on nominal operation.

An optimal multi-variable controller has been designed for a one litre continuous recycle crystallizer to indirectly control total number and average size of crystals from secondary process measurements. The system identification is solely based on experimental findings. Linear Quadratic Gaussian method based design procedure is developed to design the controller which not only shows excellent set-point tracking capabilities but also effectively rejects disturbance in the simulated closed loop runs.

to my mother and sister

ACKNOWLEDGEMENTS

The author wishes to express his sincere gratitude to the following:

Professor Alan Jones for his supervision through which he provided the right amount of support and guidance, while granting me the freedom that I needed for the project to evolve in its final form.

Dr. David Bogle for his advice and willingness to discuss the progress at all times. His efforts in arranging for the necessary courses at Denmark Technical University (DTU) and AspenTec, UK are wholeheartedly appreciated. I am also thankful to him for the SQP routine which was extensively used in the synthesis problem.

Professor Uy-Loi Ly of the Department of Aeronautics and Astronautics at the University of Washington for many helpful discussions on the control theory used in this work.

Dr Janusz Wojcik for familiarising me with different crystal size measuring devices.

Ms. Carol Welfare and Mr. Julian Perfect for their help to ensure that the experimental component was finished within the allocated time.

For their moral support, I thank all the fellow inhabitants of crystallization lab, with whom I shared the joys and the despair.

The Committee of Vice Chancellors and Principals UK, for the Overseas Research Scholarship which partly funded the project.

My family, especially father for their continual moral and financial support throughout my studies, without which this work would not have been possible.

Opinion in good men is but knowledge in the making

John Milton, (Areopagitica, 1644)

TABLE OF CONTENTS

LIST OF FIGURES

page no.

page no.

LIST OF TABLES

Chapter 1:

INTRODUCTION

This work is concerned with the development of advanced methodologies for synthesis, optimisation and control of crystallisation processes. Computers are being increasingly used to address the issues in these areas and also for equipment design, project planing, on-line parameter estimation and controller adaptation. This up surge in computer applications has resulted from a distinct trend towards sophisticated and accurate multi-faceted process models to develop reliable solutions to process problems by exploiting matured mathematical techniques. Though most of the methods formulated have been driven by the underlying paradigm; numerical solution of a set of equations, more recently there has been a shift of emphasis to develop techniques capable of articulating, representing and utilising qualitative knowledge about the process (Stephanopoulos and Han, 1996). This has been made possible by state of the art advances in computer science technology allowing seamless integration of qualitative knowledge into the general numeric solution framework. An integrated approach to systems engineering for accomplishing the aforementioned tasks is essential to inherently safe, environmentally sound, economic and flexible processes. A pre-requisite to such a task is the development of accurate multi-faceted models for unit operations of the process (Marquardt, 1996). These models could be used to validate the findings of the computations using a less rigorous process description, for instance in the synthesis problem or for generating more process data for optimisation studies. The culmination of two approaches *viz.*, numerical methods and the less physical model driven knowledge based methods have and will provide the most valuable techniques to address complex process systems problems.

These development are of paramount importance to processes such as crystallisation where the value of simple quantitative analysis is always plagued by large

uncertainties arising from the sheer complexities of the process, significantly reducing interest in the application or development of procedures that use conventional systems engineering methods. The value of new developments can be further emphasised by the vast scope of their application evident from ICI's estimate that up to 50% of its output takes up solids form during some stage of production (Rossiter and Douglas, 1986). At DuPont up to 60% of the products by value are solids and an additional 18% use solids as additives (Nelson et al., 1995).

In the present study, a holistic approach encompassing recent advances in crystallisation, artificial intelligence and systems engineering is presented to analyse a) synthesis, b) optimisation and c) control as distinct but inter-related activities. The rigour of the models is furnished by experimental data to determine kinetic models and parameters. Potassium nitrate crystallisation process has been used to illustrate the techniques developed, because of its relatively well understood crystallisation kinetics.

1.1 Dynamic Modelling and Simulation

Dynamic modelling and simulation has become an established valuable tool at all stages of plant design and operation. Traditional applications in plant operations include the study of process response to disturbances that cause deviations from the steady-state and the tuning of controllers. More recently, increasing safety and environmental concerns and stricter regulations have increased the incentives for studying "what if" operational and safety scenarios to perform the hazard and operability studies. For effective design of complex process plants, such simulations are used to determine the intrinsic controllability of the process, the design of control systems and the study of appropriate start-up and shut-down procedures.

Dynamic simulations are of particular significance to crystallisation processes, where the processes take up to ten residence times to achieve steady-state (Randolph and Larson, 1988). Furthermore, the process of crystallisation itself is not static but characterised by a crystal size distribution trajectory representing progressive change in the size of individual crystals due to different size varying phenomena. A mathematical representation of such systems not only require a mass balances, energy balances and rate equations, but also a description of how the crystals are distributed by size and in time and the way in which different phenomena that result in size change contribute to the representation often referred to as the population balance. In the following, features of versatile and rigorous models necessary for unit operations pertinent to crystallisation process flow sheets will be highlighted.

1.1.1 The MSMPR Crystallizer

Mixed-suspension, mixed-product removal type crystallizers are widely used in industry and the laboratory (Randolph and Larson, 1988). Such crystallizers behave as though they are perfectly mixed, i.e. in any arbitrary small element of the volume within the crystallizer the same full and uniform crystal size continuum is assumed to exist. Steady-state operation of MSMPR crystallizers require that the feed rate, composition and the temperature remain constant along with the volume of the vessel. The above assumptions simplify the otherwise extremely complex mathematical representation of crystallisation processes.

The distinctive nature of crystallisation process necessitates additional equations for sufficient mathematical representation of an MSMPR crystallizer in each of the three partitions of the conventional scheme to process modelling *viz.*, balances, rate and constitutive equations. Population balances and rate equations for crystal nucleation,

growth and attrition are the add-ons to the first two divisions, whereas functions describing growth mechanisms, agglomeration kernel and the dependence of physical properties on changing density are amongst the many extra equations that fall into the third category. Discretizing the size axis of integro-partial differential equation representing the population balance to transform it into a set of ordinary differential equations has emerged as the most suitable solution technique for flow sheet applications for a wide variety of systems.

1.1.2 Hydrocyclone

Hydrocyclones are used for product classification whereby the exit stream from the crystallizer is split in to two, each with crystals either predominantly above or below a cut size. The cut size is determined by the design parameters and the properties of the stream itself. These devices are extensively used because of the simplicity of their design, effectiveness and robustness.

Effective mathematical representation of the behaviour of a hydrocyclone requires adequate analysis of three distinct physical phenomenon taking place in these devices, *viz.* the understanding of fluid flow, its interactions with the dispersed solid phase and the quantification of shear induced attrition of crystals. Simplified analytical solutions to conservation of mass and momentum equations derived from the Navier Stokes equation can be used to quantify fluid flow in the hydrocyclone. Once bulk flow has been quantified in terms of spatial components of velocity, for dilute slurries crystal motion can be traced by balancing forces on the crystals themselves to map out their trajectories (Hsieh and Rajamani, 1991). The trajectories for different sizes can then be used to develop a separation efficiency curve which quantifies performance of the

vessel. Population balances can be included for crystal attrition in the above description for developing a thorough mathematical model.

1.1.3 Fines Dissolvers

Fines dissolution is employed in highly nucleating systems to dissolve small crystals so that the driving force i.e., extent of super-saturation could be directed towards the growth of larger crystals, thus increasing mean crystal size and reducing coefficient of variance. The overflow stream from the hydrocyclone or a stream withdrawn from the top of the crystallizer is often subjected to de-super-saturation through increase in temperature or solvent concentration for dissolving crystals below a certain size to extinction. Dissolution rate and the subsequent crystal number contributions to the population are modelled by equations similar to those used for the crystal growth process. The diffusion coefficient in this case, however, has to be calculated as a function of individual crystal sizes.

1.1.4 Conclusions

Dynamic models will be developed for each of the units for the reasons mentioned earlier and also because steady-state simulations for such processes can converge to an improper solution due to highly non-linear and at times inverse response from crystallizers. Furthermore, steady-state solutions could be incapable of identifying concentration multiplicities often observed in MSMPR crystallizers (Leu and Tarng, 1992). Discretized population balances capable of representing nucleation, growth, agglomeration and breakage will be solved along with mass and energy balances. Rate equations will be developed to represent both primary and secondary nucleation. Simplified analytical solutions to fluid flow equations will be used in the hydrocyclone model.

SPEEDUP™, the equation oriented simulation environment, will be employed for most of the simulation work because it provides robust algorithms for both dynamic and steady-state simulations. Facilities are available for parameter estimation and optimisation and it is equipped with a highly effective algorithm to re-initialise dynamic problems with functional and operational discontinuities. A time delay function is also provided which, for instance, can be used to delay the passage of nuclei born at the critical size to the first size interval in a discretized population balance. This would facilitate the coverage of a larger size range without employing excessively high number of intervals. The rates at which super-saturation is generated will be modelled through rigorous heat transfer analysis.

1.2 Crystallizer network Synthesis

Continuous operation of crystallizers, though beneficial in reducing capital and operating costs through smaller less expensive equipment and reduced maintenance is marked by some undesirable crystal product properties. None more so than the exponential form of crystal size distribution (CSD), particularly when most applications would desire a more uniform crystal size. A common approach for tackling this problem is to design for poor mixing so that the resulting CSD gradients could be exploited by fines dissolution and product classification loops. Such equipment is however, difficult to design, requires abnormally high in-process inventories and its operation is subject to cyclic behaviour (Randolph and Tan, 1978).

A series of MSMPR crystallizers in cascade offers a viable alternative not only capable of narrowing CSD, but also providing with improvements such as flexible operation of temperature regimes, possibility of using larger cooling surface and economies of energy consumption (Nyvlt, 1992). The performance of a cascaded

configuration is rated by crystal carry over from previous stages and super-saturation levels. The latter is not only dependent on the operating temperature but also on feed concentration and mean residence time which is in turn specified by volume and throughput for each crystallizer in the network. All these variables have to be determined optimally to achieve the desired performance.

Process synthesis, which deals with the systematic identification of optimal type and design of process units together with their interconnections determining flow sheet structure, provides numerous techniques to develop optimal networks. Since, for a specific performance, flow sheet structure and unit design cannot be determined uniquely, the task is to select a particular solution out of a large number of alternatives which meet the specified level of performance. Synthesis is usually carried out through the following series of decision levels (Nishida et al., 1982):

- System objectives
- Evaluation criterion
- Technology to achieve objectives
- Problem decomposition into smaller interconnected tasks
- Tasks within selected technologies

The first three steps are referred to as planning while the last two determine optimal design at sub-system levels often representing reactor, heat exchanger and separation sequences. The current approaches to process synthesis can be distinguished as hierarchical decomposition and mathematical programming. Their salient features are summarised below.

1.2.1 Hierarchical decomposition:

The hierarchical decomposition technique breaks the synthesis procedure into five decision levels (Douglas, 1988) *viz.*, batch vs. continuous, input-output structure, recycle structure and reactor considerations, separation systems and heat exchanger networks. The economic potential of the project is evaluated at each level after deciding the mode of operation to justify continuation of the synthesis process. Heuristics, short-cut design and cost calculations and physical insight of the process are used to formulate a base case and improvements on it. The approach provides a useful method for generating the initial flow sheet and its alternatives. Hierarchical decomposition, however fails to provide a rigorous optimal design because of its excessive reliance on heuristics. Furthermore, interactions between design variables at various sequential decision levels might not be adequately accounted for, because it is often necessary to solve sub-systems simultaneously.

1.2.2 Mathematical Programming

The mathematical programming approach utilises optimisation techniques to specify the configuration and parameters of the processing system as a whole. This approach can be further categorised into superstructure optimisation and targeting approach. The former is mainly directed at the generation and search of flow sheet structures, while the latter focuses on exploiting physical knowledge of the systems.

1.2.2.1 Superstructure Optimisation:

Superstructure based optimisation proceeds by developing a structure containing alternative processing units and interconnections modelled as discrete binary variables to depict the existence or otherwise of units. An optimal sub network within the superstructure is identified using mixed integer non-linear program (MINLP)

algorithms to maximise a performance index. The strength of this approach lies in providing a systematic framework for simultaneous modelling and optimisation to address process synthesis problems. Its weakness comes from the fact that the superstructure has to be postulated explicitly, which is not only plagued by the question of completeness but also the possibility of overlooking a better configuration. Furthermore, relatively large sizes of the problem often resulting from the postulation of an adequate superstructure, could result in poor sub-optimal solutions because global optimisation methods have to be applied to obtain an acceptable solution.

1.2.2.2 Targeting Approach:

The targeting approach, which provided the famous pinch technology for heat exchanger networks (Linhoff and Hindmarsh, 1983), exploits physical and geometric insight into the process to predict *a priori* certain features that an optimal or feasible solution should reflect. With the method only providing the guidelines, however the search for the optimal solution has to be carried out through rigorous models often solved using non-linear programming techniques. The approach has also found applications in the synthesis of azeotropic distillation networks (Doherty et al, 1985), where residual curves are used and for the design of non-isothermal chemical reactor networks (Balakrishna and Biegler, 1992a; 1996). In the latter, the procedure which is based on mixing between different reacting environments (Continuous/plug flow) to improve yield, proceeds by determining maximum possible yield within the constraints without explicitly specifying a network to achieve it. A network capable of achieving the target is then synthesised by constructive solution of small programs modelling segregated and maximum mixedness environments. The solution is directed by the concept of attainable regions in concentration space. Segregated flow

(SF) reactor model works at the heart of targeting approach for it is sufficient to establish performance bounds for isothermal processes when the concentration of product species is a concave function of feed species concentration (Glasser et al., 1987). In SF models representing both plug flow reactors (PFR) and PFR with bypasses, only molecules of the same age are well mixed while mixing between molecules of different ages only takes place at the exit.

Modelling of these reacting environments result in boundary value problems comprising differential equations for balances and other non-linear equations representing process kinetics. Orthogonal collocation on finite elements has emerged as the preferred technique to discretize the problem into a non-linear algebraic equation system, because it leads to networks easier to design in practise. The sequential solution to small problems also enables the use of more sophisticated models and robust optimisation procedures such as sequential quadratic programming. Though the formulation does not allow for parallel reactor structures or bypasses, it can be easily extended to incorporate energy integration and separation sequences for simultaneous solution of the sub-systems to determine a complete optimal configuration.

1.2.3 Conclusions:

The constructive nature of the targeting methodology, resulting in small non-linear programs to be solved sequentially, is particularly well suited for crystallisation problems to develop models comprising mass and population balances coupled through highly non-linear equations for crystal growth and nucleation. Therefore, in this work the targeting approach will be used to develop procedures for the optimal synthesis of networks for stage-wise crystallisation. Rigorous populaion balance

models will be used to verify the findings of the targeting solution and furnish it with details including the complete crystal size distribution.

1.3 Process Optimisation

Crystallisation processes have seldom been subjected to process improvement techniques for operational quality, which has emerged elsewhere as an essential pre-condition to increased profitability by fundamentally improving the design and operation of the process. These techniques involve two complementary steps; a) control within pre-specified limits and b) continuous improvement of operational performance. The first step deals with the rectification of abnormal process behaviour (as a result of special causes) through efficient control. The final level of performance thus achieved, however, is a result of common and sustained causes within the process itself which are not unavoidable. The magnitude of common cause contributions can only be reduced through the introduction of appropriate changes in operating conditions and strategies by searching for better levels and ranges of decision variables.

1.3.1 Conventional methods for process optimisation

Conventional optimisation procedures provide a systematic way of finding the best solution to process performance by developing a simplified mathematical description comprising physical behaviour of the system as well as other pre-specified constraints. The application of optimisation algorithms to address problems in chemical engineering that are often very large and comprise algebraic and/or differential equations with both continuous and discrete variables, requires an effective strategy for efficient use of available algorithms. This strategy revolves around the following three steps (Biegler, 1985);

- Choice of optimisation algorithm
- Gradient calculation strategy
- Simplified models

The two commonly used algorithms are generalised reduced gradient methods and sequential quadratic programming. The former is often used for large problems, whilst for robust solution to highly non-linear small problems the latter is preferred. Chain-ruling and direct loop perturbations are the strategies widely used for calculating gradients, the former being more efficient because it allows the inclusion of analytic modular Jacobians if they could be specified. The main disadvantages of these methods stem from the necessity of finding simplified models for complex processes.

1.3.2 Multi-variable statistical analysis

Another sound basis for the prediction of better levels of decision variables for performance improvement is from the extrapolation of past known cases. Multivariate statistical techniques such as principal-components analysis, partial least squares, factor analysis, or neural networks provide a wide range of tools for this purpose, usually based on the concept of fitting a particular class of models to the data and then hypothesising that the solution for future levels of decision variables will conform to the fitted model. All of these methods formulate a final solution consisting of a vector comprising the decision variables (x_1, ..., x_n) that defines a single best performance point (y) in the performance space. Most decision variables, however have some variability associated with them even under the best control schemes. The consequence of ignoring this variability in decision variables, could be that the final solution obtained by these approaches may be sub-optimal even when accurate models

are used, since their evaluation criterion ignores system behaviour around the optimal. The area surrounding such a point does not in general correspond to the zone where best average performance can be achieved (Saraiva, 1995).

1.3.3 Machine Learning based optimisation:

Machine learning, the study and computer modelling of learning processes in their multiple manifestations, has been used for the similar task of developing and analysing systems to improve performance from existing data, often from a less model driven standpoint. The essence of problem formulation with this approach is one in which a procedure, shown a set of process data (**x**,y) comprising quantitative and or qualitative features of the process, employs inductive inference to extract classification rules for the division of the decision space into hyperrectangles (not points) representing different levels of performance without losing the individuality of each decision variable. The procedures which discover these rules in the form of decision trees are the most mature and widely used of all the interval analysis based rules representations. These trees are developed through top-down, divide and conquer strategy which successively partitions the given set of data into smaller and smaller subsets with the growth of the tree. The symbolic induction step is based on direct sampling approach where random data sets (objects) are used to build confidence intervals for performance levels and therefore does not suffer from simplifying assumptions and numerical inaccuracies inherent to mathematical formulation in traditional optimisation procedures. The method heavily relies on the quality of data, as for quantity, Saraiva (1995) has shown that even with moderate amounts of data it is possible to construct trees resulting in significant performance improvements. Furthermore, since the trees exhibit explicit ranges of decision

variables and associated levels of performance, they can lead either directly to changes in current operation practices or to the design of a set of confirmatory experiments for validating the findings. The implementation of these suggestions would generate more novel data capable of providing operating schemes for the extension of process performance beyond currently achieved levels. These schemes are identified and passed on to the symbolic induction stage for updating classification rules by the case based reasoning component.

1.3.4 Conclusions:

Crystallisation process optimisation will, therefore, be best served by machine learning methodology which offers a flexible and mathematically de-convoluted procedure for identifying performance improvement zones by establishing ranges on the crucial decision variables. For the present study, in the absence of the required process plant data and lack of rigorous flow sheeting models in the literature, the process will be simulated using new models under ranges of decision variables to generate the necessary data. A procedure for performance improvement of a simulated potassium nitrate crystallisation process using machine learning methodology will then be developed after modifying the existing machine learning methodology (Saraiva and Stephanopoulos, 1992a) to increase efficiency of both the components *i.e.*, symbolic induction and case based reasoning.

1.4 Crystallizer Control

1.4.1 Controller Design Method:

Process control design requires 1) specification of objectives, 2) analysis of process dynamics, 3) controller design and 4) evaluation of the design. It is the requirements

on product which are related to the process that define control objectives. The desired properties (informal objectives) are then translated into process phenomena that are to be controlled. In modern control design methods, the understanding of underlying process and disturbance dynamics is essential for designing the control structure (structural relations between outputs, measurements and inputs) and the control law (algorithm that determines inputs from measurements and outputs). The controller performance is evaluated for different combinations of design parameters by repeating all the intermediate steps until all the objectives are met. The final design not only addresses the achievable nominal performance but also the achievable robust performance; that is the achievable worst case performance in the presence of a pre-specified level of model/plant mismatch. This structured approach is referred to as control design method (Gevelber et al., 1987).

1.4.2 Control issues in the continuous operation of crystallizer:

Sustained oscillations resulting from cyclic swings of the number of small crystals, open loop instability and slow damping of disturbances are important industrial issues with regards to crystallizer control. These can lead to off specification products, overload in de-watering equipment and increased fouling. Detailed studies by Sherwin et al. (1967) showed that such behaviour is characterised by the following important properties.

- Magma density has little effect on stability limits.
- Instabilities tend to decrease average crystal size and increase total variance.
- Total mass of crystals remains almost constant.

It is clear from the above inferences on the dynamics of crystallizers that an effective controller for an MSMPR crystallizer would have to control the number of particles,

i.e. the zeroth moment along with the higher moments. The total number of particles, however, cannot be measured accurately on-line for control purposes because the measurement times can be comparable to response times of the controlled variable. Readily available process measurements such as temperature, flow rate or even concentration, however, contain much process information. Development of experimental relationships between these secondary variables and the variables to be controlled (primary variables) hold the potential to make more demanding control objectives accessible. Use of processed primary measurements accumulated off line over a period of time under a wide window of operating conditions can be used to design an inferential control. The sensitivity of crystallization process to external disturbances suggests the need for disturbance modelling to effectively eradicate them.

1.4.3 Inferential control:

In addition to the benefits of less expensive and more reliable secondary measurements, inferential control can add reliability to the closed control system, as it can be designed to use both the fast and slow measurements in cascade fashion. The design of such a system consists of two parts: estimator design and the selection of a controller.

1.4.3.1 Estimator Design:

The two approaches commonly applied for estimator design and based on a) Extended Kalman filter type of design which assumes that the system can be modelled by linear superposition of the effects of disturbances and manipulated variables on the primary and secondary variables and b) partial least square regression scheme (PLS), which does not involve explicit superposition principle. In the following, some of the features of PLS based estimator will be summarised.

1.4.3.1.1 Partial least square based controller:

In all the variations to Kalman filter approach, the design is based on estimations obtained from the linearisation of a system around a pre-selected nominal operating condition. This inevitably results in reduced robustness. On the other hand, in PLS based estimators linear relationships are established over a wide range of operating conditions, without requiring the effects of disturbances and manipulated variables on both the primary and secondary control variables to obey linear superposition (Budman et al., 1992). Regression is performed directly from the manipulated and secondary measurements to the primary variable for developing models to minimise the squared error between the measurements and their estimates from the model for all the different operating conditions. The classical least square solution often results in estimators that are very sensitive to noise and therefore prinipal componenet analysis (PCA) based methods are used to develop a lower order description of the data.

In this work PCA will be performed for the primary controlled variable and process measurements (secondary control variables) to obtain the low order description through singular value decomposition. The reduced process description does not include observations with small eigenvalues. These not only have little effect on variance but are also characterised by poor signal to noise ratio. PCA (the simplest of the methods in the family) will be sufficient for controller design purposes because the control law will not be based on the model. The regression model will only be utilised in the later stages while assessing the controller design for robustness.

1.4.3.2 Controller Design:

Classical control theory does not offer adequate procedures for designing multi-input multi-output controllers for processes such as the operation of crystallizers, where

strong interactions exist between controlled variables. Modern control theory addresses these issues through two distinct but mathematically similar techniques for designing optimal controllers for multi-variable problems *viz.*, Model Predictive Control (MPC) or Dynamic Matrix Control (DMC) and optimal control based on Linear Quadratic Gaussian (LQG) method. In the following, some of the characteristics of the two design approaches will be summarised briefly. Detailed comparison can be found elsewhere (Johnson, 1993; Morari, 1991; Garcia et al., 1989).

1.4.3.2.1 Optimal control based on LQG

In the LQG design a linear finite dimensional state space model of the system is developed first. The variables are usually in terms of deviations from a given set-point; often steady-state. The model provides the description of process dynamics on either side of this set-point for small perturbations in the inputs. In order to apply state feedback, all the state variables within the model must be measured. Most of these are, however, not available for measurements and therefore a state observer (or estimator) is designed to re-construct these states from available measurements. Loop transfer recovery (LTR) procedures are used to address the robustness issues specific to the observer and the controller in general. Integral control action is usually incorporated into the controller and modelled disturbances are eradicated in feedforward fashion. Continuous time infinite-horizon quadratic cost criterion is often used. Tuning of the controller for closed loop performance is done through weighting matrices in the cost criterion and noise intensities in the observer.

Some of the advantages commonly mentioned include better controllability, increased knowledge of the process that accumulates with the modelling of the process and

controller tuning, disturbance stabilisation (Newell et al., 1972; Tiedermann et al., 1985), very high stability (Tysso and Brembo, 1978), and integrity against actuator saturation (Cori and Maffezzoni, 1984). The benefits also include ease of configuration, integral action and the advantages arising from the fact that all loops are designed together. Integral action not only provides better controllability but can also compensate for modelling errors, because these inevitably result in off-sets.

Concerns about robustness, large order of the controller, difficulties in developing state-space models, ability of Riccati equation to find solution for systems with time delays and incorporation of non-symmetric constraints have been addressed through the recent advances in LQG theory (Luo and Johnson, 1992; Benzaouia and Burgat, 1988). Procedures for adaptive optimal controller have also been developed (Bitmead et al., 1990; Chen and Guo,1986).

1.4.3.2.2 Model predictive Control

This controller design framework is more intuitive than optimal control procedure. It does not require state-space models, instead step or impulse responses are utilised as the process description. Complex dynamics and delay can therefore be incorporated with relative ease. Instead of the observer, the process model is employed directly in the algorithm to predict future levels of outputs. The method, however, requires a complete model of the process and all the control goals have to be buried into a single objective function which is then optimised. The issue of controller robustness is directly addressed by incorporating a process uncertainty description into the model as norm bound perturbations in transfer function. Such uncertainty description, however, is difficult to obtain from standard experimental and identification procedures. Furthermore, a framework to analyse stability characteristics of MPC type design and

robustness to un-measured disturbances does not exist, because the theoretical properties to develop such a framework are not very well understood. It has been shown, however, that the stability characteristics of the MPC algorithm can be affected by constraints in very surprising ways (McAvoy et al., 1989). The LQG framework has been suggested for the desired analysis (Bitmead et al., 1990), but then the advantages of MPC such as no advanced knowledge of state-space modelling and identification are lost.

1.4.4 Experimental Design for the controller:

The PCA based inferential controller requires a rich and accurate set of steady-state experimental data to establish linear relationships between primary control variables and secondary measurements. The experiments need to be performed at all the conceivable levels of disturbances that the system is likely to be subjected. This data will also be used to obtain the process gains. Step response experiments are also needed to infer system dynamics. Similar experiments have to be carried out to model the effect of disturbances.

1.4.5 Conclusions

Continuous crystallizer operation needs a multi-input, multi-output control structure, preferably not requiring on-line measurements of crystal size distribution. A PCA regression models will be developed for estimating the primary variables, *viz.* total number of from the two secondary measurements, *i.e.* conductivity and vessel temperature. The data for the models will be obtained from steady-state experiments performed over a range of operating conditions. System identification techniques will be used to develop a state-space representation of the process from step-response experiments. The state-space process models will be used along with those

representing modelled disturbances to develop an optimal LQG controller. This controller in conjunction with the PCA based regression model will provide the complete inferential MIMO design.

1.5 Concluding Remarks

Modern techniques from process systems engineering which manifest advanced research from the cutting edge of research in artificial intelligence, mathematics and process control will be transformed and refined by addressing difficult problems encountered in crystallisation systems. The focus of the work will be on the following aspects,

- Discretised population balance method for dynamic modelling and simulation of crystallisation process flow sheets.
- Optimal synthesis of stage-wise crystallisation processes using the targeting method and non-linear programming.
- Operational level optimisation of a crystallisation process flow sheet using revised machine learning methodology through inductive learning and case based reasoning.
- Design of a robust optimal controller for a continuous recycle crystallizer to inferentially control crystal number and average size without measuring them on-line by using regression models and optimal LQG/LTR techniques with real experimental data.

Chapter 2:

REVIEW OF SYSTEMS LITERATURE IN CRYSTALLISATION

"Process systems engineering (PSE) is the discipline of systematic planing, design, operation and control of chemical processes" (Ponton, 1995). The topics covered within the discipline could include fields as diverse as molecular modelling, statistical thermodynamics, computational fluid dynamics and advanced process control. The core activities centred around the "systems" approach, addressing processes as a complex whole, however, remain mathematical modelling, process synthesis, optimisation and to a lesser extent process control where the major strand branches from applied mathematics. In this chapter an extensive review of the PSE techniques as applied to crystallisation processes will be presented. Conclusions supporting the need for the techniques introduced in the preceding chapter and the advancements to be made by their application will be made at the end of each section.

2.1 Process Modelling and Simulations

Mathematical description of processes whereby crystals are undergoing nucleation, growth, aggregation and breakage during some or all phases of operation inevitably results in the inclusion of the population balance to the modelling exercise. The fact that these phenomena are dominant during different stages and the general observation that up to ten residence times are necessary to achieve steady-state in an MSMPR crystallizer, signify the importance of dynamic modelling and simulation for crystallisation processes. Dynamic population balances, however often develop into integro-partial differential equations which are entirely intractable analytically. Since the population balances lie at the heart of the models for dispersed phase systems, considerable effort has been exhausted over the years to formulate techniques for their conversion to a numerically solvable form. The dynamic population balance for a mixed-suspension, mixed-product removal crystallizer (MSMPR) will be presented

next, along with a discussion on discretization based methods for its solution. This will be followed by a review of flowsheet simulation literature focusing on crystallisation processes.

Many other methods have also been developed for the transformation of population balance equations into more solvable form, these include a) stochastic modelling (vanPeborgh Gooch and Hounslow, 1996; Jones et al., 1996; Shah et al., 1977), b) piece-wise cubic spline methods (Steemson and White, 1988), c) method of weighted residuals (Singh and Ramkrishna, 1977), d) finite element analysis (Nicmanis and Hounslow, 1996) and e) moment based solution (Hulburt and Katz, 1964).

2.1.1 Population Balance

The dynamic population balance for an MSMPR crystallizer with only crystal length as the internal co-ordinate can be written as,

$$\frac{d\,n}{dt} + \frac{d\,(Gn)}{dL} + n\frac{d\,(\log V)}{dt} = B - D - \sum_k \frac{Q_k n_k}{V} \qquad (2.1)$$

In the above equation, n is the number density function. It relates the rate of change of number of crystals in differential size range $L + dL$ to the rate of growth into and out of that range and the rates of birth and death. These birth and death events could be due to agglomeration and crystal breakage. The appropriate forms of the equations representing the two contributions for each of the two phenomena are,

$$B = \frac{L^2}{2}\int_0^L \frac{\beta(L, L'')n(L)n(L'')dL''}{L''^2} + L^2\int_L^\infty b(L, L')\,S(L')\,n(L')\,dL' \qquad (2.2)$$

$$D = n(L)\int_0^\infty \beta n(L')dL' + S(L)n(L) \qquad (2.3)$$

The nucleation rate is taken to be the rate of appearance of crystals in the smallest size range and therefore appears only as a dirac delta function in the population balance.

2.1.2 Discretization Techniques

2.1.2.1 Hounslow Method

This method discretizes particle size domain into small intervals using a $\sqrt[3]{2}$ geometric progression (details can be found in Hounslow et al., 1988 and Hounslow, 1990). The size distribution function within each interval is assumed to be constant and the integrals are replaced by summations. These transformations reduce the original integro-partial differential equation into a series of ordinary differential equations. The discretized versions of the equations for agglomeration, growth and nucleation are formulated in such a way that the total number and volume of the crystals is conserved. A correction factor representing the fraction of successful interactions from preceding size range is specifically designed for the conservation task. Recently, Russell and Seinfeld (1996) have solved three coupled population balances discretized in this manner to study the effects of aerosols and other particles on cloud formation.

Though the method is computationally efficient, it is restricted to a fixed discretization of size domain at $v_{i+1}/v_i = 2$. This could be coarse when the predictions are compared with the data obtained from sophisticated devices such as those based on the light scattering principle. Furthermore, higher moments of size distribution are not conserved, mainly due to the assumptions on the form of CSD function within the intervals and loss of mass at long times.

2.1.2.2 Kumar and Ramkrishna Method:

In this method, the most desirable properties of CSD are targeted, rather then seeking complete number density function with erroneous properties (Kumar and Ramkrishna, 1996a). This is achieved by adjusting the coarseness of discretization. In a modification to the original technique, a procedure was later developed where the variation of number density with size in a size interval was accounted by adjusting a "pivot" that represents total population of the corresponding size class (Kumar and Ramkrishna, 1996b). This enable addressing the evolution of non-uniformities within a size interval often observed due to agglomerative birth in smaller intervals. The method is superior to the Hounslow's procedure, in that any two properties of CSD function can be conserved, discretization is not restricted to $\sqrt[3]{2}$ geometric progression and a constant CSD function within a class range is not assumed. It is however, a few orders of magnitude more demanding on computation time.

2.1.2.3 Hill and Ng

Here again any two properties of CSD function could be conserved (Hill and Ng, 1995; 1996). This is achieved by using proper probability functions instead of a correction factor used in the Hounslow's method to guarantee the conservation of properties. The method allows both equal size intervals and geometric intervals of any ratio. The fact that mass is conserved can be extremely beneficial in determining the type and coarseness of grid to be used for better predictions from rough estimates obtained through large geometric ratios. The computational requirements are comparable to Kumar and Ramkrishna's method.

2.1.3 Process Simulations

Until recently, most of the flowsheet simulation studies had been based on average properties of CSD, often average crystal size and total number. The advent of

discretized population balance models and faster computers have, however provided the incentive to employ techniques routinely used for vapour-liquid flowsheets. In the following two of the more recent procedures developed for particulate processes will be analysed.

2.1.3.1 Short cut methods

The method of moments was proposed for distributed systems by Hounslow and Wynn (1992) to transform models comprising functional equations that represent CSD. These moments can be easily related to the properties of CSD including, mean crystal size, standard deviation and measures of symmetry such as skewness and kurtosis. The limitations of this approach become apparent when unit operations such as hydrocyclones and fines dissolvers are considered. Here, the lumped properties of CSD do not allow for the formulations of models unless the complete CSD is available. Hounslow and Wynn (1992) proposed the construction of complete CSD from its lumped properties by fitting an arbitrary distribution function capable of predicting up to four moments correctly. Though limited in its CSD information contents, the approach is beneficial for early stage design and simulations. Extensions to dynamic simulations were readily available because an equation oriented flowsheet simulation environment was used. With efficient algorithms available to partition a large number of equations, the equation oriented approach is not only ideal for dynamic simulations but equally suited for steady-state calculations.

2.1.3.2 Sequential-modular discretization based approach

Recently, a sequential modular flowsheet simulation program SOLIDS has been developed (Hill and Ng, 1997) to perform steady-state simulations for unit operations common to dispersed phase systems. Unlike short cut method where moments of CSD

are used, the complete CSD is simulated using discretized equations (Hill and Ng, 1995; 1996). The approach which links various units including crystallizers, dissolvers, filters and cyclones using the same general discretized population balance framework has been demonstrated for the Bayer process, potash production and salt production processes. Like all sequential modular procedures the method is restricted to steady-state solutions. Furthermore, it requires effective initialisations and good estimates for tear streams in processes with recycle. The latter could be tedious for complex flowsheets especially when initial estimates for the number of crystals in each size interval would have to be provided along with other stream variables.

2.1.4 Conclusions

Discretization has undoubtedly established itself as the most efficient and general method to transform population balance equation into forms solvable by robust algorithms for ordinary differential equations (ODE) and differential algebraic equation (DAE) systems. The different discretization forms (Kumar and Ramkrishna, 1996a; 1996b; Hill and Ng, 1995; 1996; Hounslow et al., 1988; Hounslow, 1990; Marchal et al., 1988) vary in the shape of size distribution function within the intervals, choice of discretization (geometric, linear, arbitrary), moments conserved and probability functions for agglomeration and breakage contributions.

In this work, Hounslow's discretization will be used for dynamic simulations of crystallisation process flowsheets. Though the solution could over-predict the mass of crystals by up to 14% for growth and nucleation processes and is restricted to a comparatively coarse discretization, it is by far the least demanding computationally. Litster et al. (1995) have shown that successive refinements of geometric discretization by one on a volume basis increase CPU times by at least a factor of 8.

These refinements could therefore be prohibitive for flowsheet simulations where population balances have to be solved along with mass and energy balances. The issue of lost solute, if analysed in the context of errors and inaccuracies associated with kinetic parameters, does not seem very significant. For instance, crystal mass is fourth order in growth rate and a slight error in its parameters could have far worse consequences.

For problems where a steady-state solution ignoring agglomeration and breakage would suffice, for instance during process synthesis, analytical solutions to the population balance will be used; these do not suffer from the errors discussed above.

2.2 Stage-wise crystallisation process synthesis

Modelling and simulation of the stage-wise crystallisation process have been addressed with varying levels of detail in the literature. These models have, however, rarely been used to optimise a network of crystallizers by determining best values of control profiles such as temperature, feed concentration and residence time for the desired objective. In the following, features of the efforts made to model and simulate such processes along with a detailed analysis of the only contribution on optimisation will be presented. This will be followed by a discussion justifying the use of the targeting approach for synthesis purposes.

2.2.1 Modelling and simulation

Among the early efforts to qualitatively analyse the performance of stage-wise processes was the work of Randolph et al. (1968). They developed simple equations for a network with product classification after each crystallizer and quantified its performance in terms of cut size and the fraction of inlet stream in the underflow (classification ratio) of the hydrocyclones. The hydrocyclones were modelled by very

simple equations, which did not allow for physically realisable control on their operation. Crystals were only allowed to form in the first crystallizer and a fixed value for cut size was used for every hydrocyclone. They showed that a minimum in the coefficient of variation occurs at small cut sizes and low classification ratios. It was also concluded that the assumption of non-nucleating stages, subsequent to the first stage would be difficult to achieve practically without significantly reducing the growth rates for most process.

Later, Randolph and Tan (1978) developed two alternative approaches to design techniques for stage wise crystallisation process. The methods were demonstrated on systems where classification was only allowed at the end. In the rigorous method, the population balance was solved along with the mass balance and rate equations. Different forms for separation efficiency functions were tried. An alternative technique, based on moment transformation was also presented. Here, the CSD function was developed for the classifiers by using a gamma distribution function with the moments of CSD. Effects of size dispersion due to random fluctuations in growth rates were also studied. Again, the fraction of product stream recycled through the overflow of hydrocyclone and the form of separation efficiency curve were identified as the most significant parameters while keeping all conditions in the crystallizers except for temperature constant. Whilst decreasing temperature profile was used, no reasons were provided for the selected values, neither was an attempt made to find better ones. For the crystallizers, only the effects of flowrate were quantified. These were found to be consistent with the expectations for yield and throughput, whereas the coefficient of variation and average size were shown not to respond.

Hounslow and Wynn (1992) used stage-wise crystallisation to demonstrate their short-cut methods for simulating particulate process flowsheets. They used moment transforms and a full analytical solution of the population balance for simulating such processes. Though most of the results were for simulations, there is a mention of investigations into finding the operating conditions for optimum product quality, minimum energy use and minimal capital cost. The conditions and findings for these calculations were, however, not reported. Again, only simple cascades of crystallizers were used in a pre-defined network.

2.2.2 Optimal Synthesis

Larson and Wolff (1971) have been the only authors to attempt optimisation of a network comprising up to three crystallizers in series. Analytical solution of the population balance was used and the control variables included volume of the crystallizer and fraction of solute crystallised in each crystallizer. The objective was to determine optimal values to achieve best mean size, coefficient of variation (CV) and yield by performing calculations with different randomly generated discrete combinations of control variables. It was found that multi-stage crystallizers can reduce the CV of CSD only at the expense of average size, which is often lower when compared to an equivalent single stage process. Yield can however, be increased by staging. It was also concluded that depending on the kinetics of the system, reduction in average size could easily offset the advantages of increased yield and improvements in CV.

The choice of fraction crystallised as control variable, though beneficial in simplifying modelling could be very difficult to interpret in terms of operating conditions and could even make the use of second control variable, *i.e.* volume unnecessary. The

adequacy of the procedure and therefore its findings are strongly dependent on the assumptions made during the formulation of the network, the exhaustiveness of the combinations of control variables and the fineness of their discretization. The latter is particularly important given the highly non-linear nature of crystallisation processes. Furthermore, due to *a priori* specification of the network structure and the fact that a crystallisation system is designed in isolation from energy and separation systems, the solution thus obtained could be sub-optimal, even if the above concerns were addressed (Balakrishna and Biegler, 1996).

2.2.3 Discussion

For stage wise calculations, moment transform and analytical solution to the simplified population balance have emerged as the two techniques for simulation and design. It has been noted that none of the design methods or the optimisation study pays much attention to energy balances during modelling. These considerations are, however, of paramount importance because an overall optimal solution to the synthesis problem can only be achieved if as many sub-systems as possible are considered simultaneously. Furthermore, economies of energy consumption has often been cited as another very important feature of stage-wise processes. It therefore seems odd that very little attention has been given to energy issues. Hydrocyclones have often been included at some stage to achieve CSD improvements that would not be possible to explore with the simplified models used for crystallizers and the restrictions on the structure and design parameters within the flowsheet. These devices are often modelled at a very elementary level and therefore could be extremely difficult to design and operate at levels arbitrarily prescribed.

The network structures considered heretofore are very rigid in that only a simple cascade configuration is allowed. In most cases even the same residence time has been used with only the supersaturation varied between the crystallizers. Other alternative structures which could not only help improve performance by providing more control parameters, but also by eliminating the need to operate on full feed have not been found in the literature. For instance, if feed bypass is used where only a portion of fresh feed would enter each crystallizer; the extent being determined optimally, the obvious benefits could include smaller vessels for the first few crystallizers and a lower cooling duty for each subsequent crystallizer because the inlet solute concentrations would be higher as the product stream from previous crystallizer would be mixed with fresh feed. Similarly, some product could be withdrawn from intermediate crystallizers, again reducing volumes for the latter vessels. Such network structures and choice of crystallizer types, for instance column or draft tube type designs, where PFR type of performance can be used as an approximation, along with simultaneous considerations for energy and separation networks could certainly extend the levels of performance achieved from current stage-wise processes to very high levels.

One area where the current methods for stage-wise process calculations have been particularly weak is the numerical techniques applied to solve and optimise the networks. Larson and Wolff (1971) did not use the conventional optimisation methods which are well capable of addressing the magnitude of the problems they were tackling. Robust algorithms such as generic reduced gradient (GRG) and sequential quadratic programming (SQP) are now available for optimising problems with high non-linearities. Curthall and Biegler (1987) have developed an extremely efficient

method specifically designed for the transformation of synthesis type problems represented by boundary value DAE systems into a set of non-linear equations.

In this work, the synthesis problem will be modelled as a boundary value DAE system comprising moment and mass balances. These will represent trajectories of state variables in time/volume, analogous to PFR representation except that side feeds and product removal will be allowed. An upper limit on performance will be determined within the process constraints and then the problem solved to find optimal values of the control variables for the best structure and parameters to achieve performance closest to the maximum. A network of crystallizers, which can comprise PFR type vessels and MSMPR crystallizers or just the latter, would then be extracted from the solution. Though the models would be non-isothermal, at this stage the problem will be restricted to the determination of crystallizer networks only.

2.3 Process Optimisation

The literature has been searched for both design and operational level optimisation of crystallisation processes. Very few contributions have been found in each category. In the following, their details will be summarised and a discussion on their limitations presented. This will be followed by conclusions supporting the machine learning based method proposed in the preceding chapter.

2.3.1 Design level optimisation

Rossiter and Douglas (1986) and Jones (1991) attempted to optimise a given flowsheet by determining best values of design variables. The scope of such studies can span from preliminary design; where process alternatives may have to be compared and screened economically, to determining the best conditions for equipment trails or for detailed final design. In both contributions, the focus was on

the optimisation of median size. Simplified cost correlations derived for various units were used to evaluate the impact of average size on system economics. Flowsheet decomposition analysis was carried out to identify the independent sub-systems. From individual models for crystallizers, primary product separation and drying units, a cost model for the whole process was developed. The effects of perturbations in a given design parameter while keeping others constant were used to determine an optimal set of values for all the design parameters.

The procedure was demonstrated (Rossiter, 1986) for the production process of crystalline common salt from brine. It was found that the optimal median size is determined by the entrainment limit in the crystallizer. The crystallizer had to be operated at maximum allowable temperature and the slurry density measured for quality constraints. It was also suggested that cost discontinuities should be imposed on the basis of temperatures of the available heat sources, possible materials of construction and other intrinsic properties of the system.

The limitations of the procedure were identified as, a) fixation of most design variables and b) limited number of variables due to the scarcity of the available design and cost relationships.

2.3.2 Operational level optimisation

The only work found for operational level optimisation was based on artificial neural networks (ANN), where the objective was to determine best operating conditions for a crystallizer (Woinaroschy et al., 1994). Steady-state experimental data obtained under a range of operating conditions for reactor temperature, feed concentration and mean residence time was used to develop an ANN model capable of optimising operation of a $CaCO_3$ precipitation process in a 1 litre MSMPR crystallizer. The choice of ANN

was based on the limitations of formulating an adequate simplified representation of the process from theoretical considerations to account for all the variables of interest. The ANN model had four neurones in the input layer; one for each operating variable and one for the bias. The output was selected to be cumulative mass distribution; thirteen neurones were used to represent it. A sigmoid functional form was chosen for the transfer function between inputs and outputs in the hidden and output layers. The back propagation rule was used in the learning process for training the network from 28 sets of experimental data. A compound objective function was formulated with the aim of finding vectors of operating conditions leading to a certain fixed value of mean size with minimum CSD dispersion. Adaptive search method, which involves a number of steps (details can be found in Luss and Jakoola, 1973) was used to find the optima. The steps included a) preliminary search of the random variable range in which the minimum value of objective function might be found, b) selection of these ranges to search for global minimum and c) further refinements in the vector found. The results were found to be in good agreement with the qualitative suggestions from theory and practice and showed that the optimum occurred at low temperatures. Concentration had to be increased and residence time reduced if low median sizes were desired. As expected, larger residence times resulted in larger crystals.

2.3.3 Discussion

Crystallisation process design optimisation methods are based on simple models and even simpler techniques to solve them. They utilise semi-empirical 'design and cost' models establishing a relationship with limited applicability and accuracy between very few process parameters, which often means that either the decision variable or the optimisation variable is a lumped parameter, itself a function of many independent

process variables. This feature limits the number of variables that can be considered for optimisation. For example, all the complex interactions between solubility, temperature, kinetics of nucleation and growth and evolution of final crystal size distribution with time, that characterise a crystallizer operation are often represented by an empirical relationship for optimisation between median size (decision variable) and residence time, hence the operation can only be optimised with respect to the residence time. Often such design and cost models are not available for all the major units and these are therefore ignored in the analysis. Furthermore, the correlations have been developed many years ago and need to be corrected for inflation factors.

Cost models for the entire process are developed from individual unit models. These are analysed by perturbing one variable at a time to observe and quantify its effect on the decision variable as a plot. An optimal level is determined by inspecting the plots for each variable. The procedure is not only tedious but also ignores the correlations between design variables themselves. This could mean that the performance predicted might not be obtainable. The analysis is not very useful beyond the design phase, though its limitations would have consequences for process operation.

The ANN approach is more attractive because it is based on predicting better levels for operating variables to improve performance by extrapolating from past known cases. This is done by fitting a particular class of models to the data and then hypothesising that the solution for future levels of decision variables will conform to the fitted model. The method formulates a final solution consisting of a vector comprising the decision variables (x_1, ..., x_n) that defines a single best performance point (y) in the performance space. Most decision variables, however have some variability associated with them even under the best control schemes. As a

consequence of ignoring the fact that processes usually operate in narrow bands of decision variables, the final solution obtained by this approach may be sub-optimal even when accurate models are available, since their evaluation criterion ignores the system behaviour around the optimum. The area surrounding such a point does not in general correspond to the zone where best average performance can be achieved (Saraiva, 1995).

The method also requires selection of operating variables which would best reflect the main attributes of the system. This may be trivial when a single MSMPR is considered (Woinaroschy et al., 1994), but for a complete process flowsheet with interacting and interdependent units the choice may not be straight forward. The form of transfer function at the hidden and output layer is also very crucial in determining the capabilities of an ANN model to hypothesise the solution for future levels of operating variables. Process insight could be helpful in this task to determine the functional form for mapping inputs to outputs. It has to be realised however, that fixing the function limits the relationship between inputs and outputs to a form with little physical justification. A thorough comparison of machine learning methodology and other multivariate statistical methods including ANN can be found in Saraiva and Stephanopoulos (1992b).

Crystallisation processes will, therefore, be best served by machine learning methodology which offers a flexible and mathematically de-convoluted procedure identifying performance improvement zones by establishing ranges on the crucial decision variables. In this contribution, a modified machine learning methodology will be presented. It will be illustrated by an application to a simulated potassium nitrate crystallisation process flowsheet. Sufficiently complex population balance based

models for crystallisation process unit operations will be used to simulate the process under a range of operating conditions to generate the necessary process data.

2.4 Process Control

The three most important issues in control of continuous crystallizers are,

a) on-line measurement techniques

b) use of CSD to determine dynamic process model

c) identification of most suitable process inputs

Most of the literature in control of continuous crystallizers is based on a single-input single output (SISO) control structure. Different controlled variables and manipulations have been suggested based on the relative ease and accuracy of on-line measurements and their efficiency in effectively addressing set-point tracking and disturbance rejections. Linearised physical models and black-box models have been suggested for the controller design. In the following, literature addressing these issues will be summarised under physical and black-box model based sections.

2.4.1 Physical model based control

In their control analysis for low order cycling of CSD, Rousseau and Howell (1982) considered the merits of using different measurements for stabilising a continuous crystallizer with both fines destruction and product classification. The analysis was carried out on a simulated process using population and mass balances along with kinetic equations and employed finite difference techniques to solve the system. The main advantages of using a finite difference methods in comparison with a linearised form of analytical solution were cited as, a) no modifications to the models were necessary to accommodate different removal functions and b) any form of nucleation kinetics could be used. To achieve stabilisation objectives, they considered a control

system that would stabilise growth rate rather than the nuclei density. This was done by a proportional controller based on the deviations of super-saturation from steady-state. A differential refractometer was suggested for measuring super-saturation, because its readings do not suffer from electrical noise or by the presence of crystals in the slurry. Though the measurements are easier to make than for nuclei density, it was found that a super-saturation based controller is more sensitive to measurement errors and required a controller constant 9 times higher than for nuclei density based controller to dampen the oscillations.

Randolph et al. (1987) used light scattering measurements in a continuous fines stream to infer nuclei density from slurry density measurements. A theoretical equation was used for calculating nuclei density from density measurements. An 18 litre KCL crystallizer was used to implement the controller which had the task of eliminating CSD transients (not oscillations) caused by outside disturbances such as flowrates, temperature or agitation. Nuclei density inferred from secondary measurements was controlled by manipulating the fraction of fines dissolver flow sent back to the crystallizer using a proportional action control. Only disturbances in vessel temperature were considered; these were suddenly introduced into the system at steady-state to generate a nucleation pulse. The temperature was disturbed by shutting off the cooling water, until it elevated to the desired level. The cooling water was then re-opened to initiate temperature control. Both open loop and closed loop experiments were performed and it was observed that the latter reduced root mean square of CSD fluctuations due to nucleation upset by a factor of 3.5. A recycle line was added to fines dissolver stream which enabled varying its flowrate without introducing upsets in the crystallizers due to changes in the cut size of the fines removed. It also helped

establish relationships permitting linear changes in fines destruction through linear changes in the manipulated variables.

Rawlings et al. (1992) analysed the stability of a continuous crystallizer based on the linearisation of population and solute balance. Their model did not depend on a lumped approximation of partial difference equations and successfully predicted the occurrence of sustained oscillations. They demonstrated that simple proportional feedback control using moments of CSD as measurements can stabilise the process. It was concluded that the relatively high levels of error in these measurements require robust design for effective control.

In a review on the three crucial aforementioned aspects of crystallizer control Jager et el. (1992) used a dilution unit in conjunction with laser diffraction measurement equipment. The combination could however, only determine CSD by volume while the controller required absolute values of population density. For this purpose the CSD measurements were used along with mass flowmeter. They were found to be very accurate when used to calculate higher moments of CSD. For the zeroth moment, however, the calculations resulted in standard deviations of up to 20%. This was anticipated because small particles amounted for less then 1% of volume distribution. Physical models for process dynamics were simplified by assuming isothermal operation and class II crystallizer behaviour. The latter implies a fast growing system in which solute concentration remains constant with time and approaches saturation concentration. Isothermal operation constraint enabled the simplification of mass and energy balances into a single constraint on product flowrate. Solute balance reduced to a constraint on growth rate. The model, however, did not result in the required state-space representation essential for multivariable model based control. Finite difference

approximation of size axis was used to convert population balance into a set of ODE's, which were then linearised at an operating point to obtain the required state-space representation. It was suggested that fines dissolution on its own was insufficient to achieve better control as was the scope of variations in temperature, residence time and rate of cooling/evaporation. The need for a product classification step whereby coarse crystals are removed at a finite size was highlighted. Hydrocyclones were suggested for the purpose of reducing CSD dispersion by using variable underflow diameter as an additional input for control.

2.4.2 Black box modelling for dynamics

Rohani and Paine (1991) developed a feedback controller, where process dynamics was obtained from step change responses of the outputs by fitting first order plus dead time models. Again, the rate of fines dissolution / removal was the manipulated variable with fines suspension density being the output or control variable. Control variable was interpreted using a fines suspension density sensor (FSDS) which uses a sample cell containing a representative sample stirred and heated at an appropriate rate, while the transmittence of an infra-red light beam passing through the cell is being recorded (Rohani and Paine, 1987). Temperatures are measured just outside the cell and within it until the transmittence measurement reach a plateau, *i.e.* all the crystals have dissolved. These temperature measurements along with the solubility data are used to infer fines density in a simple manner which does suffer from interference from electrical noise or other interference due to insoluble particles. FSDS was used to design a PI controller for both the set point tracking and rejecting disturbances arising from temperature fluctuations in the crystallizer. The controller gave acceptable performance in rejecting small disturbances in temperature.

Redman et. al (1997) performed a detailed analysis of a crystallization system for control variables such as mean crystal size, weight percent solids in product and fines streams, and super-saturation through manipulations in feed, product, re-circulation and fines dissolution flowrates to determine the best pairings. Open loop response to step changes in the manipulation variables were used for selecting and designing the controller. Mean size was determined by an in-line backward scattering laser light sensor, while nuclei density was inferred by the FSDS. Super-saturation was determined through density measurements and solubility data. Experiments were performed in a 1 m^3 forced circulation, evaporative crystallizer. Bristol's relative gain array analysis (Bristol, 1966) was carried out on the findings to determine the pairings which were found as,

1. Fines dissolution flowrate with average size
2. Product flowrate with weight percent solids
3. Feed flowrate with super-saturation.

A single input single output controller was designed (for mean size), even though relative gain array analysis showed possible interactions between all of the three control variables. Cascade configuration was designed with the fines dissolution flowrate as control variable in the slave loop. The internal model control (IMC) controller design techniques were used to determine controller parameters. Most process disturbances were eliminated through effective design, and after these modifications the controller was shown to be successful in tracking an increase in mean size set point. A subsequent reduction in it however, failed to bring mean size down to the new lower value even though the fines flowrate was immediately reduced to its lower limit by the controller. This happened because the improved design had

already minimised the nucleation process and thus rendered fines dissolution ineffective. The controller was also shown to be ineffective in rejecting product flowrate disturbances, where no response was observed until the disturbance had been removed.

Jager et al. (1992) again using a dilution unit and on-line measurement with light scattering devices together with mass flow meters developed a black box model based controller for a 970 litre crystallizer. System identification techniques were used; these offer a lower order state space model for multivariate analysis. A three step identification procedure was employed to obtain the model. In the first step the ARX model (Ljung, 1987) was used. The second step involved transformation of the ARX model into a state-space representation through approximate realisation (Damen and Hajdasinski, 1982). Finally, the model was used as an initial parameter combinator for fitting the actual data. Un-correlated white noise signals were added to the data used, because they could be added to process inputs simultaneously without affecting the ability of the identification algorithm to distinguish the contribution of each individual input to the output signal, thus allowing effective use of data. A model derived through these steps was used to establish relationships between inputs including heat input, product flowrate and rate of fines dissolution, and the outputs which were third moment and mass based average size. The inferences on the sufficiency of these inputs were similar to the ones summarised earlier while discussing the author's work using physical models (sec. 2.4.1).

2.4.3 Discussion

It is evident from the work reported to date that mostly either number density, average size or weight percent are considered as control variables. Often these variables are

inferred from other measurements, including density, super-saturation, refractive index etc. Inferential techniques have been shown to be particularly suitable for industrial scale applications where laser scattering devices are not yet practical for control purposes. Even when usable, these devices are characterised by noise and require very low solids concentration. Furthermore, the inversion step in which the vector of energy measurements is inverted to determine the size distribution producing the scattering pattern is mathematically ill-conditioned.

The issues of measurement uncertainty with direct measuring devices and model uncertainties where these quantities have been inferred from secondary measurements are significant with respect to the design of an effective controller. None of the contributions surveyed address these concerns. Then there is the question of what to control. It has been repeatedly suggested (Jager et. al, 1992; Sherwin et al., 1967; Redman et al., 1997) that an effective controller will have to control not a single state but multiple states through MIMO architectures. On the basis of their thorough study into the dynamics of continuous crystallizers Sherwin et al. (1967), suggested that it was necessary to control nuclei density along with any other property of CSD. Most of the work in the area, however, is based on SISO controllers which at times are shown to be unable to address either set point tracking or disturbance rejection effectively because of their heavily restricted control objectives.

Fines dissolution flowrate has almost universally been used as the manipulated variable, even though its limitations are not only obvious but have been quantified by Jager et al. (1992) and Redman et al. (1997). A simple analysis of crystallisation process would reveal that both nucleation and growth rates are strong functions of super-saturation and therefore ways of manipulating super-saturation to achieve

desired CSD properties ought to be a key concern in control exercises. Such manipulations can be brought about by changing feed concentration or crystallizer temperature. It is also obvious that residence time is of paramount importance in determining the form of product CSD. Again no interest has been evident in exploiting its merits for control studies. Lately hydrocyclone apex diameter has been suggested as an input variable to affect cut size according to the desired value for mean crystal size (Jager et al., 1992). The issues arising from the consequences of such a design including unsteady recycle flow back to the crystallizers with varying CSD were not addressed or quantified even though, Sherwin et al. (1967) showed that product classification is a major source of oscillatory behaviour in continuous crystallizers.

Models based on real process responses have begun to emerge which makes the application of modern control techniques more realisable. It can be noted, however, that most of the models have been extracted from only one or two experiments. This would not only ignore model uncertainty but also severely hamper the robustness of the controller designed. The fact that these issues were ignored by Redman et al. (1997) could describe the poor performance of their control scheme.

In the present work a two-input two-output inferential control system will be designed for a simple 1 litre continuous recycle crystallizer for KNO_3. Control objectives will include robust performance for both set-point tracking and disturbance rejection. The primary control variables will be total number density and mean crystal size, while manipulated variables will include recycle ratio and coolant flowrate. A steady-state relationship based on principal component analysis and multivariable regression will be developed for a model relating primary control variables to secondary

measurements. The data for the relationship will be obtained by performing a range of experiments to guarantee accurate estimates over a wide window of operation. In these experiments off-line steady-state measurements for primary variables will be obtained from a Coulter counter multisizer II. Step response experiments around different steady-states will be used to find first order plus dead time (FOPDT) models between secondary control variables and process inputs. LQG/LTR optimal controller would then be designed from these transfer functions and the estimator. The controller design would guarantee stability while the robustness issues for the observer will be addressed by performing loop transfer recovery. The overall robustness of the design will be checked by subjecting it to a range of values for the process model parameters.

Chapter 3:

DYNAMIC MODELLING OF CRYSTALLISATION PROCESSES

Solid processing plants differ from vapour liquid processes, to which virtually all the research papers and published applications in simulation are restricted (Evans, 1989), in that a further specification, *i.e.* physical size is required in addition to chemical composition. This additional particle characteristic accompanies with it the complexities associated with the adequate representation of crystal size distributions. Routine calculations of phase and chemical equilibria are also complicated by the possibility of the presence of many different condensed solid phases of a single compound.

In this chapter, a consistent and sufficiently complex dynamic representation of the unit operations common to crystallisation processes will be developed for subsequent use. It would therefore, be worthwhile to briefly outline underlying concepts to modelling and the systematic methodology required to develop and analyse models needed to accomplish the aforementioned goals.

3.1 Systematic approach to construction of multi-faceted dynamic models

Mathematical representation of the physical and chemical phenomenon taking place in a chemical process enhances our understanding by establishing cause and effect relationships between system variables and therefore permits the analysis of the behaviour of the entire system. Such a representation constitutes a model of the system, while the activities leading to the construction of the model are referred to as modelling.

3.1.1 Model Development:

Precise model development in engineering is usually preceded by qualitative logic induced by detailed observation of an event thereby developing its physiochemical insight. This essentially qualitative step is followed by gathering pertinent physical and chemical information, conservation laws and rate expressions. At this stage, the objectives of the mathematical exercise are outlined as they determine the ultimate complexity of the final description. The next step requires the adaptation of information accumulated for the problem at hand, for example outlining finite or differential volume elements for writing relevant conservation laws. To furnish these equations, the question of initial and boundary conditions are addressed. When the problem is fully posed in quantitative terms the model is analysed for the magnitude of parameters and nature of the equations prior to seeking an appropriate mathematical solution method which would relate dependent variables to the independent ones.

3.1.2 Model Analysis:

Model analysis is broadly divided into two distinct exercises, *viz.* analysis of the variables and the analysis and pre-processing of the equations comprising the model. Sensitive variables, *i.e.* those which show very significant variations with minute changes in the manipulated variable are identified. The magnitude and the effect of variations are analysed and quantified. If desirable, these variables are normalised so as to bring their order of variation in line with other variables in the model.

It is highly desirable to mathematically transform a model comprising partial differential equations into a set of differential algebraic equations (DAE's), because robust, efficient, accurate, versatile and verified methods have only been developed

for the numerical solution of the latter class of equations. Transformation of partial differential equations into a set of differential equations can be brought about by either finite difference or finite element methods. The mathematical model is analysed to determine degrees of freedom, and if required, additional equations are introduced to restrict specifications to physical properties, design variables, feed and operating conditions and empirical parameters. Models that result in systems of DAE's are checked for index of the equation system through the available algorithm (Pantelides et al., 1988). The system of DAE's is partitioned into ODE 's, implicit algebraic equations and a set of explicit algebraic equations. The matrix of explicit algebraic equations can be analysed for the order of precedence using the Sargent-Westerberg algorithm to convert it into block triangular form. This rearrangement of equations is often desirable, since it outlines the grouping and sequence of equations subsets that can be used for embedding them into procedures.

Once the model has been developed, transformed, analysed and structured the most suitable numerical solution technique is selected on the basis of the stiffness of the system. For stiff systems (where there is an order of magnitude difference in the eigen-values of the Jacobian) implicit methods are preferred, whereas explicit methods of solution are the obvious choice for non-stiff systems.

3.1.3 Model Validation:

The validation phase involves debugging of the model so that it can predict sensible and expected results, before seeking agreement with the available data. Sensitivity of the accuracy of simulations with respect to solution methods is also explored. The model is analysed for robustness through simulations for the different operating

conditions and uncertainties in the values of empirical parameters in all the possible configurations within a typical flowsheet.

The validated model is refined by the deletion of complexities, which have little effect on the overall outcome and through the incorporation of more variables and equations that are likely to enrich the information content. Other methods for improving the versatility and generality of the model are also sought.

3.2 MSMPR crystallizer modelling and simulation

Firstly, a rigorous dynamic model of an MSMPR crystallizer comprised of discretized population, mass and energy balances is developed to help simulate its behavior within crystallization process flowsheets and for their optimization in the subsequent sections of this thesis. Features of the model, underlying theory, simulation analysis and a discussion is then presented.

3.2.1 Features of the Model:

The model is cast in the conventional three dominion strategy i.e., balance equations, rate equations and constitutive relationships.

The population balance uses geometric progression ($r = \sqrt[3]{2}$) to discretize the internal coordinate of the dispersed phase. Number contribution relationships for growth and aggregation in the population balance are adopted from Hounslow et al. (1988), whereas Hill and Ng's (1995) development is used to model attrition effects. A time delay function for the nuclei born at critical radii to grow to the first size interval is calculated in terms of super-saturation (through growth rate and critical size expressions). The mass balance is included to calculate the change in solute concentration for specifying the extent of super-saturation. The heat balance reveals

the temperature of suspension which is essential to generate the required super-saturation.

Nucleation rate is defined as a combination of primary and secondary (power law expression) rate processes. Contact with the stirrer and walls is assumed to be the major source of secondary nucleation. Physical variables including temperature, slurry voidage, pumping capacity, surface tension at the nucleus surface etc. which affect the nucleation rate are highlighted and considerable effort has been expended in establishing accurate values for these variables and parameters for the system used for model illustration, *i.e.* potassium nitrate. It is selected because KNO_3 exhibits a moderate temperature dependence of solubility and the kinetic data is also readily available. The kinetic parameters can be found in Mullin (1993) and Garside and Davey (1980).

Growth rate is defined in terms of a power law expression. The growth rate constant is expressed as a combination of both the diffusion and surface integration steps, which are defined in terms of the size of crystal, physical properties and operating conditions of the system.

Crystal aggregation is expressed in terms of Smoluchowski' s orthokinetic kernel. Furthermore, the sticking probability function in the kernel is expressed as a function of super-saturation. Specific breakage rate for attrition is given by a parabolic expression in the volume of the crystal breaking. A fifth order polynomial is used to correlate temperature dependence of saturation concentration. Auxiliary relationships for temperature and composition dependency of the physical properties used are also added to the set of equations. A cooling jacket is modeled for simulating the cooling rate needed to achieve and maintain vessel temperature at the desired level.

3.2.2 Theory

Population balance

The number continuity equation to study the dynamics of an MSMPR can be written in discretized form as:

$$\frac{dN}{dt}=\left(\frac{dN}{dt}\right)_{growth}+\left(\frac{dN}{dt}\right)_{agg}+\left(\frac{dN}{dt}\right)_{dis}-\frac{q}{vol}\left(N-N_{in}\right) \tag{3.1}$$

Expressions for rates of change in number due to growth and agglomeration are defined by Hounslow (1990) as

$$\left.\frac{dN_1}{dt}\right)_{growth}=B+\frac{G}{L_1}[(b+cr)N_1+cN_2] \tag{3.2}$$

$$\left.\frac{dN_i}{dt}\right)_{growth}=\frac{G}{L_i}[aN_{i-1}+bN_i+cN_{i+1}] \tag{3.3}$$

$$\left.\frac{dN_i}{dt}\right)_{agg}=N_{i-1}\sum_{j=1}^{i-2}2^{j-1+1}\beta_{i-1,j}N_j+\frac{1}{2}\beta_{i-1,i-1}N_{i-1}^2-N_i\sum_{j=1}^{i-1}2^{j-1}\beta_{i,j}N_j-N_i\sum_{j=1}^{\infty}\beta_{i,j}N_j \tag{3.4}$$

$$\left.\frac{dN_i}{dt}\right)_{dis}=\frac{3}{4}\sum_{j=i+1}^{\infty}\left(2\frac{v_i^{1/3}-v_{i-1}^{1/3}}{v_{j-1}^{1/3}}\right)X_jN_j-\frac{1}{2}X_iN_i \tag{3.5}$$

where Eq. (3.5) is due to Hill and Ng (1995) and the term in the brackets represents uniform breakage of crystals.

Dynamic mass and energy balances with constant volume are formulated as

$$\frac{dC}{dt}=\frac{q}{vol}\left(C_{in}-C\right)-(\,k_s\,G\,\overline{m}_2-k_v\,B\,L_0^3\,)\rho \tag{3.6}$$

$$vol\,c_P\,\rho\frac{dT}{dt}=P+Q+\Delta H_C\,Cq+q\left(\rho_{in}\,c_{Pin}\,T_{in}-\rho\,c_P\,T\right) \tag{3.7}$$

Kinetics of nucleation, growth and attrition and agglomeration kernel are modelled by the following equations

$$B = A\exp\left(16\pi\sigma^3\upsilon^2 \Big/ 3k^3T^3(\ln S)^2\right) + k_N N_P \Big/ N_Q \overline{m}_3 s^{1.7} \tag{3.8}$$

$$G = \left(\frac{k_d k_r}{k_d + k_r}\right) s \tag{3.9}$$

$$X = X_c \nu^2 \tag{3.10}$$

$$\beta_{(i,j)} = k_\nu k_a s^{0.9}\left(L_i + L_j\right)^3 \tag{3.11}$$

Nusselt's analysis is employed to calculate the heat removal rate (cooling crystallisation) from the vessel, while published correlations (Mullin, 1993) are used to account for the effect of increasing crystal mass on viscosity, density diffusivity and thermal conductivity.

Saturation concentration against temperature data (Mullin, 1993) is approximated by the following fifth order polynomial for Potassium Nitrate solubility.

$$C_S(T) = -6106.84 + 98.896T - 0.636T^2 + 2.03\times10^{-3}T^3 - 3.24\times10^{-6}T^4 + 2.05\times10^{-9}T^5$$

3.2.3 Model Analysis:

The resulting system of Differential algebraic equations (~ 250 equations) is categorised into Ordinary differential (ODE), implicit algebraic (IAE) and explicit algebraic (EAE) equations. Most of the equations belong to the third class of equations. It is preferable for these to be embedded into procedures to reduce the size of the actual problem solved by the DAE solver, since variables in the procedures are solved internally. The Sargent-Westerberg algorithm is used for the purpose of identifying the structure within EAE's, for effective partitioning of this subset of

equations. The structuring of the model directs the order of precedence analysis (done by SPEEDUP ®) on the subsets rather than the individual equations.

3.2.4 Simulation details:

The model is used to simulate the transient behaviour of a 5 litre cooling potassium nitrate MSMPR crystallizer. The CSD profiles predict rapid increase followed by a steady decline in the number of smaller crystals, mainly due to their subsequent growth and the fact that supersaturation falls below the level necessary to sustain nucleation at the initial rate (see fig. 1).

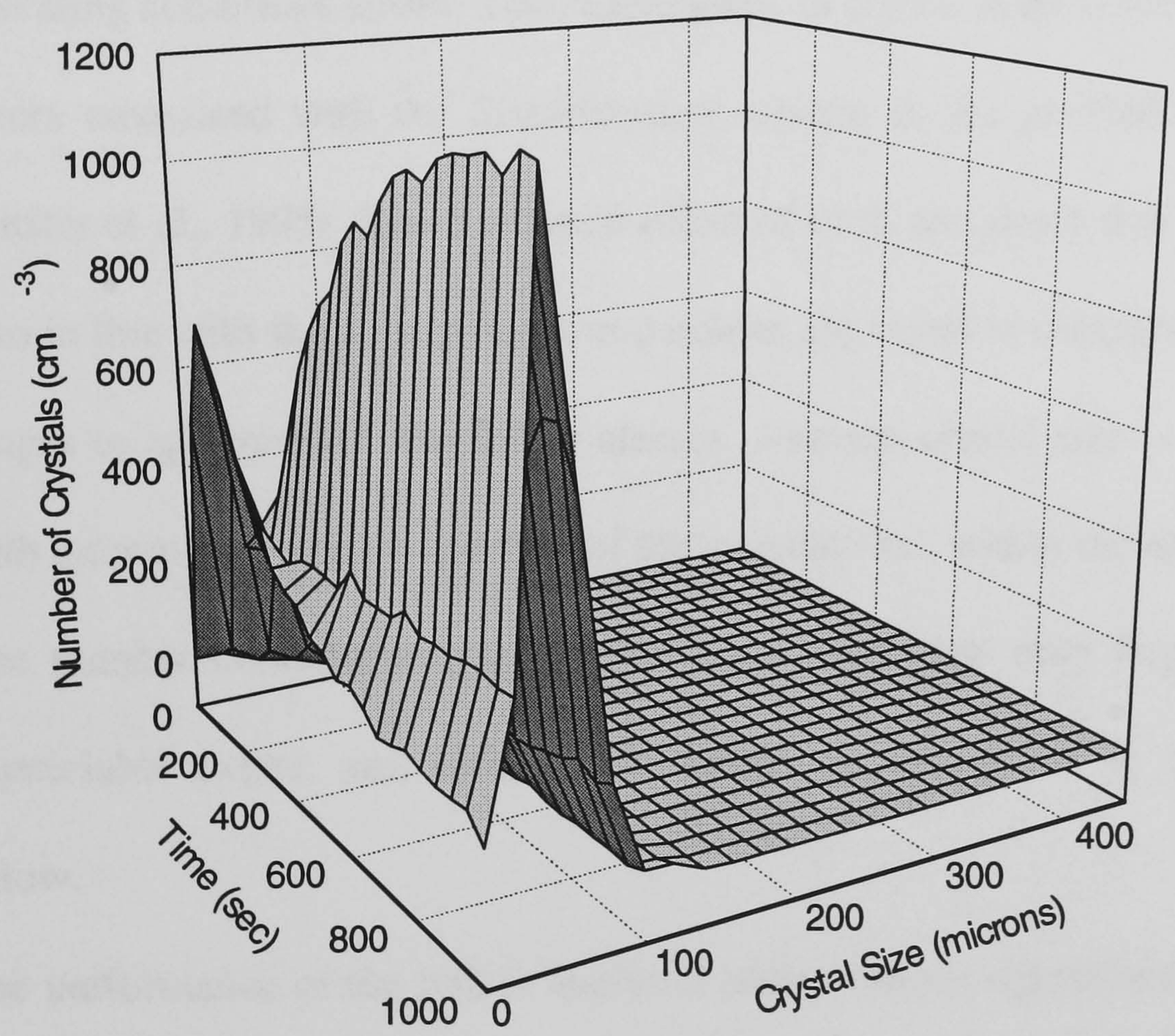

Figure 1 : Predicted development of KNO_3 CSD with time in an MSMPR

Primary nucleation exhibits a steep increase followed by a rapid decline, whereas secondary nucleation which is a function of both the supersaturation and third moment shows a steady increase to its final level. It is found that a slight decrease in

temperature results in a run away nucleation (primary) once the labile zone is penetrated for systems such as KNO_3. The effects of agitation on secondary nucleation are also observed to be consistent with the expected behaviour. The crystal mass calculated through (Eq. 3.6) by employing the moments of discretized population balance for nucleation and growth is not found to match precisely with the mass obtained from the analytical solution to the simple population balance given below.

$$M_T = 6\, k_v\, \rho_{cr}\; B\, \tau\, (G\tau)^3$$

The mass is over predicted in the range of ~3.5 - 7.5% during the limited number of operating conditions tested. This discrepancy in crystal mass could be attributed to the errors associated with the discretization scheme in the prediction of third moment (Litster et al., 1995). The combined effect of birth and death due to agglomeration is also in line with the anticipations as particles are found to disappear from smaller size ranges to agglomerate into larger classes. Average crystal size is noticed to increase with increments in the magnitude of the constant 'ka', within the agglomeration kernel. The number contributions due to breakage show that only large crystals break to appreciable extent, and most of the bigger fragments fall in classes immediately below.

The performance of the unit is analysed under various operational schemes, *viz.* high levels of supersaturation followed by reduced levels, and pronounced agglomeration and breakage. The effects of crystals in the feed are also studied. The model and the integrator perform satisfactorily under most conditions except when the crystallizer is continually operated at very low supersaturation levels without agglomeration (very few particles growing slowly) and when the system is started from heavy under-

saturation at same heat transfer rate. In the former, the response of Eq. (3.3) becomes oscillatory in early size intervals while for the latter the simulations do not progress. In conclusion, dynamic model for an MSMPR comprising thirty size classes has been successfully implemented in SPEEDUP^{TM} for its simulation within process flowsheets to predict most phenomena of interest with sufficient detail and accuracy. Further details of typical simulations and the model itself (comprising 276 equations) can be found in Sheikh and Jones (1996).

3.3 Mathematical representation of a hydrocyclone

Effective mathematical representation of the behaviour of a hydrocyclone requires adequate analysis of three distinct physical phenomena taking place in these devices, *viz*. the understanding of fluid flow, its interactions with the dispersed solid phase and the quantification of shear induced attrition of crystals. Details of the approach used to represent these phenomenon to extract particle separation efficiency curve are presented in the following section.

3.3.1 Features of the Model:

Empirical models for hydrocyclones, which by far out number the few fluid flow modelling attempts, suffer from the inherent deficiency that the model can only be used within the extremes of the experimental data from which the model parameters are determined. Therefore, mathematical models based on fluid mechanics which inevitably result in the application of the Navier Stokes equation are of great benefit if simple functional forms of quantities such as the velocity components could be obtained.

In this work, an analytical solution to the conservation of mass and momentum equations derived by Bloor and Ingham (1987) is used for the description of fluid flow. The simplified analytical solution requires specification of the angular momentum at the level in the cyclone where flow may be regarded as axially symmetric. It is also assumed that there is no azimuthal component of vorticity due to variations in the total head generated at the entry, *i.e.* the form of velocity components at the end of the transition from three dimensional to axially symmetric flow are prescribed. Comparison of Bloor and Ingham (1987) analysis with experimental findings show that the secondary motions produced from these entry conditions are of sufficient strength and do generate the commonly observed levels of vorticity inside the vessel.

The next step in the modelling work is to determine the trajectories of solid particles within the hydrocyclone, which in turn lead to the calculation of the separation efficiency curve. The liquid phase velocities and particle motion are interdependent because the liquid phase velocities are strongly related to local density and viscosity. For dilute systems where these effects are not profound, the computation of particle velocities can be performed independently by determining the lag between the particle and fluid flow which depends on particle size (Hsieh and Rajamani, 1991). The two significant latitudinal forces, *viz.* centrifugal and radial drag forces, operating on the particle in the interior of a cyclone are balanced to calculate the slip velocities in axial and radial direction. Radial drag force is dependent on Reynolds number and therefore takes different functional forms under different Reynolds number regimes. In the azimuthal direction there are no significant forces acting on the particle, and so in this direction the particle is considered to move along with the fluid. The separation curve

is then calculated using the equations due to Dietz (1981). These equations require calculation of azimuthal and radial velocities for the particles along the locus of zero vertical velocities and at the wall. The flowrates in the outlet streams are calculated from fluid flow description. The population balance is solved for particle attrition induced by high swirl velocities in the vessel.

3.3.2 Theory:

The equation of conservation of mass for an incompressible fluid in spherical polar co-ordinates system is given by (Bloor and Ingham, 1987)

$$\frac{\partial}{\partial r}\left(r^2 \sin\theta\, q_r\right)+\frac{\partial}{\partial \theta}\left(r \sin\theta\, q_\theta\right)=0 \qquad (3.13)$$

All the derivatives with respect to λ are zero because axially symmetric flow is assumed at the inlet. For steady flow momentum equation is written in vector form as

$$grad\left(\frac{p}{\rho}+\frac{1}{2}q^2\right)-\mathbf{q}\times\mathbf{w}=0 \qquad (3.14)$$

where $\mathbf{q} = (q_r, q_\theta, q_\lambda)$, $\mathbf{w} = (w_r, w_\theta, w_\lambda)$. The resulting equations (Bloor and Ingham, 1987) for dimensionless velocities in tangential, axial and radial directions respectively are

$$\frac{q_\lambda}{V}=\frac{\left[1-Q^2\sigma\psi/\left(\pi R_0 V\right)^2\right]^{\frac{1}{2}}}{r\sin\theta} \qquad (3.15)$$

The second term in the bracket provides the modifications to the free-vortex motion for secondary flow

$$q_r=2A\cos\theta-2\sigma\left[\cos\theta\, ln\left(\frac{1}{2}\tan\theta\right)\right] \qquad (3.16)$$

$$q_\theta = \frac{2\psi}{\sin 2\theta} \tag{3.17}$$

The velocity components are non-dimensionalized using $Q / 2 \pi R_0^2$ as the appropriate scale. Last two equations are transformed into cylindrical co-ordinates by

$$u = q_r \sin\theta - q_\theta \cos\theta \tag{3.18}$$

$$w = q_r \cos\theta + q_\theta \sin\theta \tag{3.19}$$

Particle velocities in radial direction are calculated from the following equations (Brayshaw, 1990).

$$\frac{\pi d_i^3}{6}(\rho_s - \rho_f)\frac{v_\lambda^2}{r_L} = 3\pi\mu_f d_i U \qquad Re_p \le 0.1 \tag{3.20}$$

$$\frac{\pi d_i^3}{6}(\rho_s - \rho_f)\frac{v_\lambda^2}{r_L} = 3\pi\mu_f d_i U\left(1+\frac{3}{16}\mathrm{Re}_p\right) \qquad 0.1 < Re_p \le 1.0 \tag{3.21}$$

$$\frac{\pi d_i^3}{6}(\rho_s - \rho_f)\frac{v_\lambda^2}{r_L} = 3\pi\mu_f d_i U\left(1+\frac{3}{16}\mathrm{Re}_p\right)^{0.5} \qquad 1.0 < Re_p \le 100 \tag{3.22}$$

The efficiency of the hydrocyclone is given by (Dietz, 1981)

$$\eta = 1 - \left[K_0 - \left\{K_1^2 + K_2\right\}^{\frac{1}{2}}\right]\exp\left[\frac{-2\pi R_C U_{pw}\left(s - a/2\right)}{Q}\right] \tag{3.23}$$

where

$$K_0 = \frac{R_C U_{pw} + R_V U_{ro} + R_V U_{pv}}{2 R_V U_{pv}}$$

$$K_1 = \frac{R_V U_{pv} - R_V U_{ro} - R_C U_{pw}}{2 R_V U_{pv}}$$

$$K_2 = \frac{R_C U_{pw}}{R_V U_{pv}}$$

Location of the locus of zero vertical velocities is found by solving the following equation obtained by setting stream function equal to one (Bloor and Ingham, 1987).

$$1=\sigma r^2\left\{A\sin^2\theta-\sin^2\theta\ln\left(\frac{1}{2}\tan\theta\right)+\cos\theta-1\right\} \tag{3.24}$$

$$\sigma=-\frac{\pi r_o^2 V^2}{QW}$$

$$A=\sigma\left\{\left[\operatorname{cosec}^2\theta-\ln\left(\frac{1}{2}\tan\alpha\right)-\operatorname{cosec}\alpha\cot\alpha\right]\sin^2\theta-\sin^2\theta\ln\left(\frac{1}{2}\tan\alpha\right)+\cos\theta-1\right\}$$

where θ is usually 0.2 α, α being the cone angle.

3.3.3 Model features

The model provides an adequate representation of the fluid movement inside a hydrocyclone for dilute particulate suspensions. It is used to find the location of the locus of zero vertical velocities by solving the appropriate equation for stream function and then point velocities for the fluid and crystals of different sizes are calculated on it and the wall. These velocities are used in the expression due to Dietz (1981) for calculating separation efficiency curve. The fluid flow description is also used to determine the two exit flowrates.

The representation of flow at the entry, which is expected to have a profound effect on the nature of flow, is effectively modelled by the assumption of pre-specified angular momentum at the onset of axially symmetric flow. The model is, however, not valid for high slurry concentrations, because liquid and particulate phase calculations in such cases cannot be carried out independently and an iterative solution where liquid and particle velocities are initially guessed to calculate changes in local density and viscosity to recalculate velocities is essential.

Since, the separation efficiency is represented by flow characteristics and dimensions of the vessel, it does provide a design and simulation tool with physically realisable control on hydrocyclone behaviour for desired performance. In table 1, the effects of

different design parameters on the stream properties of interest within the context of crystallization systems are listed.

W ($m\ sec^{-1}$)	Cone angle (rad)	Vortex angle (rad)	Spigot dia. (m)	Av. sz. feed (μm)	Av. sz. Over (μm)	Av. sz. Under (μm)	No. Over (cm^{-3})	No. Under (cm^{-3})	Flow Over ($l\ s^{-1}$)	Flow Under ($l\ s^{-1}$)
0.0100	0.1974	0.04118	0.0075	53.7	24.20	121.41	1510	836	0.186	0.064
0.0125	0.1974	0.04118	0.0075	53.7	22.13	117.92	1447	899	0.186	0.064
0.0157	0.1974	0.04118	0.0075	53.7	20.35	114.28	1384	962	0.186	0.064
0.0125	0.1800	0.04118	0.0075	53.7	24.15	120.20	1502	858	0.200	0.050
0.0125	0.2400	0.04118	0.0075	53.7	18.46	112.36	1331	988	0.140	0.110
0.0125	0.1974	0.03118	0.0075	53.7	17.43	107.66	1269	1077	0.156	0.094
0.0125	0.1974	0.05118	0.0075	53.7	26.89	126.18	1591	755	0.202	0.048
0.0125	0.1974	0.04118	0.0050	53.7	22.16	117.89	1447	899	0.221	0.029
0.0125	0.1974	0.04118	0.0100	53.7	22.12	117.95	1447	899	0.136	0.114

TABLE 1: Simulation results for hydrocyclone performance under different operations

It can be seen from the above table that all the design variables considered affect the performance through either changes in average sizes for the two outlet streams or their flowrates. Within the variations allowed, the total number of crystals reporting to either the underflow or overflow is found to be related to the average size. An increase in number for overflow always meant increase in average size, while the reverse was true for the underflow. The axial velocity into the vessel W, only affects the average sizes, while the cone and vortex finder angle change both the average size and flowrates. Increase in the cone angle drastically increases the flowrate in underflow, while an increase in vortex finder angle decreases it. This opposite correlation is also observable for the average sizes. In contrast with W, the spigot diameter only affects the flowrates while leaving the average sizes essentially unchanged. This finding is in line with the qualitative observations reported by Svarovsky (1981). (The location of

vortex finder is quantified in angles because the fluid flow uses spherical polar co-ordinates).

A check on the functional form of the relationship between the cut size and hydrocyclone diameter obtained from this model indicated that the former is proportional to the latter raised to the power of 1.5. This compares well with the form reported in the literature (Svarovsky, 1981; Bradley, 1965). The model could only be tested over a small window, mainly because diameter affected most design parameters and it was therefore difficult to isolate its impact from that of the other parameters.

3.4 Fines dissolution simulations

A virtual fines dissolver is modelled for CSTR type behaviour. An increase in temperature generates under-saturation thereby dissolving particles below a certain minimum size to extinction. The extent of under-saturation is crucial, because high values could result in a significant decrease in the size of larger particles. The dissolution rate is modelled by equations similar to growth rate law (where a first order dependence on driving force is assumed), but the diffusion coefficient-efficient in this case is calculated as a function of individual size of the particle and not the average size. A modified form of Eq. 3.3 is used to account for the change in the number of particles in a particular size range due to the decreasing size.

3.5 Conclusions

A sufficiently complex and consistent mathematical framework based on discretized population balance has been developed for an MSMPR crystallizer and hydrocyclone. These models have been tested through dynamic simulations and along with the fines dissolver will be used later for optimisation of flowsheets.

Chapter 4:

OPTIMAL SYNTHESIS OF STAGE-WISE CRYSTALLISATION

The performance of a cascaded crystallizer design is subject to operating temperature, feed concentration, crystal carry over from previous stages, volume and throughput for each crystallizer in the network. These variables have to be optimally determined through population balance models to ensure that common advantages of cascade configuration such as increased yield and improved coefficient of variance, are not markedly off-set by undesirable attributes including reduced average crystal sizes. Despite recent advances in crystallisation process modelling and the upsurge in new strategies for chemical reactor network synthesis, no prior work has been reported on crystallizer network synthesis exploiting modern synthesis strategies.

Reactor targeting methodology due to Balakrishna and Biegler (1992a) is based on mixing between different reacting environments. It proceeds by determining the maximum possible performance through reaction and mixing without explicitly specifying the network structure. A network capable of achieving this target is then devised by extending the concept of attainable regions, using simple optimisation formulations. Though the simple formulations do not allow for parallel reactor structures, they have been coupled with energy integration and separation sequences with relative ease (Balakrishna and Biegler, 1996) to provide a comprehensive framework for integrated design. An extensive review of reactor network synthesis strategies can be found in Hildbrandt and Biegler (1995).

In this work, an optimisation problem based on the targeting approach will be developed for the synthesis of stage-wise crystallisation processes. The constructive nature of the targeting methodology results in the sequential solution of small non-linear programs that is well-suited for developing models comprising mass balances, population balances and highly non-linear expressions for nucleation and growth

rates. First the basic problem formulation for chemical reactor networks due to Balakrishna and Biegler (1992a) will be reviewed. This will be followed by the derivation of the optimisation problem for a crystallisation system and its mathematical transformation into a solvable form. In the next section, a rigorous model based on the analytical solution to population balance will be presented for thorough analysis of the optimal solution. Finally, results will be presented and the conclusions drawn.

4.1 Targeting models for chemical reactors

The segregated flow (SF) reactor model works at the heart of targeting approach because it is often sufficient to establish performance bounds for isothermal processes, particularly when the concentration of product species is a concave function of reactant concentration (Glasser et al., 1987). In SF models (representing both plug flow reactors (PFR) and PFR with bypasses), only molecules of the same age are well mixed while mixing between molecules of different ages take place at the exit. Even when the concavity condition is not satisfied, *i.e.* it is possible to extend performance beyond the levels predicted by the SF solution, these models can be used in conjunction with small non-linear programs for recycle reactor extensions to improve the objective function.

The extension of SF model to non-isothermal systems, however, requires re-definition of the entire reactor model because the SF structure assumes negligible costs of mixing. In non-isothermal case this translates as zero cost of maintaining the temperature profile. For such processes, Balakrishna and Biegler (1992b) developed a cross flow reactor (CFR) model that is not only capable of allowing temperature manipulations through feed mixing and external heating or cooling but, for some

systems, also precludes the need to check for reactor extensions. The model results in a dynamic optimisation problem where temperature, feed distribution and exit flow distribution functions are the control profiles. The concavity conditions are applicable if the temperature profile can be related to the concentration profile (e.g. adiabatic reactors). More general non-isothermal reactors with arbitrary temperature profiles, however, require a sequential procedure where recycle reactor extensions are checked after solving the CFR model. In such situations the CFR model only provides the lower bound on the objective function while improvements on it through optimally designed recycle reactor extensions constructively generate the components of the complete network.

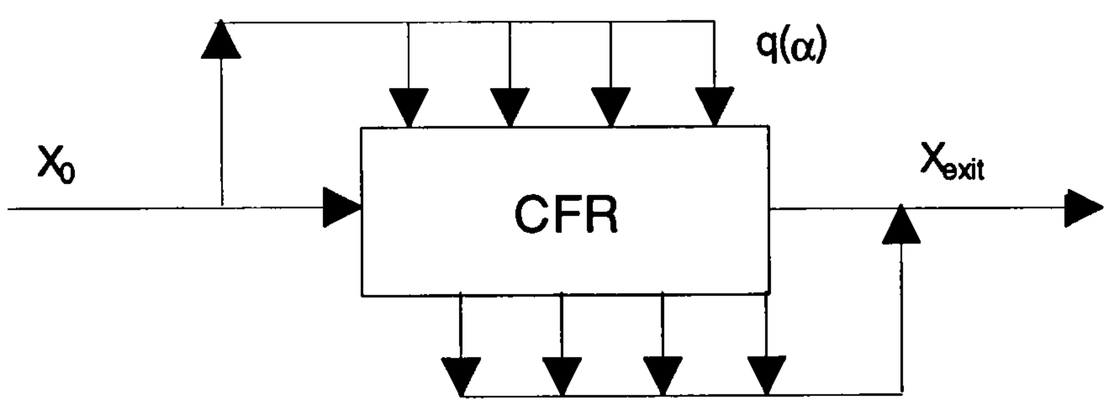

FIGURE 2 : Cross flow reactor Model (Balakrishna and Biegler, 1992b)

Figure 2 shows the schematic of a CFR as devised by Balakrishna and Biegler (1992b). X_0 is dimensionless concentration entering the reactor network and α is an independent variable representing time as the process progresses along the network. $T(\alpha)$, $f(\alpha)$, $q(\alpha)$ and $Q(\alpha)$ are the temperature, fraction of molecules leaving the network, fraction of feed and flow rate entering at α respectively. At one extreme, when $q(\alpha)$ is zero for a general value of $f(\alpha)$, the model reduces to a completely segregated flow system while a maximum mixed model is obtained for a general non-zero $q(\alpha)$ with $f(\alpha)$ as a dirac delta function at exactly one point. An optimisation

problem with T(α), f(α) and q(α) as control profiles can be formulated for maximising the performance index *J* of a CFR model as shown below,

$$\max_{q(\alpha), f(\alpha), T(\alpha)} \quad J\left(X_{exit}, \tau\right)$$

$$\frac{d\,X}{d\,t} = R\left(T(\alpha), X\right) + \frac{q(\alpha)Q_0}{Q(\alpha)}\left(X_0 - X(\alpha)\right) \tag{4.1}$$

$$X(0) = X_0 \tag{4.2}$$

$$X_{exit} = \int_0^{\infty} f(\alpha)\, X(\alpha)\, d\alpha \tag{4.3}$$

$$\int_0^{\infty}\int_0^{\alpha}\left(q(\alpha') - f(\alpha')\right) d\alpha'\, d\alpha = \tau \tag{4.4}$$

$$\int_0^{\infty} f(\alpha)\, d\alpha = 1.0 \tag{4.5}$$

$$\int_0^{\infty} q(\alpha)\, d\alpha = 1.0 \tag{4.6}$$

$$Q(\alpha)/Q_0 = \int_0^{\alpha}\left(q(\alpha') - f(\alpha')\right) d\alpha' \tag{4.7}$$

The first equation is a differential mass balance, whereas equations 4.4 and 4.7 define mean residence time and flow rate respectively. Improvements in the objective function can be sought by solving the following problems for recycle reactor extensions should the concavity condition not be satisfied. The control variables include $\lambda(\alpha')$ the convex combiner from the CFR, $f_r(\alpha)$ the linear combiner of concentration from the plug flow section of recycle reactor, T_{rr} the temperature profile in recycle reactor and Re the recycle ratio.

$$\max_{Re, \lambda, f_p, T_{rr}, f_r} \quad J\left(X_{exit}, \tau_R\right)$$

$$\frac{d\,X_{rr}}{d\,t} = R\left(T_{rr}, X_{rr}\right) \tag{4.8}$$

$$X_{rr} = \frac{Re\,X_{exit} + X_{CFR}}{Re+1} \tag{4.9}$$

$$X_{exit} = \int_0^{\infty} f_r(\alpha)\, X_{rr}(\alpha)\, d\alpha \tag{4.10}$$

$$\int_0^{\infty} f_r(\alpha)\, d\alpha = 1.0 \tag{4.11}$$

$$\int_0^{\infty} \lambda(\alpha')\, d\alpha' = 1.0 \tag{4.12}$$

$$\tau_R < \tau_{max}$$

The next iteration consists of checking for further extensions through solution of the following problem at the p^{th} iteration.

$$\max_{Re,\lambda,f_p,T_{rr},f_r} \quad J^{P+1}$$

$$\frac{d\,X}{d\,t} = R\left(T_{rr}, X_{rr}\right) \tag{4.13}$$

$$X_{rr} = \frac{Re\,X_{exit} + X_{feed}}{Re+1} \tag{4.14}$$

$$X_{exit} = \int_0^{\infty} f_r(\alpha)\, X_{rr}(\alpha)\, d\alpha \tag{4.15}$$

$$X_{feed} = \int_0^{\infty} \lambda(\alpha)\, X_{CFR}(\alpha)\, d\alpha + \sum_1^{p} f_p\ X_p \tag{4.16}$$

$$\int_0^{\infty} \lambda(\alpha')\, d\alpha' + \int_0^{p} f_p\, dP = 1.0 \tag{4.17}$$

In the above, X_{feed} is obtained through a convex combination of concentrations at the exit of p^{th} recycle reactor and the CFR. The procedure is repeated until no improvements in the objective function are observed (see fig. 3).

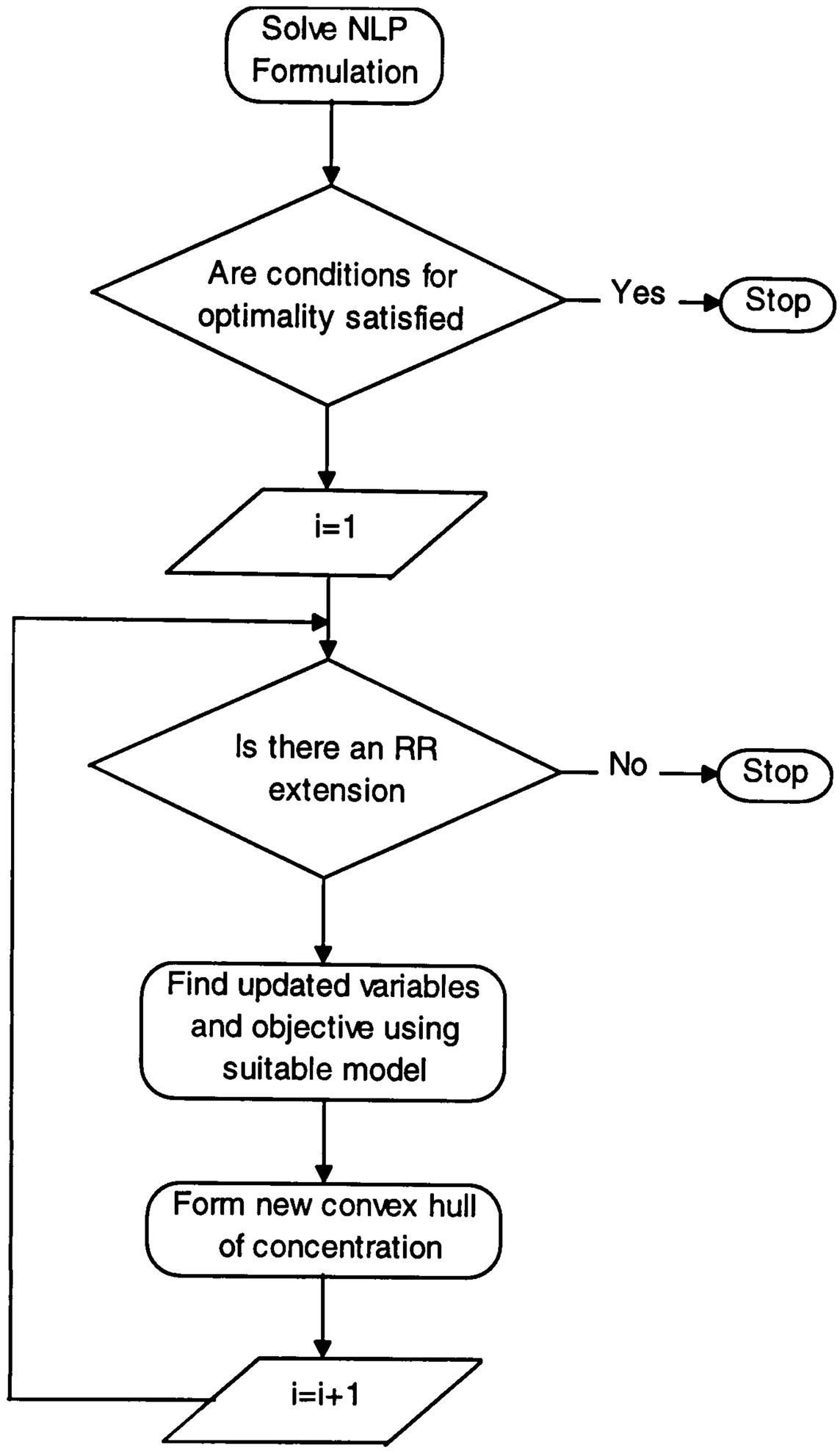

FIGURE 3 : Constructive procedure for a reactor network synthesis using targeting procedure (Balakrishna and Biegler, 1996)

4.2 Problem formulation for a crystallizer network

There are many processes in industrial practice which yield particulate products, for instance crystallisation, comminution and emulsification. Their products are distinguished by distributions of the state characteristics of the system which are not only function of time and space but also some properties of states themselves known as internal variables. Internal variables could include size and shape if particles are

formed or diameter for liquid droplets. The mathematical description encompassing internal co-ordinate inevitably results in an integro-partial differential equation called the population balance which has to be solved along with mass and energy balances to describe such processes. In most situations of engineering interest, for instance design and control, a knowledge of the complete crystal size distribution is unnecessary, rather some average or total quantities with regards to internal variable such as average size and coefficient of variance are sufficient. Moment transformation is frequently used for this purpose to obtain a lower dimension formulation of the population balance by converting it into a set of ordinary differential equations with the first four related to total number, length, area, and volume of crystals respectively. The other major difference between crystallisation and common chemical reactions is that in the former two kinetic processes occur simultaneously, *viz.* nucleation of crystals and their subsequent growth.

4.2.1 Model development for the boundary value problem

The optimal control problem analogous to the CFR model can be developed for crystallizers in a dimensionless form using moment transformation as follows

$$\max_{q(\alpha),\, f(\alpha),\, T(\alpha)} \quad J\left(X_{exit}, \tau, L_{av}\right)$$

$$\frac{dX}{dt} = -3\frac{k_v}{k_a}\,\overline{A}\,G + \frac{q(\alpha)Q_0}{Q(\alpha)}\left(X_0 - X(\alpha)\right) \tag{4.18}$$

$$\frac{dn}{dt} = \frac{q(\alpha)Q_0}{Q(\alpha)}B \tag{4.19}$$

$$\frac{dL}{dt} = nG \tag{4.20}$$

$$\frac{d\overline{A}}{dt} = 2k_a LG \tag{4.21}$$

$$L_{av} = \int_0^{\infty} f(\alpha)\, L(\alpha)\, d\alpha \Big/ \int_0^{\infty} f(\alpha)\, n(\alpha)\, d\alpha \tag{4.22}$$

$$B = A\, exp\left(-c \Big/ \left[ln\left(\frac{X}{X_{sat}(T)} \right) \right]^2 \right) \tag{4.23}$$

$$G = k_g \left(X - X_{sat}(T) \right) \tag{4.24}$$

$$X_{exit} = \int_0^{\infty} f(\alpha)\, X(\alpha)\, d\alpha \tag{4.25}$$

$$\int_0^{\infty} \int_0^{\alpha} \left(q(\alpha') - f(\alpha') \right) d\alpha'\, d\alpha = \tau \tag{4.26}$$

$$\int_0^{\infty} f(\alpha)\, d\alpha = 1.0 \tag{4.27}$$

$$\int_0^{\infty} q(\alpha)\, d\alpha = 1.0 \tag{4.28}$$

$$Q(\alpha) \Big/ Q_0 = \int_0^{\alpha} \left(q(\alpha') - f(\alpha') \right) d\alpha' \tag{4.29}$$

The first four equations define differential solute mass and crystal moment balances, while equations 4.23 and 4.24 couple them through kinetic expressions. The optimal solution to this boundary value problem provides a lower bound on performance by simultaneously considering all the relevant properties of CSD along with the yield.

4.2.2 Model transformations using orthogonal collocation

Common adjoint techniques can be used to solve the above DAE optimisation problem. Orthogonal collocation on finite elements has, however, emerged as the preferred discretisation technique (Cuthrell and Biegler, 1987) for it leads to solutions that are easier to interpret physically. Furthermore, the integrals within the problem are automatically evaluated at Gaussian quadrature points. These features, along with

the fact that state constraints can be imposed directly are very important within the context of the synthesis problem for they allow use of CSTR type rate equations in the differential mass balance (Cuthrell and Biegler, 1987). These properties are even more significant to the crystallisation model because integrated forms (continuous MSMPR type equations) of the differential moment balances (Eq. 4.19 - 4.21) can be used within the collocation points to calculate the rate of solute loss.

Figure 4 shows the equivalent discretised CFR environment, where state equations are optimally solved at collocation points within the finite elements.

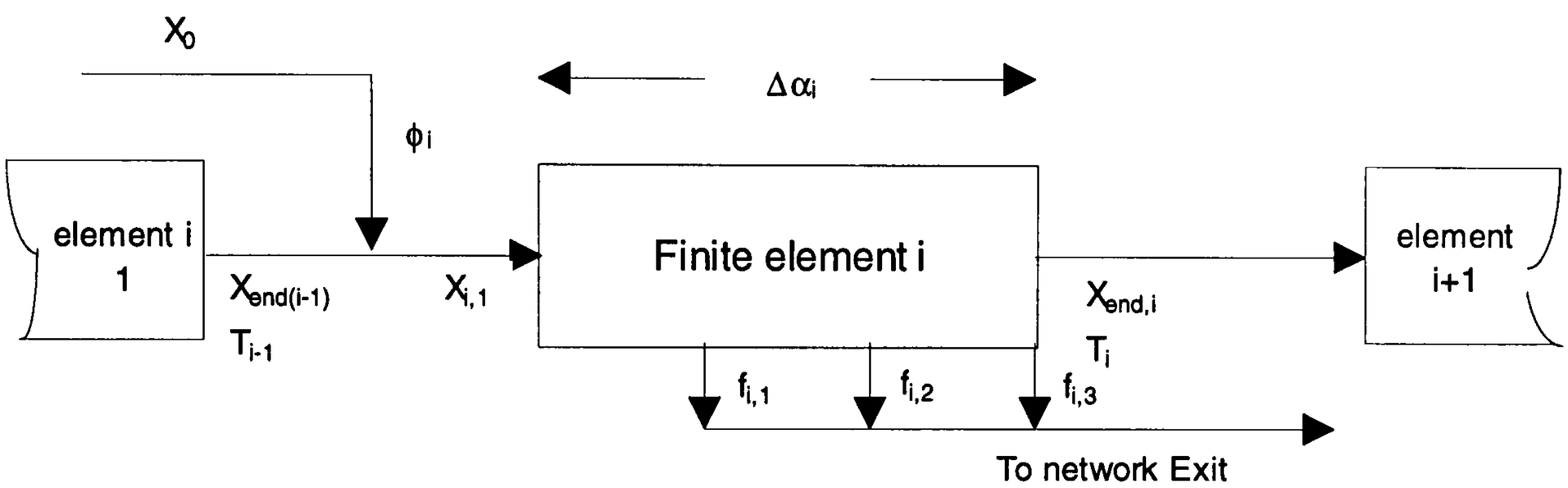

FIGURE 4 : Discretized CFR model for non-isothermal synthesis

The following simplified non-linear program can be developed to find optimal performance by orthogonal collocation on finite elements with Lagrange interpolation functions

$$\max_{q_i, f_{ij}, T_i} \quad J\left(X_{exit}, \tau, L_{av}\right)$$

$$\sum_k X_{ik}\, \mathbf{L}'_{\mathbf{k}}\left(\alpha_{ij}\right) - R\left(X_{ij}, T_i\right)\Delta\alpha_{ij} = 0 \tag{4.30}$$

$$n_{ij} = B_{ij}\left(\alpha_{ij} - \alpha_{ij-1}\right) Q_{ij} + \left(\left(1 - \left(\frac{f_{ij-1}}{Q_{ij-1}}\right)\right) \times n_{ij-1}\right) \tag{4.31}$$

$$L_{ij} = n_{ij}\; G_{ij}\; \tau_{ij} + \left(\left(1 - \left(\frac{f_{ij-1}}{Q_{ij-1}}\right)\right) \times L_{ij-1}\right) \tag{4.32}$$

$$A_{ij} = L_{ij}\ G_{ij}\ \tau_{ij} + \left(\left(1 - \left(\frac{f_{ij-1}}{Q_{ij-1}}\right)\right) \times A_{ij-1}\right) \tag{4.33}$$

$$R\left(X_{ij}, T_i\right) = A_{ij}\ G_{ij}\ \tau_{ij} \tag{4.34}$$

$$L_{av} = \frac{\sum_i \sum_j L_{ij}\ f_{ij}}{\sum_i \sum_j n_{ij}\ f_{ij}} \tag{4.35}$$

$$B_{ij} = A\, exp\left(-c \Big/ \left[ln\left(\frac{X_{ij}}{X_{sat}(T_i)}\right)\right]^2\right) \tag{4.36}$$

$$G_{ij} = k_g \left(X_{ij} - X_{sat}(T_i)\right) \tag{4.37}$$

$$X(0) = X_0 \tag{4.38}$$

$$X_{i,0} = \phi_i\ X_0 + \left(1 - \phi_i\right) X_{i-1,end} \tag{4.39}$$

$$X_{i,end} = \sum_k X_{ik}\ \mathbf{L_k}\left(\alpha_{i+1,0}\right) \tag{4.40}$$

$$X_{exit} = \sum_i \sum_j X_{ij}\ f_{ij} \tag{4.41}$$

$$n_{exit} = \sum_i \sum_j n_{ij}\ f_{ij} \tag{4.42}$$

$$\tau = \sum_i \sum_j \alpha_{ij} \left(q_i - f_{ij}\right) \tag{4.43}$$

$$Q_{ij} = \sum_i \sum_j \left(q_i - f_{ij}\right) \tag{4.44}$$

$$\phi_i = Q_{i,0} \Big/ Q_{ij} \tag{4.45}$$

$$\sum_i q_i = 1.0 \tag{4.46}$$

$$\sum_i \sum_j f_{ij} = 1.0 \tag{4.47}$$

The discretised differential solute balance at the j^{th} collocation point in the i^{th} finite element is represented by equation 4.30. Equations 4.31-4.33, the constituents of the rate of solute removal due to crystallization (Eq. 4.34) are dimensionless analogues of

zeroth, first and second moments of CSD in their integrated forms. The second terms in these equations manifest the effects of crystal carry over from the previous intervals. The balance between feed and crystallising streams is represented by equation 4.39 while 4.46 and 4.47 are the discretised forms of 4.27 and 4.28 obtained through Gaussian quadrature. The values of state variable X, in an element are extrapolated to find its magnitudes at the end through equation 4.40.

The collocation points are optimally selected as roots of a Jacobi polynomial of an equivalent order that takes the following general form (Rice and Do, 1995)

$$J_N(x) = \sum_{i=0}^{N} (-1)^{N-i} \gamma_{N,i} x^i \tag{4.48}$$

where $\gamma_{N,i}$ is calculated from the following recurrence formula, starting with $\gamma_{N,0} = 1$.

$$\frac{\gamma_{N,i}}{\gamma_{N,i-1}} = \frac{N-i+1}{i} \times \frac{N+1}{i} \tag{4.49}$$

$\mathbf{L_k}(\alpha)$ is the Lagrange interpolation function while $\mathbf{L'_k}(\alpha)$ representing its derivative is a matrix of dimension k × k. These are determined from the following equations (Rice and Do, 1995),

$$\mathbf{L_k}(\alpha) = \prod_{\substack{j=1 \\ j \neq k}}^{N+1} \frac{(\alpha - \alpha_{jk})}{(\alpha_k - \alpha_j)} \tag{4.50}$$

$$\mathbf{L'_{k,j}} = \begin{cases} \dfrac{1}{2} \dfrac{p_N^{(2)}(\alpha_k)}{p_N^{(1)}(\alpha_k)} & j = k \\ \dfrac{1}{(x_k - x_j)} \dfrac{p_N^{(1)}(\alpha_k)}{p_N^{(1)}(\alpha_j)} & j \neq k \end{cases} \tag{4.51}$$

where $p^{(1)}{}_N$ and $p^{(2)}{}_N$ are calculated from the following recurring formula

$$p_o(\alpha) = 1, \qquad p_o^{(1)}(\alpha) = p_o^{(2)}(\alpha) = 0.0$$

$$p_j(\alpha) = (\alpha - \alpha_j)\, p_{j-1}(\alpha); \qquad j = 1,2,\ldots,N$$

$$p_j^{(1)}(\alpha) = (\alpha - \alpha_j)\, p_{j-1}^{(1)}(\alpha) + p_{j-1}(\alpha)$$

$$p_j^{(2)}(\alpha) = (\alpha - \alpha_j)\, p_{j-1}^{(2)}(\alpha) + 2p_{j-1}^{1}(\alpha)$$

This discretised model only solves the solute balance through interpolation functions because the ability to use the integrated form of moment balances between collocation points eliminates the need for a similar representation of differential moment balances. As a result the problem is greatly simplified, it would, however, require a large number of points for a satisfactory solution. These are not only needed for the validity of MSMPR type equations between the points but also for mathematical reasons stemming from highly non-linear discontinuous equations within the problem. Descending temperature profiles are often used in stage-wise crystallisation to compensate reductions in super-saturation levels (Nyvlt, 1992). This relationship between temperature and concentration satisfies the modified sufficiency condition to interpret CFR type solution as optimal for any concave objective function. The need to check for recycle extensions (see figure 3) is therefore eliminated. This is not to suggest, however, that the constructive approach should not be used to find more complex networks using arbitrary temperature profiles.

4.2.3 Implementation details and solution technique

General performance specifications for stage-wise systems do not exist, especially in terms of CSD parameters and therefore the objective functions for such problems often depend upon the end use envisaged for the product. In this work, a composite objective function comprising yield and average size is developed in such a way that the total number of crystals is penalised.

Twenty collocation points over five equi-sized finite elements (same $\Delta\alpha$) are used during discretization. The value of temperature drops from 291 to 288 K over these elements. Cooling crystallisation of potassium nitrate is selected for illustration due to its relatively well-established kinetics and moderate temperature dependence of solubility. The kinetic parameters are appropriately scaled to determine the coefficients for nucleation and growth rate expressions in the dimensionless problem. The problem is simplified by calculating nucleation rate (Eq. 4.36) from the entry-level concentration into the elements instead of its local point value. This will over-predict the number of crystals. With all the variables normalised and retention times very small, however, the effect on diminutive changes in dimensionless yield is not expected to be significant. A maximum of 0.6 is imposed on both q_i and f_{ij} to ensure a more even distribution of flow within the elements.

The non-linear program is solved using the sequential quadratic programming (SQP) algorithm because the dimension of the problem is relatively small ($n < 100$) and it comprises highly non-linear constraints appearing as discretised state equations. Furthermore, the convergence is quadratic and, unlike the reduced gradient method without restoration (MINOS), the method does not require linearisation of active constraints around the starting points.

4.3 Rigorous models for complete crystal size distribution

The simplified non-dimensional nature of the above optimisation problem necessitates the development of rigorous models for detailed analysis and comparison of its findings. The model reported below is based on the analytical solution to a simplified population balance that ignores effects of crystal agglomeration and disruption. It provides complete CSD in each crystallizer and does not suffer from errors in mass

balances, often observed in discretized solutions (Litster et al., 1995). The simple population balance representing number flow for the i^{th} stage takes the following general form (Hounslow and Wynn, 1992),

$$\frac{\partial n_i}{\partial L} = \frac{n_{i-1} - n_i}{G_i \ \tau_i}$$

$$\text{subject to } n_i(0) = {V_i \ B_i^0}/{G_i \ \tau_i} \qquad (4.52)$$

This steady-state form is amenable to analytical solution and the application of an integrating factor followed by subsequent integration yields

$$n_i(L) = exp\left(-{L}/{G_i \ \tau_i}\right)\left(\frac{V_i \ B_i^0}{G_i \ \tau_i} + \int_o^L \frac{n_{i-1}}{G_i \ \tau_i} exp\left({L}/{G_i \ \tau_i}\right) dL\right) \qquad (4.53)$$

Nucleation rate in the above equation has often been modelled by a power law equation with the rate constant being an exponential function of temperature. Experimental studies, however, have shown that nucleation rate drops with increasing temperature even when the resulting effects on saturation concentration have been accounted for. In this work, an Arrhenius reaction velocity type equation is therefore used

$$B = 1.8 \times 10^{16} \exp\left(\frac{-0.5}{(\ln(s))^2}\right) \qquad (4.54)$$

$$G = 2.27 \times 10^{-5} \ \left(X - X_{sat}(T)\right) \qquad (4.55)$$

Kinetic parameters in these equations are taken from Mullin (1993) with the coefficients based on rates expressed in $cm^{-3}\ s^{-1}$ and $cm\ s^{-1}$ respectively. Other details, including checks for numerical accuracy of the results can be found in the FORTRAN code used for simulations (see Appendix A(2)).

The optimal network will be simulated with five MSMPR crystallizers; each designed according to the specifications determined from the non-linear program for the five finite elements. Though adequate for illustration purposes, these simulations will be a simplified representation of the optimal solution because the latter employs MSMPR type approximations for crystallization rate between collocation points and not over the elements.

4.4 The optimal configuration and its analysis:

The results from the optimisation program and its detailed simulation are presented in the following sections. Comparisons with other possible configurations are used to analyse the findings.

4.4.1 The non-linear program:

The solution to the NLP representing crystallizer synthesis model determined an optimum configuration with dimensionless yield, average crystals size and CV of 0.3749×10^{-3}, 0.1157×10^{-3} and 0.6654 respectively. This solution represents the best compromise between two extremes in design, *viz*. MSMPR and simple cascade. The former provides largest average sizes and coefficient of variance at a reduced yield, while the reverse is true for simple cascade (Larson and Wolff, 1971). Flow distribution of each finite element within the optimal network is depicted in figure 5 while the temperature profile across it is shown in figure 6. Since no experimental or simulated data are available, three other design configurations with similar characteristics (designs involving flow distribution) were developed to compare and analyse the performance of the optimal network. The cases include,

a) descending temperature profile and same flow distribution for all the finite elements (q_i and f_i equal to 0.2 throughout)

b) constant temperature and optimal flow distribution as determined by the NLP

c) constant temperature and same flow distribution.

Table 2 depicts predictions for the three criterion variables from different schemes. It can be seen that it is possible to improve CV by operating at constant temperature (cases b and c). Average size can also be increased when optimal flow distribution is used in conjunction with constant temperature profile (case b). These improvements could be due to the shift of reduced super-saturation towards crystal growth. None of the schemes, however, succeed in improving the yield beyond the levels obtained from optimal solution. The latter out-performs case (a) which only differs from it in flow distribution in all three criterion.

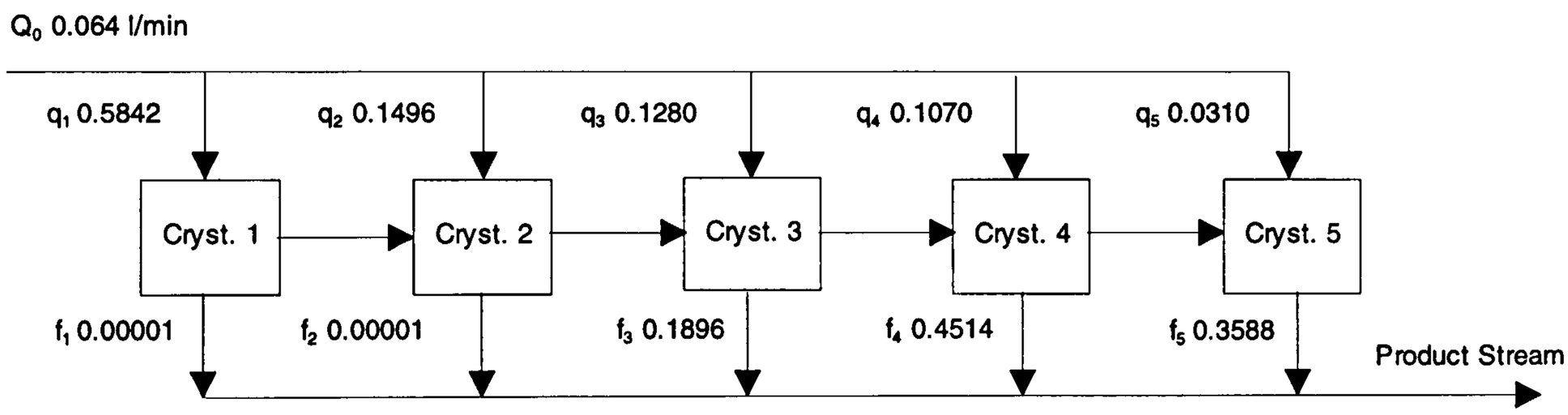

FIGURE 5 : Optimal flow profiles for KNO_3 crystallisation process

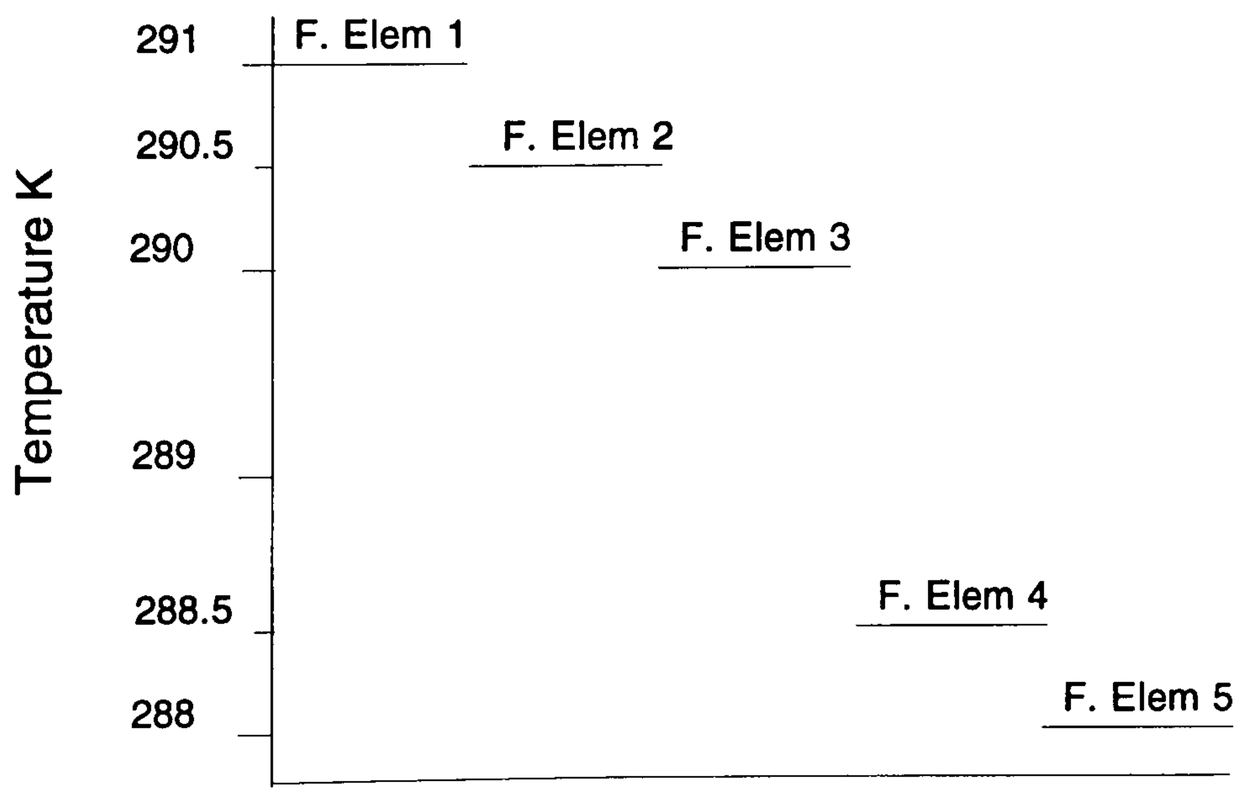

FIGURE 6 : Temperature profile within the network

Case	Yield (dimensionless)	Average crystal size (dimensionless)	Coefficient of variance
Optimal Solution	0.3749×10^{-3}	0.1157×10^{-3}	0.6654
a	0.2508×10^{-4}	0.6468×10^{-4}	0.7375
b	0.7676×10^{-5}	0.2267×10^{-3}	0.6382
c	0.3666×10^{-6}	0.9328×10^{-4}	0.6121

TABLE 2 : Case studies results for yield, average size and CV

4.4.2 Detailed simulations of the network

In this section, results from detailed simulations of the optimal network comprising five MSMPR type crystallizers are reported. The findings are compared with equivalent MSMPR crystallizers and a simple cascade. Finally the performance of the optimal network is quantified at very high levels of super-saturation.

Each crystallizer has a volume of 9.07 m^3, while the feed concentration is 3.52 kmol m^{-3} and the same temperature profile as in the NLP is used. The total flows (fresh feed plus stream from the preceding crystallizer as determined from the NLP) to each vessel are 0.13668, 0.17168, 0.20163, 0.1826 and 0.0889 m^3 sec^{-1} respectively. It is worth noting that these optimally determined flowrates, if transformed into variable vessel volumes, would show that the volume of individual crystallizers increases down the network. This observation is in line with the general findings of chemical reactor engineering which suggest a similar configuration for higher order reactions (Levenspiel, 1972). A check on the levels of super-saturation indicate that they drop along the network to such extents that nucleation is only significant in the first vessel, following which crystal growth pre-dominates. Consequently, the number of crystals do not increase while the growth rate steadily drops. Figure 7 shows predicted CSD in the crystallizers and the product stream. The shape of product CSD shows all the

attributes of a system where not all the small crystals stay in the reacting environment for the same average retention time (Randolph and Larson, 1988). The fact that nucleation virtually ceases after the first stage can also be observed from figure 7. In figure 8, normalised CSD for the five vessels are plotted to qualitatively present the effect of staging. It can be seen that as the system progresses down the network, the peaks in CSD shift to the right and the symmetry of the distribution deteriorates. The markedly reduced heights of curves 4 and 5 reflect significant reductions in the number of crystals within the system due to intermediate product removal. It can also be inferred that the average size of the product stream lies between the sizes from crystallizers 4 and 5.

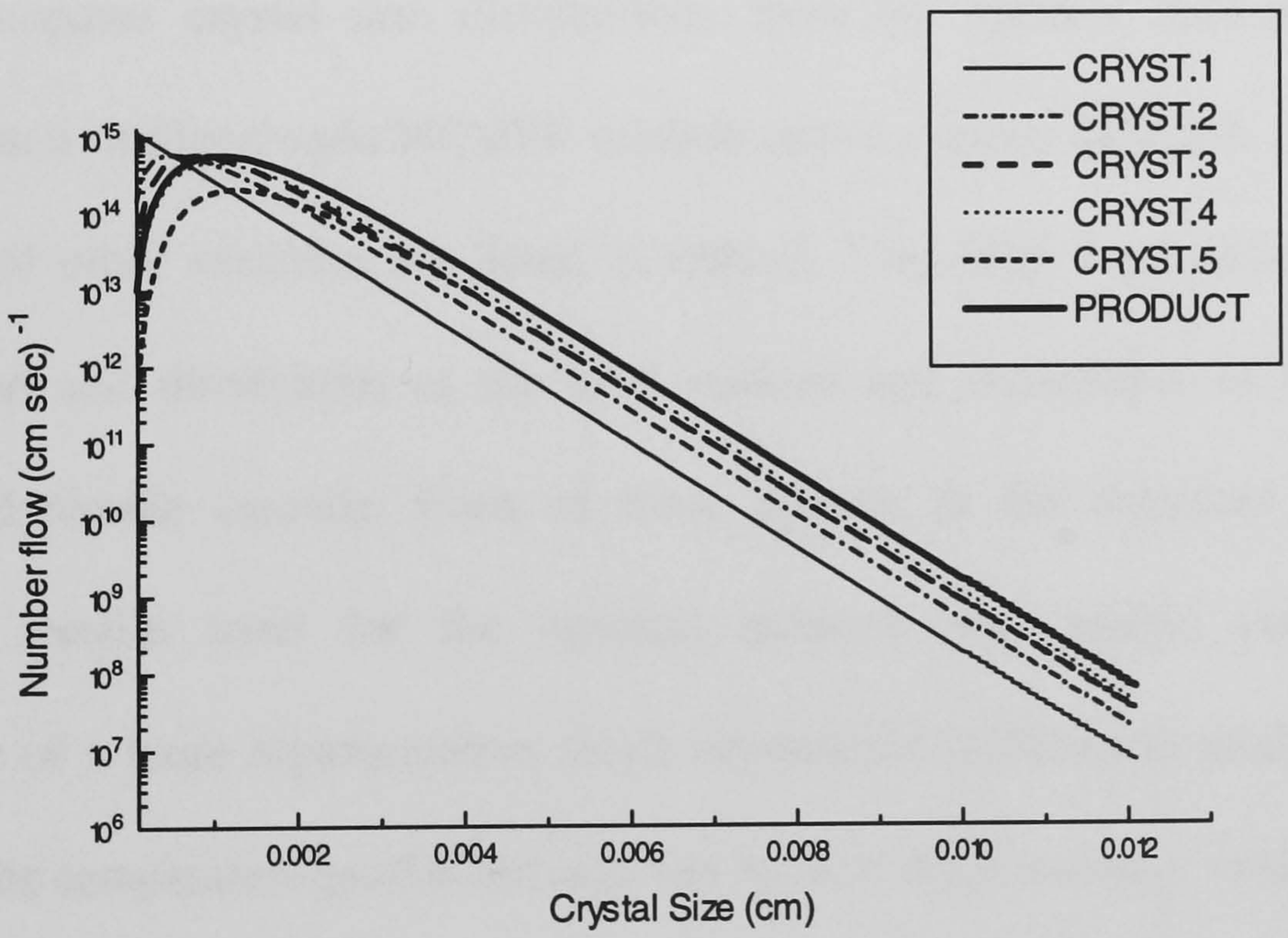

FIGURE 7 : Crystal size distributions from each crystallizer and product stream

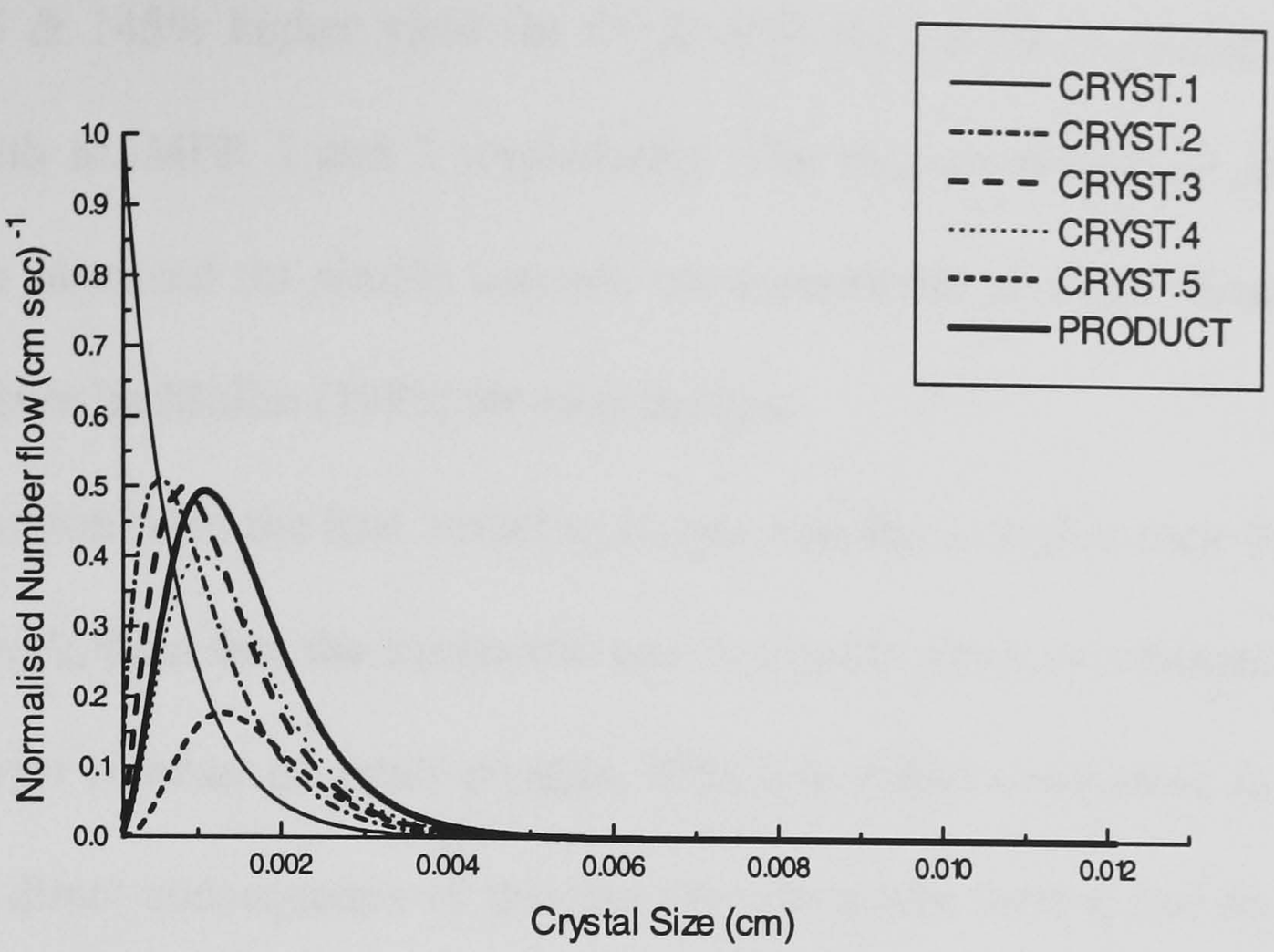

FIGURE 8 : Normalised CSD from the optimal network

Figure 9 compares crystal size distributions from the optimal network to those obtained from a similar simple MSMPR cascade and two single MSMPR crystallizers. The details of other variables are listed in table 3. The single crystallizers have the same volume and throughput as the total volume and throughput in the optimal network and simple cascade. Each of these operate at the extremes within the temperature profile used for the optimal network and simple cascade. The performance of a more representative single crystallizer (difficult to model, not only because of the temperature profile but also due to flow distributions), would therefore lie between these two crystallizers. The results confirm that the optimal solution performs between the cascade and single crystallizers. It succeeds in increasing the yield by 280% when compared with the single crystallizer operating at higher temperature (MSMPR 1) for a 17% reduction in average size. Though the yield is only up 115% on single crystallizer operating at the lower temperature (MSMPR 2), it also accompanies reductions in the degradation of average size (~8%). The simple cascade

achieves 365 & 145% higher yield for 54 & 45% reductions in average size when compared with MSMPR 1 and 2 respectively. The magnitudes of the reductions in average sizes observed for simple cascade are comparable to those obtained from a correlation given by Mullin (1993) for such designs.

Exit concentration from the first vessel in simple cascade is higher then that from the optimal network, therefore the nucleation rate is greater which is reflected in figure 9 through a larger number of small crystals. This low initial conversion in the simple cascade is a direct consequence of the fact that the entire feed is fed in a vessel of similar volume. The steeper slope manifests the effects of full crystal carry over from stage to stage that relieves super-saturation at a faster rate and consequently lower growth rates when compared with the optimal solution. The MSMPR crystallizers provide the best average size because the mean residence time is much higher. The coefficient of variance for MSMPR crystallizers is 1.0, because the moments are calculated on the basis of number flow and not density.

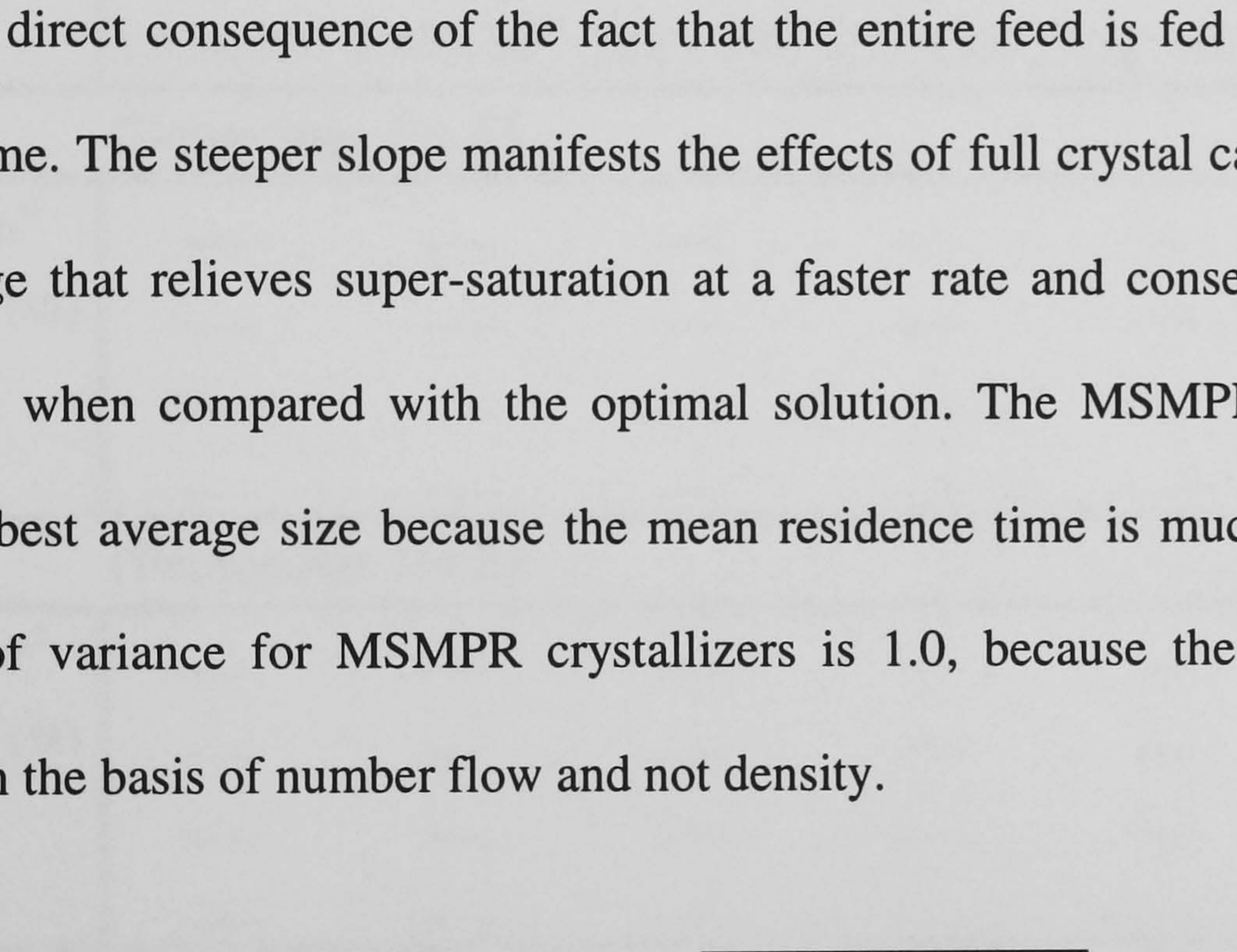

FIGURE 9: The product CSD from optimal network, simple cascade and MSMPR's

	MS 1	MS 2	MS 3	MS 4	MS 5	PRODUCT
Optimal Solution						
C_out Kmol m^{-3}	3.318	3.165	3.018	2.871	2.669	2.827
Overall Yield (%)	—	—	—	—	—	19.6
CV	1.000	0.727	0.617	0.545	0.487	0.512
LBAR cm	6.30×10^{-4}	1.02×10^{-3}	1.26×10^{-3}	1.49×10^{-3}	1.74×10^{-3}	1.61×10^{-3}
Simple Cascade						
C_out Kmol m^{-3}	3.337	3.111	2.933	2.778	2.644	2.644
Overall Yield (%)	—	—	—	—	—	24.8
CV	1.000	0.726	0.622	0.562	0.523	0.523
LBAR cm	3.83×10^{-4}	6.20×10^{-4}	7.58×10^{-4}	8.57×10^{-4}	9.32×10^{-4}	9.32×10^{-4}
MSMPR 1	(Temperature 291 K)					
C_out Kmol m^{-3}	—	—	—	—	—	3.281
Overall Yield (%)	—	—	—	—	—	6.6
CV	—	—	—	—	—	1.000
LBAR cm	—	—	—	—	—	1.93×10^{-3}
MSMPR 2	(Temperature 288 K)					
C_out Kmol m^{-3}	—	—	—	—	—	2.918
Overall Yield (%)	—	—	—	—	—	17.1
CV	—	—	—	—	—	1.000
LBAR cm	—	—	—	—	—	1.74×10^{-3}

TABLE 3 : Average size, CV, yield and exit concentration from different environments

Significant differences in average size and coefficient of variance between the optimal network and simple cascade can be explained by analysing the moments within each environment. These are listed in table 4 in their conventional dimensions. In the optimal design the number of crystals (zeroth moment) continually drops not only due to the increasing flowrates into the vessels that do not accompany new crystals but also because the intermediate product removal becomes significant. The first and second moments, however, continually increase with the exception of fourth vessel

where the first moment shows a drop. The reason for this could be that the increase in its magnitude due to growth fails to compensate for very low number density as the flowrate reaches its maximum value. These moment trends are in sharp contrast to those observed in a simple cascade, where the zeroth moment remains constant, while the others continually increase. Whilst longer residence time in the first vessel within the optimal network could also contribute to significantly higher average sizes, CV is greatly affected by the changes in moments resulting from flow distribution. The first two vessels in both the cascade and the optimal network operate in identical manner, since insignificant amounts of product is withdrawn from the first vessel in the optimal configuration. This can be observed from the near identical values for CV in both the environments upto the second vessel. However, as the flow patterns and consequently the trends in moments start to diverge, CV drops more rapidly in the optimal network. This could be due to the reductions in standard deviation of the CSD around the mean and also because of more rapid increase in the average sizes. The optimal solution, hence out-performs simple cascade in both the attributes of CSD considered in the present model.

		Moment 0 ($\times 10^{-6}$ cm^{-3})	Moment 1 ($\times 10^{-6}$ cm cm^{-3})	Moment 2 ($\times 10^{-6}$ cm^{2} cm^{-3})
Optimal network				
	MS 1	6403765.6	4036.85	5.089533
	MS 2	5098058.9	5181.95	5.052975
	MS 3	4340749.2	5474.86	9.537487
	MS 4	3619397.0	5415.80	10.4402
	MS 5	3206364.8	5830.89	12.5756
Simple cascade				
	MS 1	25786219.2	9898.68	7.59975
	MS 2	25786219.2	16010.93	15.1900
	MS 3	25786219.2	19561.13	20.5763
	MS 4	25786219.2	22117.11	24.9609
	MS 5	25786219.2	24056.87	28.5802

TABLE 4 : Moments for the optimal network and simple cascade

The performance of optimal network is also studied at very high super-saturation throughout the network. Though the resulting network is no longer optimal because the non-linear program finds the optimum using super-saturation levels, it is nevertheless considered worth-while to analyse the system with significant nucleation in each vessel. In figure 10, product CSD from such a design is compared with a similar simple cascade and the earlier findings. It can be seen that the new solution still out-performs a similar simple cascade, the magnitude of improvements in average size is, however, significantly reduced. This is not only due to the reduction in sizes for the network based on the optimal configuration resulting from an increase in the number of crystals but also because the average size from the simple cascade increases. The latter could be attributed to the fact that nucleation ceases earlier in such a design, leaving the driving force only for crystal growth.

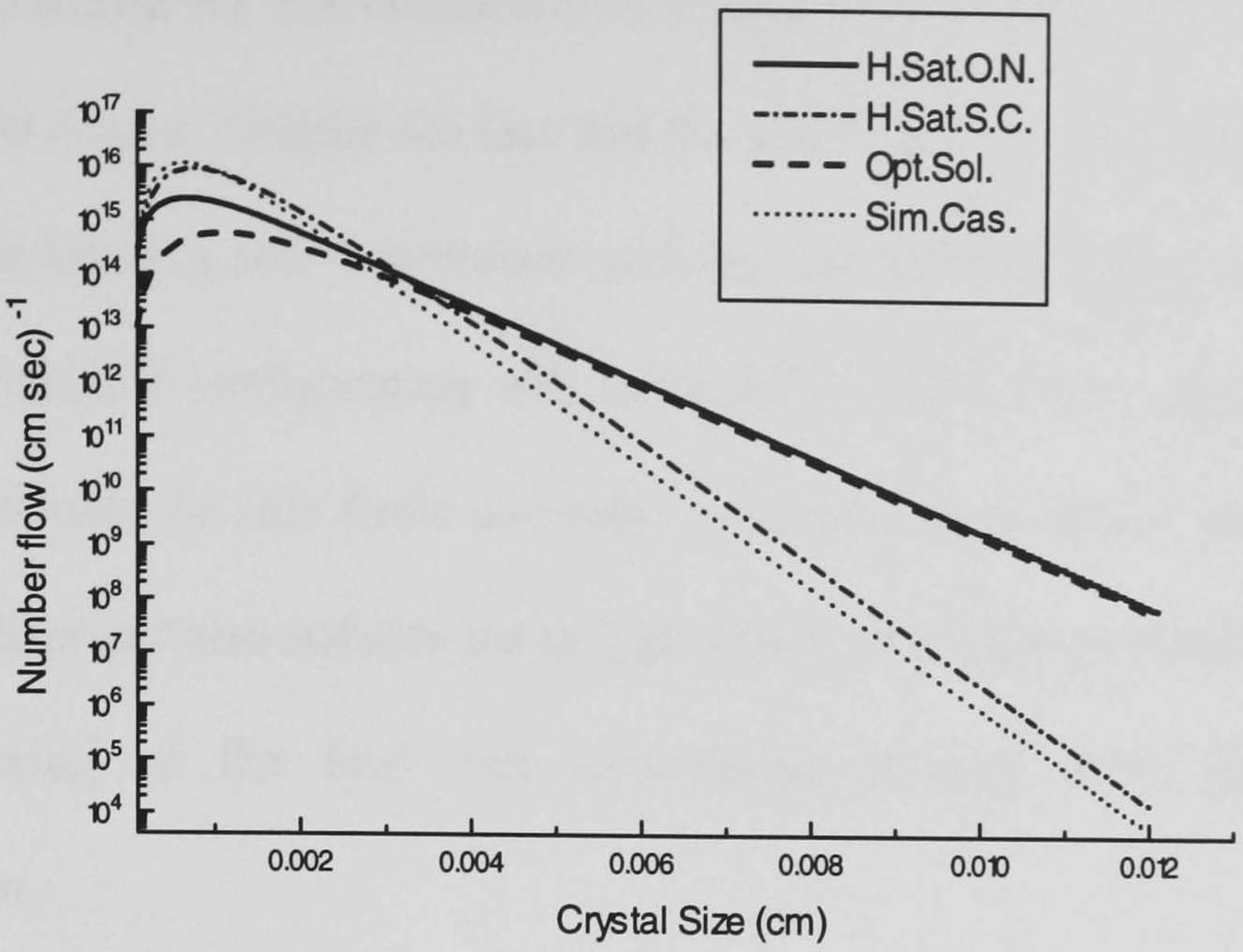

FIGURE 10: CSD from high super-saturation analogues of optimal network and simple cascade

4.5 Conclusions

In this chapter a targeting based method is developed for optimal synthesis of stage-wise crystallisation processes. The methodology draws its structure from a similar approach developed by Balakrishna and Biegler (1996) for chemical reactor networks. It provides an optimisation based method for trading between maximum yield (simple cascade) and best average size (MSMPR) by fundamentally changing the characteristics of stage-wise design through innovative flow distributions. The procedure has been demonstrated for a KNO_3 crystallisation process. With the conditions used in the simulations of optimal network, an increase of more than 115% is achieved in yield when compared with the best performing MSMPR of similar volume and throughput at the expense of at the most a 17% reduction in average size (worst MSMPR). Though higher yield (340%) can be obtained from a simple cascade, the degradation of average size is more pronounced (~50% reductions on the size

from a single MSMPR). The coefficient of variance is also reduced to a greater extent in the optimal design. Despite the fact that the magnitude of these results are strongly related to the kinetics and temperature profiles, the methodology is of more general utility. The optimal configuration will inherently result in more efficient networks, since the provision of side feeds not only eliminates the need for equal volumes of each crystallizer but also reduces the energy requirements for cooling the suspension, because mixing of the feed and crystallising streams itself increases solute concentration.

Chapter 5:

MACHINE LEARNING BASED OPTIMISATION OF CRYSTALLISATION PROCESSES

Crystallisation processes have seldom been subjected to process improvement techniques at the operational level. Rather process improvement studies have been restricted to the design level through simple "design and cost" relationships, (Rossiter and Douglas, 1986; Jones, 1991), for they are characterised by mathematical complexities associated with the adequate representation of crystal size distribution (CSD) and functional discontinuities in kinetic processes, beyond current optimisation algorithms (Cuthrell and Biegler, 1987; Biegler et al., 1995). These calculations require a thorough understanding of the process so that it can be effectively represented in simplified mathematical form to find the best solution to a process within the imposed constraints.

Machine learning, the study and computer modelling of learning processes in their multiple manifestations, has been used for the similar task of developing and analysing systems to improve performance from existing data, often from a less model driven standpoint (Saraiva and Stephanopoulos, 1992; Saraiva 1995). The essence of problem formulation with this approach is one in which a procedure, shown a set of process data (**x**,y) comprising quantitative and or qualitative features of the process, employs inductive inference to extract classification rules for the division of decision space into hyperrectangles (not points) representing different levels of performance without losing the individuality of each decision variable. The procedures which discover these rules in the form of decision trees are the most mature and widely used of all the interval analysis based rules representations. These trees are developed through top-down, divide and conquer strategy which successively partitions the given set of data into smaller and smaller subsets with the growth of the tree (Quinlan, 1990). Symbolic induction is based on direct sampling approach where random data

sets (objects) are used to build confidence intervals for performance levels and therefore does not suffer from simplifying assumptions and numerical inaccuracies inherent to mathematical formulation in traditional optimisation procedures. The method relies on the quality of data, as for quantity Saraiva (1995) has shown that even with moderate amounts of data it is possible to construct trees resulting in significant performance improvements. Furthermore, since the trees exhibit explicit ranges of decision variables and associated levels of performance, they can lead either directly to changes in current operation practices or to the design of a set of confirmatory experiments for validating the findings. The implementation of these suggestions would generate more novel data capable of providing operating schemes for the extension of process performance beyond currently achieved levels. These schemes are identified and passed on to the symbolic induction stage for updating classification rules by the case based reasoning component. Crystallisation processes will, therefore, be best served by machine learning methodology which offers a flexible and mathematically de-convoluted procedure identifying performance improvement zones by establishing ranges on the crucial decision variables. By way of illustration, a potassium nitrate process flowsheet will be optimised.

Firstly, features of the crystallization process and its simulations will be presented. This will be followed by a thorough explanation of the modifications made herein to the existing machine learning methodology (Saraiva and Stephanopoulos, 1992a). These changes have lead to the simplification and increase in the efficiency of both of its components *i.e.*, symbolic induction and case based reasoning. This section will be followed by the stepwise illustration of the revised methodology as applied to the

crystallisation process problem after simulating it under a range of different operating conditions to develop the necessary process data.

5.1 The process

5.1.1 Flowsheet description and its solution

In this study a simplified potassium nitrate flowsheet comprising an MSMPR crystallizer, a hydrocyclone and a fines dissolver has been developed for simulating crystallisation processes (see fig. 11) on SPEEDUP® through the models developed earlier in chapter 3. Dynamic simulations are performed from start up of steady state.

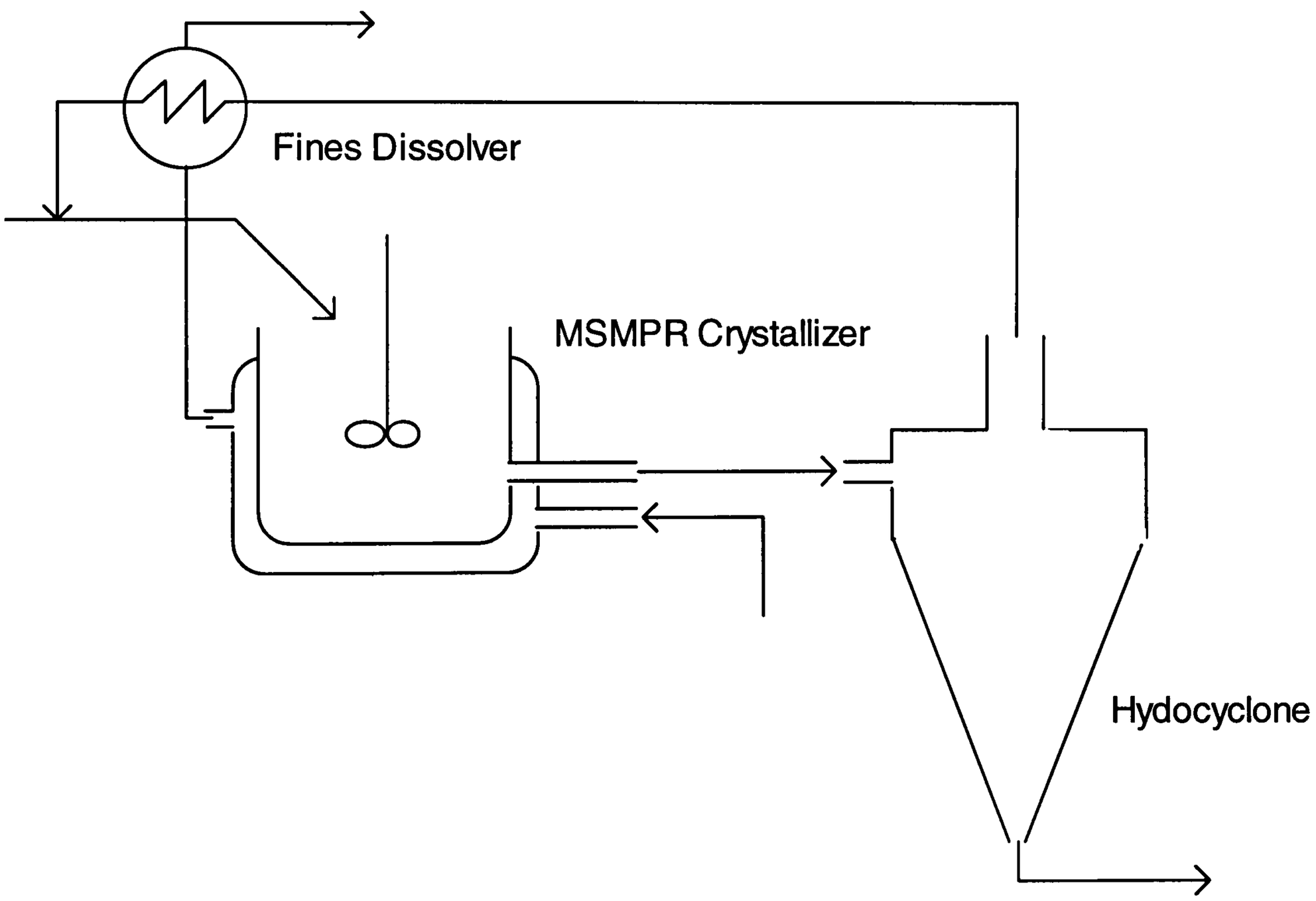

FIGURE 11 : The crystallisation process flowsheet

As a consequence of non-minimum phase (initial response opposite to final transient response) for the crystals to be dissolved and a delayed increase in temperature, the SPEEDUP® solver fails with fines dissolver. The problem can be resolved by either using a separate utility stream with a steady temperature or by switching the unit off

from the simulations until the temperature and / or the profiles of the crystals to be dissolved show a near steady state response. The latter has been adapted by tailoring functional discontinuities in the model formulation, where a set of equations is only activated after a certain specified time has lapsed. A time delay function in the crystallizer, which accounts for the crystals to grow from critical radius to first size range, is also used. Run times are around ~ 300 CPU seconds on an IBM RS-6000/250, for simulating 10 residence times in the crystallizer. Figure 13 shows typical CSD profiles from the crystallizer and underflow of hydrocyclone. Nucleation and growth transients are depicted in figure 12.

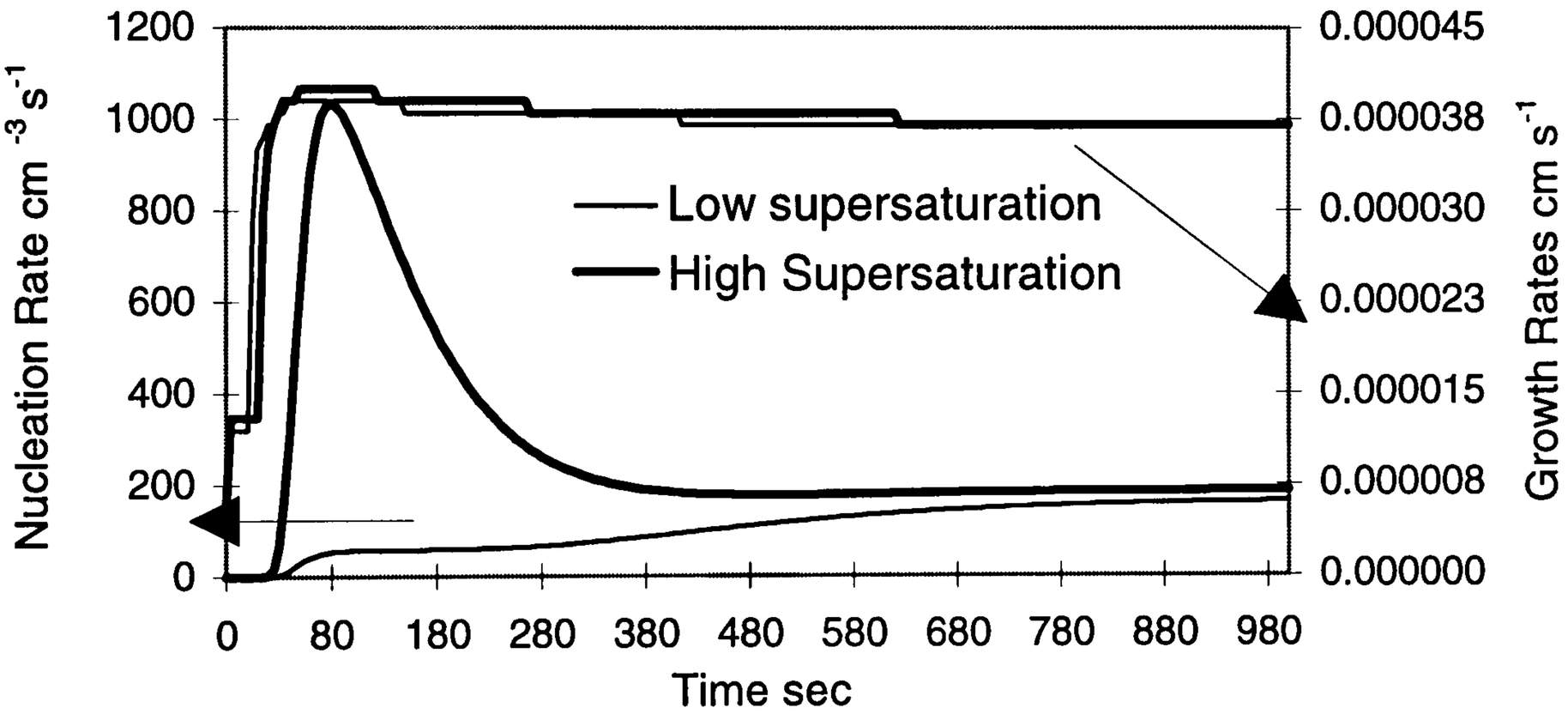

FIGURE 12 : Nucleation and Growth rates at two different levels of super-saturation.

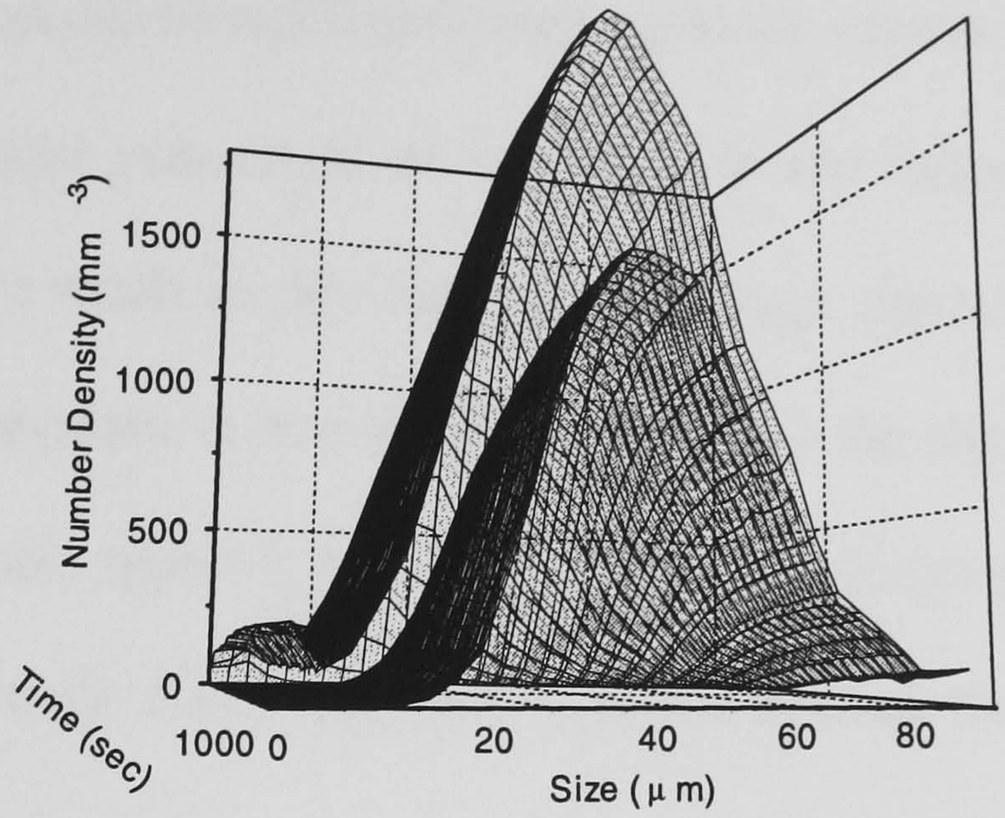

FIGURE 13 : Development of KNO_3 CSD in the Crystallizer and Product Stream

5.1.2 Analysis of the findings

The simulation of the crystallisation circuit shown in figure 11, help establish some of the very complicated and highly coupled interactions not only within the units but also across them. Some of the observations of interest are summarised in the following.

- Slurry recycle is found to effect the level of super-saturation and hence the kinetics of nucleation and growth through two of its conflicting attributes, *viz.* reduced temperature and reduced concentration. The former results in an increase in super-saturation due to lowering of the temperature of combined feed, whereas reduced solute concentration has a negative impact on super-saturation. From the limited number of cases simulated, however, the net effect of recycle seemed to

be an increase in super-saturation; enough to initiate a runaway increase in primary nucleation without significantly increasing the growth rate. This undesirable effect can be rectified through effective control of vessel temperature.

- Study of the axial component of velocity into the hydrocyclone showed that higher velocities result in the lowering of average crystal size for the product stream; and vice-versa. It is worth re-iterating that the physical interpretation of this un-measurable quantity is subject to many simplifying assumptions and its accurate and simple functional form in terms of feed flow properties is non-existent.
- The introduction of a fines dissolver on the overflow stream reversed the undesirable effect of recycle as the temperature of combined feed is increased to an acceptable value thereby leading to cessation of primary nucleation. The specification for temperature within fines dissolver was made to ensure that only particles in the first few classes dissolved to extinction. This increase in temperature was desirable even after primary nucleation had ceased because as the crystal mass increased, secondary nucleation took over.

These inferences lead to an interesting observation on the conceptual design of the circuit. Had the conventional method been adopted, whereby two separate loops for fine dissolution and classified product removal are used, the desirable effect of fines dissolution could not have off set the unwanted increase in super-saturation. This is because, in the two loop design a very small volume of suspension (usually from the top of the crystallizer) is withdrawn for fines removal and the rest of the bulk is sent for product classification. As a consequence, inter-stage heating would be required for the recycle from the product classifier along with the heater in fines loop.

5.2 Machine learning approach to process improvement

The sequence of steps undertaken by the global machine learning approach are depicted in Figure 14 (details can be found in Saraiva and Stephanopoulos, 1992). It comprises two major components *viz.*, one for screening the objects to maintain a reduced subset of data conveying novelty (these constitute the feedback from the process' s attempt to perform at the desired level) and the other for detecting interesting conceptual patterns or revealing structure in collections of observations. The former employs case based reasoning whereas the latter is based on symbolic inductive learning which involves operations of generalising, specialising, transforming, correcting and refining knowledge representations. In the following we will summarise the features of the procedures used by these two components as employed in the existing methodology before highlighting the merits of the modifications suggested in this work.

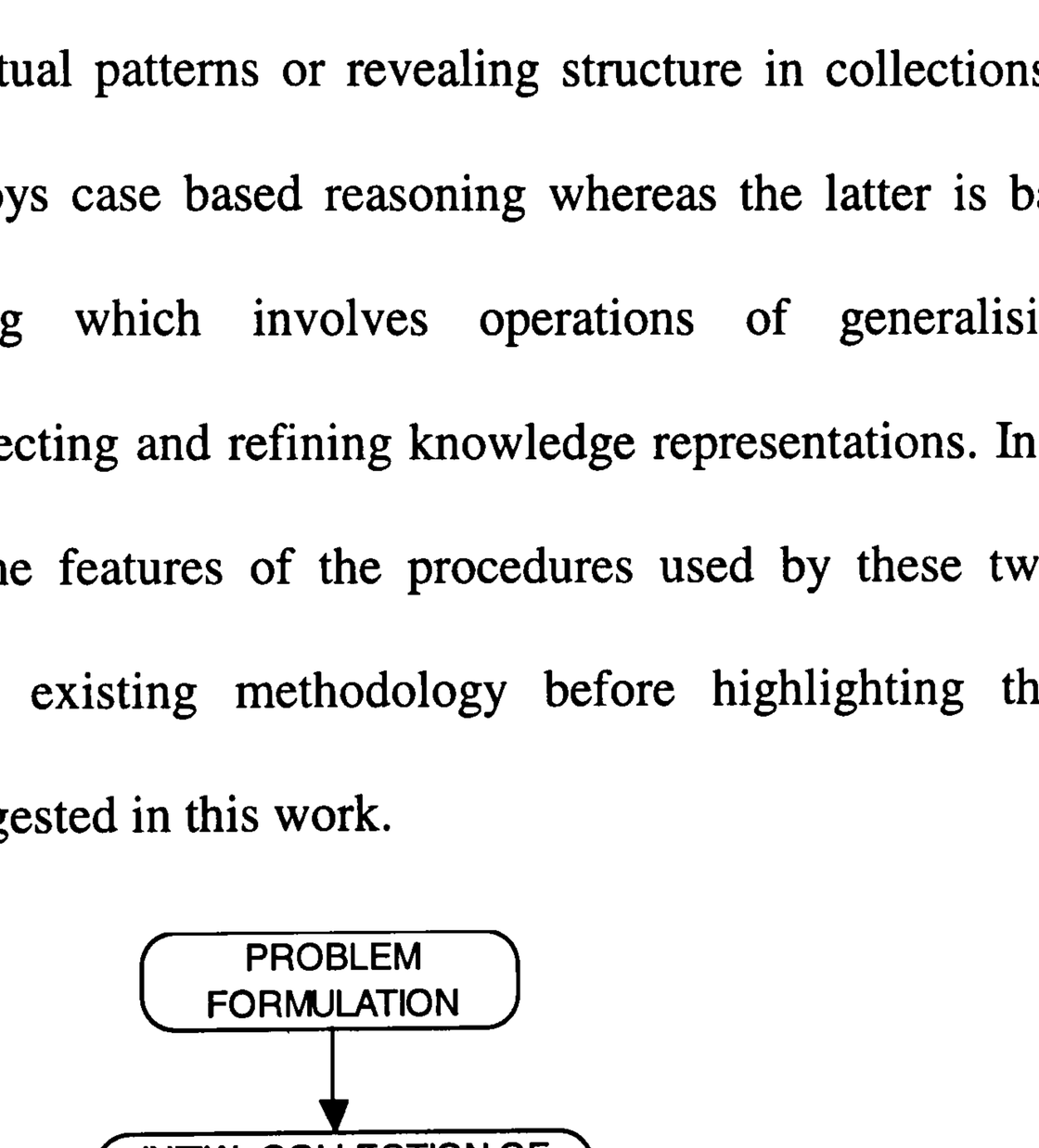

FIGURE 14 : Global Machine Learning Methodology (Saraiva and Stephanopoulos, 1992a)

5.2.1 The ID3-CART Induction of Decision Trees:

The non-incremental construction of a decision tree based on the *ID3* algorithm starts at the root node of the tree where all the objects are located. For continuous valued attributes, the threshold value for discretising the range is calculated by minimising the information entropy function (E-score) over all the possible splits (for *N* objects there are *N-1* possible splits for each of the continuous attributes). The E-score, which is a measure of the ambiguity associated with a particular split can be calculated by:

$$E = -\sum_{K=1}^{K} P_k \log P_k + \sum_{c=1}^{R} \frac{N_c}{N} \sum_{k=1}^{K} P_k^c \log P_k^c$$

where P_k is the relative frequency of objects that belong to class k of the performance variable among all the N objects, and N_c is the number of objects allocated to the c^{th} node. The attribute with lowest E-score is selected as test attribute for splitting the node and sending the subsets of objects through branches emanating from it to children nodes. E-score based selection of test attribute ensures that only the most significant attributes contribute to the classification rules. New threshold values are calculated at each of the new nodes for all the attributes to select test attributes for further splitting of the objects. The procedure continues until a terminal node is reached where all the objects belong to the same class.

The lower levels of the tree are developed from a progressively smaller number of objects and therefore many of branches could be reflecting chance occurrences in the particular data rather then representing underlying principles. Pruning methods identify the least reliable branches and remove them. The Error-Complexity (CART) pruning method due to Breiman et al. (1984), is used in the existing methodology. It is

a two stage method, first generating a series of trees pruned by different amounts, and then selecting one of these by examining the number of classification errors each of them makes on an independent set of objects. During pruning, the error-complexity method takes account of both the number of errors and the size (complexity) of the tree. The scheme, however, requires an independent set of objects for selecting the tree.

5.2.2 Case Based Reasoning:

This step involves a screening procedure whereby existing and continually generated data from on-line applications is analysed to obtain a reduced data set (active memory of exemplars, AME) situated near the decision boundaries. The procedure is also capable of periodically updating AME 's contents during serial learning tasks (process generating a stream of training objects where one would like to be able to detect novelty instantaneously and revise the contents accordingly). A distance nearest neighbour (DNN) classifier is used to predict the classes of incoming objects. It uses a set of objects and a distance metric on them to find the nearest neighbours of the incoming object to find its class. The miss-classified objects are stored in an incremental training set and whenever the total number in this training set reaches a pre-determined fraction of the present cardinality of AME, a revision point is reached. An object is excluded from AME if the misclassifications made by it exceed a predetermined threshold. A global measure of significance, considering reliability, frequency of use and age is used as a second criterion to remove objects from AME. The revised AME is used to induce a new generation of decision trees.

5.2.3 Modifications

5.2.3.1 Revised Scheme for the Induction of Decision Trees:

For non-incremental learning tasks, *ID3* is a useful concept learning algorithm because it can efficiently construct a decision tree that generalises well. Serial learning tasks would, however, be better served by an algorithm that could accept objects continually to revise the tree, without needing to build a new tree each time. Most of the incremental algorithms perform on decision trees induced through non-incremental methods by restructuring them to account for the incoming object which cannot be classified by the existing tree. Failure of the tree to classify the new object is attributed to the fact that at one of the nodes traversed by this object, the criterion for selection of the test attribute does not hold. The *ID5R* algorithm (Utgoff, 1989) is one such algorithm and involves the use of E-scores to change the test attribute at a node to one with the lowest value, followed by a tree restructuring process which preserves consistency with the existing objects without re-examining them. The algorithm is depicted in Table 5. When a new object is introduced to the existing tree, attribute value counts (number of attribute values in each class) are updated for the test and non test attributes. If the test attribute no longer has the lowest score, the tree is restructured by the procedure outlined in Table 6.

1. If the object is from the same class then update the number of objects at the leaf.

2. otherwise,

   a. For the test attribute and all the non-test attributes at all the nodes traversed by the incoming objects, update the attribute counts.

   b. If the current node contains an attribute test that does not have the lowest E-score then,

      i) Restructure the tree so that an attribute with the lowest E-score is at the root.

      ii) Recursively re-establish a best test attribute in each subtree except the one updated in step 2c.

   c. Recursively update the decision tree below the current decision node along the branch for the value of the test attribute that occurs in the object description. Grow the branch if necessary.

TABLE 5 : *ID5R* Algorithm for incremental induction of Decision trees

1. If the attribute a_{new} to be pulled up is already at the root then stop.

2. otherwise,

   a. Recursively pull the attribute a_{new} to the root of each immediate subtree.

   b. Transpose the tree, resulting in a new tree with a_{new} at the root, and the old root attribute a_{new} at the root of each immediate subtree.

TABLE 6 : Tree Re-structuring procedure

All the algorithms for inducing decision trees require the attributes to be categorical and therefore continuous valued attributes (the term continuous covers both real and integer values) must be discretized prior to test attribute selection. We will employ a corollary due to Fayyad and Irani (1992) on the discretization of continuous attributes based on the information entropy minimisation heuristic to gain computational efficiency by reducing the number of possible candidates for cut point. The corollary states that a binary partition based on the information entropy minimisation principle will always partition the data on a boundary point in the sequence of objects ordered by the attribute value. The boundary points refer to those attribute values in their ascending sequence where the class of performance variables changes. Speedups of upto 7 times have been reported for some types of objects as a direct consequence of the corollary (Fayyad and Irani, 1992).

Pessimistic pruning (Quinlan, 1993) has been adapted in preference to CART for two reasons; a) it is much faster than any of the other pruning methods because it only makes one pass and only looks at each node once and b) it does not require an independent set of objects for choosing the pruned tree. The method however, results in larger trees than those pruned by error-complexity method (CART). Pruning proceeds from the root downwards by comparing the corrected number of misclassifications at a node with the leaves in the corresponding subtree. A tree is pruned if the following condition is satisfied

$$SE\left(n'\left(T_t\right)\right) + n'\left(T_t\right) > n'\left(t\right) \tag{5.1}$$

where $n'(t)$ and $n'(T_t)$ are corrected misclassification rates at a node and for the subtree respectively. $SE(n'(T_t))$ denotes standard error for the subtree. Following equations are used to calculate these quantities.

$$n'(t) = e(t) + 1/2 \tag{5.2}$$

$$n'(T_t) = \sum e(i) + N_i/2 \tag{5.3}$$

$$SE(n'(T_t)) = \sqrt{\frac{n'(T_t) \times [N(t) - n'(T_t)]}{N(t)}} \tag{5.4}$$

A thorough comparison of different methods available for pruning decision trees can be found in Mingers (1989). Though the incremental algorithm leads to instantaneous incorporation of novel objects into the decision trees, it is the evaluation process which determines the maturity of newly acquired information for application. The branches representing obsolete objects are pruned automatically by the chosen pruning method.

5.2.3.2 Present state of Case based Reasoning Process:

The existing procedure for screening objects is applied to the initial training set to obtain a reduced subset of objects. The application of DNN also provides an indication on the adequacy of the data where similar cardinality of the complete and reduced sets indicate the need for further collection of data. With the modifications to the symbolic learning procedure, the need for dynamic memory to adapt AME for updating the decision tree vanishes as the objects reflecting drifts or other temporal changes in the process behaviour once detected could lead to instantaneous update of the classifier. We propose to replace the DNN method with the current version of the tree to serve as the classifier at the case based reasoning step for tightening the

passage of objects to the incremental induction step. The DNN classifier is not the most effective classifier especially when used in isolation. Furthermore, its effectiveness is very sensitive on the metric definition and it is computationally expensive as well, because a representative set of objects must be stored and the inter-point distances and classification rule calculated for each incoming object (Breiman et al., 1984).

The simplified case based reasoning procedure, however, leaves only the pruning mechanism to exclude obsolete objects which can be an inefficient and slow procedure. To overcome the potential problem of exceedingly large decision trees with a significant proportion of obsolete rules, we suggest eliminating all the branches leading to these leaves after a proposed scheme of the tree for performance improvement has been agreed upon for implementation. The implementation would ensure that no objects are subsequently generated for the lower levels of performance represented by the eliminated branches.

5.2.4 Formulation of Improvement Suggestions:

Some of the procedures and tests developed by Saraiva and Stephanopoulos (1992) for the formulation of improvement suggestions from the decision trees will be summarised in the following. The process can be divided into three distinct activities *viz.*, refinement, evaluation and validation.

Refinement entails the enlargement of the partitions of feature space defined by the leaves of the decision tree without significantly lowering their purity (fraction of objects with the correct class label). The surface boundaries for each of the leaves are examined to identify borders with partitions of the same class. The leaf is then expanded by extending each of these borders in turn (while leaving the others fixed),

until no further extensions are possible for any boundary without including space of different class. This procedure is repeated for all the leaves. A statistical test of significance is performed on all the expanded leaves, followed by a check to ensure that hard process constraints on any of the variables are not violated due to the expansion.

Evaluation tests include a) *certainty factors*; the fraction of objects from an independent test set that are correctly classified by the extended leaves, b) *Pareto index*; which allows the identification of those regions of the feature space where most of the objects of each class from the test set are being placed and c) *demographic density*; the ratio of total number of objects in the set that belong to a particular leaf.

The validation process involves an extensive analysis of the evaluation scores for the identified promising and feasible pathways to process improvement. This distilled information is re-evaluated to ensure that all the process and safety constraints are satisfied, prior to plant personnel deciding on whether to perform pilot tests or implement the improvement schemes on-line (see Saraiva and Stephanopoulos, 1992a; for details).

5.3 Performance improvement of the crystallisation process

In this section we present stage-wise development of two generations of decision trees for performance improvement of KNO_3 crystallisation through a revised machine learning methodology. The first generation construction of decision trees is closely based on the existing methodology (Figure 14), however for continual improvement of process performance the revised scheme presented in Figure 15 is employed. Three

zones of high level performance are identified, with each representing an improvement of upto 12% on the nominal average levels.

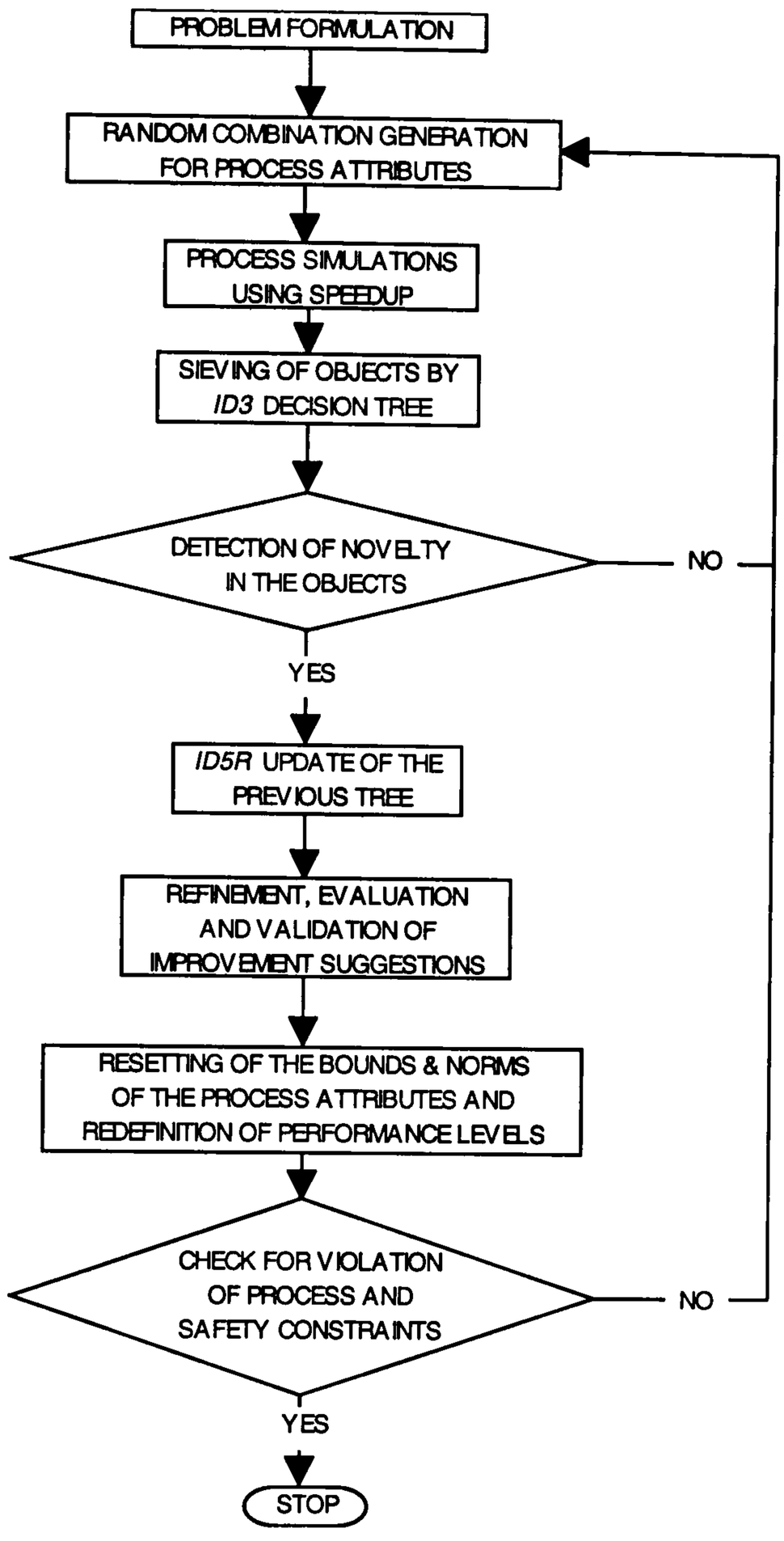

FIGURE 15 : Revised Machine Learning scheme as applied to Crystallisation Problem

5.3.1 Problem Formulation and process simulations:

The performance of crystallisation system is measured as a combination of total number of crystals and their average size in the underflow from the hydrocyclone. These two features of crystal size distribution manifest the effects of nucleation and growth rates and there is always an optimum driving force for the two kinetic processes beyond which they do not increase simultaneously, rather the average size

falls while the number of crystals increases. In the process under consideration, the operation for all three units *viz*., crystallizer, hydrocyclone and fines dissolver can be affected to achieve desired performance. The behaviour of the crystallizer is modified through feed temperature, concentration and flowrate and coolant temperature. These variables allow to manipulate both the super-saturation driving force and residence time within the crystallizer. Axial velocity of the stream into the hydrocyclone is used to adjust particle efficiency curve, whereas fines dissolution temperature allows control of the number of fine crystals recycled. The operating data is constructed by generating 150 random combinations of these six variables with the following means and standard deviations; TF (295.00 K, 2.0); CF (3.52 kmol/m^3, 0.03); FF (0.10 l/s, 0.01); TC (281.25 K, 1.5); TD (296.5 K, 0.35); W (0.01257, 0.00075). Dynamic simulations are carried out for each combination of operating data by interfacing it to SPEEDUP® through external data interface. The results for total crystal number and average size are stored with the corresponding vector of decision variables to develop a complete training set.

5.3.2 Case Based Reasoning to obtain a Reduced subset of objects:

The application of distance nearest neighbour (DNN) classification procedure to the complete training set results in a reduced subset of 125 objects conveying all the information relevant for the identification of the decision boundaries. Reduction in size indicates the adequacy of the data for effective induction.

5.3.3 ID5R Induction of decision trees:

The induction algorithm can handle fuzzy, functional or crisp discretization for the performance criterion (Saraiva and Stephanopoulos, 1992). In this study, however,

with the objective being the identification of zones encompassing best average performance, we will restrict ourselves to crisp discretization of the performance criterion based on the following thresholds, $y < 2.5\times 10^6$ sec^{-1} ($L_{av.} < 55.0$ microns) as low (A); $2.5\times 10^6 < y < 4.2 \times 10^6$ ($55.0 < L_{av.} < 63.5$ microns) as normal (B) and $y > 4.2\times 10^6$ ($L_{av.} > 63.5$ microns) as high (C). Each object in the reduced subset is labelled a performance class according to these thresholds. Of the 125 objects, 100 are used to induce the decision tree while 25 are reserved to estimate the true misclassification rate of the pruned tree. The average performance of these 100 objects is 3.58×10^6 sec^{-1} crystals with an average size of 56.3 microns. In figure 16 we present a projection of these objects in FF-TC co-ordinates along with the corresponding classes. Although these two variables are not enough to produce a complete discrimination, there are clearly zones of the FF-TC plane where it is very likely to get points from only one particular class. It is the boundaries of these zones which will be discretely identified by the decision tree.

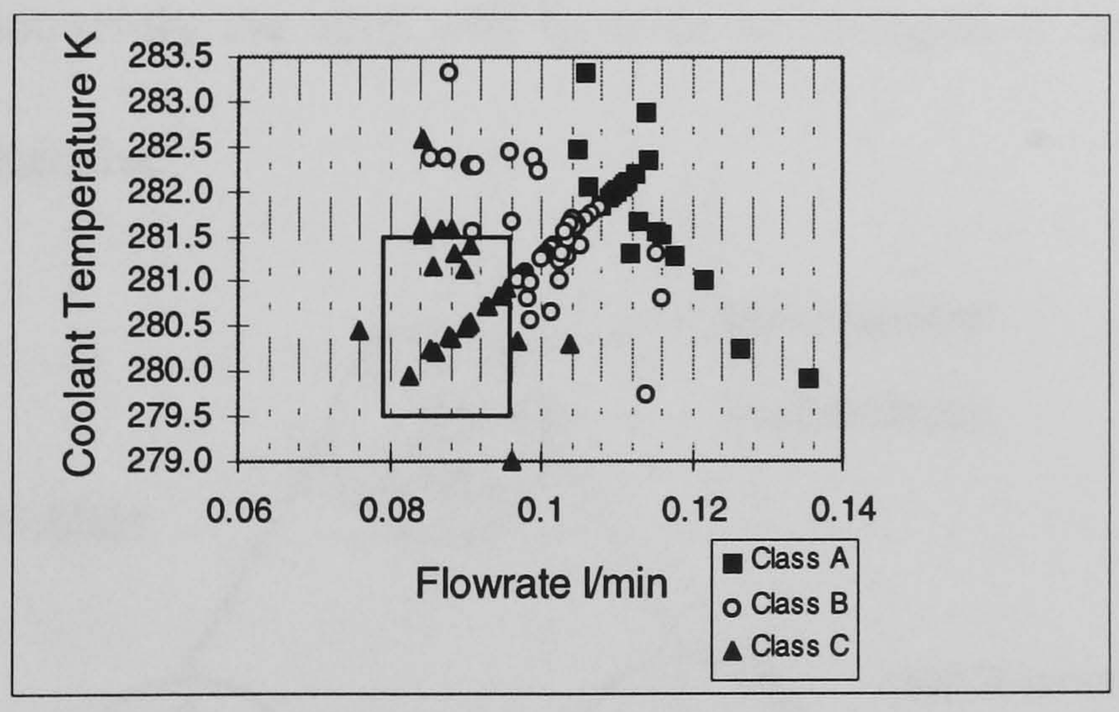

FIGURE 16 : FT-TC scatter of the reduced training set

The *ID5R* algorithm which constructs an identical tree to *ID3* for the same training set was used to develop a fully expanded decision tree. All the attributes in the training set were discretized using information entropy minimisation heuristic, and the

attribute value counts associated with each split were recorded at each node to enable the update of E-scores for incorporating new process information into the tree as it becomes available. Pessimistic pruning was used to prune the tree by removing statistically insignificant branches to improve its understanding. Figure 17 shows the schematic description of the features of a decision tree, while the pruned tree itself is depicted in Figure 18.

It exhibited a misclassification rate of 15% on an independent test set. Since the tree has not seen these objects during induction, the miss-classification test provides a good measure of the validity of the induced rules, especially with regards to the split thresholds which are the prime pointers to the ability of trees in classifying unseen objects. This cross validation procedure is more testing then a similar approach in, for instance PCA based regression models, because every miss-classified object is affixed same weight irrespective of the drift in magnitude. Since, the splits are not calculated with the withheld data and therefore should the tree fail to classify properly, the test attribute and consequently the split will have to be changed if the misclassification was considered excessive.

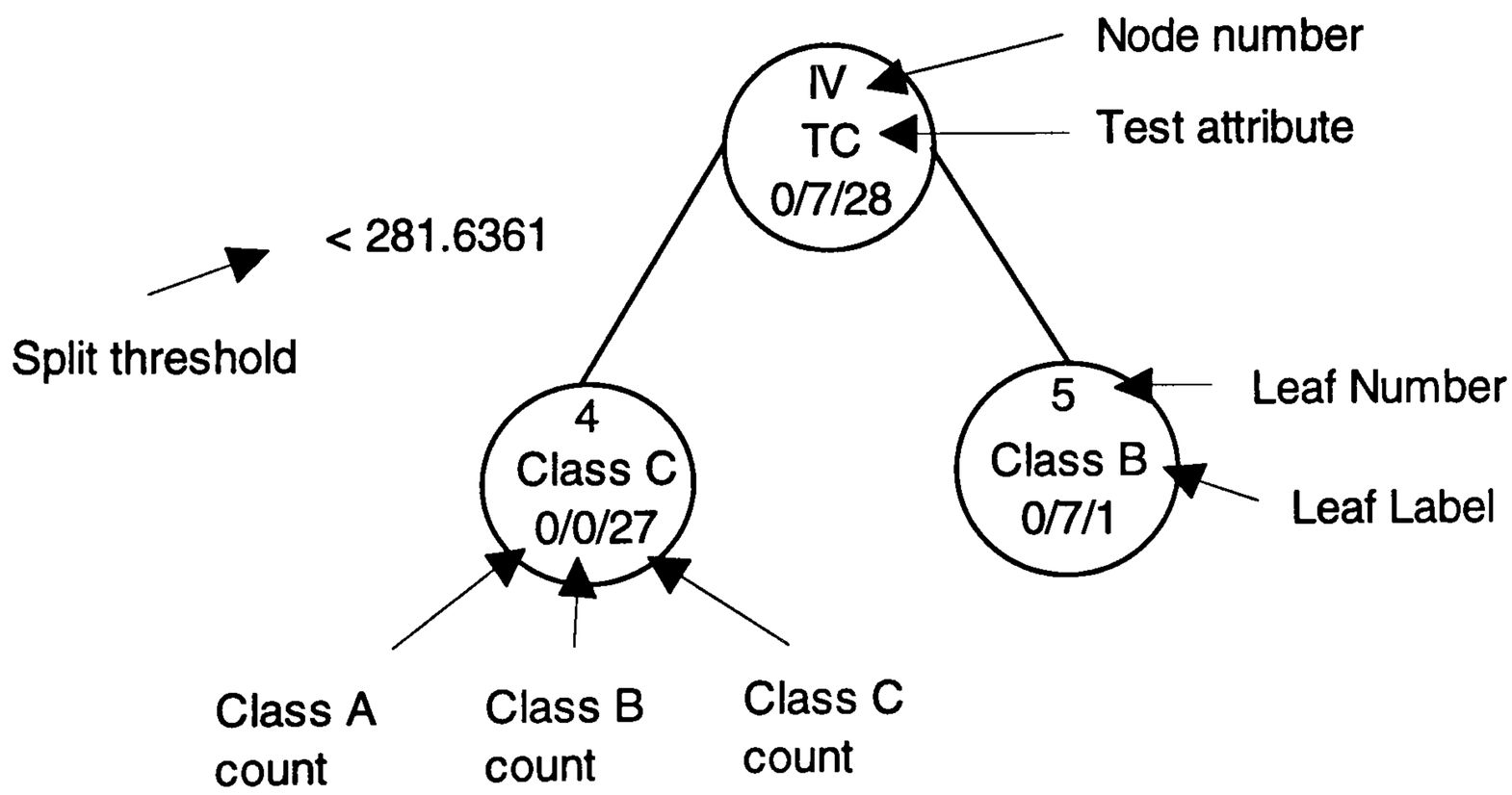

FIGURE 17: Description of the features of a decision tree

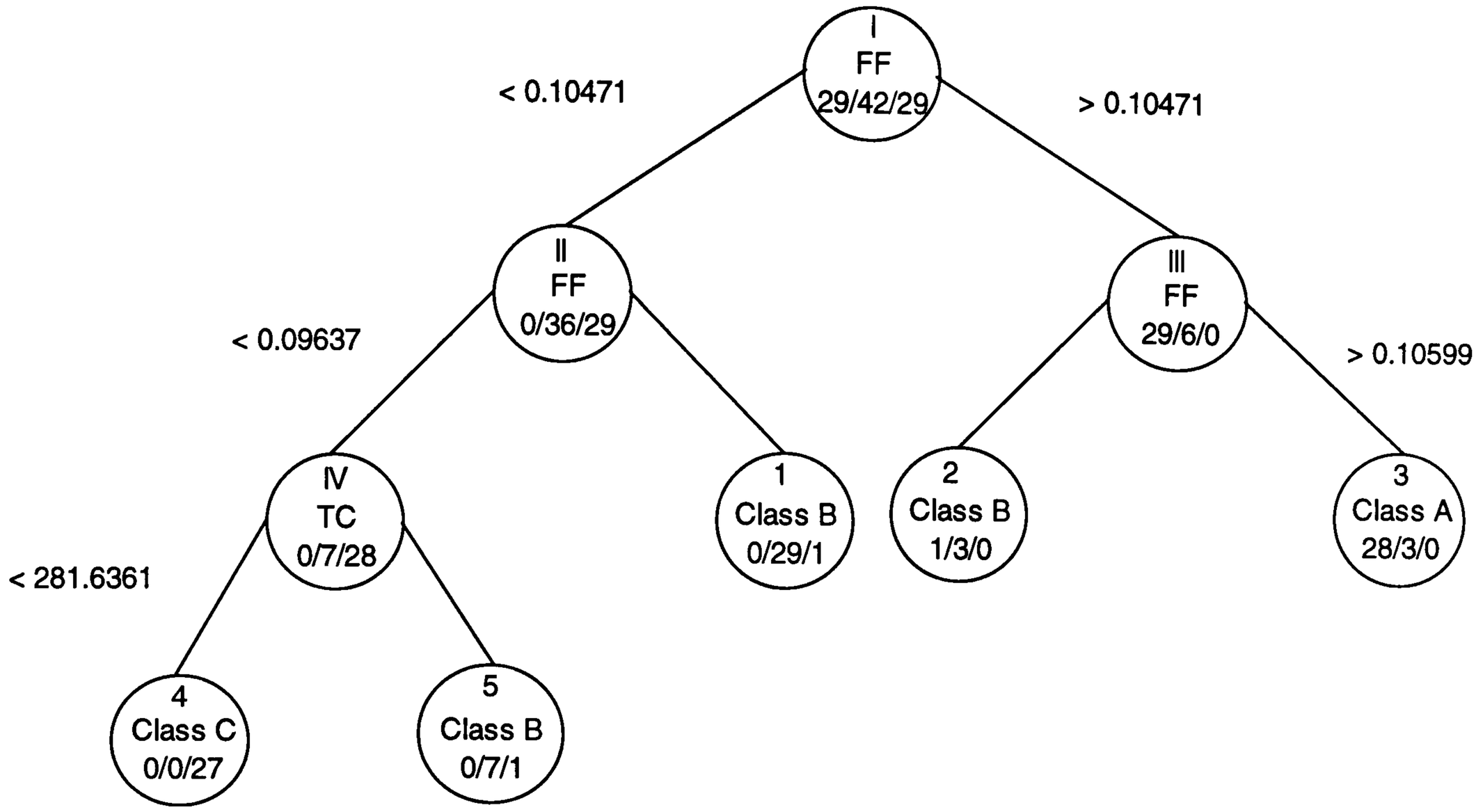

FIGURE 18 : *ID5R* Decision Tree from the reduced training set

5.3.4 Evaluation, refinement and validation:

It can be seen from the pruned tree that only the most significant amongst all the attributes appear in the trees. For example, feed temperature, feed concentration, fines dissolver temperature and axial velocity of fluid into the hydrocyclone are found to have undetectable effects on the performance variable within their allowed variations. Only feed flowrate which is a measure of residence time, is sufficient to distinguish normal from low levels of performances whereas high or class "C" leaf requires three pre-conditions in two variables to be satisfied. Leaf 4 representing class C performance has a certainty factor of 1.00, which means that all the objects within this constrained feature space represent class C whereas *Pareto* index evaluation for it indicates that 93 % of all the high performance objects are concentrated here. The average performance within this zone is 5.34×10^{6} sec^{-1} crystals with an average size of 65.5 microns. The best class "B" leaf scores 0.966 and a mere 0.69 on the two indices respectively. The subsequent refinement procedures leave most of the rules

essentially unchanged especially those regarding class B. The findings are validated by simulating the process under the identified conditions.

5.3.5 Implementation and Case based Reasoning using the decision tree:

To illustrate the incremental induction algorithm we will explore the boundaries between classes B and C and try to obtain multiple regions of class C in the feature space for increased flexibility of operation. It can be seen from the induced decision tree that by setting the flowrate at less than 0.1047 l/min., only class B or C performance will be achieved. The bounds and norms are adjusted accordingly and a set of 50 objects is compiled through simulations. Of the 50 objects, only 30 pass through revised case base reasoning employing current decision tree. The FF-TC and CF-TC scatters of these and other objects from the original reduced training set meeting the flowrate criterion (figures 19 a and b), show that only CF-TC scatter is capable of vaguely identifying the decision boundaries.

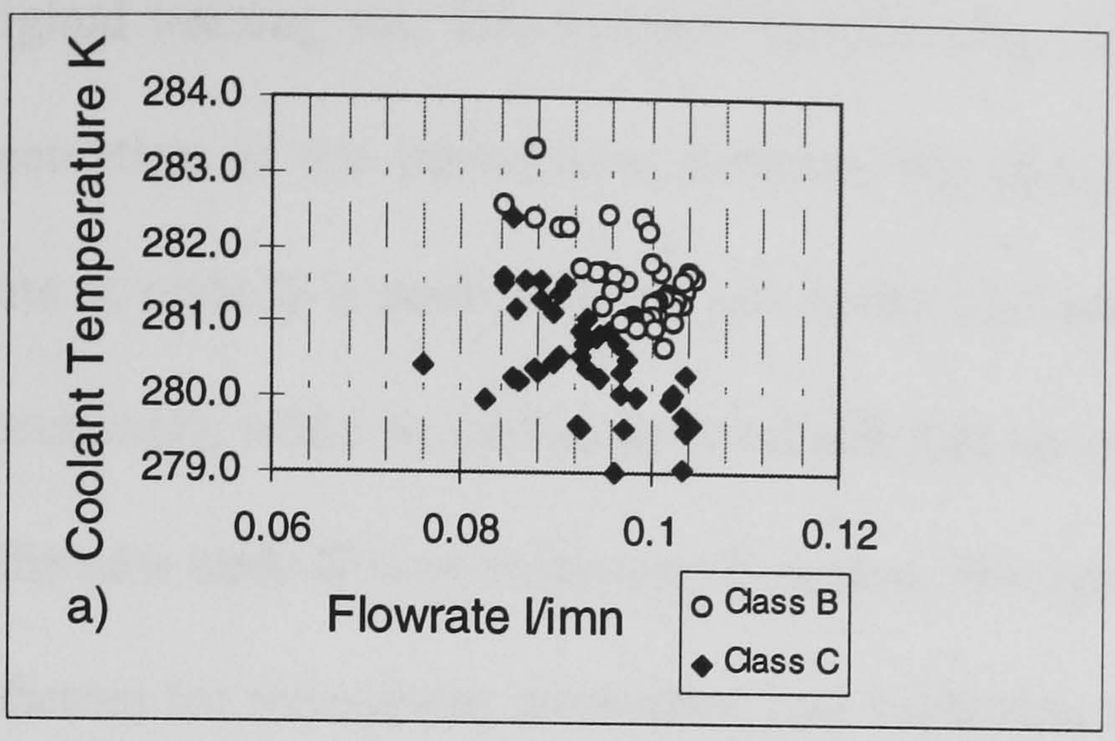

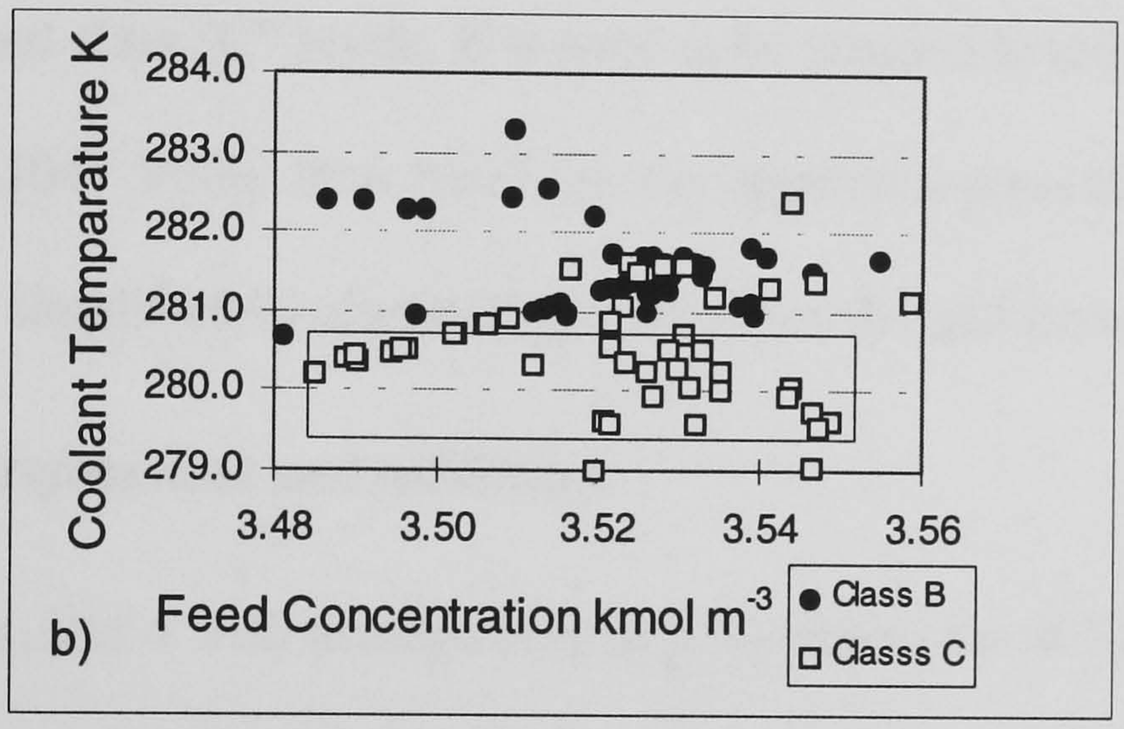

FIGURE 19 : a) FF-TC and b) CF-TC scatter of all objects with feed flowrate less then 0.1047 l/min

5.3.6 Second generation decision tree:

The current tree is updated using E-scores through the procedures sketched in Tables 4 and 5. The *ID5R* algorithm uses original discretization of continuous valued attributes during incremental induction process. As a consequence, even though the algorithm updates the tree to a form similar to one that would be induced by the non-incremental *ID3* algorithm for the enlarged training set, the attribute splits associated with the latter are more accurate with lower information entropy. This added ambiguity resulting from the use of old discretization in the revised tree is, however, offset by the exclusion of their calculation at each node in the subtree during re-

structuring which would otherwise involve substantial computational effort and re-examination of original training set. The updated version (Fig. 20) presents a more complicated representation of the interactions between the decision variables. The original test attribute at node II is pushed down two levels (TC and CF appearing at levels 2 and 3 respectively), while restructuring to ensure that all the test attributes in the subtree below the new node II have minimum E-scores. The updated tree provides three alternative schemes for refinement, evaluation and validation to improve process performance beyond class "C" levels. If it were to be decided to reduce the flowrate to a maximum of 0.1047 l/min, then based on the argument presented earlier the tree (Fig. 20) could be simplified by eliminating nodes I and III and leaves 1 and 2.

5.3.7 Evaluation, refinement and validation:

Of the three leaves, leaf 4 with average crystal production rate of 5.83×10^6 sec^{-1} and size of 67.6 microns seems most promising, for it represents 76.59 % of class C objects and has a certainty factor of 0.923. The operating conditions corresponding to this leaf are, a) FF < 0.1047 l/min, b) TC < 280.94 K and c) CF > 3.508 $kmol/m^3$. Even though the certainty factors associated with leaves 6 and 8 are perfect 1.0, they only represent 12.76 and 10.65 % of the total current class C objects respectively. Average performance of objects in these two zones are 4.68×10^6 sec^{-1} and 65.4 microns and 5.0×10^6 sec^{-1} and 66.3 microns respectively. Process and safety constraints and ease of implementation would determine which of three schemes should be implemented.

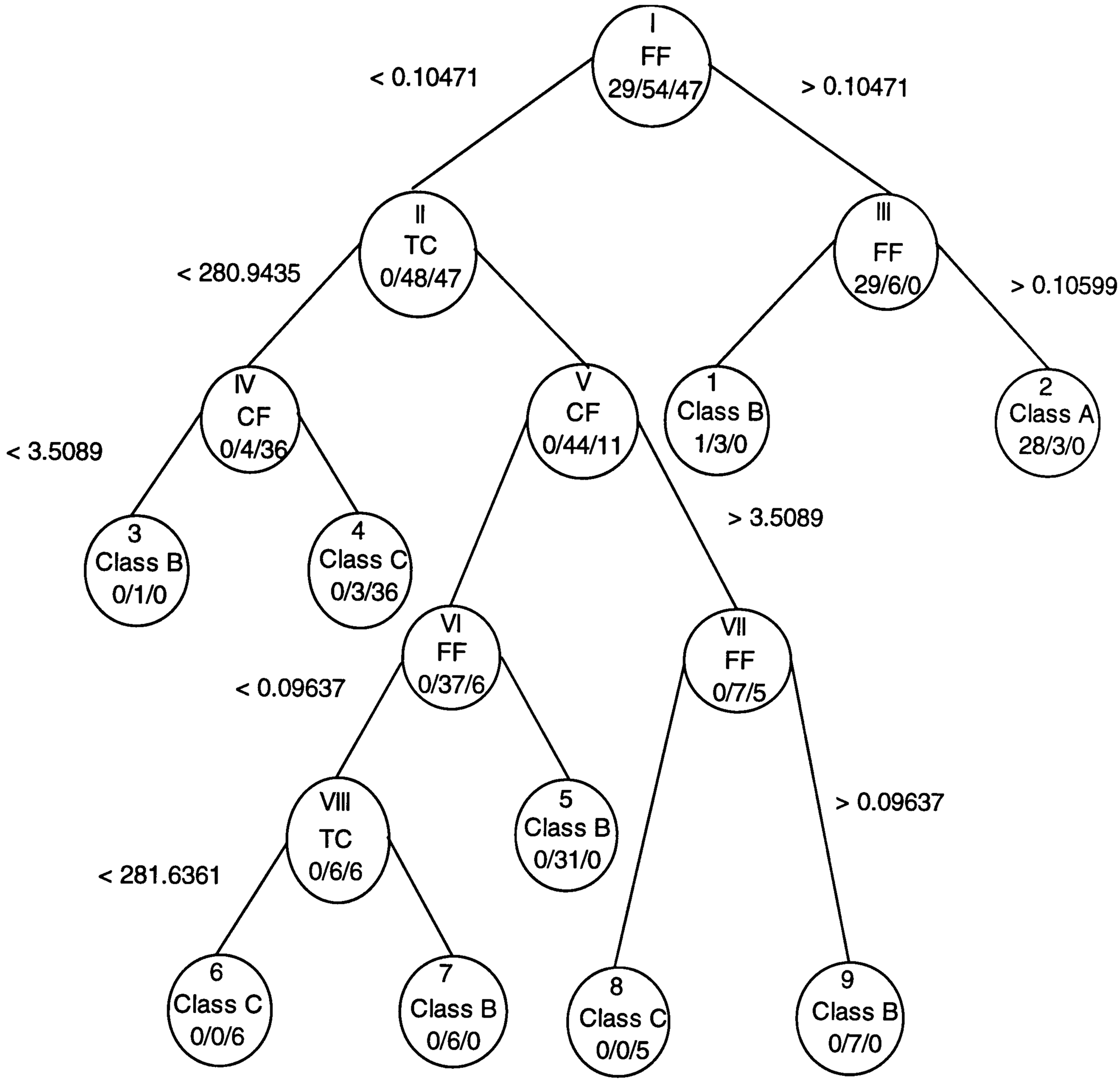

FIGURE 20 : Revised Decision Tree through *ID5R* Algorithm

The update procedure can be re-initiated whenever a novel object is detected by the current generation tree (at case based reasoning step), after implementing one of the performance improvement schemes suggested by it. Since the level of super-saturation and residence time characterise the crystallisation process, it seems reasonable that the three significant features capturing their effect are cooling stream temperature, feed concentration and feed flowrate.

5.4 Conclusions

The revised methodology presented here has been successfully used to quantify performance of the crystallisation process in terms of operating conditions. In two generations of symbolic induction three different operational schemes, representing an increase of nearly 12% on nominal average performance are identified by the methodology without altering the levels of variations specified at the start. The performance level is found to be a strong function of feed concentration and flowrate and cooling stream temperature. These variables reflect the underlying characterisation of the process by super-saturation levels and residence time in the crystallizer. After the implementation of one of the schemes, the performance levels could be re-defined and the procedure for searching further improvements re-initiated. Application of revised machine learning methodology thus provides a new tool for optimisation of crystallisation processes which can utilise both simulated or real plant.

Chapter 6:

EXPERIMENTAL INVESTIGATION INTO THE CONTINUOUS CRYSTALLIZATION OF KNO_3

The operation of continuous crystallizers is marked by cyclic behavior of small crystals and slow damping of disturbances. Effective eradication of these concerns require controlling the number of crystals along with other states of the system. The total number of crystals, however, cannot be measured with accuracy for control purposes because measurement times can be comparable to response times to changes in the inputs, particularly in small scale operations. Development of experimental relationships between available process measurements such as, temperature, flowrate, concentration etc., and the primary control variables hold the potential for making more demanding control objectives accessible. Appreciable interactions between different states, evident from theory and practice together with the sensitivity of process to external disturbances, justify multi-variable control design through modern control theory in feedforward/feedback configuration. Figure 21 shows the general block diagram for the proposed control design. In this scheme, unmeasured but modeled disturbances are fed forward.

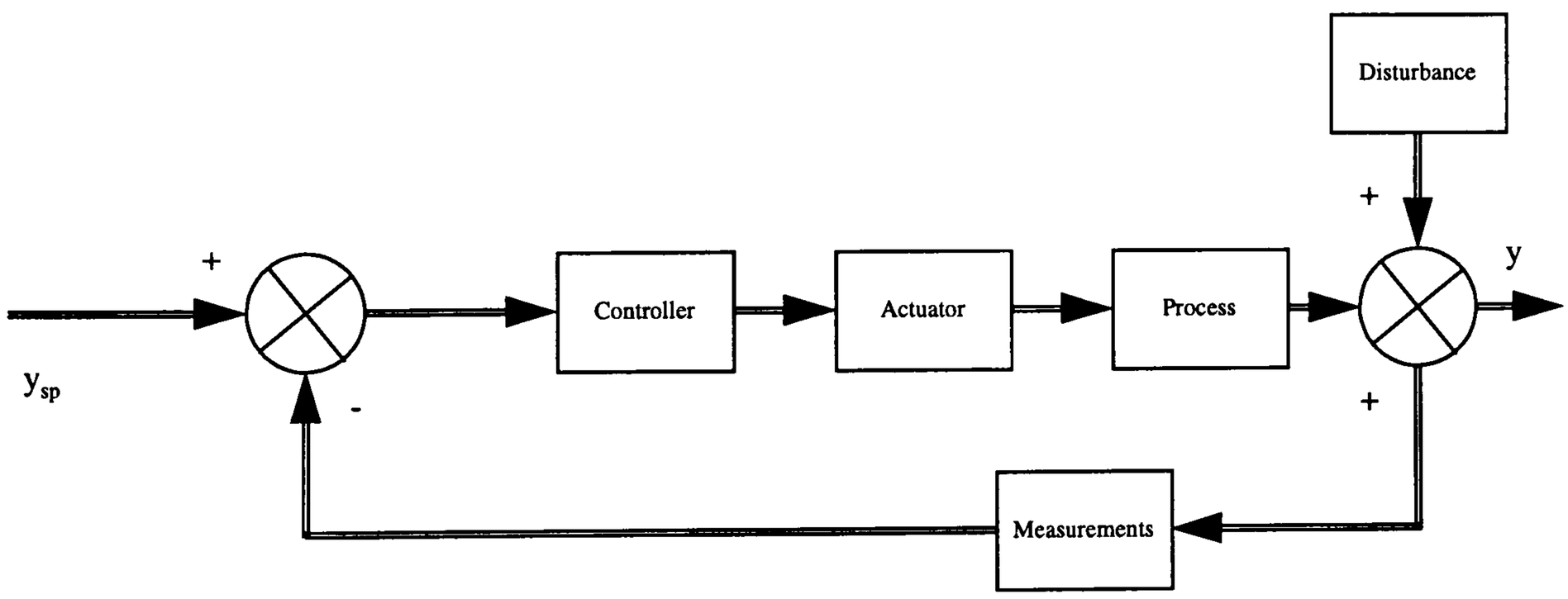

FIGURE 21: Block diagram for feedback control with disturbance rejection capabilities

In this chapter, the experimental investigations necessary to accomplish the above tasks are reported. The experiments are conducted in both steady state and step

response modes for extracting parameters to model the system in Laplace domain and develop regression models relating secondary control variables to primary control variables (see fig. 22). Methods for parameter extraction are also presented. From hereafter, secondary control variables will be referred to as measurements, while inputs will be used interchangeably with manipulated variables.

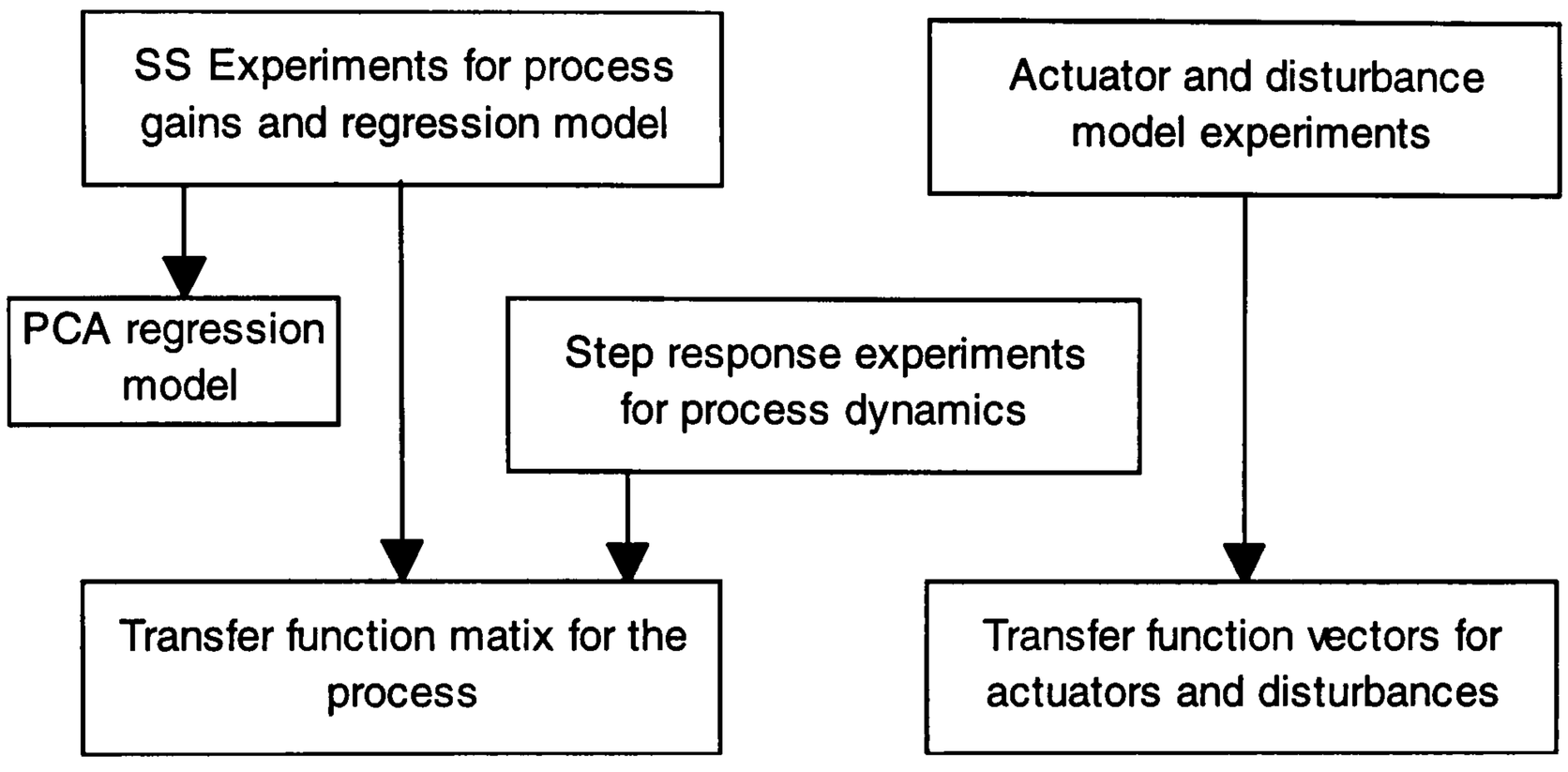

FIGURE 22 : Objectives for the desired experiments

6.1 Apparatus

A schematic of the crystallization system is shown in figure 23. Feed to the crystallizer was supplied from the feed tank at a rate specified through the PC LAB® program. Solution concentration was kept constant throughout the study at a value equivalent to saturation concentration at 288 K, i.e. 2.88 kmol m^{-3}. The flat bottom crystallizer was made out of glass with a working volume of 1 liter and had four equally spaced baffles. Set point temperature within the crystallizer was maintained through a jacket whose temperature and flowrate were regulated by a HAAKE® cooling/heating system. A marine propeller type impeller was used to keep the magma in suspension by forcing the slurry down the center and up against the inside walls of

the vessel. Exit streams, to the product tank and recycle were withdrawn in a way that ensured crystal magma flow was in the same direction. The product stream flowrate was regulated in the same way as the feed stream, while an external variable speed static pump was used in conjunction with a calibrated rotameter to control recycle stream flow. This stream was mixed with fresh feed before re-entering the vessel.

Conductivity and turbidity measurements were recorded and stored on-line through PC LAB® which also logged temperature profiles within the vessel and the jacket. Turbidity measurements obtained from an Analite® 156a nephelometer did not show significant variations until a large fraction of solute had crystallized. This was mainly because KNO_3 crystals are transparent and at small sizes do not contribute to the opaqueness of the solution. The conductivity meter, on the other hand, tracked the reaction curve with reasonable accuracy. Off-line measurements were performed using a Coulter Multisizer II® to obtain a complete crystal size distribution using an orifice tube of 200 μm aperture diameter. The Coulter determines the number and size of crystals suspended in an electrolyte solution by monitoring the electrical current between two electrodes immersed in the conductive liquid on either side of a small aperture through which the crystals are forced to flow. When a crystal passes through the aperture, the impedance between the electrodes changes which produces an electrical pulse with a magnitude proportional to crystal volume. A constant volume of 150 ml Standard Coulter electrolyte, ISOTON II was mixed with 40 ml of slurry from the vessel to prepare the sample. Time mode was used for sampling with a fixed period of 30 seconds.

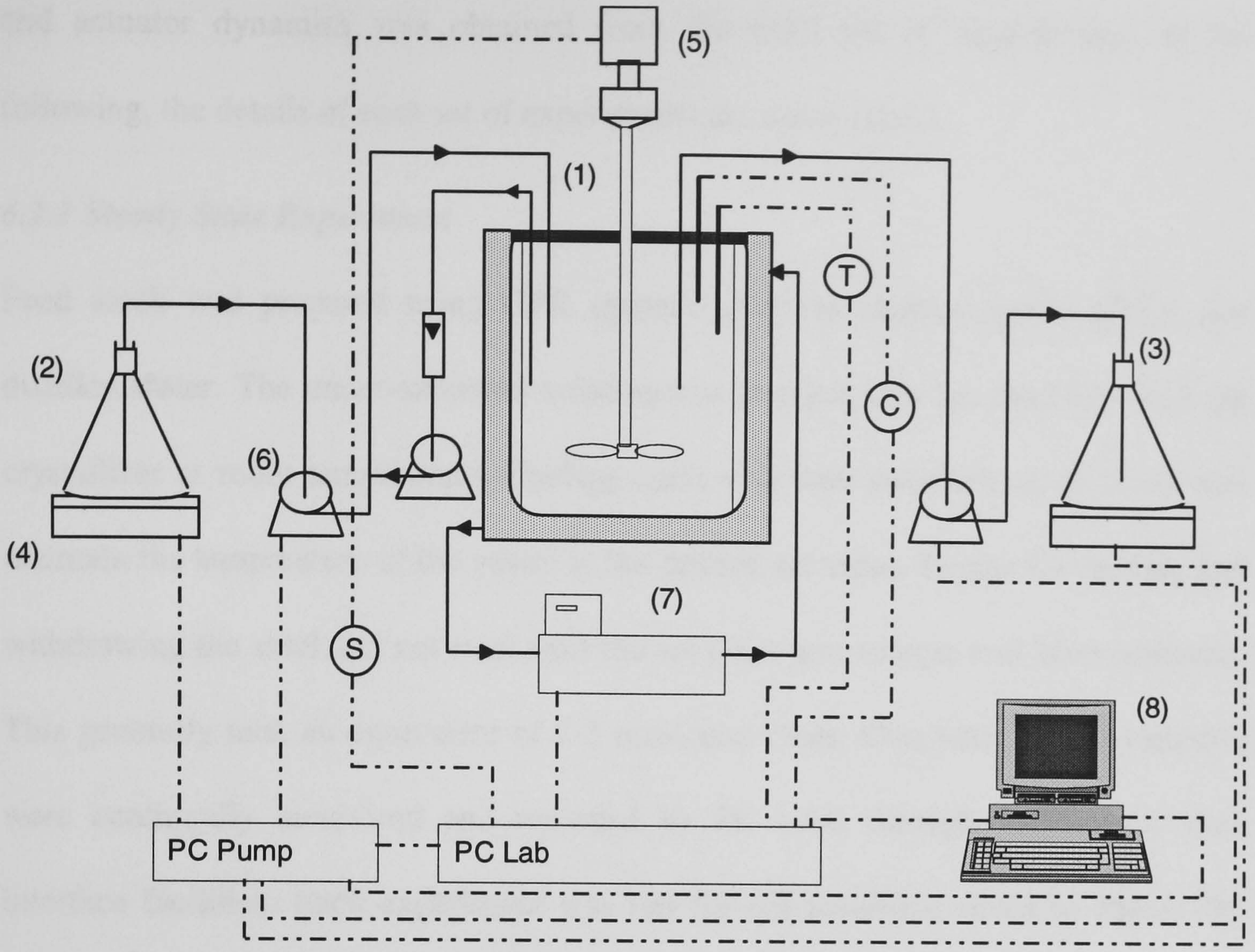

(1) MSMPR crystallizer
(2) Feed tank
(3) Product tank
(4) Balance
(5) Motor
(6) Static pump
(7) Haake heating/cooling unit
(8) On-line PC
(C) Conductivity measurements
(T) Vessel temperature
(S) Stirrer speed measurements

FIGURE 23 : Schematic of the experimental rig

6.2 Experimental

As depicted in figure 22, three different types of experiments were performed. The first set of experiments were steady state experiments which are used to develop a PCA based regression model and to calculate steady state process gains for measurements to inputs. The second set of experiments were performed to model process dynamics for changes in the inputs. In these experiments system response (observed through on-line measurements) was monitored after introducing step change in one of the input to a process at steady state. Data for modelling disturbance

and actuator dynamics was obtained from the third set of experiments. In the following, the details of each set of experiments are summarized.

6.2.1 Steady State Experiment

Feed stock was prepared using GPR (general purpose reagent) grade KNO_3 and distilled water. The under-saturated solution was charged into the feed tank and the crystallizer at room temperature. Cooling cycle was then switched on to lower and maintain the temperature of the vessel at the desired set value. Pumps for feeding and withdrawing the stock did not start until the set point temperature had been achieved. This generally took an equivalent of 2-3 residence times. Conductivity and turbidity were continually monitored and recorded by PC LAB through its external data interface facilities. Each experiment was run for ten residence times to ensure the attainment of steady state. Over this period, three off-line measurements were made for CSD using Coulter Counter.

Seventeen different combinations of operating conditions (listed in table 7) were used to perform an equivalent number of experiments. They cover a broad range of residence times at three different levels of recycle ratios (0.33, 0.6, 1.0) and crystallizer temperatures (285, 286, 287 K). The conditions referred to in experiment 1 were classed as the nominal operating policy. The agitation speed was kept constant at 400 rpm throughout the study.

Experiment No.	Temperature (K)	Flowrates (ml/min)		Residence time (minutes)
		Feed/Product	Recycle	
1	286.0	125.00	75.00	8.0
2	286.0	150.00	50.00	6.6
3	286.0	100.00	100.00	10.0
4	285.0	125.00	75.00	8.0
5	285.0	150.00	50.00	6.6
6	285.0	100.00	100.00	10.0
7	287.0	125.00	75.00	8.0
8	287.0	150.00	50.00	6.6
9	287.0	100.00	100.00	10.0
10	285.0	124.00	42.60	8.0
11	285.0	83.33	83.33	12.0
12	287.0	124.00	42.60	8.0
13	287.0	83.33	83.33	12.0
14	285.0	156.25	93.75	6.4
15	285.0	125.00	125.00	8.0
16	287.0	156.25	93.75	6.4
17	287.0	125.00	125.00	8.0

TABLE 7: Operating conditions for the continuous steady-state experiments

For larger residence times, the experiments had to be paused for re-charging due to the small capacity of feed tank. The operational discontinuity was introduced as early in the experiment as possible to minimize its effect on the final findings. Larger diameter tubes were also used in these experiments for charging/discharging to avoid clogging due to the increased yield of bigger crystals.

6.2.2 Open loop reaction curve experiments

Two reference open loop reaction curves for each measurements were obtained at the conditions represented by experiments 1 & 2 in table 8. Four more curves were derived for each measurement at the two extreme conditions. These correspond to experiments 11 and 16 in table 7.

Since PC LAB does not allow changes in the input file during execution, nor does it have provisions for specifying two sets of operating conditions, an operational discontinuity was unavoidable when perturbing the operation. The perturbations were introduced by momentarily shutting down the system at steady-state for switching over to the input file with new settings. The experiment was allowed to run a further five residence times with these settings to ensure full development of the reaction curve. Table 8 lists the steady-state operating conditions and the conditions after introducing step changes in the inputs for each of the six experiments. A fixed step increase of 30% was used for recycle ratio, while the jacket temperature was dropped by 10% (for most cases the change in RR do not result in a residence times beyond the range depicted in table 7, and therefore would not affect the validity of the gains obtained from steady-state experiments when used with the dynamics estimated from these experiments).

Exp. No	Flowrate ml/min		RR	Jacket Temp K	Flowrate ml/min		RR	Jacket Temp K
	Flow	Recycle			Flow	Recycle		
1	125	75	0.6	288.4	112.35	87.64	0.78	288.4
2	125	75	0.6	288.4	125	75	0.6	286.9
3	83.3	83.3	1.0	287.0	72.46	94.19	1.3	287.0
4	83.3	83.3	1.0	287.0	83.3	83.3	1.0	285.6
5	156.3	93.7	0.6	289.8	140.45	109.55	0.78	289.8
6	156.3	93.7	0.6	289.8	156.3	93.7	0.6	288.1

TABLE 8: Steady state and perturbed levels for the inputs

6.2.3 Experiments for actuator dynamics and disturbance models

Incorporation of actuator dynamics is very important in designs for optimal control, especially for slow reacting actuators. In the current problem the response of jacket temperature to a command is rather slow and therefore of more importance than the

responses of pumps to re-adjust the flowrates. The proposed control design also need disturbance models to relate their effects to the measurements.

6.2.3.1 Actuator Dynamics Experiments

The reaction curve for jacket temperature can be obtained from both the start up data of the steady state experiments or from the step response experiments. Fresh experiments could also be done for the sole purpose of determining the minimum (at highest cooling/heating rate) response time. Since, in all the three experimental modes, an operational discontinuity is unavoidable, in the present study the start-up data was used. It depicts the largest possible changes in the input that could be encountered during control and therefore the response times thus extracted will be an over-estimate, since for both the actuators it was observed that these times increase with the magnitude of command. The actuator curve for jacket temperature was constructed from the transient data depicting its profile from the initial value of room temperature to the final setting. The pumps used the rates of mass removal (from the feed tank) from the time they were switched until the desired rate had been achieved. Similar dynamics was assumed for all three pumps

6.2.3.2 Experiments for Disturbance modeling

In the present design, only fluctuations in product stream flowrates were considered for modeled disturbances. Experiments similar to those for modeling process dynamics were performed. Again the changes were introduced at steady-state in a discontinuous fashion and the affect of disturbance on the two measurements observed over a period of time. In these experiments, however, the magnitude of variations introduced was kept low (~5%) in order to minimize changes in the level of

magma within the crystallizer resulting from an increase in exit flow. Data were recorded from both pulse and step changes, however, the latter was found to be more useful.

6.3 Results and their transformation

In this section, findings of the aforementioned experiments will be summarized and briefly discussed along with the methods used for data transformation. The data relating total number and average size of crystals as measured at steady-state using Coulter counter from the first set of experiments will be subjected to principal component analysis. This will be followed by the development of a regression models relating the two measurements to each of average size and total number. Steady state process gains will also be computed from the findings. Dynamic data from the second and third set of experiments will be used to infer dynamic parameters for Laplace domain modeling of the process, disturbances and the actuators. The technique used for transforming reaction curves into first order plus dead time and first order models will also be discussed.

6.3.1 Steady-state experiments

Though crystals with average size as large as 600 μm have been reported in the literature (Helt and Larson, 1977) for very large residence times (~30 minutes), in the present experiments much smaller crystals were obtained. This was mainly due to the fact that residence time was considerably small and the degree of initial super-saturation was also lower. A maximum mean size of 12.19 μm was obtained from experiment 13 while the largest number of crystals, i.e. 9883 (for 40 ml of slurry diluted with 150 ml of electrolyte sampled for 30 seconds) were obtained during experiment 11. Both the loss of crystals and reductions in average size were expected

during sampling because of dilution. Attempts were made to circumvent the problem by saturating the electrolyte with the solute. Due to the high solubility of KNO_3, however, the conductivity of electrolyte was significantly affected and disabled Coulter Counter from determining a related constant during calibration which rendered the apparatus un-usable. As a consequence, the effect of dilution on dissolution was assumed to be uniform for all the experiments and therefore the actual magnitude of the findings for average size and total number will not truly represent the slurry. The relative magnitudes of average size and number from the experiments which are listed table 9, however, represent the trends correctly and will suffice for the control purposes of the experimentation. The complete size distribution as measured by the Coulter counter for experiment 1 is shown in figure 24. Conductivity entries represent the net change over the length of the experiment in milli-siemens (mS).

Exp. No.	Input 1 TJ (K)	Input 2 RR	Measurement 1 Vessel Temp, TV (K)	Measurement 2 Cond. (mS)	1" Control variable 1 Total Number	1" Control variable 2 Av. Size
1	288.40	0.60	286.00	16.00	2886	7.64
2	289.20	0.33	286.00	14.00	2613	7.46
3	287.60	1.00	286.00	20.00	5747	8.32
4	287.30	0.60	285.00	22.00	7728	7.42
5	287.90	0.33	285.00	16.00	2720	7.69
6	286.80	1.00	285.00	24.00	6181	8.92
7	290.20	0.60	287.00	13.00	2390	9.53
8	290.70	0.33	287.00	10.00	2312	8.64
9	289.80	1.00	287.00	15.00	2360	10.52
10	288.00	0.33	285.00	18.00	3355	8.64
11	287.00	1.00	285.00	26.00	9883	9.85
12	290.90	0.33	287.00	12.00	2086	8.93
13	290.00	1.00	287.00	17.00	2958	12.19
14	287.10	0.60	285.00	15.00	7141	5.67
15	286.50	1.00	285.00	17.00	3620	6.92
16	289.80	0.60	287.00	10.00	2206	6.51
17	289.50	1.00	287.00	8.00	2178	7.14

TABLE 9: Summary of the results from steady-state experiments.

The readings for jacket temperature are at the exit of the jacket; this means that an increase in vessel temperature would be indicated by an increase in jacket temperature and vice-versa. It can be seen from the above table that conductivity (measurement 2), shows a positive relationship with recycle ratio and negative with jacket temperature. The reverse is true for vessel temperature which drops with an increase in recycle ratio and increases with increasing jacket temperature.

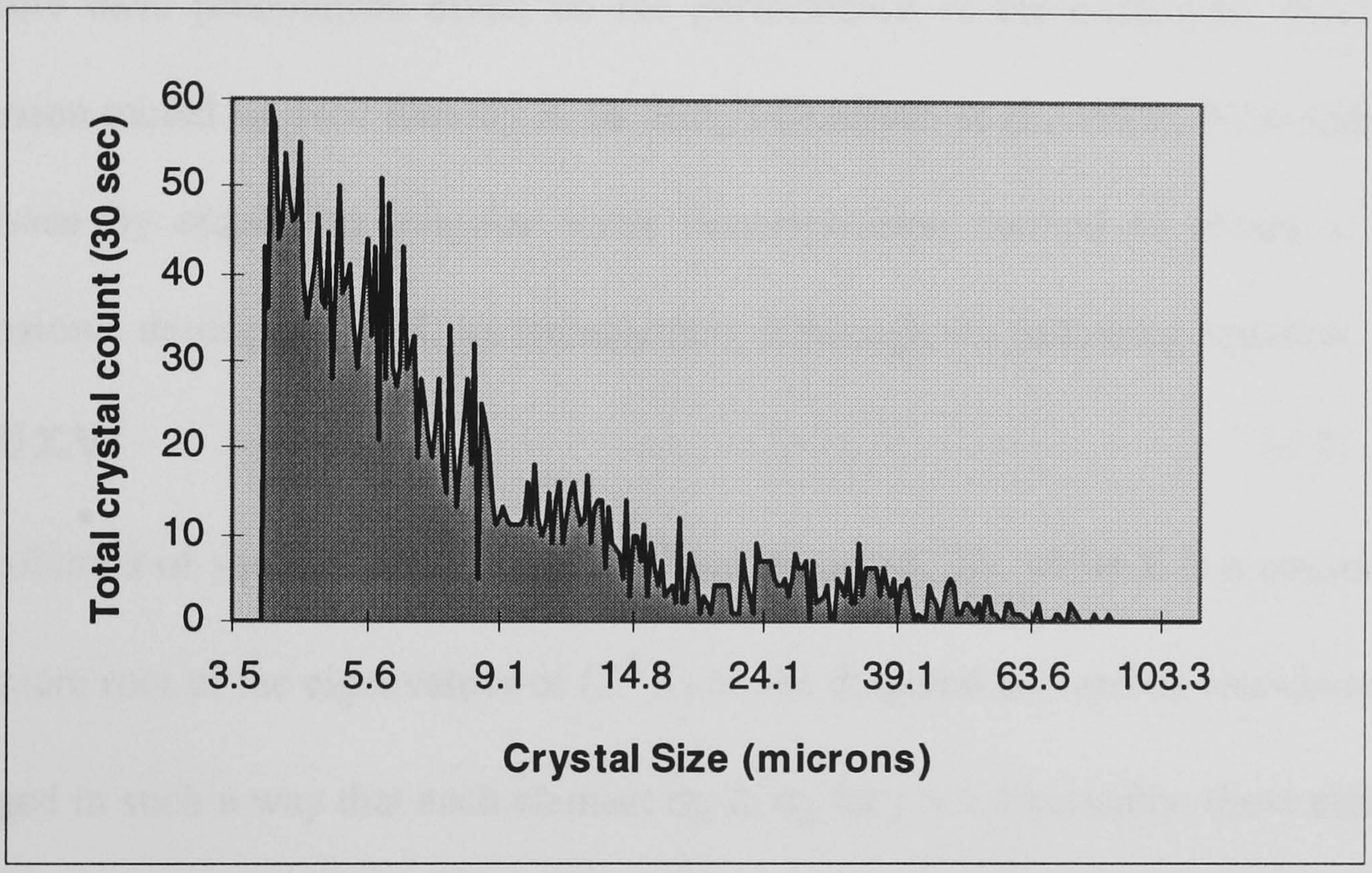

FIGURE 24 : Crystal size distribution of KNO_3 crystals from experiment 1 (table 6)

6.3.1.1 Theoretical background to PCA based regression analysis

Principal component analysis, which in conjunction with multi-variable linear regression is used to develop relationships between the two measurements and each primary control variable, seeks to minimize the squared error between measurements of primary variables and their predictions from secondary measurements. The technique is directly related to classical least squares linear regression methods that

attempts to find the elements of vector $\boldsymbol{r}$ (dimension equal to the number of measurements) in equation 6.1 through the manipulations depicted in equation 6.2.

$$y = \mathbf{X}r \tag{6.1}$$

$$r = \left(\mathbf{X}^{\mathrm{T}}\mathbf{X}\right)^{-1}\mathbf{X}^{\mathrm{T}}\,y \tag{6.2}$$

Though $\boldsymbol{r}$ is optimally determined through Eq. 6.2, the relationship thus obtained can be very sensitive to noise if the condition numbers for the matrix $\mathbf{X}$ are high, and will therefore have pronounced effect on the performance of the controller, should the regression model be used directly in its design (Budman et al., 1992). PCA addresses this issue by employing singular value decomposition method to obtain a lower dimensional description of $\mathbf{X}$, by transforming it through the following equation.

$$\mathbf{X} = \mathbf{U}\,\boldsymbol{\Sigma}\,\mathbf{V}^{\mathrm{T}} \tag{6.3}$$

The columns of square matrix $\mathbf{V}$ are eigenvectors of $(\mathbf{X}^{\mathrm{T}}\mathbf{X})$, while $\boldsymbol{\Sigma}$ is a matrix with the square root of the eigenvalues of $(\mathbf{X}^{\mathrm{T}}\mathbf{X})$ on the diagonal and zeroes elsewhere. $\boldsymbol{\Sigma}$ is arranged in such a way that each element $\sigma_{ii} \geq \sigma_{jj}$ for $j > i$. Physically, these elements provide a measure of variance within the data in the direction described by the columns of $\mathbf{V}$. Directions with small eigenvalues have little variance and therefore their removal is desirable because it tend to decrease noise sensitivity. This is done by building a matrix $\mathbf{W}$ with first n columns of $\mathbf{V}$, where n is specified by the user. These columns correspond to directions with n largest eigenvalues. The regression parameters of vector r for the reduced system are obtained from equation 6.4.

$$\bar{r} = \left(\mathbf{W}^{\mathrm{T}}\mathbf{X}^{\mathrm{T}}\mathbf{X}\mathbf{W}\right)^{-1}\mathbf{W}^{\mathrm{T}}\,\mathbf{X}^{\mathrm{T}}\,y \tag{6.4}$$

The number of directions is usually determined through cross validation, where only a portion of available data is used to develop a trial relationship with pre-determined

number of directions. As the number of directions is varied, the performance on the withheld data used for model evaluation varies. The procedure is continued until an optimum number for data size is determined.

6.3.1.2 The PCA based model

The procedure outlined in the preceding section was employed to develop two empirical relationships between measurements and each of the two primary control variable. NAG® routine G03AAF was used to perform principal component analysis. It provided both the principal component loadings and principal component scores. These were analyzed to determine the optimal size of matrix, **W**, which was found to be ten. The data from the corresponding ten experiments was used to develop the following equations that provide estimates for average crystal size and total number in the same units as those from Coulter counter.

$$L_{est} = 0.33973 \times Cond + 1.88197 \times T_{vessel} - 21.57008 \qquad (6.5)$$

$$N_{est} = 322.61582 \times Cond - 502.81154 \times T_{vessel} + 5377.13121 \qquad (6.6)$$

Table 10 exhibits the comparison between actual measurements for the two primary control variables and their estimates from regression equations at the extremes.

Real Measurements		Estimates		% Error	
T. Number	Av. Size	T. Number	Av. Size	T. Number	Av. Size
2886	7.635	4002	8.331	27.9	8.4
2360	10.15	3117	9.873	25.7	2.8
5747	8.322	5293	9.690	8.57	14.1

TABLE 10: Accuracy of estimates from PCA based regression models

6.3.1.3 Process Gain Estimates

Steady state process gains are simply calculated by dividing the net change in measurements with a corresponding change in the inputs from any two steady state

experiments. The values for process gains are calculated from all the possible pairs of experiments listed in table 7. These were used to determine the mean and bounds for gains that are depicted in table 11. The means will be used in the transfer functions approximating process dynamics, while the bounds will be employed during the robustness analysis of the controller.

Gain	Mean	Bounds
$K_{TV,TJ}$	0.66	±0.1
$K_{TV,RR}$	-0.25	±0.04
$K_{CO,TJ}$	-5.0	±0.4
$K_{CO,RR}$	11.1	±1.3

TABLE 11 : Mean and bounds for the four steady-state gains

6.3.2 Dynamics experiments

In the following, the dynamic data is reported. All the responses have been scaled up according to the steady-state gain values to facilitate comparison of their relative significance.

6.3.2.1 System Dynamics

The reaction curve for vessel temperature (fig. 25) obtained from experiment as defined in table 7, shows that it falls with jacket temperature. This is in line with the findings from steady-state experiments (direct relationship as seen in the gain) and the physics of the apparatus. It can also be observed that, though initially small in magnitude, an immediate response is shown by the vessel temperature to changes in jacket temperature. This would suggest the opportunity for approximating the dynamics between this pair of input and output without dead time compensation. The reaction curve nearly took 140 seconds (~ 2.5 minutes) for completion. Very little

noise is observed in the response curve which would help accurate extraction of transfer function parameters.

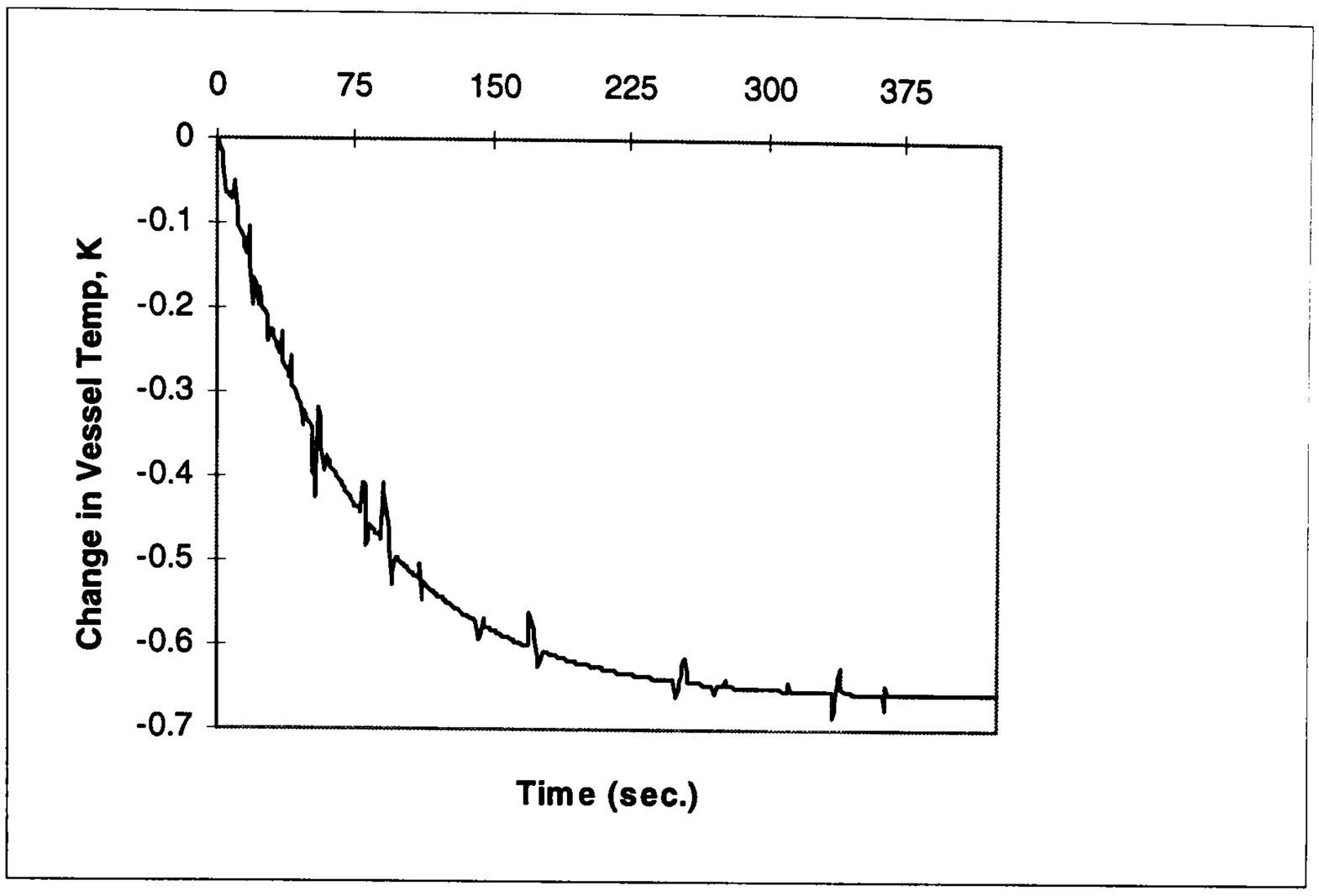

FIGURE 25: Response of vessel temperature to unit step change in jacket temperature

The response of conductivity to the change in jacket temperature (fig. 26) also shows a tame but immediate response. It, however takes 400 seconds or nearly 1.25 residence time to completion. Some noise is observed during the early stages.

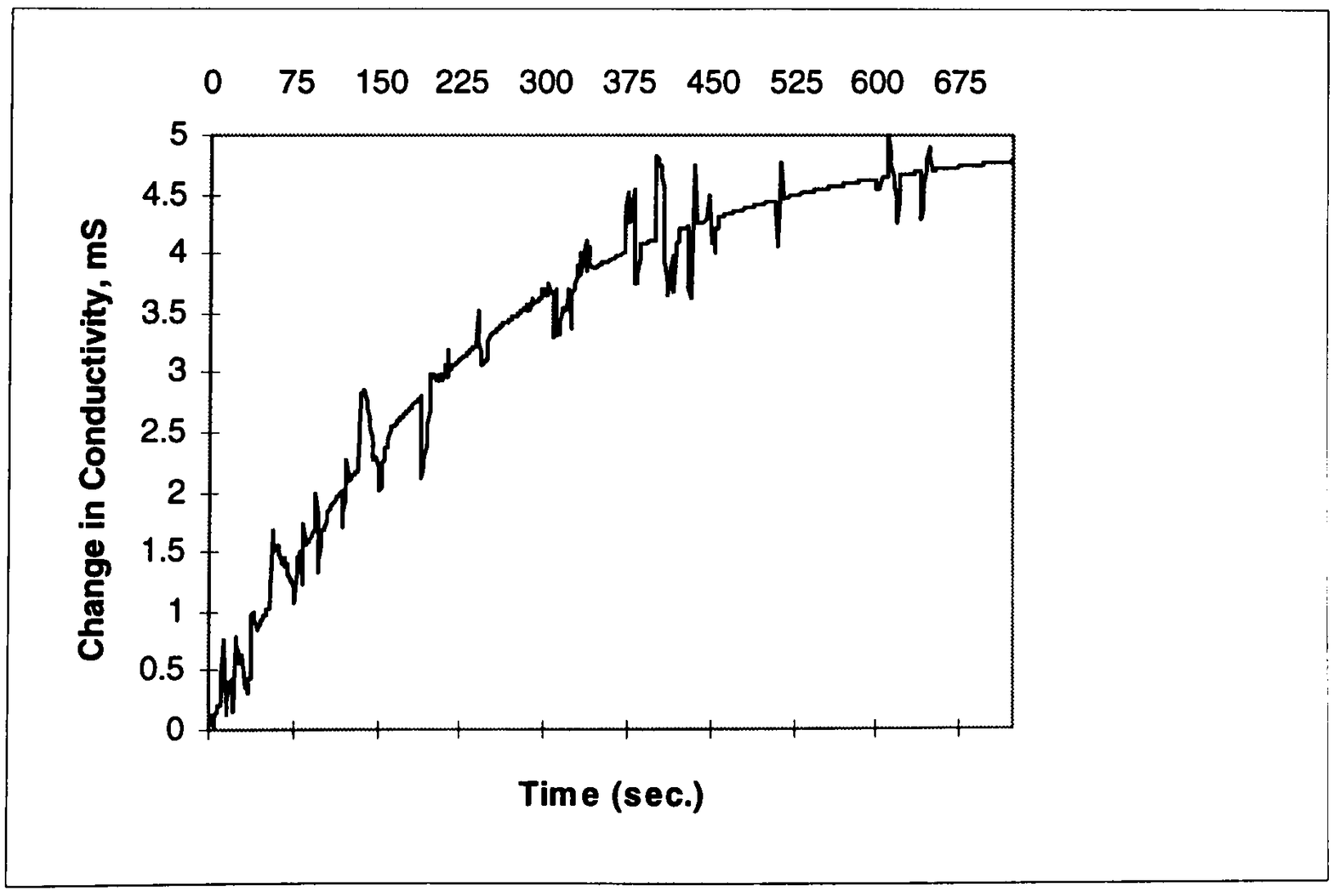

FIGURE 26: Conductivity response to unit change in jacket temperature

Figure 27, shows the response of vessel temperature to change in recycle ratio. No immediate changes were observed. This suggests the need for dead time compensation in transfer function for effective modeling of the dynamics between the two variables. The profile took nearly 3.5 minutes (217 seconds) to fully develop.

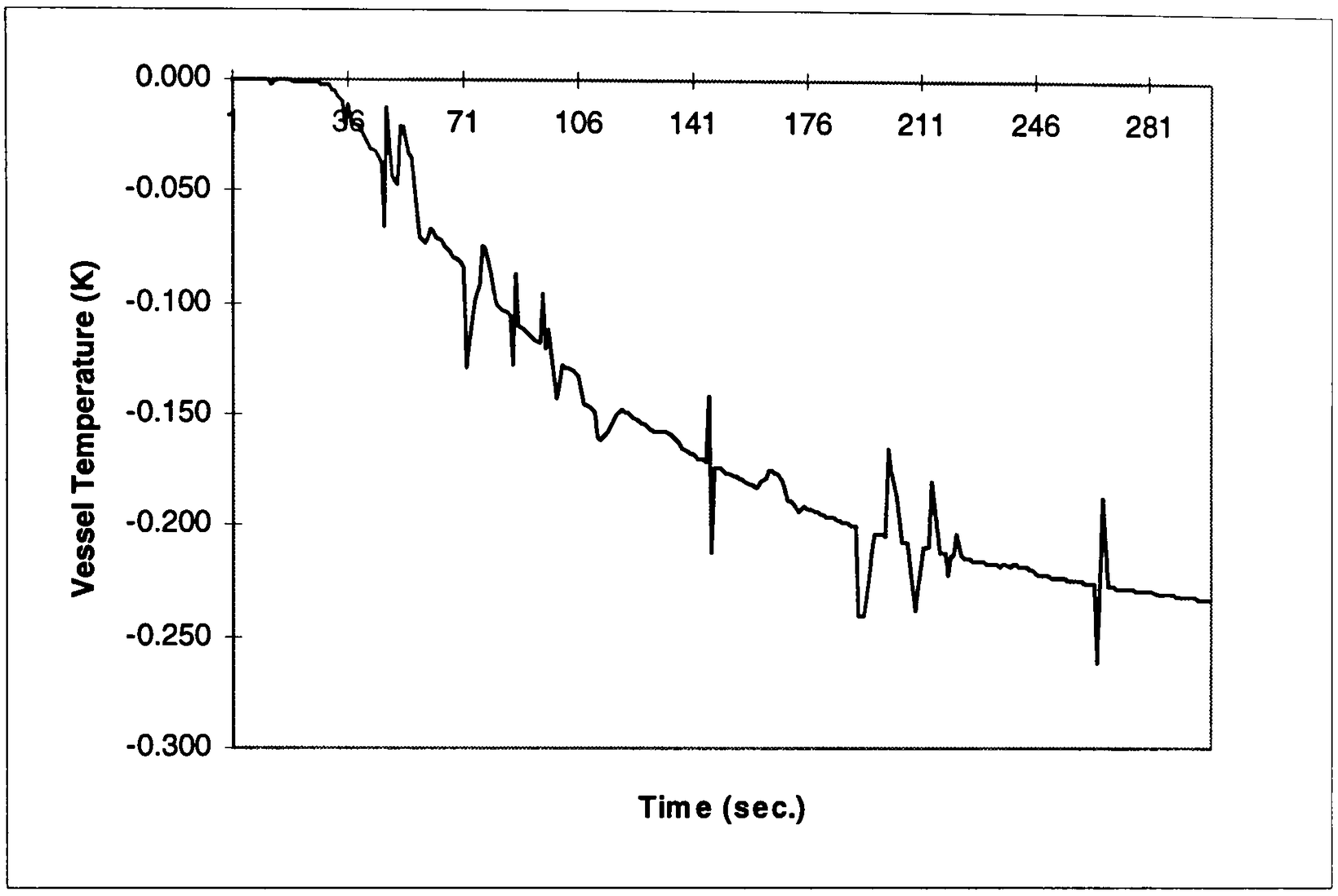

FIGURE 27 : Vessel temperature response to changes in recycle ratio

The conductivity response also suggested the need for dead time compensation, this time, however, of a slightly larger magnitude (fig. 28). The response time to completion was 368 seconds. Given the nature of conductivity measurements, some noise is again apparent.

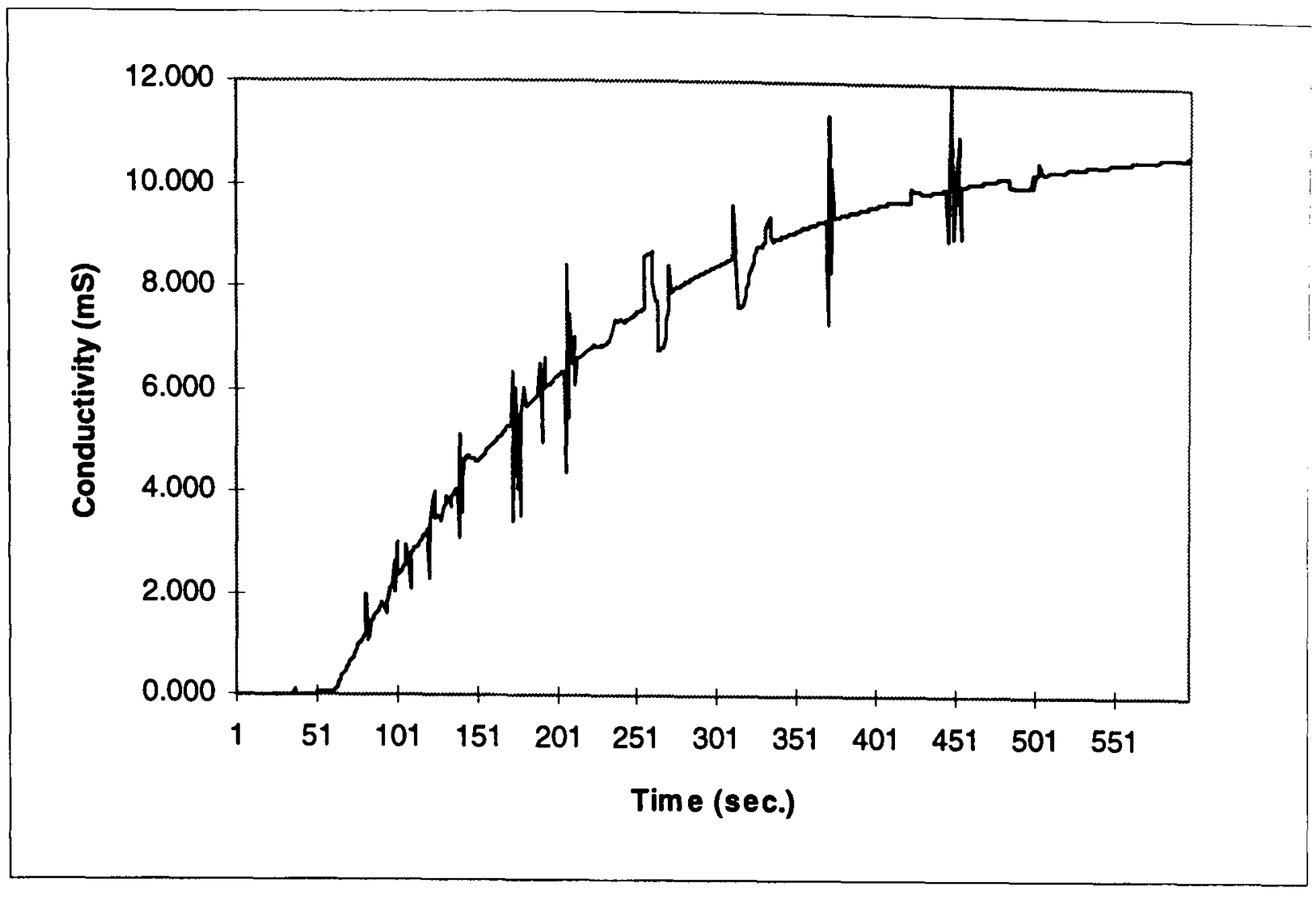

FIGURE 28 : Conductivity response to nominal change in recycle ratio

The other four experiments listed in table 8 (3-6 inclusive), were monitored in a similar way. Their findings will be used to establish bounds on the parameters extracted from the experiments performed under nominal operating conditions.

It is evident from the above findings that responses to changes in jacket temperature can be approximated by first order models only, whereas curves for conductivity and vessel temperature obtained by perturbing recycle ratio also require dead time compensation.

6.3.2.2 Actuator dynamics and disturbance modeling

Step response experiments for determining actuator dynamics reveal that the pumps respond quicker to changes in command then the jacket temperature (see figures 29 and 30). It took nearly 50 seconds for the attainment of a 1 K change in jacket temperature, while the pumps achieved the new set point in under 10 seconds. The gains are one in these, because the output is a response to change in its own set point.

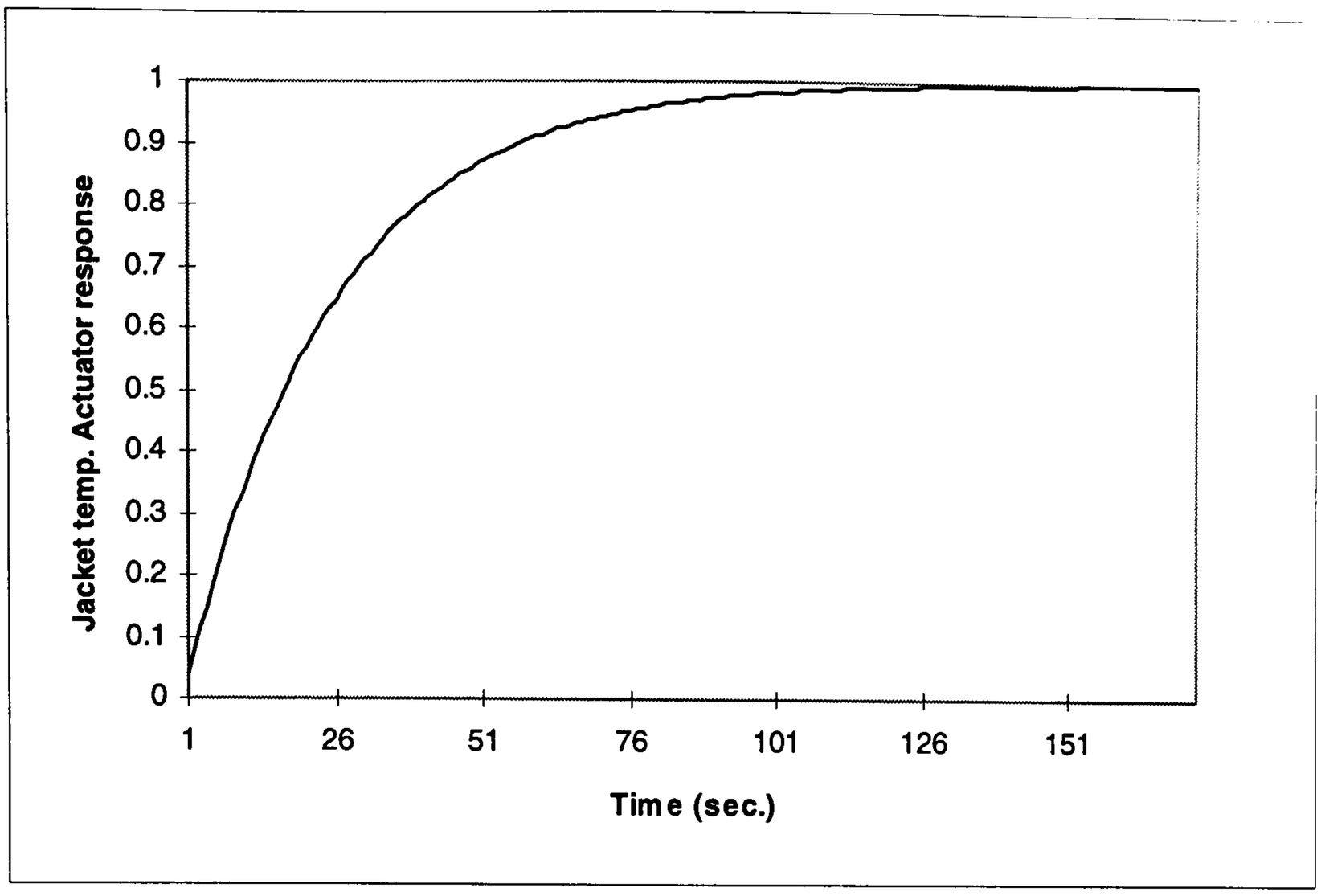

FIGURE 29: Actuator Response time for the jacket temperature

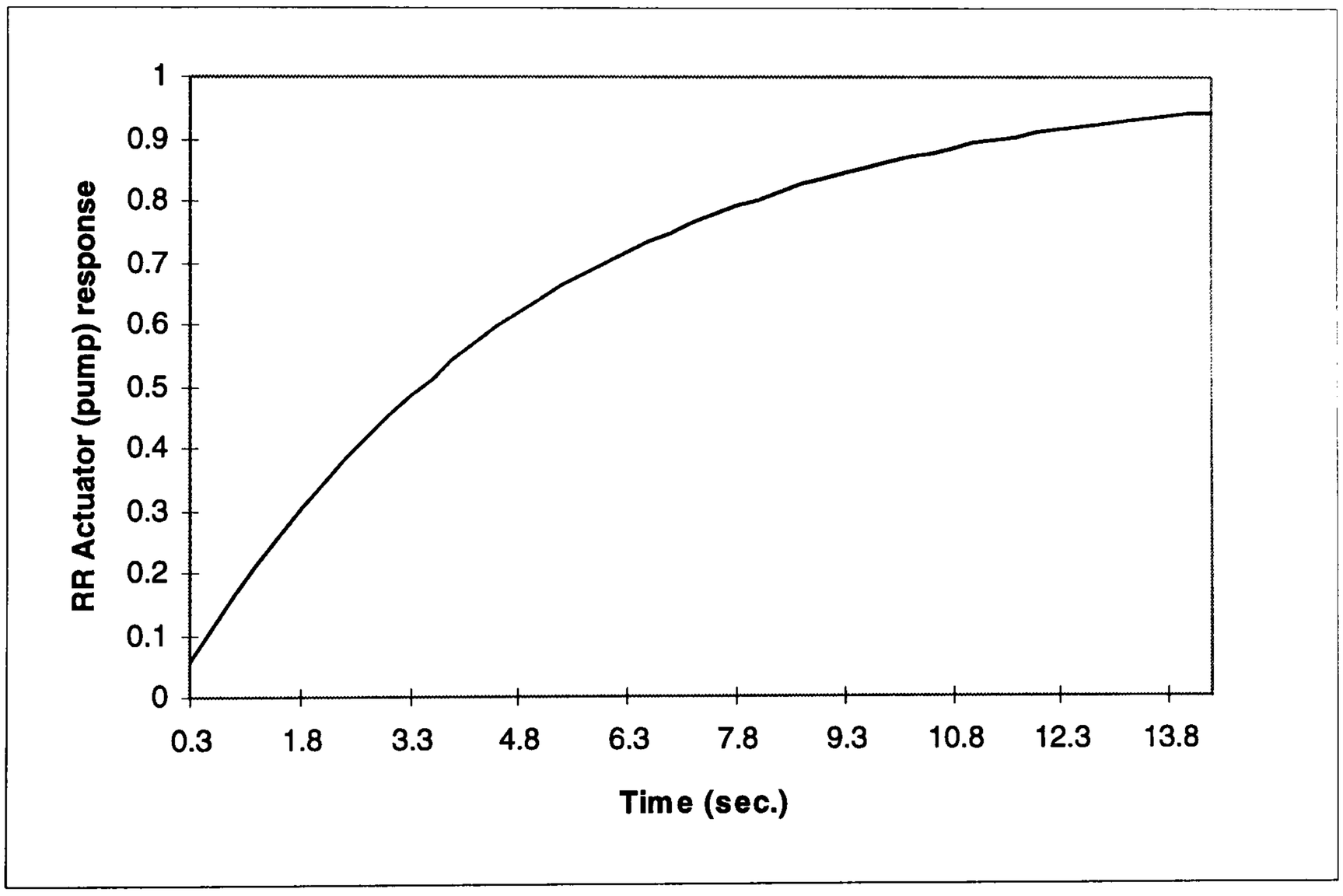

FIGURE 30 : Dynamics of the actuator for controlling recycle ratio through the pumps

Similar experiments to quantify the effects of fluctuations in exit stream flow rate on conductivity and vessel temperature indicated that the latter responds quicker than the former. It took 3 minutes for vessel temperature to register response completion while nearly four minutes were required for the development of the conductivity reaction

curve to reach the new steady state (fig. 31 and 32). The gains for the measurements were found to be 0.05 and -3.0 respectively for a unit change in the input defined earlier.

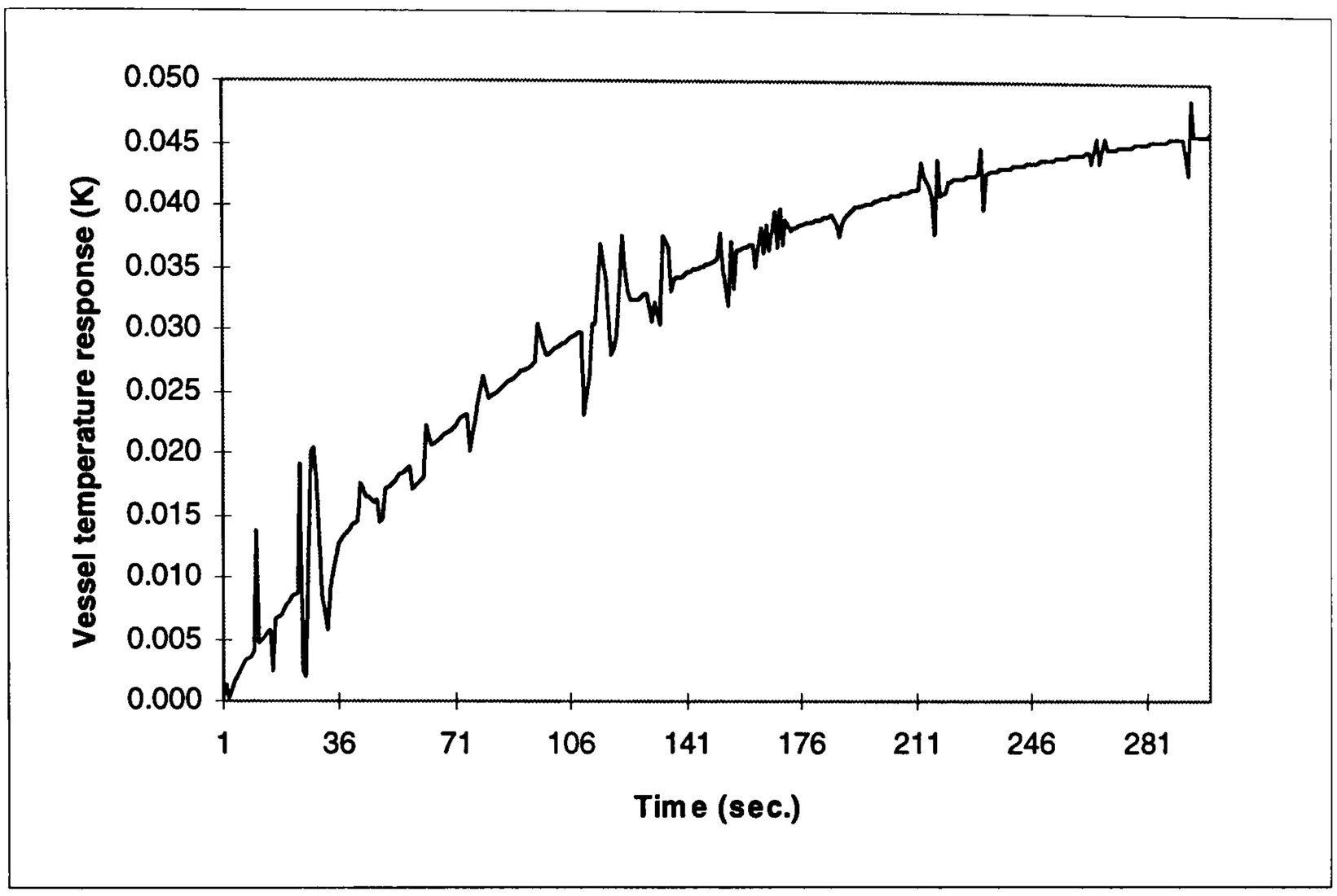

FIGURE 31: Response of vessel temperature to disturbance in product flow rate

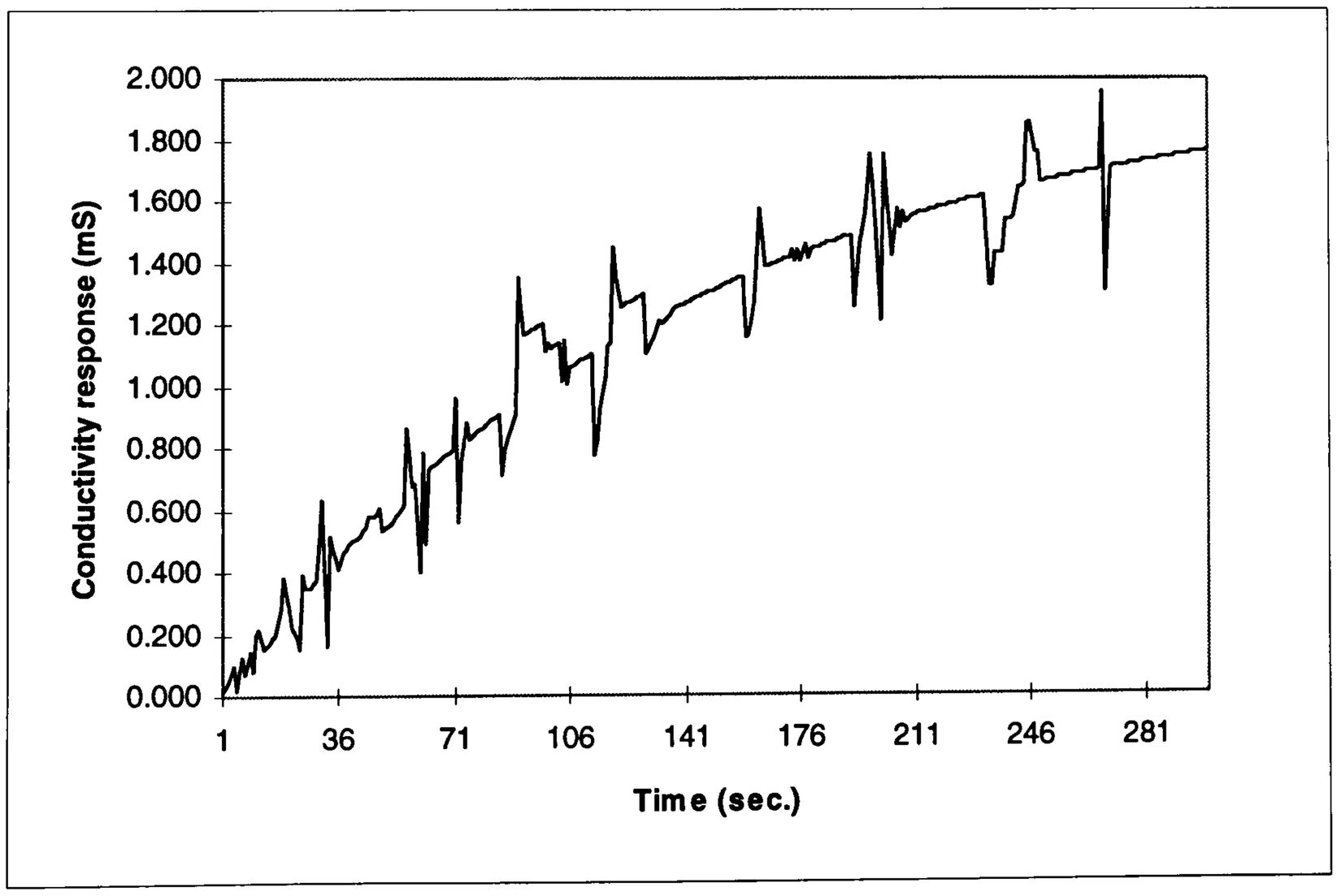

FIGURE 32 : Response of conductivity to disturbance in product flow rate

6.3.3 Estimation of time delays and time constant

In this work, a method developed by Sundaresan and Krishnaswamy (1978) to optimise "two points selection" in Smith's procedure (Smith, 1972) will be used for estimating delays and time constants in first order plus dead time (FOPDT) and first order approximations of system dynamics. The models take the following general form

$$G(s) = \frac{k}{\tau_s s + 1} \tag{6.7}$$

$$G(s) = \frac{k\, e^{(-\tau_d s)}}{\tau_s s + 1} \tag{6.8}$$

The method requires FOPDT approximation curve, $\bar{y}(t)$ to intersect the actual response curve $y(t)$ at least at two points (fig. 33). The FOPDT equation is solved in time domain at these intersection points to obtain the following equations for τ_d and τ_s,

$$\tau_d = \frac{t_2 \ln f_1 - t_1 \ln f_2}{\ln\left(f_1 / f_2\right)} \tag{6.9}$$

$$\tau_s = \frac{t_2 - t_1}{\ln\left(f_1 / f_2\right)} \tag{6.10}$$

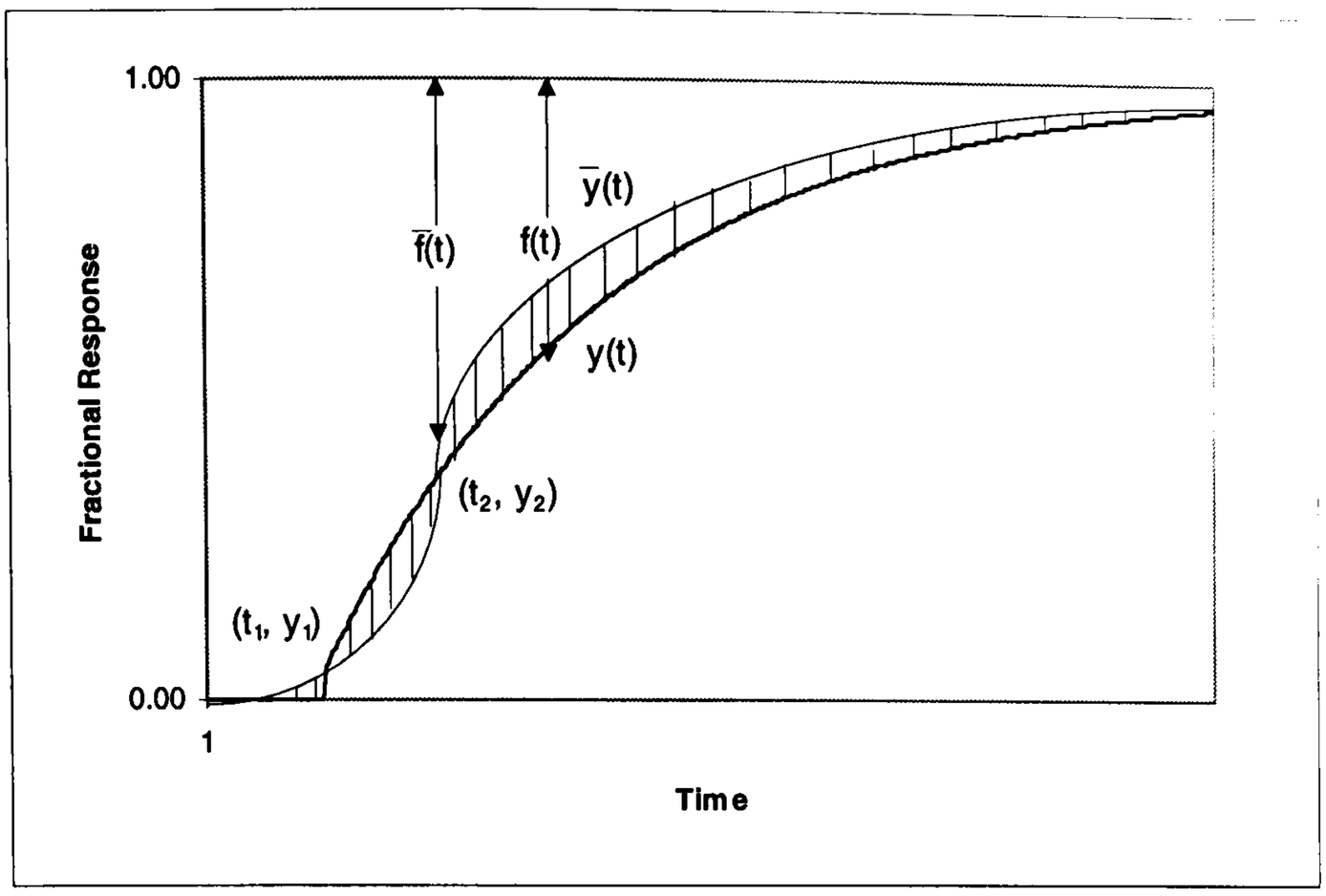

FIGURE 33: Process transient response and delay time approximation

Equation for the enclosed area between the curves (fig. 33) is then,

$$I = \tau_d + \tau_s - \int_0^{\infty} f(t)dt + 2\int_{t_1}^{t_2} \left[f(t) - \bar{f}(t) \right] dt \qquad (6.11)$$

This is differentiated with respect to τ_d and τ_s and the derivative equations set equal to zero to obtain the following relationships for f_1 and f_2,.

$$f_1 = f_2 + 1/2 \qquad (6.12)$$

$$f_1 \ln f_1 = f_2 \ln f_2 \qquad (6.13)$$

Simultaneous solution of these equations provide the optimal values for f_1 and f_2, which minimize the cumulative area of the region representing the deviations between the actual and approximated response. These values can then be used in equations 6.8 and 6.9 to find the corresponding values for the delay and time constant. The solution yields a value of 0.647 for f_1 and 0.147 for f_2.

Based on the above method, the appropriate parameters for the four transfer functions representing system dynamics and two each for actuator and disturbances are

calculated by reading the values for time at f_1 and f_2. The complete set of parameters for all the transfer functions are tabulated in table 12.

Transfer Function	Time constant (sec.)	Dead time (sec.)	Nominal Gain
$G_{TV,TJ}$	70		0.66
$G_{TV,RR}$	102	30	-.25
$G_{CO,TJ}$	230		-5.0
$G_{CO,RR}$	168	63	11.1
$G_{AC,TJ}$	30		1.0
$G_{AC,RR}$	5		1.0
$G_{TV,\eta}$	120		0.05
$G_{CO,\eta}$	138		-3.0

TABLE 12: Parameters for experimental dynamics of the crystallization system

6.4 Conclusions

In this chapter, details of the experiments performed for steady state analysis and system identification have been provided. The experimental data has been analyzed and transformed to obtain a transfer function matrix for the process along with similar vectors representing actuator dynamics and disturbance models. These findings will be used in the next chapter to develop a multi-variable optimal control system for the present problem.

Chapter 7:

MULTI-VARIABLE OPTIMAL CONTROL FOR A CONTINUOUS KNO_3 CRYSTALLIZER

In this chapter, a multi-variable robust controller capable of inferentially controlling average size and total number of crystals is developed through optimal control theory by using LQG/LTR design procedure with MATLAB. Requirements on the controller include specifications for stability, responses to changes in set points and disturbances, transient behaviour of the process itself and controller robustness. The robustness with regards to the observer is addressed through loop transfer recovery (LTR) method where the original problem for observer design is modified by introducing fictitious process noises at the control inputs. In effect, the estimator is over designed at the LQG step, so that the lost robustness due to state estimation could be recovered in the closed-loop. Controller robustness is analysed by observing performance through closed loop simulations with the extremes in process parameters identified in the previous chapter. The design steps which have been isolated with the aid of case studies presented in Gangaas et al. (1986) are sequenced in the flowchart presented in figure 34. Figure 35 elaborates on the decision steps within figure 34.

The crystallization system described in the previous chapter has many inputs and outputs which are interrelated in complicated manner. To analyse such a system, it is essential to reduce the mathematical complexity of the system representation. The state-space approach which forms the basis of modern control is best suited from this viewpoint.

In the next sub-section, the general form of state-space representation, its properties, state space realisation from transfer functions and augmentation of such representations to develop a complete experimentally determined model will be presented. This section will be followed by a sequence, closely based on the design steps depicted in figure 34.

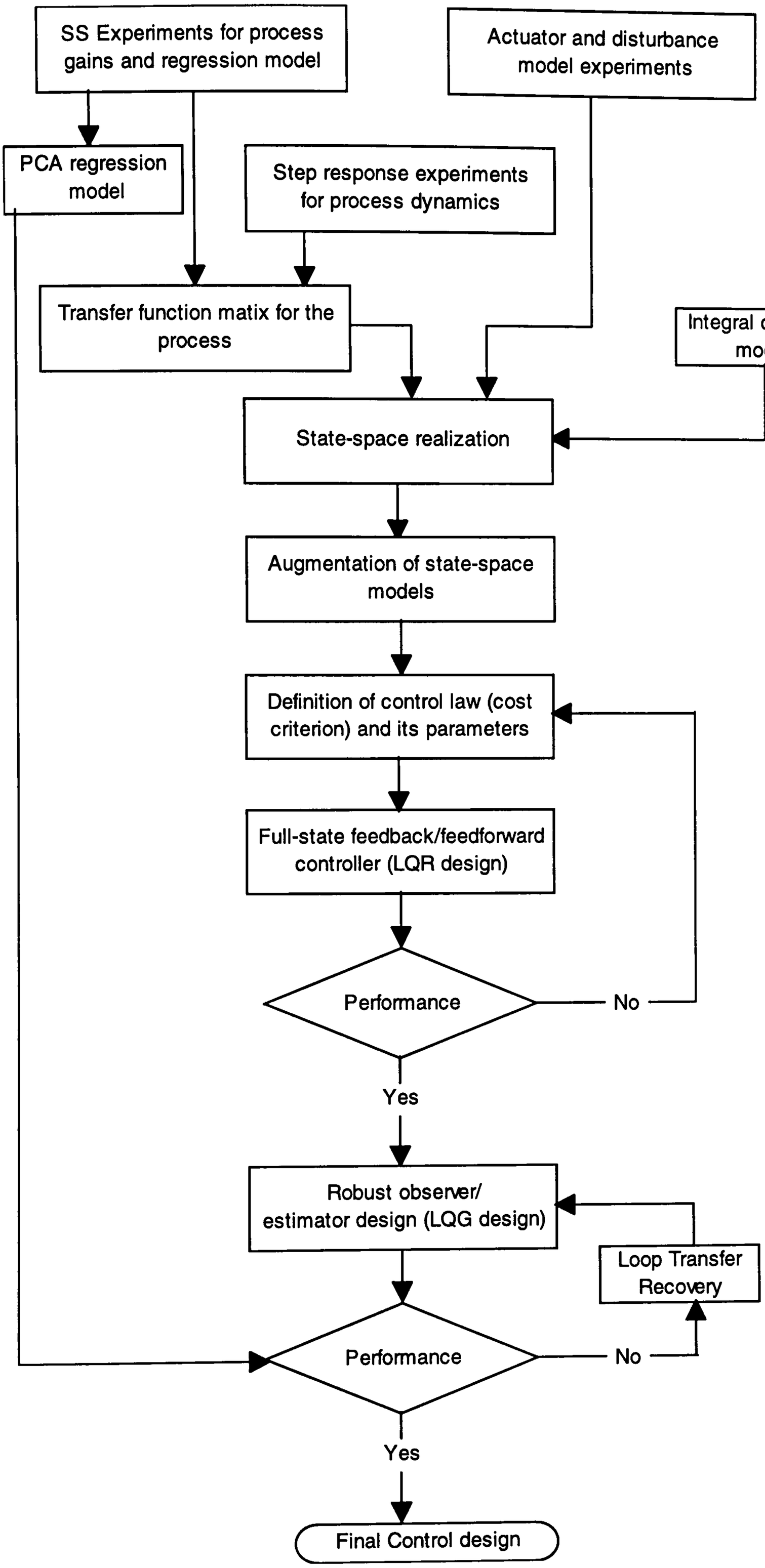

FIGURE 34 : Multi-variable optimal controller design procedure

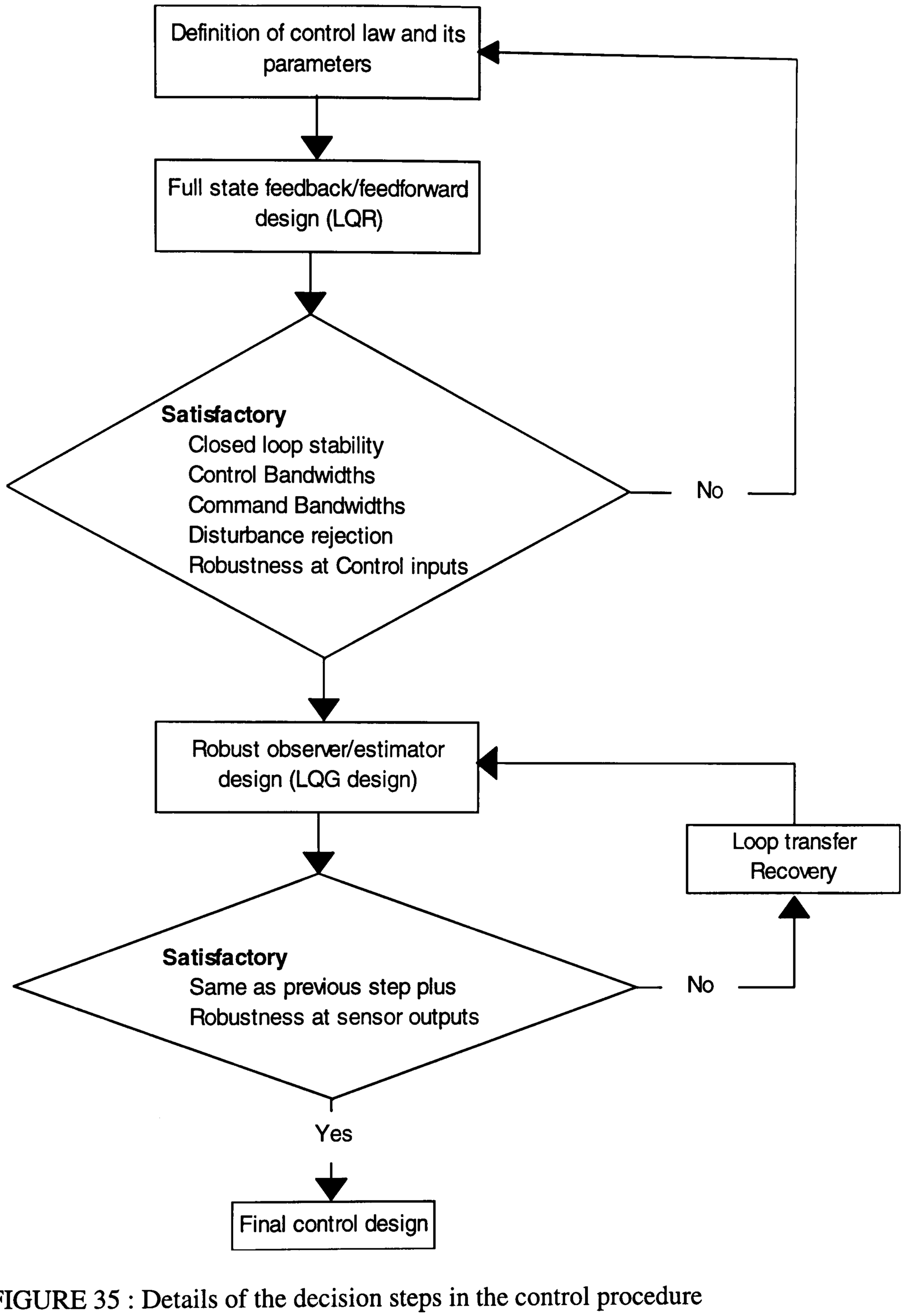

FIGURE 35 : Details of the decision steps in the control procedure

7.1 State-space representation

As stated earlier, modern control theory is based on state-space process models. They represent first order differential equations that may be combined into a first order vector matrix. The notation simplifies the underlying mathematics to an extent, that analysis of complex MIMO systems can be carried out by procedures that are only slightly more complicated then those used for the study of first order scalar differential equations (Ogata, 1997).

The general description of dynamic system in time domain with state space representation is given by

$$\sum : \begin{cases} \dot{x} = \mathbf{A}\, x(t) + \mathbf{B}\, u(t) \\ y = \mathbf{C}\, x(t) + \mathbf{D}\, u(t) \end{cases} \tag{7.1}$$

The system is completely defined by the constant matrices **A**, **B**, **C** and **D** of dimensions; $\mathbf{A} \in \mathcal{R}^{n \times n}$, $\mathbf{B} \in \mathcal{R}^{n \times m}$, $\mathbf{C} \in \mathcal{R}^{p \times n}$ and $\mathbf{D} \in \mathcal{R}^{p \times m}$ respectively.

The frequency domain description in Laplace form can be recovered from the above four matrices through the following equation.

$$G(s) = \mathbf{C}(s\mathbf{I} - \mathbf{A})^{-1}\mathbf{B} + \mathbf{D} \tag{7.2}$$

Stability of the system represented in state-space form is governed by the eigenvalues of the state matrix **A**. These are the roots of the characteristic polynomial, det ($\lambda\mathbf{I}$-**A**)=0 and are often referred to as the poles of the system. The system (eq. 7.1) is asymptotically stable if the real parts of eigenvalues are strictly negative. It is neutral or marginally stable if one of the eigenvalues has a real part equal to zero and the process is unstable if the real part of at least one of the eigenvalues is strictly positive. Besides the stability of the system, there are two other fundamental properties of the system that need to be considered in the analysis of open loop dynamics for control

design through state-space representation; they are controllability and observability. The conditions of controllability and observability govern the existence of a complete solution to the control system design problem since the problem is deemed unsolvable if the process is not controllable, while unobservability necessitates the development of state estimator.

7.1.1 Controllability

A system is said to be controllable at time t_0 if, with the system at state $x(t_0)$, it is possible by means of an unconstrained control vector to transfer the system from any initial state to any other state in a finite interval of time (Ogata, 1997). Controllability is a property between system inputs, and the system states only. It is often checked by a procedure which consists of evaluating controllability matrix $\boldsymbol{C}$, and determining its rank.

$$\boldsymbol{C} = \begin{bmatrix} \mathbf{B} & \mathbf{AB} & \mathbf{A^2B} & \cdots & \mathbf{A^{n-1}B} \end{bmatrix} \tag{7.3}$$

If the rank of the above matrix is smaller than that of **A**, the system is classed as uncontrollable.

7.1.2 Observability

A system is said to be completely observable if any state can be determined from the observation of y(t) over a finite time interval, when the inputs are assumed to be known (Ogata, 1997). This is a property between system output and system states only. As with controllability, observability is determined by constructing an observability matrix $\boldsymbol{O}$, defined as shown below

$$O = \begin{bmatrix} \mathbf{C} \\ \mathbf{CA} \\ \mathbf{CA}^2 \\ \vdots \\ \mathbf{CA}^{n-1} \end{bmatrix} \tag{7.4}$$

A deficiency in the rank of the above matrix, when compared with matrix **C**, indicates unobservable system.

Having defined the three most fundamental properties of state-state representation within the context of control system design, the focus will now shift to state-space realisation from frequency domain representation of the process. In the following, methods for scalar transfer functions, matrices of transfer functions and techniques for augmenting component state-space models to obtain a complete representation of system dynamics will be presented for the KNO_3 crystallization system.

7.1.3 State-space realisation for SISO systems

The dynamics of a general SISO system can be written in frequency domain as shown below

$$G(s) = \frac{b_n s^n + b_{n-1} s^{n-1} + \cdots + b_1 s + b_0}{s^n + a_{n-1} s^{n-1} + \cdots + a_1 s + a_0} \tag{7.5}$$

In a controllable form, the four matrices can be obtained as follows (Ly, 1996)

$$\mathbf{A} = \begin{bmatrix} 0 & 1 & 0 & \cdots & 0 \\ 0 & 0 & 1 & \cdots & 0 \\ \vdots & \vdots & \vdots & \vdots & \vdots \\ 0 & 0 & 0 & \cdots & 1 \\ -a_0 & -a_1 & -a_2 & \cdots & -a_{n-1} \end{bmatrix}$$

$$\mathbf{B} = \begin{bmatrix} 0 \\ 0 \\ \vdots \\ 0 \\ 1 \end{bmatrix} \tag{7.6}$$

$$\mathbf{C} = \begin{bmatrix} b_0 - a_0 b_n & b_1 - a_1 b_n & b_2 - a_2 b_n & \cdots & b_{n-1} - a_{n-1} b_n \end{bmatrix}$$

$$\mathbf{D} = b_n$$

The above transformation is used for the transfer functions representing actuator dynamics and disturbance models. Following are the command lines used in MATLAB to carry out the transformations with the "tf2ss" command.

```
n_act1=1/25;
d_act1=[1 1/25];
n_act2=1/5;
d_act2=[1 1/5];
[Act1,Bct1,Cct1,Dct1]=tf2ss(n_act1,d_act1);
[Act2,Bct2,Cct2,Dct2]=tf2ss(n_act2,d_act2);

n_dist1=0.05/120;
d_dist1=[1 1/120];
n_dist2=-2/140;
d_dist2=[1 1/140];
[Ad1,Bd1,Cd1,Dd1]=tf2ss(n_dist1,d_dist1);
[Ad2,Bd2,Cd2,Dd2]=tf2ss(n_dist2,d_dist2);
```

The sets of four matrices for each actuator and disturbance model are coupled to obtain a complete representation of actuator and disturbance dynamics through the following commands

```
Act=[Act1, 0;
    0,Act2];
Bct=[Bct1, 0;
    0,Bct2];
Cct=[Cct1, 0;
    0,Cct2];
Dct=[Dct1, 0;
    0,Dct2];

Ad=[Ad1, 0;
    0,Ad2];
Bd=[Bd1, 0;
    0,Bd2];
Cd=[Cd1, 0;
    0,Cd2];
```

```
Dd=[Dd1,  0;
    0,Dd2];
```

The dynamics defined by these matrices will subsequently be augmented with the process dynamics to obtain complete representation of the system.

7.1.4 MIMO systems

In this section a procedure to develop state-space model from a transfer function matrix of a MIMO system is presented. The following method ensures controllability, just as was the case with SISO derivation. Considering a general transfer function matrix,

$$G(s)=\begin{bmatrix} G_{11}(s) & G_{12}(s) & \cdots & G_{1m}(s) \\ G_{21}(s) & G_{22}(s) & \cdots & G_{2m}(s) \\ \vdots & \vdots & \vdots & \vdots \\ G_{p1}(s) & G_{p2}(s) & \cdots & G_{1pm}(s) \end{bmatrix} \tag{7.7}$$

where,

$$G_{ij}(s)=\frac{b_{ij}^{n}s^{n}+b_{ij}^{n-1}s^{n-1}+b_{ij}^{n-2}s^{n-2}+\cdots+b_{ij}^{1}s+b_{ij}^{0}}{s^{n}+a_{n-1}s^{n-1}+\cdots\cdots+a_{1}s+a_{0}} \tag{7.8}$$

and assuming that all the elements of G_{ij} (s) share the same denominator as eq. 7.8, a state-space realisation can be obtained as follows. (The assumption of common denominator is not restrictive, since it is always possible to obtain a common denominator by modifying the corresponding numerators appropriately.)

$$\mathbf{A}=\begin{bmatrix} \mathbf{A_0} & 0 & \cdots & 0 & 0 \\ 0 & \mathbf{A_0} & \cdots & 0 & 0 \\ \vdots & \vdots & \vdots & \vdots & \vdots \\ 0 & 0 & \cdots & \mathbf{A_0} & 0 \\ 0 & 0 & \cdots & 0 & \mathbf{A_0} \end{bmatrix}_{(mn\times mn)}$$

$$\mathbf{B}=\begin{bmatrix}\mathbf{B}_0 & 0 & \cdots & 0 & 0\\ 0 & \mathbf{B}_0 & \cdots & 0 & 0\\ \vdots & \vdots & \vdots & \vdots & \vdots\\ 0 & 0 & \cdots & \mathbf{B}_0 & 0\\ 0 & 0 & \cdots & 0 & \mathbf{B}_0\end{bmatrix}_{(mn\times mn)} \tag{7.9}$$

$$\mathbf{C}=\begin{bmatrix}\mathbf{C}_1 & \mathbf{C}_2 & \cdots & \mathbf{C}_{m-1} & \mathbf{C}_m\end{bmatrix}_{(p\times mn)}$$

$$\mathbf{D}=\begin{bmatrix}\mathbf{D}_1 & \mathbf{D}_2 & \cdots & \mathbf{D}_{m-1} & \mathbf{D}_m\end{bmatrix}_{(p\times m)}$$

where

$$\mathbf{A}_0=\begin{bmatrix}0 & 1 & 0 & \cdots & 0\\ 0 & 0 & 1 & \cdots & 0\\ \vdots & \vdots & \vdots & \vdots & \vdots\\ 0 & 0 & 0 & \cdots & 1\\ -a_0 & -a_1 & -a_2 & \cdots & -a_{n-1}\end{bmatrix}_{(n\times n)}$$

$$\mathbf{B}_0=\begin{bmatrix}0\\ 0\\ \vdots\\ 0\\ 1\end{bmatrix}_{(n\times 1)}$$

$$\mathbf{C}_i=\begin{bmatrix}b_{1i}^0-a_0b_{1i}^n & b_{1i}^1-a_1b_{1i}^n & \cdots & b_{1i}^{n-1}-a_{n-1}b_{1i}^n\\ b_{2i}^0-a_0b_{2i}^n & b_{2i}^1-a_1b_{2i}^n & \cdots & b_{2i}^{n-1}-a_{n-1}b_{2i}^n\\ \vdots & \vdots & \vdots & \vdots\\ b_{pi}^0-a_0b_{pi}^n & b_{pi}^1-a_1b_{pi}^n & \cdots & b_{pi}^{n-1}-a_{n-1}b_{pi}^n\end{bmatrix}_{(p\times n)}$$

$$\mathbf{D}_i=\begin{bmatrix}b_{1i}^n\\ b_{2i}^n\\ \vdots\\ b_{pi}^n\end{bmatrix}_{(p\times 1)}$$

The transfer function matrix for KNO_3 crystallization comprising 4 elements is converted into the above form using the following commands. The dead time

contributions are approximated by second order Pade function while the common denominator for the transfer functions is obtained through the "conv" command.

```
% N1, D1 represent the num and den for the first transfer function relating
% T_vessel to T_jack., Subscript 2 indicates G(s) between T_vessel and RR
% Sub. 3 is for G(s) between Cond. and T_jack
% Sub. 4 for Cond. and RR

[num1,den1]=pade(30,2);
[num2,den2]=pade(60,2);
N1=-0.66/70;
D1=[1 1/70];
N2=(-0.25/100)*num1;
D2=conv([1 1/100],den1);
N21=(1/D2(:,1))*N2;
D21=(1/D2(:,1))*D2;
N3=5/230;
D3=[1 1/230];

N4=(11.1/168)*num2;
D4=conv([1 1/168],den2);
N41=(1/D4(:,1))*N4;
D41=(1/D4(:,1))*D4;


% Reformation of the above transfer function to obtain common denominators
% and corresponding numerators
com_den=conv(D41,conv(D3,conv(D1,D21)));
 com_num1=conv(N1,conv(D21,conv(D3,D41)));
 com_num2=conv(N21,conv(D1,conv(D3,D41)));
 com_num3=conv(N3,conv(D1,conv(D21,D41)));
 com_num4=conv(N41,conv(D1,conv(D21,D3)));


% State-space realisation of transfer function matrix

A0=[0 1 0 0 0 0 0 0;
   0 0 1 0 0 0 0 0;
   0 0 0 1 0 0 0 0;
   0 0 0 0 1 0 0 0;
   0 0 0 0 0 1 0 0;
   0 0 0 0 0 0 1 0;
   0 0 0 0 0 0 0 1;
      -com_den(:,9)      -com_den(:,8) -com_den(:,7) -com_den(:,6) -com_den(:,5) -com_den(:,4) -
com_den(:,3) -com_den(:,2)];


A=[A0 zeros(size(A0));
   zeros(size(A0)) A0];


B0=[zeros(7,1);1];

B=[B0 zeros(size(B0));
   zeros(size(B0)) B0];
```

```
c11=[com_num1(1,8)      com_num1(1,7)   com_num1(1,6)   com_num1(1,5)      com_num1(1,4)
com_num1(1,3) com_num1(1,2) com_num1(1,1)];
c21=[com_num3(1,8)      com_num3(1,7)   com_num3(1,6)   com_num3(1,5)      com_num3(1,4)
com_num3(1,3) com_num3(1,2) com_num3(1,1)];
c12=[com_num2(1,8)      com_num2(1,7)   com_num2(1,6)   com_num2(1,5)      com_num2(1,4)
com_num2(1,3) com_num2(1,2) com_num2(1,1)];
c22=[com_num4(1,8)      com_num4(1,7)   com_num4(1,6)   com_num4(1,5)      com_num4(1,4)
com_num4(1,3) com_num4(1,2) com_num4(1,1)];

C=[c11 c12;
  c21 c22];
D=zeros(2,2);
```

It is worth noting that the Pade approximation of dead times within transfer functions 2 and 4, result in an increased order system, shown to be sixteenth by matrix **A**. It can also be observed from the above extract of MATLAB file (complete listing can be found in the appendix) that the matrix **D** is zero; this stems from the fact that the order of numerator is strictly less then that of the denominator for all the transfer functions within the convoluted system. The system can therefore, be defined as strictly proper, which means that there is no direct transmission from inputs to outputs and the relationships between them only exist through the states.

The following listing of the eigenvalues for matrix **A** indicates that the open loop system is asymptotically stable. The first four modes are however, comparatively slow with frequencies up to an order of magnitude smaller then the faster modes. The pairs in eigen-values originate from the diagonal formulation of **A** martix through $\mathbf{A_0}$.

Eigenvalues		Damping	Frequency(rad/sec)
-4.34783e-03	0.00000e+00i	1.000	4.34783e-03
-4.34783e-03	0.00000e+00i	1.000	4.34783e-03
-5.95238e-03	0.00000e+00i	1.000	5.95238e-03
-5.95238e-03	0.00000e+00i	1.000	5.95238e-03
-1.00000e-02	0.00000e+00i	1.000	1.00000e-02
-1.00000e-02	0.00000e+00i	1.000	1.00000e-02
-1.42857e-02	0.00000e+00i	1.000	1.42857e-02
-1.42857e-02	0.00000e+00i	1.000	1.42857e-02
-5.00000e-02	2.88675e-02i	0.866	5.77350e-02
-5.00000e-02	-2.88675e-02i	0.866	5.77350e-02
-5.00000e-02	2.88675e-02i	0.866	5.77350e-02
-5.00000e-02	-2.88675e-02i	0.866	5.77350e-02
-1.00000e-01	5.77350e-02i	0.866	1.15470e-01

-1.00000e-01	-5.77350e-02i	0.866	1.15470e-01
-1.00000e-01	5.77350e-02i	0.866	1.15470e-01
-1.00000e-01	-5.77350e-02i	0.866	1.15470e-01

Checks on controllability and observability show that though the system is controllable, it is, however, not fully observable. This is to say that not all states contribute directly to the output vector. Though an ideal system, would have full observability, the consequences of this nature of the system do not restrict the continuation of control synthesis procedure as depicted in figure 34.

7.1.5 Synthesis of control system and augmentation of the individual models

In the preceding section models for system dynamics, disturbances and actuator dynamics were developed. To synthesise the complete control system, two additional states representing the drift between measurements and their set points (command) need to be defined to enhance integral control properties of the final design. These will be termed as integral states and are defined for the measurements, *i.e.* conductivity and vessel temperature as

$$\dot{x}_{\int \Delta C} = y_C - y_{C,cmd} \tag{7.10}$$

$$\dot{x}_{\int \Delta T} = y_T - y_{T,cmd} \tag{7.11}$$

These new states, that are only observable through the measurements can be calculated through matrix **C** which relates measurements to states.

The effect of disturbances/noise is usually incorporated into the state space model by defining two additional terms in the general representation given in eq. 7.1. These terms add their effects on states and measurements respectively. The more general model takes the following form,

$$\sum : \begin{cases} \dot{x} = \mathbf{A}\, x(t) + \mathbf{B}\, u(t) + \Gamma\, y_{dist} \\ y = \mathbf{C}\, x(t) + \mathbf{D}\, u(t) + \Omega\, y_{dist} \end{cases} \tag{7.12}$$

where, y_{dist} is a vector of length equal to the number of measurements, i.e. two, Γ is a scalar matrix of dimension equal to the number of states times the number of measurements and Ω is a square matrix of size equal to the number of measurements. In the present problem, since the effects of process noise are not considered at this stage, the Γ matrix has zeros for all the entries. The Ω matrix on the other hand, is a negative identity matrix of size 2×2. The negative sign ensures that the actual measurements in the model are calculated after substracting the effects of white noise disturbance inputs.

Besides the 16 states describing the convoluted process dynamics of corresponding order, the six new states, viz. two each for the actuators, disturbances and the integral action have to be augmented into the system model to obtain a complete control system. In the following the augmented matrices for the problem will be presented, along with the description of their derivation.

```
Aaug=[A B*Cct gama*Cd zeros(16,2);
    zeros(2,16) Act zeros(2,4);
    zeros(2,18) Ad zeros(2,2);
    C zeros(2,6)];
```

It can be seen from the Aaug matrix that its dimension has increased from 16×16 to 22×22, due to the incorporation of six new states. The term B*Cct couples actuator dynamics with the process model (B appears in the term because actuators affect the inputs), while gamma*Cd links process model to the disturbance models. In the last two rows which represent the new integrals states, the whole matrix **C** is placed along with zeros of the appropriate dimension. As mentioned previously, this is because the integral states can only be measured as functions of outputs.

```
Baug=[zeros(16,2);Bct;zeros(4,2)];
```

Of all the twenty two states, only those related to the actuators are of relevance, because the relationship between the original inputs and the states have already been established in Aaug. Furthermore, the original inputs are no longer inputs; they are functions represented by the output of the actuators.

The matrix "gammaug", represents the relationship between the $\dot{x}$ vector and both the disturbances and the two integral states. It is formulated as follows,

```
gamaug=[zeros(18,4);Bd zeros(2,2);zeros(2,2) [-1 0;0 -1]];
```

The fact that there are four columns in gammaug, verifies that the matrix is accounting for the sensors and integral states. The Bd matrix at rows 19 and 20, establishes the relationships for disturbance, while [-1 0;0 -1] allows the integral states to contribute to $\dot{x}$ through gammaug.

```
Caug=[C D*Cct omega(:,1)*Cd(1,1) omega(:,2)*Cd(2,2) zeros(2,2);
      zeros(1,16) 1/3 zeros(1,5);
      zeros(1,17) 1/3 zeros(1,4);
      zeros(2,18) Cd zeros(2,2);
      eye(18) zeros(18,4);
      zeros(2,20) eye(2)];
```

In the above matrix, the term D*Cct couples actuator to the process, while omega(:,1)*Cd(1,1) and omega(:,2)*Cd(2,2) incorporate the effects of disturbances on the measurements. In the two terms with omega, the first adds the disturbance effect to measurement 1, while the second term adds to measurement 2. The subsequent rows are again zero because new states can only observed through the measurements.

The following representation of Daug indicate zero transmittence of inputs directly to the outputs, while omegaug has all entries equal to zero because the effects of disturbances and integral states on the output have already been accounted through the states via gammaug.

```
Daug=zeros(26,2);
```

```
omegaug=zeros(26,4);
```

Augmentation of these six matrices accomplishes the design of control system, which will now be used to develop the appropriate control law for feedback design.

7.2 Full-state Feedback Control

The traditional design techniques such as Bode diagram and root loci are well suited for SISO systems. When designing multi-variable feedback control systems, these methods however, can be extremely time consuming and therefore are less attractive. In this section a method to synthesise feedback control law based on "full state" feedback will be presented. It would yield best control systems in terms of achievable performance such as control bandwidth and saturation limitations (Ogata, 1997; Johnson 1993; Gangsaas et al., 1986). With adequate controllability, all the design performance and specifications can be met under full state feedback design. If such a state-feedback control-law cannot be found to meet control design requirements, then it would be futile to pursue other linear feedback control structures such as output feedback and feedback with lead/lag compensation (Ly, 1996; Gangsaas et al., 1986). For a process represented by eq. 7.12, a linear static feedback control law has the following form

$$u(t) = \mathbf{G}\, x(t) \tag{7.13}$$

where **G** is a full-state feedback gain matrix of dimension m×n (m is the length of vector u(t) and n that of x(t)). The control law synthesis reduces to the determination of this gain matrix so that the following design objectives can be achieved:

1. Closed-loop stability: The closed-loop system (**A** + **BG**) must be stable with the required damping factors and frequencies.

2. Command responses: Responses of the system to command inputs must have the desired settling times, little overshoots and robustness to external disturbances.
3. Disturbance rejection: Feedback control system must be able to attenuate undesirable responses due to disturbances of deterministic or stochastic nature.

With feedback control the closed-loop system becomes

$$\sum : \begin{cases} \dot{x} = (\mathbf{A} + \mathbf{BG})\, x(t) \;+\; \mathbf{B}\, u_{cmd}(t) + \Gamma\, y_{dist} \\ y = (\mathbf{C} + \mathbf{DG})\, x(t) \;+\; \mathbf{D}\, u_{cmd}(t) + \Omega\, y_{dist} \end{cases} \tag{7.14}$$

where $u_{cmd}(t)$ represent the external control input commands.

Many design methods such as H^2- optimal control, H^∞- norm bound control and eigenassigment are available for determining the gain matrix. In the following, the theory of optimal control for the synthesis of linear quadratic regulator will be presented and the appropriate control law formulated.

7.2.1 Linear quadratic regulator (LQR)

The problem with this method is to determine an acceptable feedback control law for "u" such that the following cost function is minimised for optimal regulatory performance

$$J = \int_0^\infty \left[y^T(t)\mathbf{Q}y(t) \;+\; u^T(t)\mathbf{R}u(t) \right] dt \tag{7.15}$$

The first term in the above cost function is used to penalise deviations of the regulated output through the **Q** matrix, while the second term discourages the use of excessively large control efforts, this time by using the matrix **R**. Optimisation of this function yields the following feedback control law,

$$u = -\mathbf{R}^{-1}\mathbf{B}^{\mathrm{T}}\mathbf{S}_0\; x(t) \tag{7.16}$$

where $\mathbf{S_0}$ satisfies the steady-state matrix solution of the Riccati equation given by the following equation

$$-\mathbf{A}^T\mathbf{S}_0 - \mathbf{S}_0\mathbf{A} + \mathbf{S}_0\mathbf{B}\mathbf{R}^{-1}\mathbf{B}^T\mathbf{S}_0 = \mathbf{Q} \qquad (7.17)$$

The matrix $\mathbf{S_0}$, obtained from the above equation is usually symmetric and positive semi-definate. The equation itself comes from the following differential matrix Riccati equation after setting $\dot{\mathbf{S}}(t) \to 0$ and $\mathbf{S}(t) \to \mathbf{S}_0$ (Ly, 1996),

$$\dot{\mathbf{S}}(t) = -\mathbf{A}^T\mathbf{S}(t) - \mathbf{S}(t)\mathbf{A} + \mathbf{S}(t)\mathbf{B}\mathbf{R}^{-1}\mathbf{B}^T\mathbf{S}(t) - \mathbf{Q} \qquad (7.18)$$

with $\mathbf{S}(t_f) = \mathbf{S_0}$ as the boundary condition.

The solution of control law (eq. 7.16) thus reduces to the calculation of a constant feedback gain matrix given by the following equation

$$\mathbf{G} = -\mathbf{R}^{-1}\mathbf{B}^T\mathbf{S}_0 \qquad (7.19)$$

The optimal full state feedback control system derived from the above procedure posses the following guaranteed robustness properties in the control loops (Siouris, 1996),

- Gain margins: -6 dB $\leq$ Gain variation $< \infty$
- Phase margins: $-60^o <$ Phase variation $< +60^o$

7.2.2 Selection of design weights and criterion variables

As stated earlier, the regulatory problem involves penalising the relevant outputs from the vector y(t) through weighting matrix **Q**, along with penalties on certain controls from u(t) by proper selection of weights in the **R** matrix. The selection procedure for the parameters within these matrices which are usually selected to be diagonal is iterative and involves complete re-evaluation of each step in the design.

The performance index for the crystallization process has been based around defining and penalising two criterion variables ccrit 1 and ccrit2. These are defined as $(T\text{-}T_{dist})\text{-}T_{cmd}$ and $(C\text{-}C_{dist})\text{-}C_{cmd}$. The additional target transmission zeros between the inputs and these criterion variables are appropriately placed in the left half *s* plane by formulating the following shaping factors and adjusting their parameters according to the asymptotic regulator design procedure

$$ccrit1(s) = \left[K_{D1}s + K_{P1} + {K_{I1}}/{s}\right]\left[\left(T_v(s) - T_{v.dist}(s) - T_{v,cmd}(s)\right)\right]$$

$$ccrit2(s) = \left[K_{D2}s + K_{P2} + {K_{I2}}/{s}\right]\left[\left(C(s) - C_{dist}(s) - C_{cmd}(s)\right)\right]$$

where $K_D = 1.0$, $K_P = 2\omega\zeta$, $K_I = \omega^2$. The location of target zeros in the *s* plane can be found by the following equation.

$$s = -\zeta\omega \pm \sqrt{1-\zeta^2\omega}$$

By specifying ζ as 1.0, for the current problem, it was ensured that a damping of 1.0 is achieved. A value of 0.02 was chosen for ω, which would provide a settling time of 100 seconds. The settling time is defined as the time required for the response curve to reach and stay within a range about the final value of size specified by absolute percentage of the final value (Ogata, 1997).

The selected value of settling time will suffice for the current dynamics of the process, where the largest time constant is over 200 seconds. Following is the extract of the MATLAB program defining the criterion formulation and listing the appropriate parameters

```
% Regulator Design
% Creating target zeros using shaping filter on T-Tcmd and C-Ccmd

zeta=1; omega1=0.02;
ktdot=1.0;kt=2.0*omega1*zeta;kintt=omega1*omega1;
ccrit1=[ktdot,kt,kintt]*[Caug(1,:);Caug(1,:);Caug(25,:)];
```

```
dcrit1=[ktdot,kt,kintt]*[Baug(1,:);Daug(1,:);Daug(25,:)];
zeta=1;omega1=0.02;
kcdot=1.0;kc=2.0*omega1*zeta;kintc=omega1*omega1;
ccrit2=[kcdot,kc,kintc]*[Caug(2,:);Caug(2,:);Caug(26,:)];
dcrit2=[kcdot,kc,kintc]*[Baug(2,:);Daug(2,:);Daug(26,:)];
ccrit3=Caug(4,:);dcrit3=Daug(4,:);
ccrit=[ccrit1;ccrit2;ccrit3];dcrit=[dcrit1;dcrit2;dcrit3];
```

Besides, the two criterion defined for regulatory purposes, a third criteria was also formulated for penalising the effects of process disturbance on conductivity measurements. It appears as ccrit3 and dcrit3 in the foregone extract.

```
Q=[10000000000   0  0;
  0 10000000  0
  0  0  1000] ;

R=[1000  0;
    0 10000];
```

The first two diagonal elements of weighting matrix **Q**, select the bandwidth of command path for vessel temperature and conductivity respectively. The third element on the other hand allows to improve the load factor responses to disturbances affecting conductivity. The diagonal elements of matrix **R** are used to specify the bandwidth of the controls with the first related to jacket temperature and the second to recycle ratio. In the MATLAB file "lqrcross" command is used for the augmented **A** and **B** matrices along with the criterion functions and the weighting matrices to compute the optimal full state feedback controller gain matrix **G**.

7.2.3 Closed loop LQR design

The block diagram of the system after excluding the integral states from the augmented description of the system is shown in figure 36. The two integral states have been removed to emphasise the ability of the controller in achieving zero off-set.

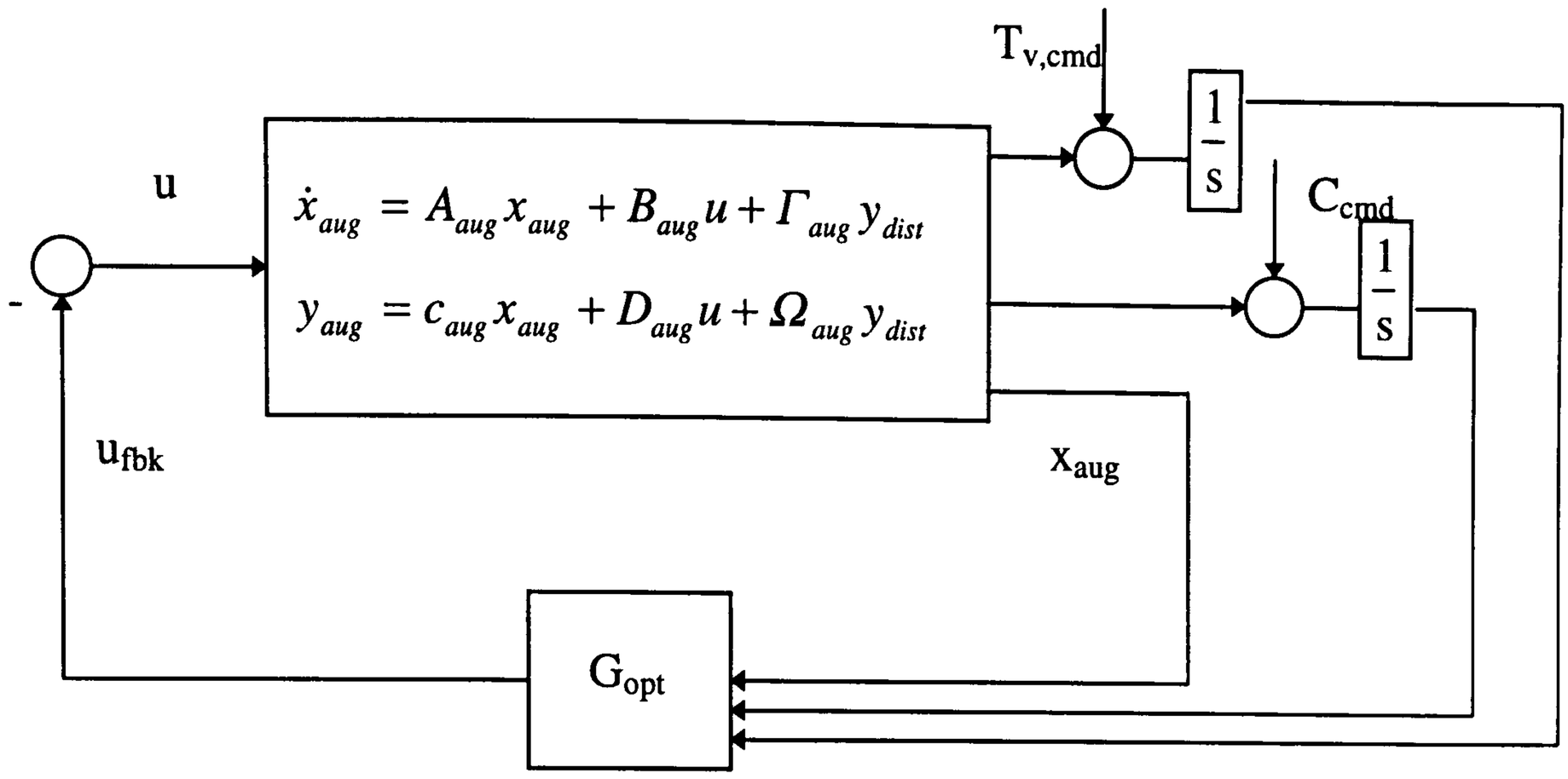

FIGURE 36 : Block diagram for the LQR design

7.2.3.1 Stability Analysis of the design

Two methods are used to determine the stability characteristics of the closed loop system with full-state feedback control. These include the examination of eigenvalues of the closed loop $\mathbf{A}_{cl}$ matrix and the analysis of Bode plots for the two measurements.

$\mathbf{A}_{cl}$ matrix is determined from the following equation

$$\mathbf{A}_{cl} = \mathbf{A}_{aug} - \mathbf{B}_{aug} \times \mathbf{G} \qquad (7.20)$$

where **G** is the optimal control gain matrix. Following is the listing of eigenvalues of the closed loop **A** matrix.

Eigenvalues		Damping	Frequency(rad/sec)
-4.65217e-03	0.00000e+00i	1.000	4.65217e-03
-4.89872e-03	0.00000e+00i	1.000	4.89872e-03
-5.95238e-03	0.00000e+00i	1.000	5.95238e-03
-7.14286e-03	0.00000e+00i	1.000	7.14286e-03
-8.33333e-03	0.00000e+00i	1.000	8.33333e-03
-8.61538e-03	0.00000e+00i	1.000	8.61538e-03
-8.61538e-03	0.00000e+00i	1.000	8.61538e-03
-9.79394e-03	0.00000e+00i	1.000	9.79394e-03
-1.00000e-02	0.00000e+00i	1.000	1.00000e-02
-1.42857e-02	0.00000e+00i	1.000	1.42857e-02
-5.00000e-02	2.88675e-02i	0.866	5.77350e-02
-5.00000e-02	-2.88675e-02i	0.866	5.77350e-02
-5.75124e-02	2.46042e-02i	0.919	6.25543e-02
-5.75124e-02	-2.46042e-02i	0.919	6.25543e-02
-1.00000e-01	5.77350e-02i	0.866	1.15470e-01
-1.00000e-01	-5.77350e-02i	0.866	1.15470e-01
-1.08034e-01	5.57743e-02i	0.889	1.21581e-01

-1.08034e-01	-5.57743e-02i	0.889	1.21581e-01
-4.35753e-01	4.15894e-01i	0.723	6.02370e-01
-4.35753e-01	-4.15894e-01i	0.723	6.02370e-01
-8.33329e-01	8.26417e-01i	0.710	1.17363e+00
-8.33329e-01	-8.26417e-01i	0.710	1.17363e+00

It can be seen from the above listing that all the eigenvalues are stable with adequate damping. In can also be noticed that the frequencies of the two integral states (the last two in the list) are much higher then any other states. These higher values reflect the ability of the design to achieve significant improvements.

In figures 37 and 38, the bode plots are depicted for each of the two integral states in the closed loop system.

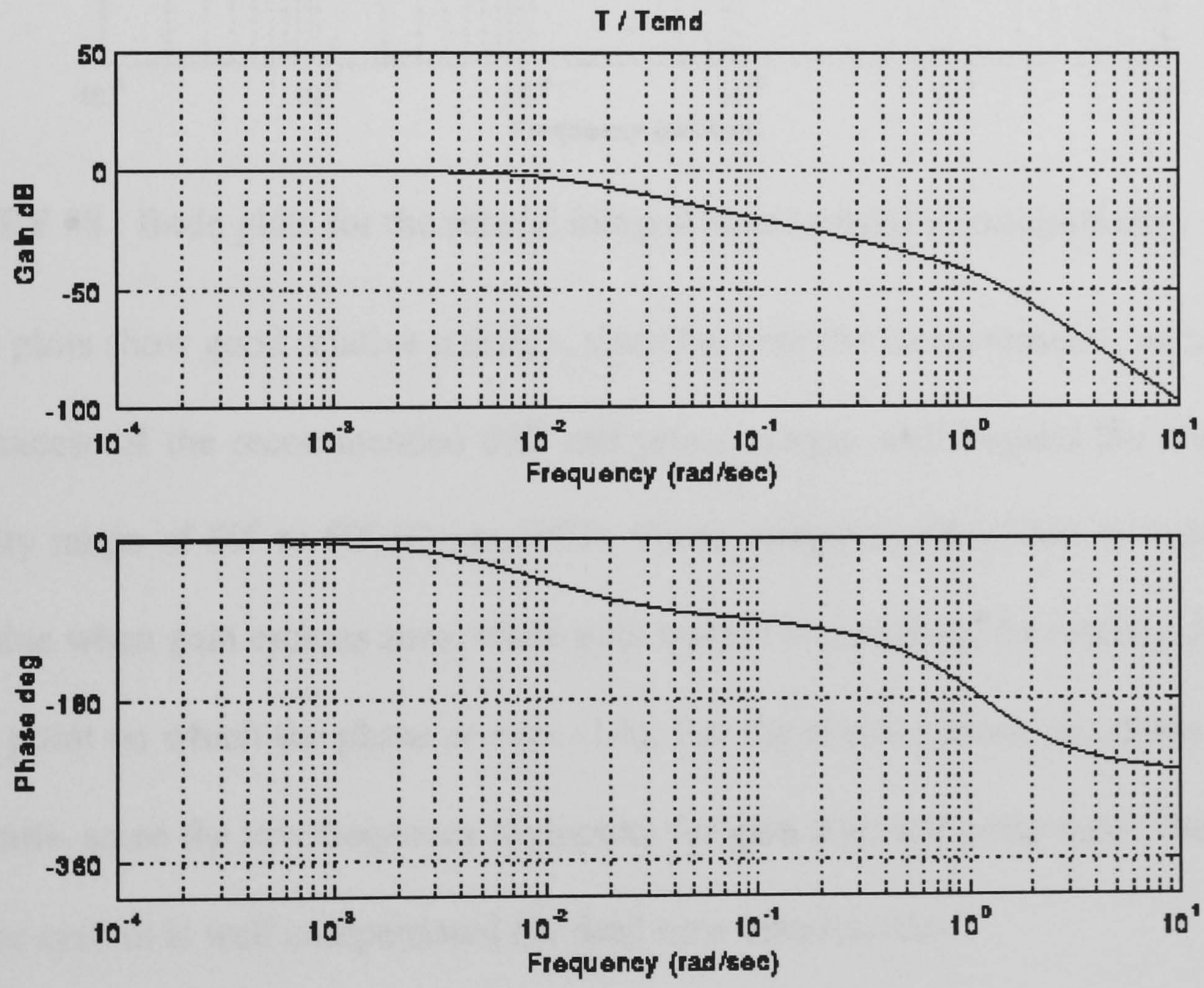

FIGURE 37 : Bode plots for the first integral state (Vessel temperature related)

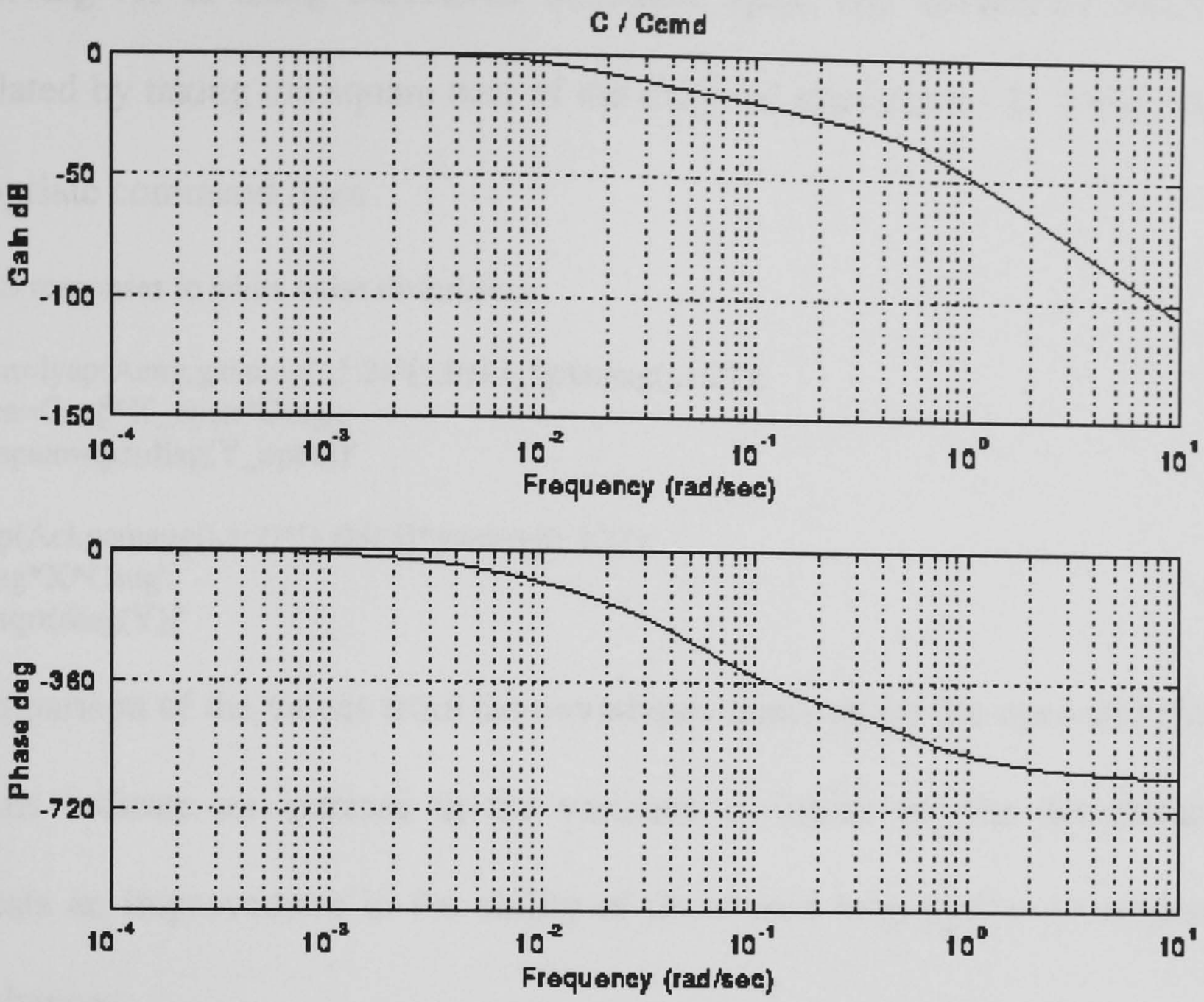

FIGURE 38 : Bode plots for the second integral state (related to conductivity)

These plots show good relative stability, since for both the measurements, gain margin is in excess of the recommended 6dB and phase margin well beyond the close loop stability range of 30^{o} to 60^{o} (Ogata,1997). Phase margin is calculated by reading off the value when gain crosses zero, while gain margin is calculated by reading the value at the point on which the phase crosses -180. For the above system, the phase margin is infinite, since the low frequency asymptote for gain does not cross zero. This means that the system is well compensated for dead time uncertainties.

7.2.3.2 Analysis of the affect of disturbances

The covariance of process outputs to moderate disturbances are calculated using Lyapunov matrix equation

$$\mathbf{A}_{aug}\mathbf{X}+\mathbf{X}\mathbf{A}_{aug}^{T}= -\Gamma_{aug}\,\Gamma_{aug}^{T} \qquad (7.21)$$

by solving for **X** using MATLAB command lyap. The covariance matix is then calculated by taking the square root of the diagonal elements of **X**. Following are the appropriate command lines

```
% RMS responses to white noise disturbance

X_open=lyap(Aaug,gamaug(:,1:2)*[1,0;0,1]*gamaug(:,1:2)');
Y_open=Caug*X_open*Caug';
sigY_open=sqrt(diag(Y_open))'

X=lyap(Acl,gamaug(:,1:2)*[1,0;0,1]*gamaug(:,1:2)');
Y=Caug*X*Caug';
sigY=sqrt(diag(Y))'
```

A comparison of the values from the covariance matrices for the open and closed loop systems indicate an increase in the variance of inputs for the disturbances. This suggests an improvement in the ability of the closed loop system to respond to the disturbances.

7.2.4 Single loop robustness analysis

The robustness analysis is carried out breaking one input loop in the feedback design and evaluating the performance of the remaining loop for tracking set point changes and disturbance rejection. The findings for jacket temperature loop are shown in figure 39. The bode plot for the attainable characteristics from the recycle loop is depicted in figure 40. Though the gain and phase margins for the two situations have reduced when compared with frequency response of the complete closed loop system, they are still well inside the stability region. The actual magnitudes of the margins for the Bode plots are;

1. Jacket temp. loop only: Gain margin = infinite, phase margin = 180-(-259.6)
2. RR loop only: Gain margin = 14.65 dB, phase margin infinite

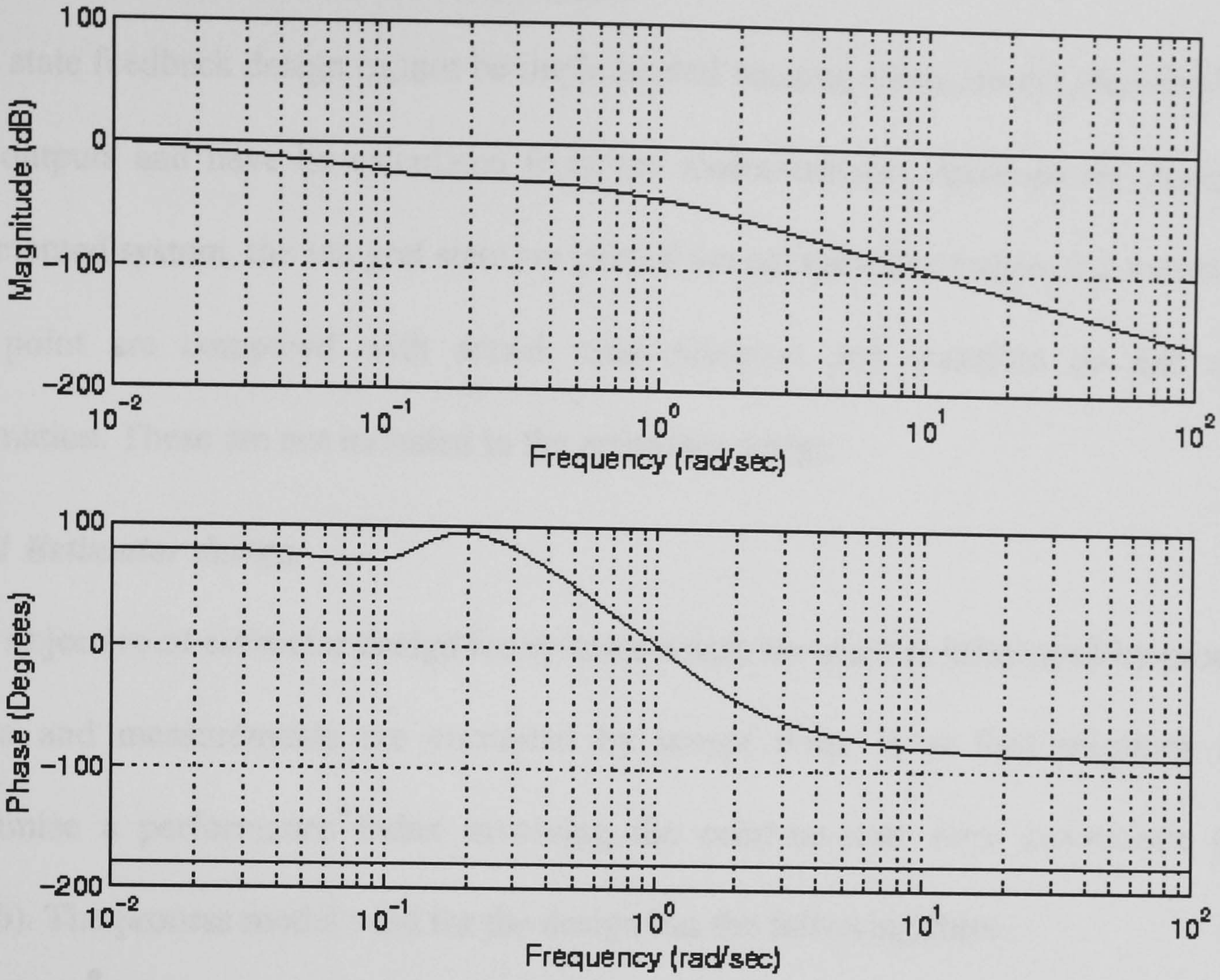

FIGURE 39 : Bode plot of the closed loop system with just jacket temperature loop

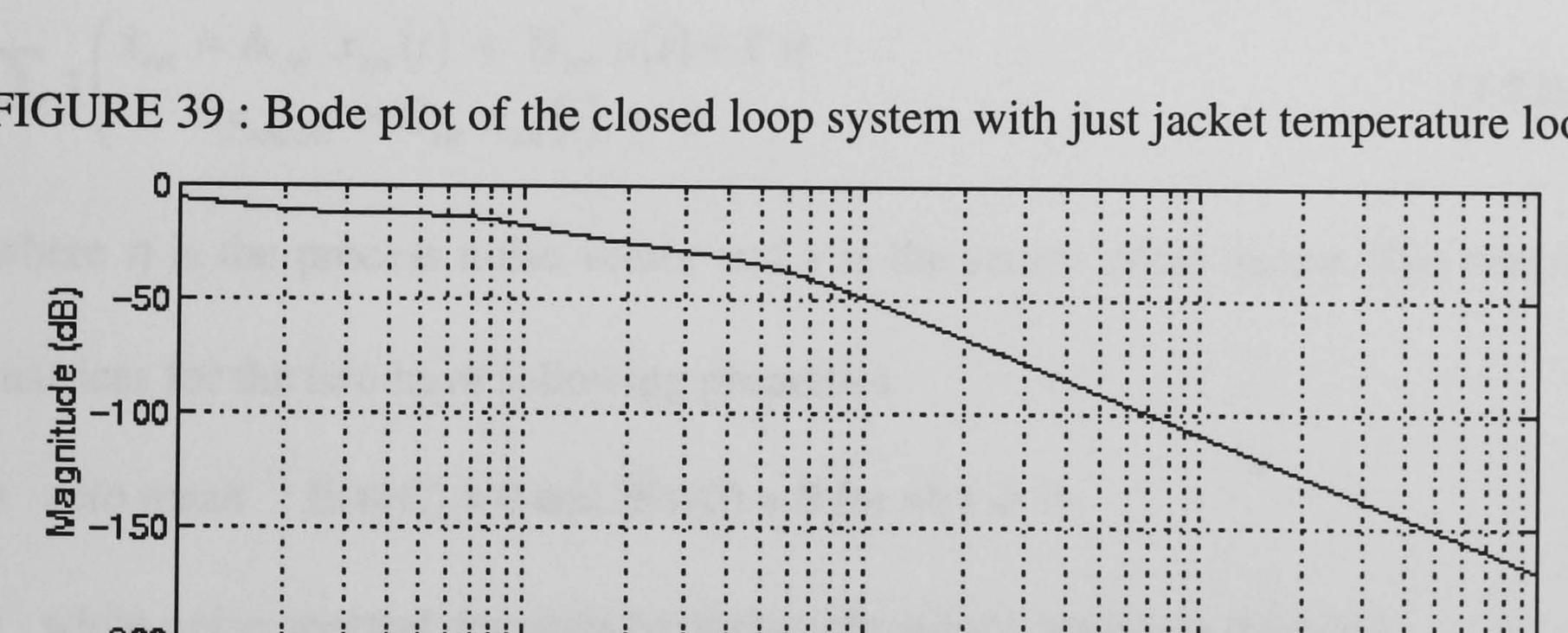

FIGURE 40 : Bode plot of the closed loop system with just recycle loop

7.3 Estimator design and LQG Controller

Full state feedback design cannot be implemented because states are not observable in the outputs and have be calculated from the measurements. Amongst the states of augmented system, the integral state are part of the compensator (where the values for set point are compared with actual measurements) and therefore do not need estimation. These are not included in the estimator design.

7.3.1 Estimator design

The objective of estimator design for systems where the plant is influenced by process noise and measurements are corrupted by sensor noise is to find solutions that minimise a performance index involving the estimate-state error covariance (Ly, 1996). The process model used for the design has the following form

$$\sum : \begin{cases} \dot{x}_{est} = \mathbf{A}_{est}\ x_{est}(t) + \mathbf{B}_{est}\ u(t) + \Gamma \eta \\ y_{sensors} = \mathbf{C}_{est}\ x_{est}(t) + \upsilon \end{cases} \tag{7.22}$$

where η is the process noise vector and v is the sensor noise vector. The correlation matrices for the two have following properties

- zero mean : $E(\eta(t)) = 0$ and $E(v(t)) = 0$ for all $t \geq 0$
- white noise spectral densities have the following correlation matrices

$$E[\eta(t+\tau)\eta^T(t)]=W_o y_{dist}(\tau)$$

$$E[v(t+\tau)v^T(t)]=V_o y_{dist}(\tau)$$

where W_o is a symmetric positive, semi-definite matrix usually selected to be identity matrix of appropriate size. V_o is a symmetric positive, definite with diagonal elements of co-variance response of the plant to disturbances (calculated earlier using Lyapunov matrix equation).

The matrices of equation 7.22 are formulated using the following command lines.

```
% Estimater design

Aest=Aaug(1:20,1:20);
Best=Baug(1:20,:);
Gest=gamaug(1:20,1:2);
%Sensors:{T,C}
Cest=[C D*Cct omega(:,1)*Cd(1,1) omega(:,2)*Cd(2,2)];

Dest=zeros(2,2);
Gest1=[Best,Gest];

% Process noise and sensor noise covariance matrices

Wo=eye(2);
Vo=0.1*diag([sigY(1,1),sigY(1,2)]);
```

It can be seen from the above extract that the only difference between the representation of the process for full feedback and the estimator design is that the integral states have been excluded.

The problem of optimal linear state estimator is solved by finding the best estimates, $\hat{x}(t)$ such that the following performance index is minimised.

$$J = \lim_{t\to\infty} E\left[\left\{\hat{x}(t) - x(t)\right\}^T Q \left\{\hat{x}(t) - x(t)\right\}\right] \tag{7.23}$$

For the above performance index, the steady state error co-variance matrix of the estimated states $\overline{\mathbf{X}}$, can be defined as

$$\overline{\mathbf{X}} = \lim_{t\to\infty} E\left[\left\{\hat{x}(t) - x(t)\right\}\left\{\hat{x}(t) - x(t)\right\}^T\right] \tag{7.24}$$

where $\overline{\mathbf{X}}$ is determined from the steady-state solution of Riccati equation through the following matrix equation

$$\mathbf{A}_{est}\overline{\mathbf{X}} + \overline{\mathbf{X}}\mathbf{A}^T - \overline{\mathbf{X}}\mathbf{C}_{est}{}^T\mathbf{V}_o{}^{-1}\mathbf{C}_{est}^T\overline{\mathbf{X}} + \Gamma\mathbf{W}_o\Gamma^T = 0 \tag{7.25}$$

The optimal estimator gain matrix, $\mathbf{K}_{opt}$ is therefore given by

$$\mathbf{K}_{opt} = -\overline{\mathbf{X}}\mathbf{C}^T\mathbf{V}_o^{-1} \tag{7.26}$$

With the substitution of the above gain matrix, the estimator has the following design,

$$\dot{x}_{est} = \mathbf{A}_{est} x_{est} + \mathbf{B}_{est} u + K_{opt} [\, y_{est} - y_{sensors} \,] \tag{7.27}$$

where

$$\mathbf{B}_{est}\, u = \left[\mathbf{B}_{est}\mathbf{G}_{est}\mathbf{X}_{est} - \mathbf{B}_{est}\mathbf{G}_{I}\mathbf{X}_{I}\right]$$

y_{sensor} and X_I are found from the following equations

$$y_{sensor} = \mathbf{C}_{est}\mathbf{X}_{est}\mathbf{K}_{opt}$$

$$\dot{\mathbf{X}}_{I} = \begin{bmatrix} 0 & 0 \\ 0 & 0 \end{bmatrix} + \begin{bmatrix} 1 & 0 \\ 0 & 1 \end{bmatrix} \begin{bmatrix} \Delta T \\ \Delta C \end{bmatrix}$$

The appropriate command lines to calculate the optimal estimator gain matrix **K**, are

```
% Optimal estimator gain matrix (Solving Steady-state Riccati equation)
k=lqrcross(Aest',Cest',Gest',Dest,Wo,Vo);k=k';
```

7.3.2 LQG Controller design

The feedback control law with LQG design is given by;

$$u(t) = \mathbf{G}_{est}\, \mathbf{X}_{est} - \mathbf{G}_{I}\, \mathbf{X}_{I} \tag{7.28}$$

where the optimal gain matrix for the full-state feedback can be recovered from the following equation

$$[\mathbf{G}_{est}, \mathbf{G}_{I}] = \mathbf{G}_{opt}$$

The stability of the closed loop system with LQG design is guaranteed if $\mathbf{A}_{est}$ and Γ_{est} matrices can be disturbed and are detectable. The latter translates into the observability of the unstable eigenvalues of $\mathbf{A}_{est}$. The closed loop eigenvalues of the complete system are simply the sum of the values for optimal regulator design, $\lambda(\mathbf{A}_{aug}$-$\mathbf{B}_{aug}\,\mathbf{G}_{opt})$, and optimal state estimator design, $\lambda(\mathbf{A}_{est}$-$\mathbf{K}_{opt}\,\mathbf{C}_{est})$. This additive property allows design of the controller in isolation from the estimator without the loss of optimality when the two are combined. The state-space representation of the LQG controller is as follows,

$$\dot{x}_{cont} = \begin{bmatrix} \mathbf{A}_{est} - \mathbf{B}_{est}\mathbf{G}_{est} - \mathbf{K}_{opt}\mathbf{C}_{est} & -\mathbf{B}_{est}\mathbf{G}_{I} \\ 0 & 0 \end{bmatrix} \begin{bmatrix} x_{est} \\ x_{I} \end{bmatrix} + \begin{bmatrix} -\mathbf{K}_{opt} & -\mathbf{K}_{opt} \\ 1 & 0 \\ 0 & 1 \end{bmatrix} \begin{bmatrix} \Delta T \\ \Delta C \end{bmatrix} +$$

$$\begin{bmatrix} 0 & 0 \\ -1 & 0 \\ 0 & -1 \end{bmatrix} \begin{bmatrix} \Delta T_{cmd} \\ \Delta C_{cmd} \end{bmatrix} \tag{7.29}$$

$$y_{cont} = -\begin{bmatrix} \mathbf{G}_{est} & \mathbf{G}_{I} \end{bmatrix} \begin{bmatrix} x_{est} \\ x_{I} \end{bmatrix}$$

The closed loop system with the estimator can therefore be written as follows.

$$\begin{bmatrix} \dot{x}_{est} \\ \dot{x}_{cont} \end{bmatrix} = \begin{bmatrix} \mathbf{A}_{est} & \mathbf{B}_{est}\mathbf{C}_{cont} \\ \mathbf{B}_{cont}\mathbf{C}_{sensors} & \mathbf{A}_{cont} \end{bmatrix} \begin{bmatrix} x_{est} \\ x_{cont} \end{bmatrix} + \begin{bmatrix} 0 & \\ -1 & 0 \\ 0 & -1 \end{bmatrix} \begin{bmatrix} \Delta T_{cmd} \\ \Delta C_{cmd} \end{bmatrix} + \begin{bmatrix} \Gamma_{est} \\ 0 \end{bmatrix} \begin{bmatrix} v \\ w \end{bmatrix} \tag{7.30}$$

The complete block diagram for an implementable LQG design is shown in figure 41.

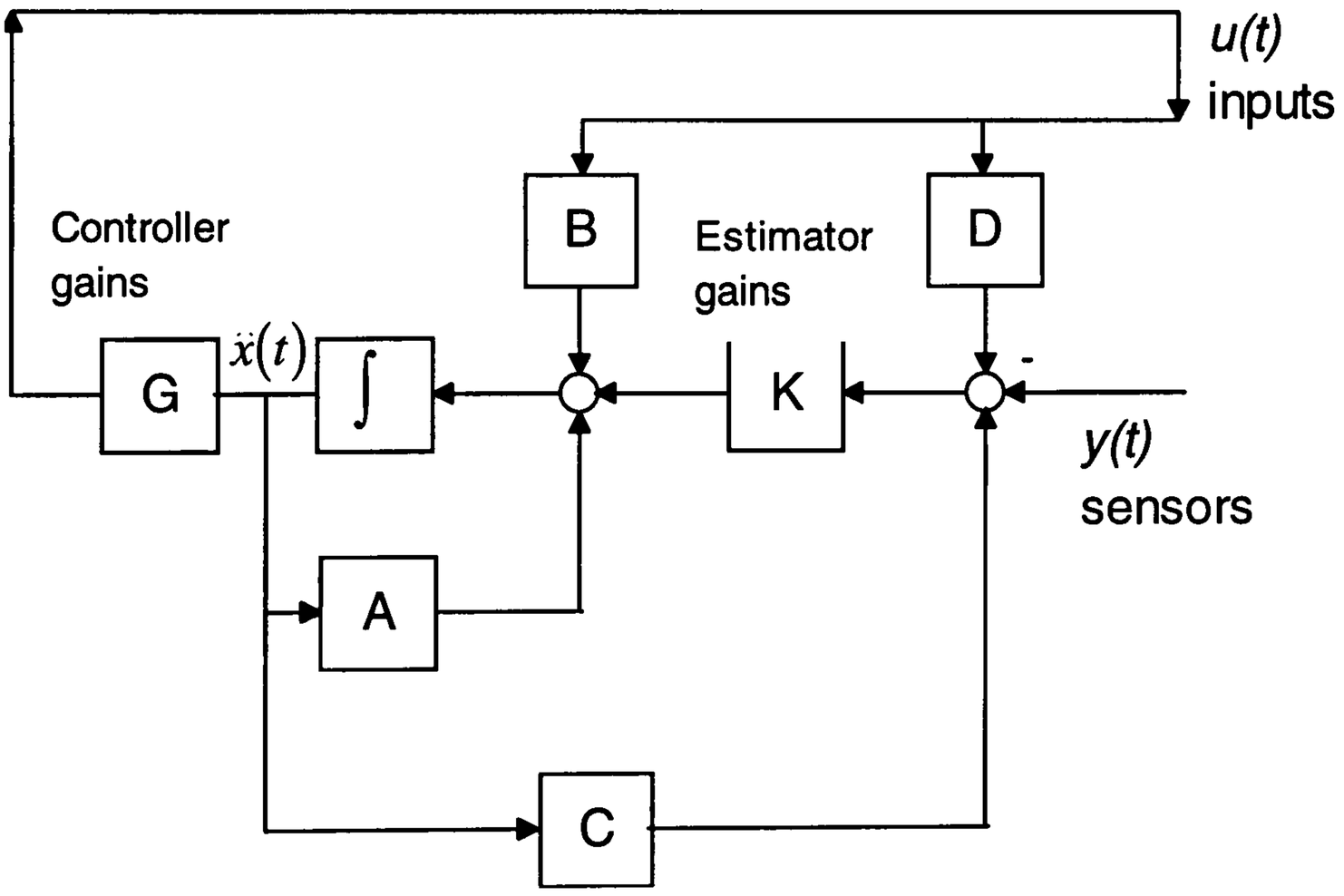

FIGURE 41: Block diagram of an implementable LQG controller

7.3.3 Closed loop performance

In figure 42, the development of vessel temperature profile and the affects on conductivity are shown when the set point for the former is changed by 0.5 K through the following function.

$$T_{cmd} = 0.5 \times \left(1 - exp(-0.05\,t)\right)$$

where t is the real time.

The conductivity command is generated by the following function

$$C_{cmd} = 4.0 \times \left(1 - exp(-0.05\,t)\right)$$

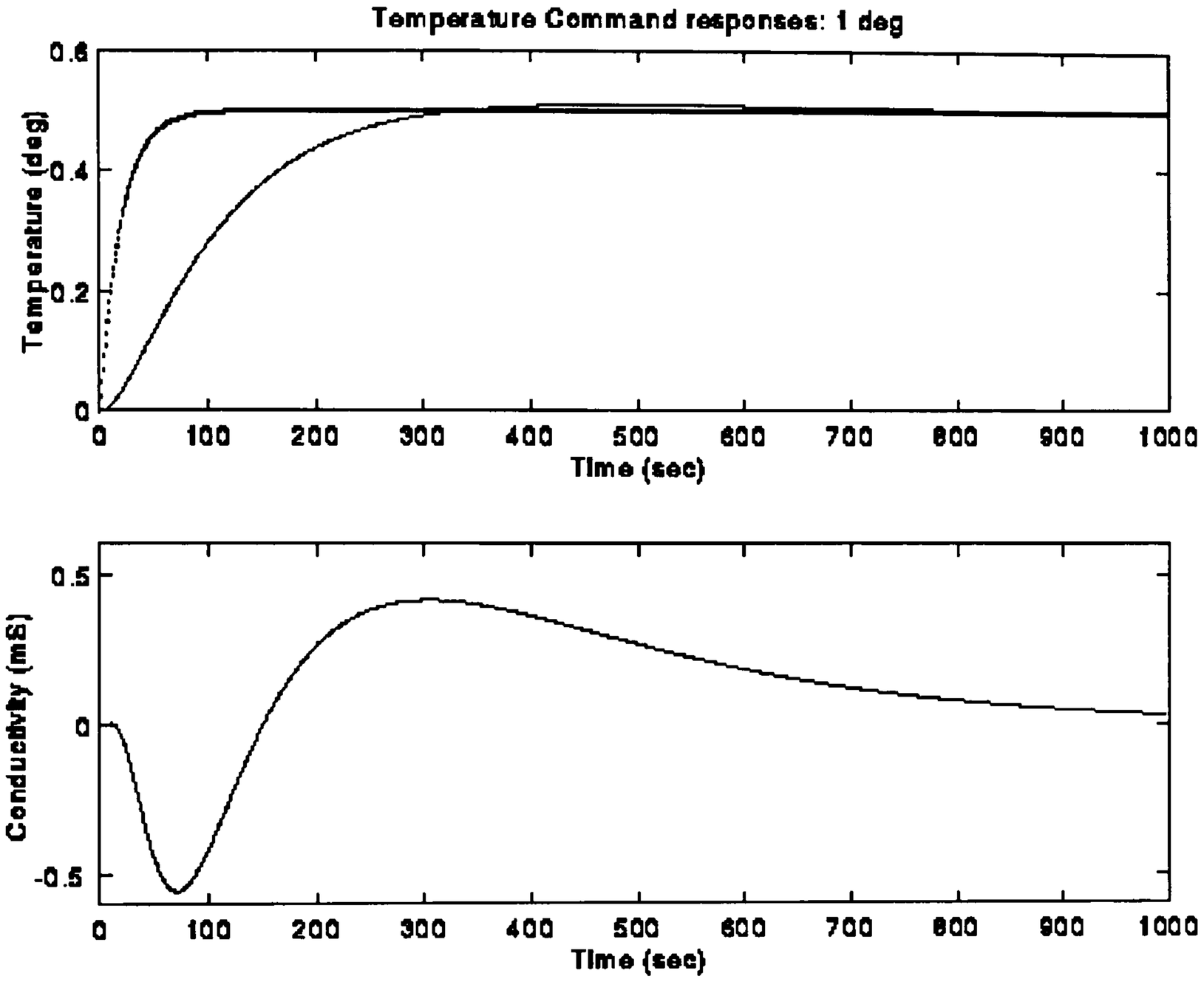

FIGURE 42 : Responses to set point change in vessel temperature

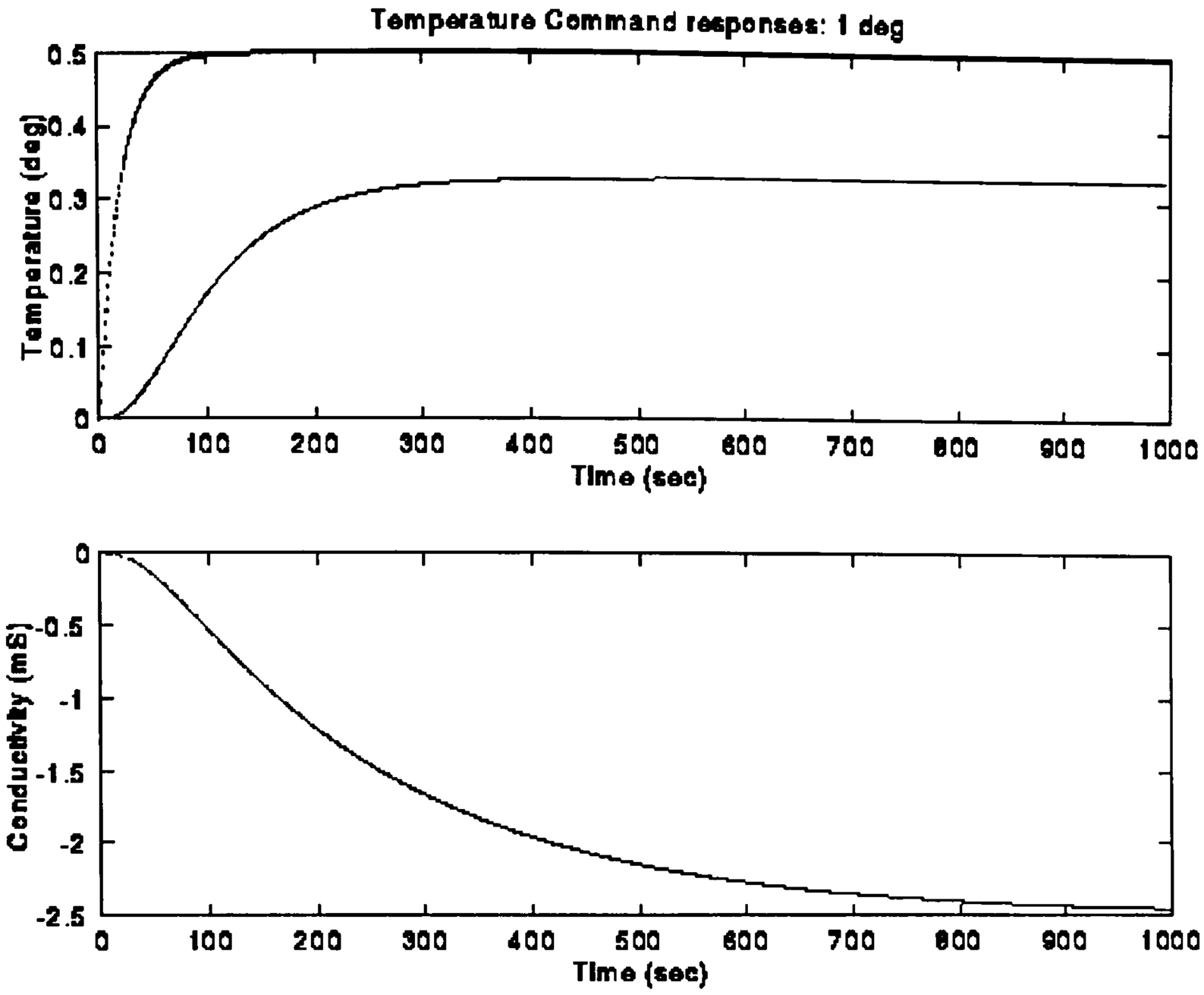

FIGURE 43 : Open loop response to change in vessel temperature set point

In figure 43, the corresponding open loop responses are shown. The lower curves in the upper plots of fig. 42 and 43, show the vessel temperature response to similar variations in the set point introduced according to the function represented by the upper curves. It can be noticed that zero off-set is achieved through the controller. In the open loop case, however, the final value of temperature is less than 0.3 for similar variations in inputs as for the closed loop system. Furthermore, the uncontrolled action increases the conductivity by nearly 2.5 mS whereas there is very minute change in conductivity with control action when the system achieves its new steady state.

In figures 44 and 45, responses of the measurements are shown when the set point for conductivity is changed by 4 mS for simulated controlled and open loop system.

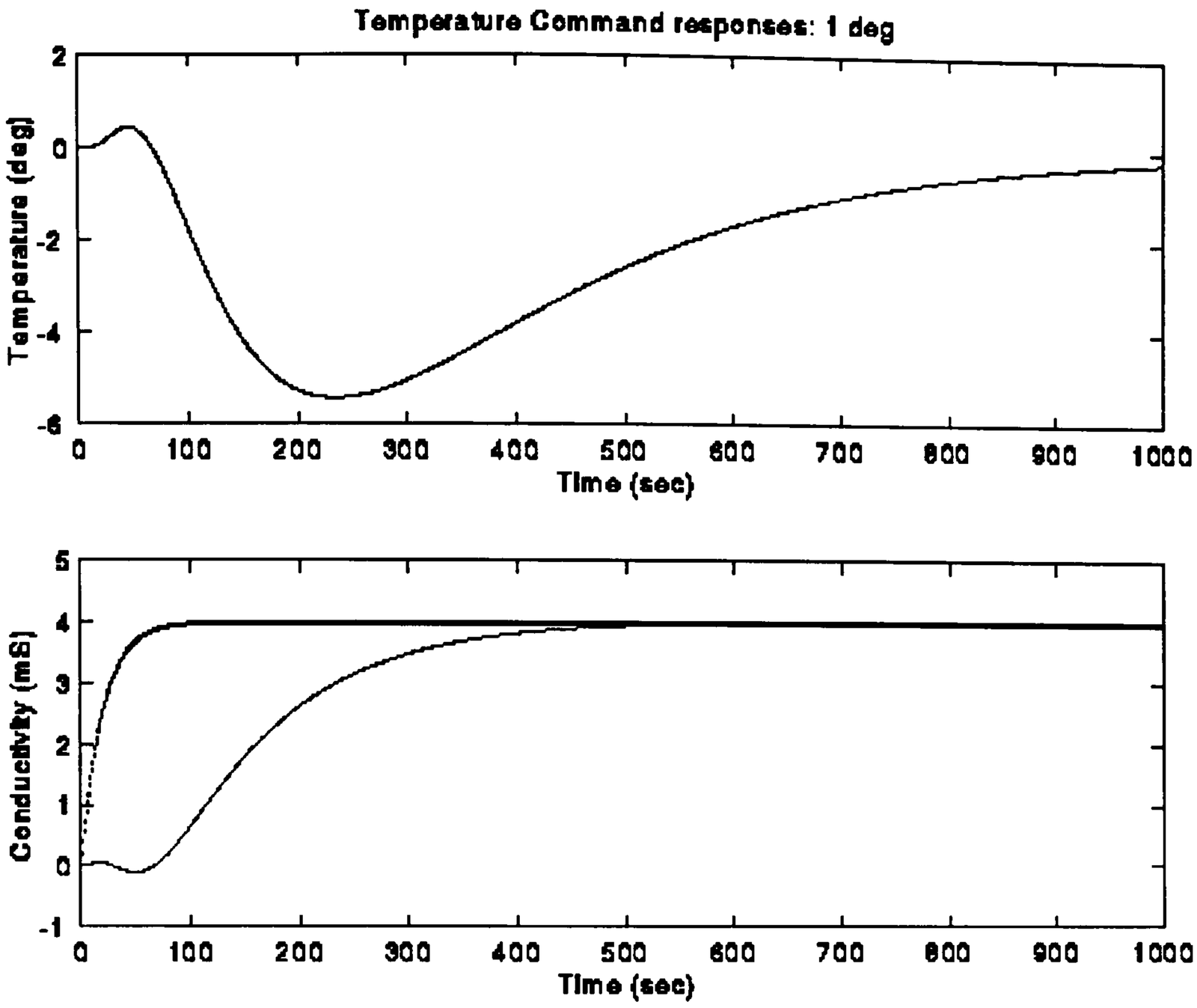

FIGURE 44 : Responses to set point change in conductivity

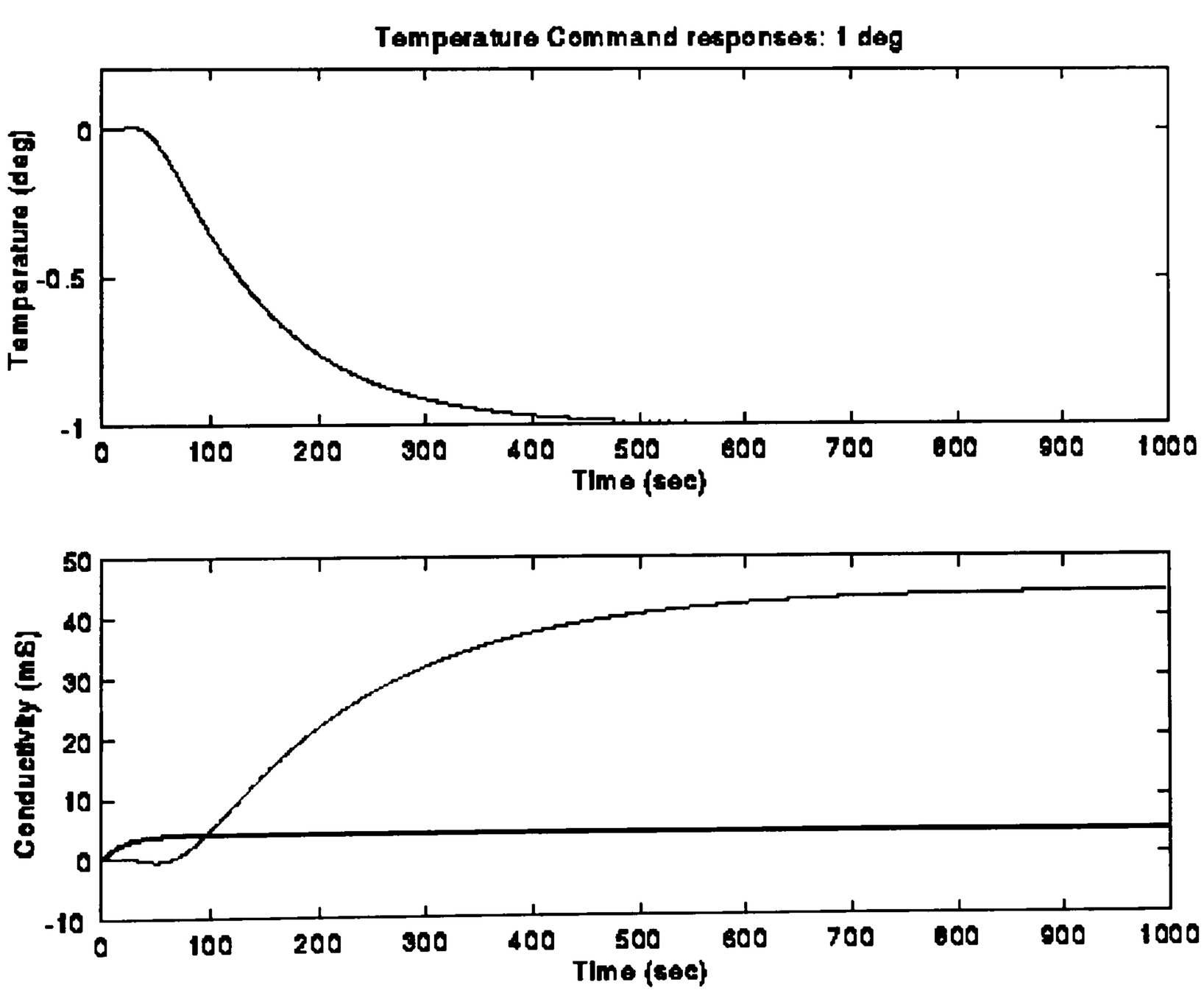

FIGURE 45: Open loop responses of the system to set point changes in conductivity

Again no off-set is observed and though, large variations are noticed during the early stages of the reaction curve for vessel temperature, it eventually settles to a value very close to its initial settings. The open loop performance for similar manipulations in the inputs fail in both respects, as a run-away increase in conductivity is observed due to a sharp decline in vessel temperature.

7.3.4 Closed loop stability analysis

As with the LQR, three different types of analysis are carried out for the LQG design to determine its stability characteristics. These include the study of covariance responses of the states due to the controller, eigenvalues of the closed loop **A** matrix and the frequency responses from the single loop analysis.

The covariance responses of the output with LQG controller are also calculated using the Lyapunov matrix equation with the $\mathbf{A}_{cl}$ and closed loop gain matrix for the full-state estimator based controller. The comparison of the values with LQR design show that the responsiveness of the design to states is slightly deteriorated. It however, becomes more sensitive to the actual measurements (apparent from the increase in the magnitude of numbers in column 3 and 4 in appendix E).

The examination of eigenvalues of the system determined through the $\mathbf{A}_{cl}$ matrix shows that the system is stable with a slight reduction in the relative magnitude when compared with the values obtained from LQR design. Following is the listing of roots.

Eigenvalues		Damping	Frequency(rad/sec)
-4.34783e-03	0.00000e+00i	1.000	4.34783e-03
-4.34783e-03	0.00000e+00i	1.000	4.34783e-03
-5.95238e-03	0.00000e+00i	1.000	5.95238e-03
-5.95238e-03	0.00000e+00i	1.000	5.95238e-03
-1.00000e-02	0.00000e+00i	1.000	1.00000e-02
-1.00000e-02	0.00000e+00i	1.000	1.00000e-02
-1.42857e-02	0.00000e+00i	1.000	1.42857e-02
-1.42857e-02	0.00000e+00i	1.000	1.42857e-02
-2.44971e-02	0.00000e+00i	1.000	2.44971e-02
-4.00000e-02	0.00000e+00i	1.000	4.00000e-02
-5.00000e-02	2.88675e-02i	0.866	5.77350e-02
-5.00000e-02	-2.88675e-02i	0.866	5.77350e-02

-5.00000e-02	2.88675e-02i	0.866	5.77350e-02
-5.00000e-02	-2.88675e-02i	0.866	5.77350e-02
-1.00000e-01	5.77350e-02i	0.866	1.15470e-01
-1.00000e-01	-5.77350e-02i	0.866	1.15470e-01
-1.00000e-01	5.77350e-02i	0.866	1.15470e-01
-1.00000e-01	-5.77350e-02i	0.866	1.15470e-01
-1.28382e-01	0.00000e+00i	1.000	1.28382e-01
-2.00000e-01	0.00000e+00i	1.000	2.00000e-01

Single loop analysis is again performed by tearing one loop and analysing the stability of the resulting system by studying their Bode plots. The gain and phase margins show that though, the former remain unchanged from the previously determined values for LQR design, the phase margins are greatly reduced. The values for the latter are calculated as -247.65 and -253.43 for the jacket and recycle loops respectively.

7.4 Robustness properties of the LQG controller

In this section, a comparison between the loop properties of a full-state feedback control law (LQR) and those for an LQG controller is presented. Loop transfer function for an LQR design broken at control inputs is,

$$L_{LQR} = \mathbf{G}(s\mathbf{I} - \mathbf{A})^{-1}\mathbf{B} \tag{7.31}$$

while for an LQG, similar transfer function is given by (Stein and Athans, 1987)

$$L_{LQG} = \mathbf{G}(s\mathbf{I} - \mathbf{A} - \mathbf{BG} - \mathbf{KC} - \mathbf{KDG})^{-1}\mathbf{K}\left[\mathbf{C}(s\mathbf{I} - \mathbf{A})^{-1}\mathbf{B} + \mathbf{D}\right] \tag{7.32}$$

Since $L_{LQR} \neq L_{LQG}$, the robustness properties of the two design are not similar. It is not even possible to guarantee robustness for an estimate-state feedback controller (Stein and Athans, 1987). Many different methods have however, been developed for recovering loop properties lost during the estimator design (Saberi et al., 1993). In the following the method due Stein and Athans (1987) for loop transfer recovery will be explained. The findings of the procedure for current design will also be reported.

7.4.1 LQG/LTR design through process noise and control inputs

The simple procedure due to Stein and Athans (1987) recovers the LQR properties by using the mechanism of the Riccati equation. The idea is to introduce additional fictitious process noise at the control inputs while designing the estimator (or over-design the LQG controller). It has been successfully shown that increasing the intensity of added noise results in a significant resemblance of the properties for the two designs, viz. LQR and LQG/LTR (Stein and Athans, 1987; Saberi et al., 1993). The analysis is carried out to find the appropriate gain matrix **K** such that the closed loop estimator dynamics represented by the system matrix (**A+KC**) is asymptotically stable and the recovery error E(s) given by the following equation is very small.

$$E(s) = -\mathbf{M}(s)\left[\mathbf{I} - \mathbf{M}(s)\right]^{-1}\left[\mathbf{I} - \mathbf{L}_{LQR}(s)\right] \tag{7.33}$$

where

$$\mathbf{M}(s) = \mathbf{G}\left(s\mathbf{I} - \mathbf{A} - \mathbf{KC}\right)^{-1}\left(\mathbf{B} + \mathbf{KD}\right)$$

The necessary and sufficient condition for the recovery error E(s) to be small is to have the magnitude of entries in the matrix **M** as small as possible, because the matrix itself represents the recovery. After proper definition of the appropriate cost function, the optimal gain matrix with loop transfer recovery can be formulated as (Stein and Athans, 1987)

$$K_{LQG/LTR} = -\left(\mathbf{BD}^T + \mathbf{PC}^T\right)\overline{\mathbf{R}}^{-1} \tag{7.34}$$

Matrix **P**, satisfies the solution of the following Riccati equation

$$\overline{\mathbf{A}}^{\mathrm{T}}\mathbf{P} + \mathbf{P}\overline{\mathbf{A}} - \mathbf{PC}^{\mathrm{T}}\overline{\mathbf{R}}^{-1}\mathbf{CP} + \mathbf{BB}^{\mathrm{T}} - \mathbf{BD}^{\mathrm{T}}\overline{\mathbf{R}}^{-1}\mathbf{DB}^{\mathrm{T}} = 0 \tag{7.35}$$

where

$\overline{\mathbf{A}} = \mathbf{A}^T - \mathbf{C}^T\overline{\mathbf{R}}^{-1}\mathbf{DB}^T$ and $\overline{\mathbf{R}} = \mathbf{DD}^T + \varepsilon\,\mathbf{I}$.

ε being the intensity of the arbitrary noise added at the control inputs. Following are the command lines for calculating the optimal gain matrix for the LQG/LTR and the subsequent control design.

```
%%%Loop Transfer Recovery

Gest2=[Gest1];
Wox=diag([0.0,0,1,1]);
Vox=Vo;
Destx=zeros(4,2);
kx=lqrcross(Aest',Cest',Gest2',Destx,Wox,Vox);kx=kx';
%Controller formulation
gestx=g(:,1:20);
gix=g(:,21:22);
Acontx=[Aest-Best*gestx-kx*Cest,-Best*gix;
      zeros(2,22)];
Bcontx=[kx;[1,0;0,1]];
Bccontx=[zeros(20,2);-eye(2)];
Dcontxx=zeros(2,4);
Bcontxx=[Bcontx,Bccontx];
Ccontx=-g;
Dcontx=zeros(2,2);
```

In the above, the new gain matrix for the LQG/LTR controller is given by kx, while g denote the LQR gain matrix.

7.4.2 Closed loop stability analysis of the final LQG/LTR design

The eigenvalues for LQG/LTR (see the values for **ACLx** in appendix E) again show that all the poles are stable and their magnitudes have slightly increased, which reflects improved stability and performance. The covariance response of the states also shows a general increase for all the states. The values though not very close to LQR design, better resemble them than those from the LQG design.

The gain and phase margins for the single loop analysis are lower when compared with the LQR design, they are, however, well inside the stability region. The actual magnitudes are as follows;

1. Jacket temp. loop only: Gain margin = infinite, phase margin = 180-(-259)
2. RR loop only: Gain margin = 11.88 dB, phase margin infinite.

7.5 Incorporation of the PCA model and overall robustness analysis

The PCA model establishes linear relationships between primary control variables and measurements that would have only translated as scaling up the measurements. It was not, therefore, deemed necessary to base the design on estimated primary control variables. The issue of uncertainty within the regression model and its implications for the controller performance is addressed by evaluating the performance of the design by introducing variations into the model parameters that were identified in chapter 6. This is done by running six control simulations after introducing variation of between 10-15% in either the dead times, time constants or the steady-state process gains. In the first run the time constants for the four transfer functions were changed from 70, 100, 230 and 168 respectively to 75, 110, 250 and 180. For the second experiments the values considered were 60, 90, 210 and 158. In third and fourth simulated experiments the dead times were perturbed from 30, 60 to 38, 68 and 22, 52 respectively. The variations in gains for the four transfer functions during experiment 5 and 6 were 0.86, 0.47, 8, 14.1 and 0.45, 0.05, 2, 7.0 with the base values being 0.66, 0.25, 5, and 11.1.

It was found that changes in time constant only affect settling times for the control variables. For the first simulation these approached nearly 450 seconds for both measurements while the lower values reduced settling times to under 200 seconds (under nominal operation the settling times are around 400 sec.). Variations in gains had a similar affect where the settling times for experiment six were in excess of 500 seconds. Significant changes were, however, not observed during experiment five. None of these variations resulted in off-set or over-shoot.

The performance of the controller deteriorated when changes of the magnitudes specified for experiments 3 and 4 were introduced in the dead times. The results for the former are given in figures 46 and 47, while figures 48 and 49 display the response curves when the dead times are reduced. It can be seen that increases in dead time greatly affect settling times; these now approach nearly 1000 seconds for conductivity. The vessel temperature, however does not show significant adverse affects. Reductions in dead times manifest through over-shoots in the responses for both the conductivity and vessel temperature for respective step changes. The conductivity response over-shoots by nearly 25% before quickly settling at the set-point. The vessel temperature, on the other hand experiences an over-shoot of just under 10%. It is worth noting that the settling times do not increase as a result of this oscillatory behaviour and the system achieves its new steady-state within the nominal time.

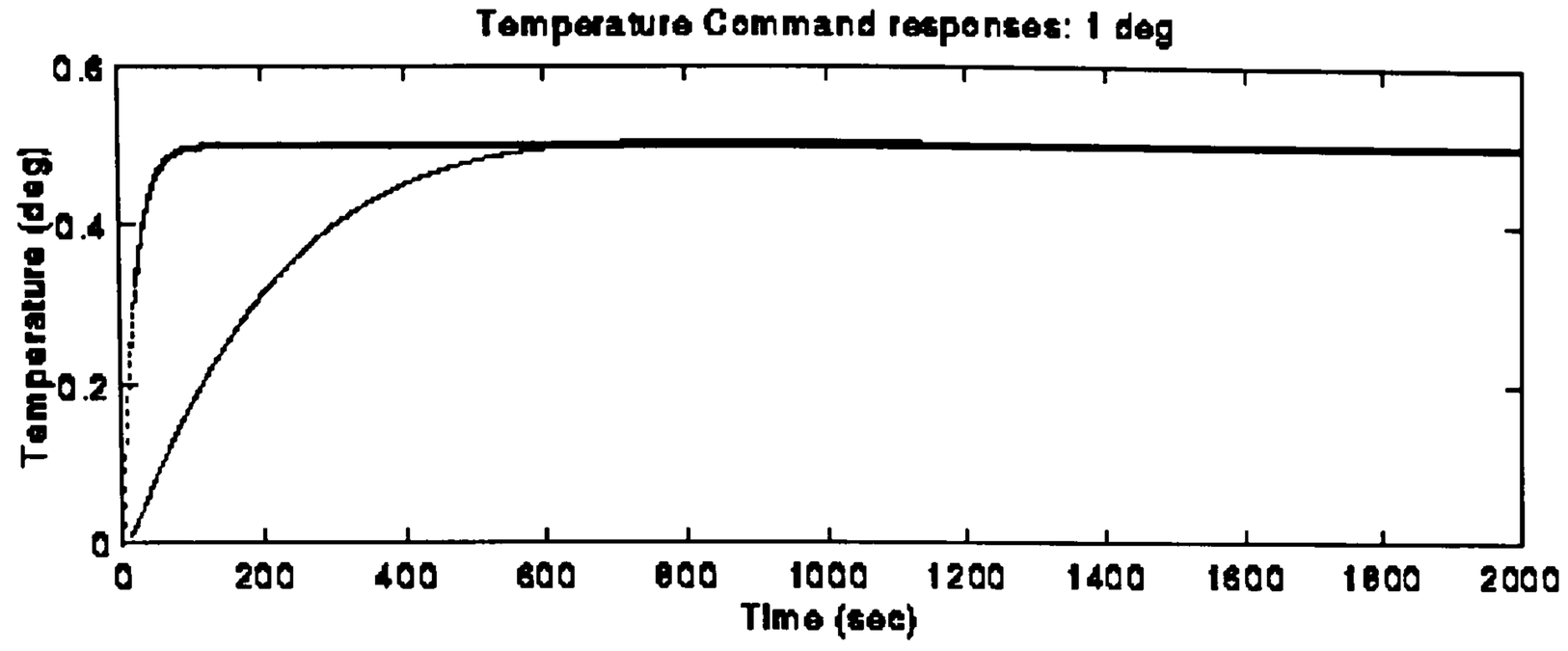

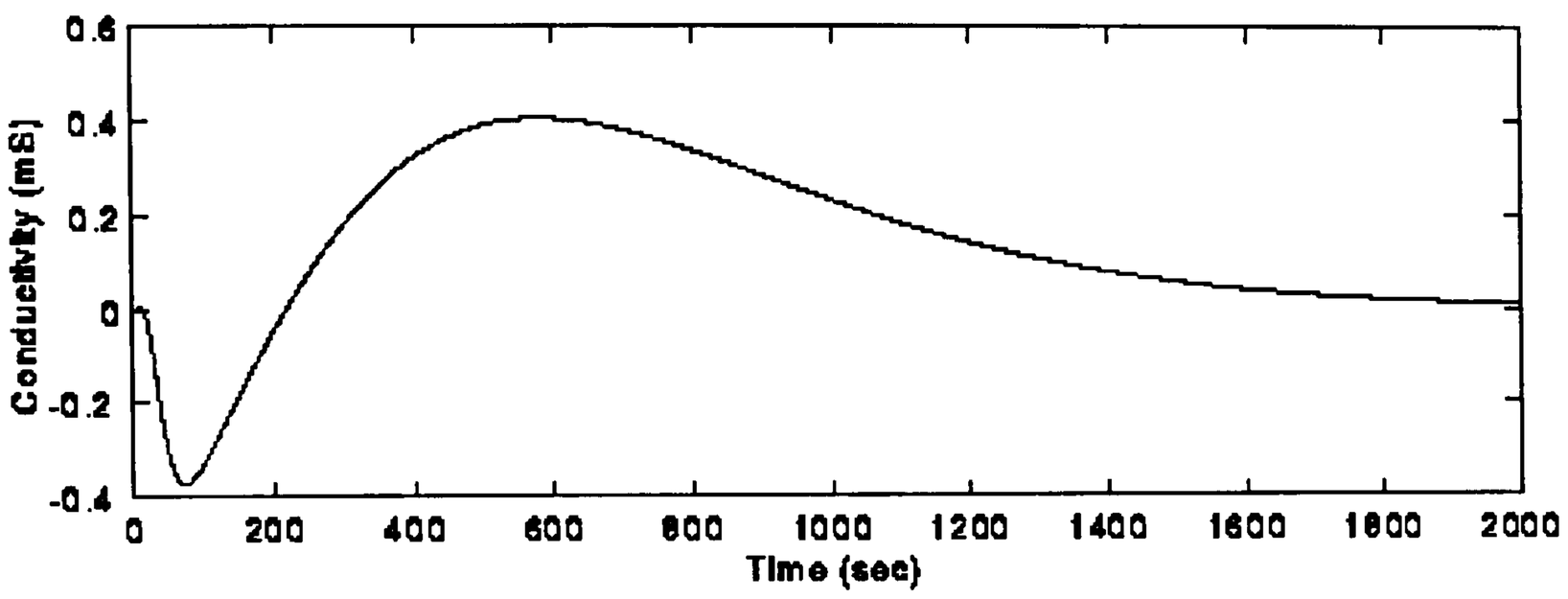

FIGURE 46 : Responses to set point change in vessel temperature for high dead times

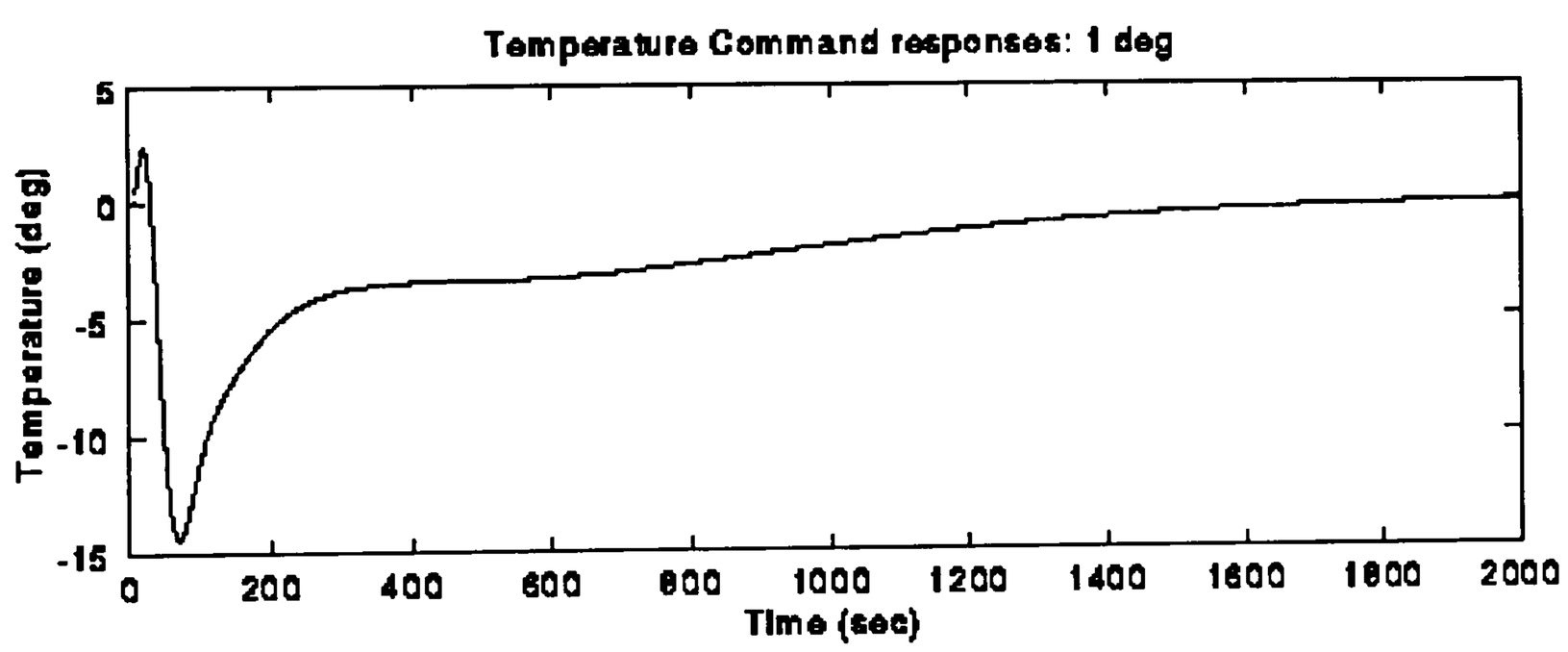

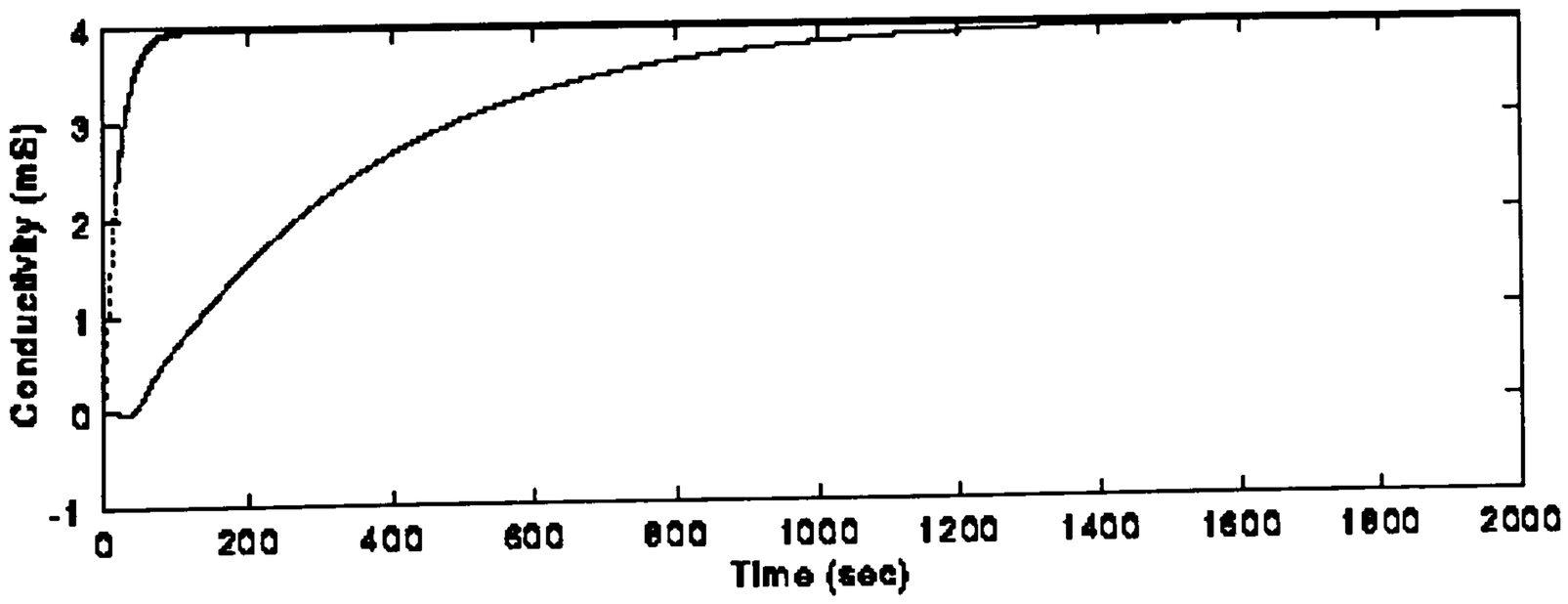

FIGURE 47 : Responses to set point change in conductivity for high dead times

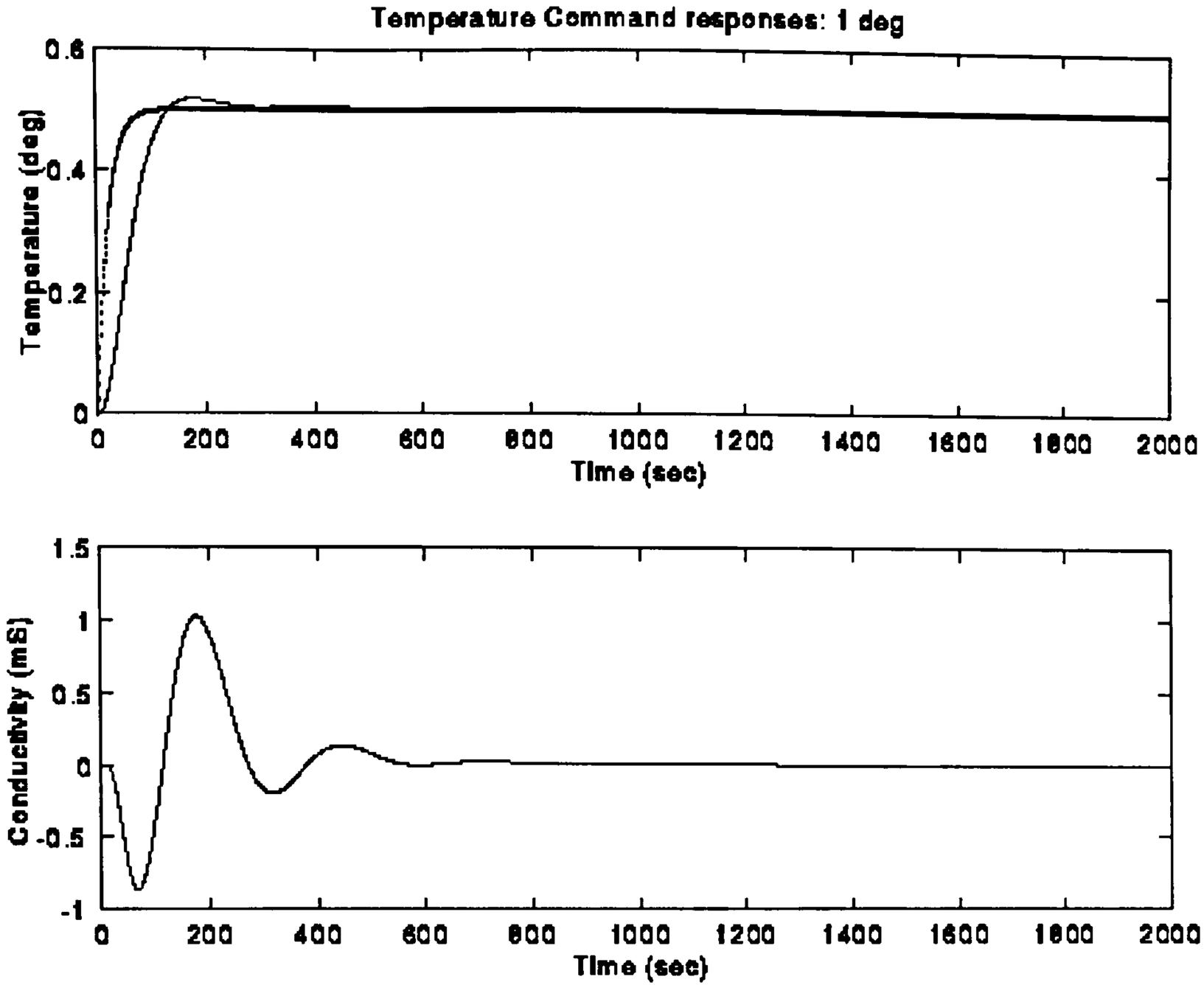

FIGURE 48 : Responses to set point change in vessel temperature for low dead times

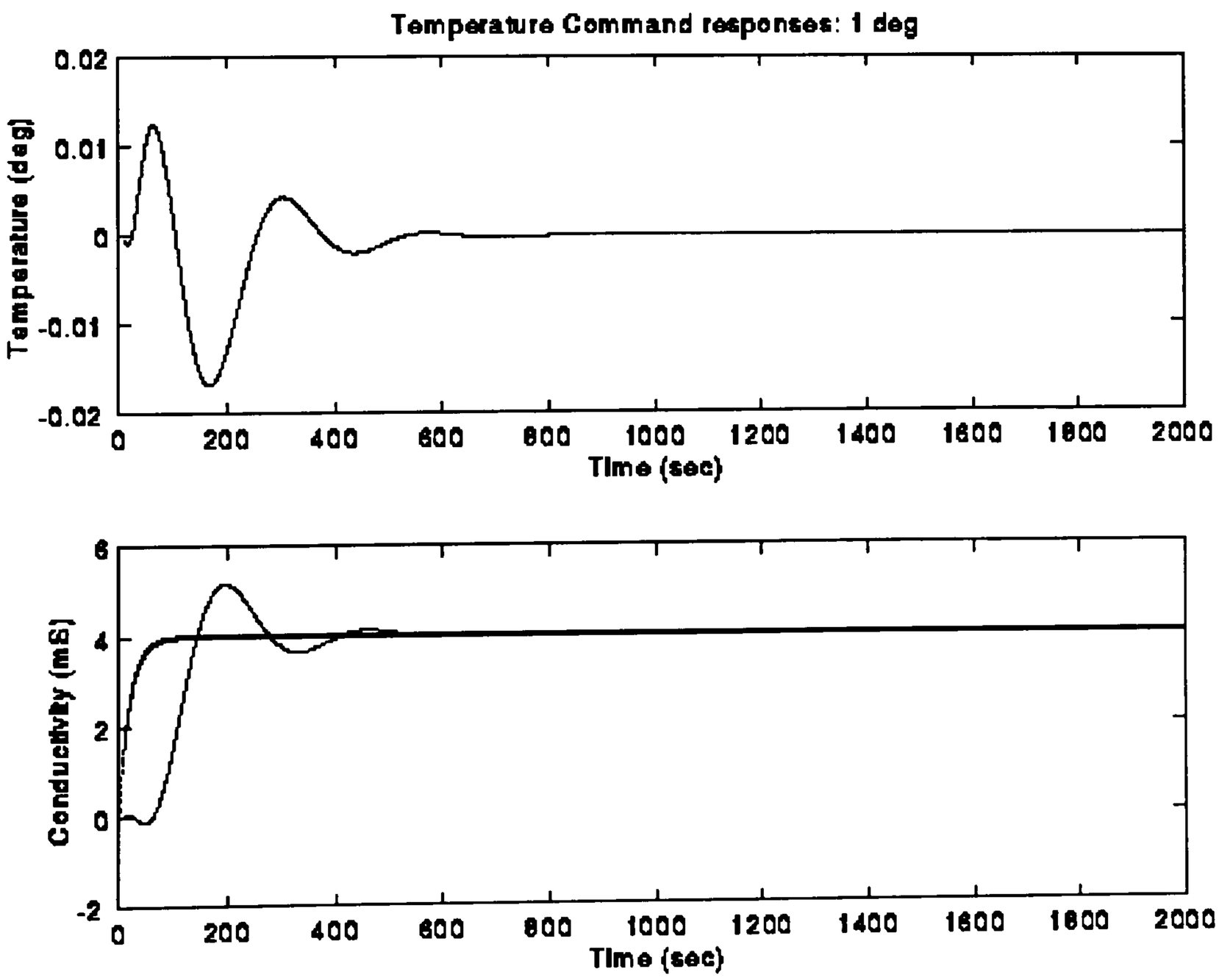

FIGURE 49 : Responses to set point change in conductivity for low dead times

If the above worst case performances were to be unacceptable, the controller could be modified by increasing the penalties on the drift from the required trajectory of the outputs through **Q** matrix in the LQR cost function. The placing of the target transmission zeros for both the outputs could also be re-adjusted by analysing the open-loop eigen-values of the system represented by the worst case. This would be achieved by re-defining the values of ω (please refer to sec. 7.2.2).

It can be seen that the controller retains acceptable levels of stability and performance even under worst case of pre-specified mismatch between the model and plant. It can therefore, be expected to achieve similar performance for primary control variables inferred through PCA model which can be in errors comparable to the model parameter variations considered here.

7.6 Conclusions

A robust multi-variable optimal controller has been designed to inferentially control both the number and average size of crystals by establishing linear relationships between these variables and the available measurements for conductivity and vessel temperature. As evident from the comparison between open loop responses and the controlled closed loop results, the controller achieves zero off-set for both measurements and also effectively eradicates process disturbances. The controller is found to retain stability and most of its performance under a range of scenarios representing plant/model mismatch and primary variable inference uncertainites.

Chapter 8:

REFLECTIONS AND FUTURE DIRECTIONS

In this chapter, the significant issues raised in each of the three major aspects of this thesis, *viz.* synthesis, optimisation and control are presented. This is accompanied discussions on how the work reported here might be improved and extended.

8.1 Synthesis of stage-wise crystallization processes

In this work, a new method has been developed for innovative design of stage-wise crystallization processes. The method results in major improvements for the two main attributes of crystal size distribution, *viz.* average size and coefficient of variance, without significant reductions in yield when compared with the conventional cascade design. This is achieved through a fundamental design shift, whereby innovative flow distributions are isolated for optimal trade-off between CSD properties and yield.

The technique is based on targeting approach which proceeds by evaluating the maximum attainable performance for a given kinetics within the design constraints without explicitly specifying the network. Points are then sequentially generated in concentration space through the kinetics equations, and the mass and moment balances while maximising a performance index. The moment balances ensure that the search direction is based on both the yield and CSD parameters. The sequential mapping of optimal trajectories in the concentration space is then used to infer the appropriate network. The mathematical model takes the form of a boundary value differential equation system which is transformed into a set of non-linear equations through orthogonal collocation. The resulting set of equations is solved to determine the optimal control profiles for best achievable performance through SQP algorithm.

It has been demonstrated that even with many simplifying assumptions and limitations of SQP routine, it is possible to significantly improve performance. For the KNO_3 crystallization considered in this work, a minimum increase of 115% in yield was

achieved on the best (yield-wise) single MSMPR crystallizer with comparable volume and throughput. The degradation in average size was no more than a mere 17% when compared with the a similar crystallizer with lowest average sizes. This compared with an improvement of over 300% in yield for a simple cascade but at a 60% reduction in average size. Reductions in CV were also more pronounced in the optimal network. These results manifest the capabilities of the model to effectively balance improvements in CSD properties with reductions in yield through a novel approach based on optimal flow distribution.

Some issues and concerns

A large number of collocation points have been found to be essential for an acceptable solution. The number of collocation points, however, defines the length of control variable vectors which gets large enough to affect the efficiency of the SQP routine in obtaining the optimal solution. These issues restricted us to consider only independently determined optimal temperature profiles during the case studies.

The consequences of such limitations can be costly, especially when the current model is expanded to encompass inter-connected sub-systems comprising series of hydrocyclones for product classification and energy integration networks. Such expansions can be readily done for heat integration networks, mainly due to the simplicity of their incorporation into the CFR model (Balakrishna and Biegler, 1996) and the availability of heuristics on the optimal form of temperature profiles. Inclusion of a hydrocyclone network is, however, not straight forward because the heuristics on specification of their performance within networks do not exist. Furthermore, the conventional models often represent performance in terms of separation efficiency

curves. They require the knowledge of complete crystal size distribution which is rarely modelled at design level calculations.

Suggestions for improvements

In order to formulate and solve larger problems to simultaneously consider sub-systems within the flowsheet, the MINOS algorithm could be used. Though, most efficient for large non-linear problems (n > 100), it requires linearisation of all the active constraints around the starting points. This will result in large number of function calls and possibly higher numerical errors, because all the highly non-linear state equations obtained through the transformation of the differential equations are solved as constraints.

To retain the SQP method for robust solution, a new method has to be devised for the discretisation of the boundary value problem. This new method will have to reduce the length of the existing control vectors without significant penalties on the accuracy of the transformed set of equations. This would help incorporate new vectors for heating or cooling profiles (for heat-exchanger network integration) and performance representation for hydrocyclones. We suggest replacing Lagrange basis function with the wavelet basis function for this purpose. These bases are extremely effective in determining the coarseness of the discretisation mesh according to the form of the function at a particular value of the independent variable. Their utility has been demonstrated through solution of equations representing propagation of shock waves through fluids (Erlrebacher et al., 1996).

The interpretation of segregated solution within finite elements has been based on MSMPR crystallizers. This would result in degradation of the estimated performance which can only be recovered if exact analogues for PFR can be found and modelled

during detailed analysis. Future work could also therefore focus on developing mathematical relationships between PFR type behaviour and its possible counterparts in crystallization such as draft-tube and column crystallizers. This would enable extending networks to comprise different types of vessels, along with different operational specifications.

It has been repeatedly reported in the literature that hydrocyclones play an extremely important role in determining the final characteristics of the crystalline product through their size classification capabilities which are well capable of improving CSD characteristics beyond the levels possible by manipulating the behaviour of the crystallizers themselves. Work could be done on developing heuristics for their incorporation within the crystallizer networks and for developing simple yet physically interpretable models for synthesis purposes.

The above suggestions would enable the realisation of maximum possible performance from stage-wise processes by optimally synthesising the complete process and rating the performances of the devices within it.

8.2 Process optimisation

In this work first attempt is made to optimise crystallization process flowsheets at operational level by generating and analysing process data. The method used is better then the conventional procedures for process optimisation because the latter are often based on simplified mathematical representations of the system which, though sufficient for design level calculations, can be inadequate to achieve continual improvements in operational performance. It is also a significant improvement on the multi-variable statistical techniques for extracting opportunities leading to improved performance through data analysis, because of its superior representation of results.

The method is based on machine learning approach to continuous performance improvement which identifies bands of crucial decision variables leading to zones of best average performance. Such representation in the form of hyper-rectangular zones addresses the issue of process variability during operation. This variability can often result in sub-optimal performance because the area surrounding an optimal point does not in general correspond to the zone where best average performance is achieved.

The methodology in its original form (Saraiva and Stephanopoulos, 1992) comprised two components; one for screening the data to maintain a reduced subset conveying novelty and the other for revealing structure in the collection of observations. The former employ case based reasoning, while the latter is based on symbolic induction which involves operations of generalising, specialising, transforming, correcting and refining knowledge representation.

The symbolic induction component of the methodology has been modified to include an incremental algorithm for updating the decision trees in the wake of incoming data. This not only eliminates their periodic re-induction with the old methodology but also simplifies the case based reasoning step. Its scope reduces from keeping an active memory of exemplars, updating it as new data becomes available, identifying novelty, removing obsolete data and determining when to re-induce the new version of the tree, to simply recognising an incoming object as novel and passing it onto the induction stage for its continual update through the incremental algorithm. These along with the other modification introduced here have resulted in the reduction of upto 55% in computational effort.

The methodology is demonstrated through KNO_3 crystallization process flowsheet where three opportunities with each representing an increase of 12% on nominal

performance are identified within two generations of symbolic induction. These are isolated without altering the variation levels initially specified for operational variables.

Issues and possible future advancements

The essence of problem with this approach is one in which a procedure, shown a set of process data comprising quantitative and or qualitative features of the process, employs inductive inference to extract classification rules for the division of decision space into hyper-rectangles representing different levels of performance without losing the individuality of each decision variable. These partitions are generated through orthogonal partition of the space which accounts for the non-linearities in the system through a large number of small partitions. In small problems with limited number of process features and data, the existing method infers decision trees of acceptable size and the identified zones of interest can be easily expanded, based on the features of the process around them. For larger problems, however, the tree could get excessively large that would complicate the inference procedure, since a large number of variables would have to be traversed. The size of the tree also affects case-based reasoning step, and therefore the overall efficiency of the methodology in quickly and accurately identifying the regions of interests will be further reduced.

The common approach to curb the size of the trees is by more stringent pruning, which though beneficial for problems where the objective is to extract broad generalisation about the system would b extremely detrimental for our purpose of isolating incidences that yield above average performances. We therefore, propose to replace the existing uni-variate tree induction algorithm with a procedure based on Brodley and Utgoff's (1995) method for multivariate induction. Though the procedure

is not restricted to orthogonal partition and therefore finds more compact trees by checking for linear combinations of a range of variables at each node, in its present form it only provides a non-incremental algorithm similar to the *ID3* used by Saraiva and Stephanopoulos (1992). A new incremental multivariate tree induction procedure could therefore be developed for the scaling up the revised methodology presented in this work.

The issue of multiple objective functions could be another possible future focus of attention. Saraiva (1995) extended the old methodology to include multiple operational objectives by modifying two of its aspects, viz. definition of performance variable and identification and refinement of the rules themselves. In the former a new performance function was defined through combination of the p individual performance variables which was then used as the criterion for subsequent symbolic induction. During the induction phase this translated into an increased number of tests, equal to p times the number of variables at each node. The other accompanying complication was the fact that a trade-off criterion had to be defined, should the most desired combination of performance were not achieved.

This particular approach was actually used in our case study, where the accompanying complications were hidden by the correlation between average size and total number over the range of interest. Further developments on this front, using multivariate decision trees could be an extremely interesting and challenging project for the future.

An alternative methodology for multi-objective optimisation could be devised for a more versatile technique by using the concept of blackboard architectures (Nii, 1986a; 1986b). It is based on opportunistic reasoning based problem solving model where pieces of knowledge are applied either backward or forward at the most opportune

time. The overall model consists of three major components; the knowledge sources, the database and the control. The knowledge source encompasses different techniques that would be needed to solve the components of the problem while the database which is termed as the blackboard is where all the data is kept. Knowledge sources produce changes to the blackboard that incrementally lead to the solution of the problem. The control determines the knowledge source required to respond. Though the method provides a comprehensive structure for employing all the relevant techniques at the appropriate levels of hierarchy to obtain an overall solution, it is difficult to realise as a computational entity. That is where the challenge lies.

8.3 Control of continuous crystallizer

An optimal multi-variable controller has been designed for indirectly controlling total number of crystals and average size. The controller is found to be robust under process uncertainty over a wide window of operation with capabilities for both set-point tracking and disturbance rejection. The design is far superior to any of the work previously reported in the literature on the control of crystallizers not only because the most developed state of the art mathematical techniques have been employed but also a much wider range of control objectives have been considered and the design is based on real process data obtained over a range of operating conditions.

The experiments were performed for a range of objectives that included development of multi-variable regression models for estimating primary control variables from process measurements, system identification in terms of first order plus dead time models and disturbance modelling. The optimal control theory is used to design a robust optimal controller through the LQG/LTR design procedure which requires state-space realisation of the system dynamics identified in frequency domain from the

experiments. These individual state-space models are augmented together with two new integral states corresponding to the differences in the set-points and actual measurements to obtain the complete description of the system. Continuous time infinite horizon quadratic cost function is solved to obtain the "full-state" optimal control gain matrix. An optimal state observer is then designed by minimising the error covariance-variance of the estimated states. The robustness properties of the full state controller which are lost with the observer are recovered by the simple loop transfer recovery procedure, where in essence the observer is fictitiously over-designed by using higher then normal intensities for measurement noises and process disturbances. The final LQG/LTR design is then used for the experimentally determined variations in process parameters to quantify controller robustness in the wake of process/plant mismatch. The high levels of variations considered in the analysis also cover for the relatively large deviations possible in estimating the number of crystals from vessel temperature and conductivity measurements.

During simulated runs, the controller has demonstrated excellent set-point tracking capabilities for both the outputs along with disturbance rejection arising from fluctuations in exit stream flowrates. The integral states ensured zero off-set while the fully coupled design helped maintain steady-state values of the other measurement at its original level. The open simulations for similar control efforts not only resulted in significantly large off-sets but also completely failed in maintaining the other output at the desired level.

Issues and possible future refinements

A multi-variable optimal controller has been systematically designed for obtaining best achievable performance in terms of control bandwidth and saturation limits. The

sequence of steps undertaken together with the techniques adapted in each of them, leaves only the definition of control objectives and the exhaustiveness of the process models used as the two major areas of possible improvements should the LQG/LTR design procedure be used which is by far the most developed in terms of the available techniques for thorough analysis and evaluation of design at each step in the synthesis. The only possible improvement to the controller itself could be the reduction of its order which in the present design is same as that of the complete system. This step, though customary for sound controller design practise is not essential given the powers of hardware available for the implementation of such controllers.

First and foremost is the issue of implementation of this design on the real process to gauge its effectiveness and further tune its performance on the actual crystallizer. For this purpose, the rig used in this work would need a few alterations, such as computer based commands for the external pump used to regulate recycle stream flowrate. The software running the controller will also need to be interfaced with the PC LAB program.

In the present inferential configuration the dynamics of primary control variables and the measurements are implicitly assumed to be identical. This assumption though crudely verified through experiments by taking three off-line measurements for the primary variables during the reaction curve experiments for the measurements, could be eliminated by including appropriately designed lead-lag elements between these variables. This can be achieved by implementing the inferential engine on-line and comparing its predictions with the actual off-line measurements over the entire reaction curve.

The overall performance of the controller in effectively tailoring the CSD will require extending the primary control variables to include other properties of the system. This could initiate finding parameters that influence and hence would regulate the shape of CSD within each interval of interest in the size range besides, considering other common properties such as CV, yield etc. The appropriate manipulatable variables would than have to be identified. An even wider window of operation could be used to test the controller performance, this time under more pronounced affects of disturbances.

The procedure for inferring number of crystals from process measurements through regression models is found to accompany large uncertainties. Though, the extent of discrepancies will reduce as the number of available measurements increase, it will be worthwhile to consider more realistic functional forms in the regression model, such as exponential components within higher order polynomials. Physical understanding of the process would be key to the development of such relationships. Similarly better models could be developed by not only fitting the reaction curves with more realistic higher order functions but also by rectifying the experimental curves to smoothen their forms for better inferences. We propose wavelet decomposition for the latter because it has a mechanism that could be used for isolating peaks that represent process behaviour from measurement noise (Erlrebacher et al., 1996; Daubechies, 1990).

Though LQG/LTR method provides the most comprehensive procedure for thorough design and analysis of multi-variable controller, other techniques could also be explored for the same purpose. A fuzzy logic based controller is particularly attractive in this respect for reasons that bear striking resemblance to those stated earlier in favour of using machine learning based optimisation techniques. In fact, the decision

tree induced there could be easily transformed into the appropriate rules representation at the fuzzifying step. Furthermore, since the trees are continually updated, the controller could easily be equipped with adaptive properties. These advantages are in addition to the common belief that fuzzy logic based design is more suitable when compared with other design methods for complex processes where simple model development is prone to high uncertainties (Rhinehart and Murugan, 1996). It is however, worth reminding that analysis tools for evaluating such a design are not very well developed.

8.4 Final remarks

Throughout this work, the underlying motivation has been to employ and develop diverse and most advanced yet inter-related techniques to address complex issues in synthesis, optimisation and control of crystallization without losing the overall focus from the important unit operation of crystallization. This is not only evident from the innovative and superior results presented here but also through the suggested possible improvements in the findings by furthering the understanding of both the techniques and the process itself. For instance, in the problem on optimisation the most promising opportunities for advancement could only be uncovered by developing the methods themselves, whereas in synthesis both the methods and the exploitation of the lacking understanding of the process itself are crucial for realising the full potential of the presented method. Finally, in the control problem the improvements are heavily related to the process aspect of the problem.

NOMENCLATURE

Chapter 3

Crystallizer

A	= frequency factor for primary nucleation, $cm^{-3}\ s^{-1}$
a, b, c	= constants in Eq. (3.3)
B	= overall nucleation rate, $cm^{-3}\ s^{-1}$
β	= agglomeration kernel $cm^3\ s^{-1}$
C	= solute concentration, $kg\ m^{-3}$
c_P	= specific heat capacity, $kJ\ kg^{-1}$
ΔH_C	= heat of crystallization, $kJ\ kg^{-1}$
G	= linear growth rate, $cm\ s^{-1}$
k	= Boltzman constant $J\ K^{-1}$
k_d, k_r	= diffusion and surface integration coefficients
k_N	= secondary nucleation rate coefficient
k_s	= surface shape factor
L_0	= size of the nucleus, μm
$\overline{m}_i$	= i^{th} moment, $\mu m^i\ cm^{-3}$
N	= number of particles in a class range, cm^{-3}
N_P, N_Q	= power and pumping number for the stirrer
P	= specific power input of the stirrer, $kJ\ s^{-1}$
Q	= heat transfer rate, $kJ\ s^{-1}$
q	= volumetric flowrate, $m^3\ s^{-1}$
S	= supersaturation expressed as fraction
s	= supersaturation expressed as difference
σ	= interfacial tension, $J\ m^{-2}$
υ	= molecular volume, m^3
ν	= volume of a crystal, μm^3
vol	= volume of the vessel, m^3
X	= specific attrition rate, s^{-1}

Hydrocyclone

A	= constant of integration
a	= feed inlet diameter, m
d_i	= equivalent diameter of the particle, μm
Q	= feed flowrate, $m^3\ s^{-1}$
q_i	= i^{th} component of fluid velocity
θ	= angle for radial direction
R_0	= length of the hydrocyclone, m
R_C	= radius of the cone in cylindrical region, m
R_V	= radius of the vortex finder, m
s	= engagement length, m
σ	= dimensionless group
U	= particle velocity
U_{pw}	= radial particle velocity near the wall of cyclone
U_{pv}	= radial particle velocity at the locus of zero vertical velocities
U_{ro}	= radial velocity of the liquid into the cone

V		= swirl velocity at the entrance
v_i		= liquid velocity in the i^{th} direction
W		= axial velocity at the inlet
w_i		= i^{th} component of vorticity
ψ		= stream function

Chapter 4

A	=	pre-exponential factor in nucleation rate expression, m^{-3} s^{-1}
$\overline{A}$	=	second moment of size distribution
B	=	nucleation rate, m^{-3} s^{-1}
c	=	constant on nucleation rate expression
G	=	crystal growth rate, m s^{-1}
$f(\alpha)$	=	fraction of crystals exiting CFR at point α
f_{ij}	=	fraction of crystals exiting discretised CFR at point α_{ij}
f_p	=	fraction of crystals obtained from the solution at p^{th}iteration
f_r	=	linear combinator of concentrations from PFR section of recycle reactor
i,j,k	=	index of finite element *i* at collocation point *j,k*
J	=	objective function
k_g	=	growth rate constant
$L_K(\alpha)$	=	Lagrange interpolation polynomial of degree k
$L'_K(\alpha)$	=	derivative of Lagrange interpolation polynomial
L	=	first moment of size distribution
n	=	number of crystals
$q(\alpha)$	=	fraction of feed entering the system at point α
q_{ij}	=	fraction of feed entering discretised CFR at point α_{ij}
Q_0	=	flowrate at the entry of the network
$Q(\alpha)$	=	total flowrate at point α
R(X)	=	reaction rate, s^{-1}
R_e	=	recycle ratio
$T(\alpha)$	=	temperature at point α
X	=	dimensionless concentration
$X_{i,k}$	=	dimensionless concentration at point *i,k*
$X_{i,end}$	=	dimensionless concentration at the end of element i
X_0	=	dimensionless concentration at network entry

Greek Letters

α	=	time along the length of the network
$\Delta\alpha_i$	=	length of finite element i
ϕ_i	=	ratio of feed flow to element i to bulk flow entering element i
λ	=	convex combinator for CFR
τ	=	mean residence time
τ_R	=	residence time in recycle reactor

Chapter 5

CF	=	feed concentration, kmol m^{-3}
E	=	Statistical measure of data ambiguity
e	=	mis-classification rate
FF	=	feed flowrate, litre s^{-1}
K	=	Number of classes
L_{av}	=	average crystal size, μm
n	=	mis-classification rate
N	=	number of objects
P	=	Frequency of objects from a certain class
R	=	Number of splits from a node
SE	=	Standard Error
TC	=	coolant temperature, K
TD	=	dissolver temperature, K
TF	=	feed temperature, K
W	=	hydrocyclone inlet axial velocity
y	=	rate of crystal production per unit volume, s^{-1}

Chapter 6

AC	=	actuator
CO	=	change in conductivity, mS
f	=	compliments of the dependent variable, y
G	=	transfer function
η	=	disturbance input (non-deterministic)
K	=	steady-state process gain
$\bar{L}_{est}$	=	estimated average crystal size, μm
N_{est}	=	estimated number of number of crystals
r	=	regression parameter vector
RR	=	recycle ratio
Σ	=	matrix with the square root of eigenvalues of $\mathbf{X^TX}$
t	=	time, s
τ_d	=	dead time, s
TJ	=	jacket temperature, K
τ_s	=	time constant, s
TV	=	vessel temperature, K
U	=	unitary matrix with all eigenvalues as 1
V	=	square matrix of eigenvectors of $\mathbf{X^TX}$
W	=	Reduced order description of **X**
X	=	matrix of measurements from different experiments
y	=	dependent variable

Chapter 7

a	=	co-efficients of the denomenator polynomial in G(s)
A	=	state matrix
b	=	co-efficients of the numerator polynomial in G(s)
B	=	input matrix
C	=	output matrix
ccrit	=	shaping filters

$\boldsymbol{C}$	=	controllability matrix
D	=	direct transmission matrix
ε	=	intensity of process noise
E	=	Statistical operator for stochastic variables
G	=	LQR controller gain matrix
Γ	=	process noise matrix
G(s)	=	transfer function in Laplace domain
J	=	cost criterion
K	=	optimal estimator gain matrix
K	=	shaping filter gains
L	=	loop transfer function
M	=	error recovery matrix for LTR
m	=	number of inputs
n	=	number of states.
$\boldsymbol{O}$	=	state observability matrix
p	=	number of outputs
P	=	Riccati matrix for LTR
Q	=	Measurement / state error penalty matrix
R	=	input efforts penalty
$\mathbf{S_0}$	=	Riccati matrix in LQR design
u	=	vector of inputs
$\mathbf{V}_0$	=	fraction of sensor noise matrix used for LQG design
$\boldsymbol{\Omega}$	=	measurement noise matrix
ω	=	settling frequency
$\mathbf{W}_0$	=	process noise matrix used for LTR design
x	=	vector of states
$\dot{x}$	=	vector of state derivatives
y	=	vector of outputs
ζ	=	damping factor

Subscripts

aug	=	augemented
cl	=	close loop
cmd	=	command
cont	=	controller
est	=	estimated
I	=	integral
dist	=	disturbance

PUBLICATIONS AND PRESENTATIONS FROM THIS WORK

1. Sheikh AY and AG Jones, "Crystallization process optimisation via a revised machine learning methodology", *AIChE J*, **43**(6), 1448 (1997)
2. Sheikh AY and AG Jones, "Operation of crystallization processes under uncertain conditions through machine learning methodology", In AIChE Annual Meeting, Recent advances in crystallization and precipitation, Nov. 10-15, 1996, Chicago, Il. AIChE, New York, Paper 3c.
3. Sheikh, AY and AG Jones, "Dynamic flowsheet model for an MSMPR crystallizer", In Industrial Crystallization '96. Eds. B. Biscans and J. Garside, Toulouse: PROGEP, 16-19 September 1996. pp. 583-588.

Publications Pending

1. Sheikh AY and AG Jones, " Optimal synthesis of stage-wise crystallization process using a targeting approach", (in preparation for Ind. Chem. Res. Des.)
2. Sheikh AY and Jones AG, "Multi-variable optimal Controller for a continuous recycle crystallizer I: The system and its dynamics", (in preparation for Ind. Chem. Res. Des.).
3. Sheikh AY and Jones AG, "Multi-variable optimal Controller for a continuous recycle crystallizer II: LQR/LQG design for the MIMO controller", (in preparation for Ind. Chem. Res. Des.).

REFERENCES

Balakrishna S, LT Biegler, "Targeting strategies for the synthesis and energy integration of non-isothermal reactor networks", *Ind. Eng. Chem. Res.*, **31** (9), 2152 (1992b)

Balakrishna S, LT Biegler, " Constructive targeting approach for the synthesis of chemical reactors", *Ind. Eng. Chem. Res.*, **31** (1), 300 (1992a)

Balakrishna S, LT Biegler, "Chemical reactor network targeting and integration: An optimisation approach" in Anderson JL (Edn.), *Advances in Chemical Engineering*, **23**, 243 (1996)

Benzaouia A, C Burgat, "Regulator problem for linear discrete time system under non-symmetrical state and control constraints", *Int. J Control*, **48**, 2441, (1988)

Biegler LT and IE Grossmann, "Strategies for the optimisation of chemical processes", *Reviews Chem. Eng,* **3** (1), 1-48 (1985)

Biegler LT, J Nocedal, C Schmid, "A reduced Hessian method for large scale constrained optimization", *SIAM J. Opt.*, **5** (2), 314 (1995)

Bitmead RR, M Gevers, V Wetz, *Adaptive optimal control- The thinking Man's GPC*, Prentice-Hall (1990)

Bloor MIG, DB Ingham, "Flow in Industrial Cyclones", *J. Fluid Mech.*, **178**, 507 (1987)

Budman HM, C Webb, TR Holcomb, M Morari, "Robust inferential control for a packed bed reactor", *Ind. Eng. Chem. Res.*, **31** (7), 1665 (1992)

Bradley D, *The Hydrocyclone*, Pergamon Press, Oxford (1965)

Brayshaw MD, " Numerical model for the inviscid flow of a fluid in a hydrocyclone to demonstrate the effects of changes in the vorticity function of the flow field on particle classification", *Int. J. Miner. Process.*, **29**, 51 (1990)

Breiman L, JH Friedman, RA Olshen, CJ Stone, *Classification and Regression Trees*, Wadsworth and Brooks (1984)

Bristol EH, "On a new measure of interactions for multivariable process control", *IEEE Trans Auto Control*, **AC-11**, 133 (1966)

Brodley CE, PE Utgoff, "Multivariate Decision Trees", *Machine Learning*, **19**, 45 (1995)

Chen HF, L Guo, "Optimal stochastic adaptive control with quadratic index", *Int. J Control*, **43**, 869, (1986)

Cori R, C Maffezzoni, "Practical optimal control of a drum boiler power plant", *Automatica*, **20**, 163, (1984)

Cuthrell JE, LT Biegler, "On the optimisation of Differential-Algebraic process systems", *AIChE J*, **33** (8), 1257 (1987)

Damen AAH, AK Hajdasinski, *in Proc. 6th IFAC Symp. Identification and System Parameter Estimation,* Washington DC, 903 (1982)

Daubechies I, "The wavelet transform, time-frequency localization and signal analysis", *IEEE Trans Info Theo*, **36**(5), 961-1005 (1990)

Dietz PW, "Collection efficiency of cyclone separators", *AIChE J*, **27** (6), 888 (1981)

Doherty MF, "Pre-synthesis problem for homogeneous azeotropic distillation has a unique solution", *Chem Eng Sci*, **40** (10), 1885 (1985)

Douglas JM, *Conceptual design of Chemical processes*, McGraw-Hill (1988)

Erlrebacher G, MY Hussaini, LM Jameson, *Wavelets: theory and applications*, Oxford University Press, New York (1996)

Evans LB, "Simulation with respect to solid fluid systems", *Comp Chem Eng*, **13**, 343 (1989)

Fayyad UM, KB Irani, "On the handling of Continuous-Valued Attributes in Decision Tree Generation", *Machine Learning*, **8**, 87 (1992)

Gangsaas D, Blight J, Bruce KR, Ly U, "Application of modern synthesis to aircraft control: Three case studies", *IEEE Trans Auto Control*, **AC-31**, 995 (1986)

Garcia CE, DM Prett, M Morari, "Model predictive control: theory and practice-a survey", *Automatica*, **25**, 599, (1989)

Garside J., RJ Davey., "Secondary contact nucleation: Kinetics, growth and scale-up", *Chem. Eng. Comm.*, **4**, 393, (1980)

Gevelber MA, MJ Wargo, G Stephanopoulos, "Advanced control design considerations for the Czochralski process", *J Crystal Growth,* **85**,256-263 (1987)

Glasser D, CM Crowe, D Hildebrandt, "A geometric approach to steady flow reactors: The attainable region and optimization in concentration space", *Ind. Eng. Chem. Res.*, **26**, 1803 (1987)

Hart M, R Hart, *Quantitative Methods for quality and productivity Improvements*, Quality Press (1989)

Helt JE, MA Larson, "Effects of temperature on the crystallization of potassium nitrate by direct measurement of super-saturation", *AIChE J*, **23** (6), 822 (1977)

Hildebrandt D, LT Biegler, "Synthesis of chemical reactor networks", in LT Biegler and MF Doherty (Eds.), *Foundations of Computer aided process design (FOCAPD '94)*, Snowmass CO, 52 (1994)

Hill PJ, KM Ng, "New discretization procedure for the breakage equation", *AIChE J*, **41** (5), 1204 (1995)

Hill PJ, KM Ng, "New discretization procedure for the agglomeration equation", *AIChE J*, **42** (3), 727 (1996)

Hill PJ, Ng KM, "Simulation of solids processes accounting for particle size distribution", *AIChE J*, **43** (3), 715 (1997)

Hounslow MJ, "Discretized population balance for continuous system at steady state", *AIChE J*, **36** (1), 106 (1990)

Hounslow MJ, EJW Wynn, "Short-cut models for particulate processes", *Comp Chem Eng*, **17** (5/6), 505 (1993)

Hounslow MJ, RL Ryall, VR Marshall, "Discretized population balance for nucleation, growth, and aggregation", *AIChE J*, **34** (11), 1821 (1988)

Hulburt HM, SL Katz, "Some problems in particulate technology; A statistical mechanical formulation", *Chem. Eng. Sci.*, **19**, 555 (1964)

Hsieh KT, Rajamani RK, "Mathematical model of the hydrocyclone based on physics of fluid flow", *AIChE J*, **37**(5), 735 (1991)

Jager J, HJM Kramer, E deJong, S deWolf, OH Bosgra, A Boxman, HG Merkus and B Scarlett, "Control of industrial crystallizers", *Powder Tech.*, **69**, 11-20 (1992)

Johnson A, "LQG applications in the process industries", *Chem Eng Sci*, **48** (16), 2829 (1993)

Jones AG, J Hostomsky, S Wachi, "Modelling and analysis of particle formation in agglomerative precipitation systems", *Chem Eng Comm*, **14**(6), 105-130 (1996)

Jones AG, "Design and performance of Crystallization Systems", *Advances in Industrial Crystallization 91*, Butterworth-Heinemann (1991)

Kokossis AC, CA Floudas, "Optimisation of complex reactor networks - I: Isothermal operation", *Chem Eng Sci*, **45** (3), 595 (1990)

Kumar S, D Ramkrishna, "On the solution of population balance equations by discretization II. A fixed pivot technique", *Chem. Eng. Sci.*, Apr 1996, **51**, 1311 (1995a)

Kumar S, D Ramkrishna, "On the solution of population balance equations by discretization II. A moving pivot technique", *Chem. Eng. Sci.*, Apr 1996, **51**, 1333 (1995b)

Larson MA, PR Wolff, "Crystal size distributions from multistage crystallizers", *Chem. Eng. Prog. Symp. Ser.*, **67** (110), 97-107 (1971)

Leu L, SL Tarng, "Multiciplity and Stability of Continuous MSMPR crystallizer", *J of Chin. I. Ch. E.*, **23** (1), 17-23

Linhoff B, E Hindmarsh, "The pinch design method for heat exchanger networks", *Chem Eng Sci*, **38**, 745 (1983)

Ljung L, *System Identification: Theory for the user*, Prentice-Hall, New York (1987)

Litster JD, JD Smit, MJ Hounslow, "Adjustable discretised population balance for growth and aggregation", *AIChE J*, **41** (3), 591 (1995)

Lou JS, A Johnson, "Stability robustness of the discrete-time LQG system under plant perturbation and noise uncertainty", *Int. J Control*, **55**, 1491, (1992)

Luss R, TH Jaakola, "Optimisation by direct search and systematic reduction of the size of search region", *AIChE J*, **19**, 760 (1973)

Ly U, *Linear multivariable control*, Univ. of Washington Press, Seattle (1996)

McAvoy TJ, Y Arkun, E Zafiriou, *Model based process control*, Pergamon Press (1989)

Marchal P, R David, JP Klein, J Villermaux, "Crystallization and Precipitation engineering - I: An efficient method for solving population balance in crystallization with agglomeration", *Chem Eng Sci*, **43** (1), 59 (1988)

Marquardt W, "Trends in computer aided process modelling", *Comp. Chem. Eng.*, **20**, 591 (1996)

McCabe WL, "Crystal growth in aqueous solutions", *Ind Eng Chem*, **21**, 112 (1929)

Mingers J, "An Empirical Comparison of Pruning Methods for Decision Tree Induction", *Machine Learning*, **4**, 227 (1989)

Morari M, "Process control theory: Reflections on the past decade and goals for the next" in Coulton C (Edn.), *Advances in Chemical Engineering*, **16**, 525 (1991)

Mullin JW, *Crystallization*, 3 rd Edn, Butterworth Heinemann (1993)

Nelson RD, R Davies, K Jacob, "Teach 'em particle technology", C*hem. Eng. Educ.*, **29**, 12 (1995)

Newell RB, DG Fisher, DE Seborg, "Computer control using multivariable feed-forward feedback algorithms", *AIChE J,* **18**, 976 (1972)

Niemanis M, MJ Hounslow, "Finite element analysis of steady-state population balance equation for particulate systems; aggregation and growth", *Comp. Chem. Eng.*, **20**, S261 (1996)

Nii HP, "Blackboard systems: The blackboard Model of problem solving and the evolution of blackboard architectures", *The AI Mag*, **7**(2), 38-53 (1986a)

Nii HP, "Blackboard systems: Blackboard application systems, blackboard system from a knowledge engineering perspective", *The AI Mag*, **7**(2), 82-106 (1986b)

Nishida N, G Stephanopoulos, AW Westerberg, "A review of Process synthesis", *AIChE J,* **27**, 321 (1981)

Nyvlt J, *Design of crystallizers*, CRC Press, Boca Raton (1992)

Ogata K, *Modern control engineering*, 3rd Edn., Prentice Hall, Upper Saddle River N.J., (1997)

Pantelides CC, D Gritsis, KR Morison, RWH Sargent, "Mathematical modelling of the transient systems using differential algebraic equations", *Comp. Chem. Eng.*, **12** (5), 449 (1988)

Ponton J, "Process systems engineering: Halfway through the first century", *Chem. Eng. Sci.*, **50** (24), 4045-4059 (1995)

Quinlan JR, "Decision Trees and Decision making, *IEEE Trans Systems Man Cybernetics*, **20** (2), 339 (1990)

Quinlan JR, *C4.5: Programs for Machine Learning*, Morgan Kaufmann (1993)

Randolph AD, C Tan, " Numerical design techniques for staged classified recycle crystallizers: Examples of continuous Alumina and sucrose crystallizers", *Ind. Eng. Process Des. Dev.*, **17**, 189-200 (1978)

Randolph AD, L Chen, A Tavana, "Feedback control of CSD in a KCl crystallizer with a fines dissolver", *AIChE J*, **33** (4), 583-591 (1987)

Randolph AD, MA Larson, *Theory of Particulate Processes*, 2 nd Ed, Academic Press (1988)

Rawlings JB, WR Witkowski, JW Eaton, "Modelling and control of crystallizers", *Powder Tech.*, **69**, 3 (1992)

Redman T, S Rohani, G Strathdee, "Control of the crystal mean size in a pilot plant potash crystallizer", *Trans. IChemE,* **75** (Part A), 183 (1997)

Rhinehart RR, P Murugan, "Improve process control using fuzzy logic", *Chem Eng Prog*, **91**(11), 60 (1996)

Rice RG, DD Do, *Applied Mathematics and modelling for chemical engineers*, Wiley, New York (1995)

Rohani S, K Paine, "Feedback control of CSD in a continuous cooling crystallizer", *Can. J. Chem. Eng.*, **69**, 165 (1991)

Rossiter AP, "Optimisation of a crystalline salt plant using a novel procedure", *Chem Eng Res Des*, **64**, 191 (1986)

Rossiter AP, JM Douglas, "Design and Optimization of Solids Processes", *Chem Eng Res Des*, **64**, 175 (1986)

Rousseau RW, TR Howell, " Comparison of simulated crystal size distribution control systems based on nuclei density and super-saturation", *Ind. Eng. Process Des. Dev.*, **21**, 606 (1982)

Russell LM, JH Seinfeld, "Dynamics of mixed aerosol population in clouds", In AIChE Annual Meeting, Chicago Il., Paper 108d, Nov 10-15 (1996)

Saberi A, Chen BM, Sannuti P, *Loop transfer recover: Analysis and design*, Springer-Verlag (1993)

Saraiva PM, "Inductive and Analogical Learning: Data-Driven improvement of Process operation", in Stephanopoulos G and C Han (Eds.), *Advances in Chemical Engineering*, **22**, 377 (1995)

Saraiva PM, G Stephanopoulos, "Continuous process improvement through inductive and analogical learning", *AIChE J*, **38** (2), 161 (1992a)

Saraiva PM, G Stephanopoulos, "An exploratory data analysis robust optimisation approach to continuous process improvement", *Working Paper*, Dept. Chem. Eng. MIT, Cambridge MA. (1992b)

Sherwin MB, R Shinner, S Katz, "Dynamic behavior of the well-mixed isothermal crystallizer", *Chem. Eng. Prog. Symp. Ser.*, **65** (95), 59-90 (1967)

Shah BH, D Ramkrishna, JD Borwanker, "Simulation of bubble populations in a gas fluidised bed", *Chem. Eng. Sci.*, **32**, 1419 (1977)

Singh PN, D Ramkrishna, "Solution of population balance equation by MWR", *Comp. Chem. Eng.*, **1**, 23 (1977)

Siouris GM, *An engineering approach to optimal control and estimation theory*, John Wiley, New York (1996)

Smith CL, *Digital computer process control*, Intext Publishers, Pittsburgh (1972)

Stephanopoulos G, C Han, " Intelligent systems in process engineering: A review", *Comp. Chem. Eng.*, **20**, 743 (1996)

Steemson M, ET White, "Numerical solution of steady state continuous crystallization process using piece-wise cubic spline function", *Comp. Chem. Eng.*, **12**, 81 (1988)

Stein G, Athans M, "The LQG/LTR procedure for multivariable feedback control design", *IEEE Trans Auto Control*, **AC-32**, 105 (1987)

Sundaresan KR, PR Krishnaswamy, "Estimation of time delay and time constant parameters in time, frequency and Laplace domains", *Can. J. Chem. Eng.*, **56**, 257 (1978)

Svarovsky L, *Solid-liquid Separation*, Butterworths, London (1981)

Tiedermann AR, RM Dekkers, WL de Koning, "Digital optimal control of continuous-time systems with delays ", *Int. J Control,* **42**, 1337 (1985)

Tysso A, JC Brembo, "Installation and operation of a multivariable ship boiler control system", *Automatica*, **14**, 213, (1978)

Utgoff PE, "Incremental Induction of Decision Trees", *Machine Learning*, **4**, 161 (1989)

Woinaroschy A, R Isopescu, L Fillipescu, " Crystallization process optimisation using artificial neural networks", *Chem. Eng. Tech.*, **17**, 269-272 (1994)

APPENDIX A:
(1) Listing of the subroutine for synthesis problem

```
C The subroutine, with the contraints and objective function
C It is interfaced with the SQP rooutine itself for solution

      SUBROUTINE SETPARS(NX,NC,X,BL,BU,INF,HESSIN,PERT)
      IMPLICIT NONE
      INTEGER I ,NX , NC
      REAL*8 BL(*) , BU(*) , X(*) , INF, HESSIN, PERT
      REAL*8 BLI(54) , BUI(54) , XI(31)
C
C BL and BU are the upper and lower bounds on the variables
C AIXi's and MULi are the parameters from orthogonal collocation
C These have been included in the program itself because this routine
C  is repeatedly called by the SQP and therefore interfacing these
C through data file would not be efficient
C
      REAL*8 z1,AIX1,AIX2,AIX3,AIX4,AIX5,GK
      REAL*8 MUL1,MUL2,MUL3,MUL4,MUL5,T
      COMMON /points/z1(20),MUL1(6),MUL2(3),MUL3(2),MUL4(3),MUL5(6)
      COMMON /mat/AIX1(0:6,6),AIX2(0:3,3),AIX3(0:2,2),AIX4(0:3,3),
     &          AIX5(0:6,6),GK,T
      DATA XI/  0.2D0,0.2D0,0.2D0,0.2D0,0.2D0,
     &  0.2D0,0.2D0,0.2D0,0.2D0,0.2D0,
     & .4D-8,.9D-8,.1D-7,.5D-7,.7D-7,.6D-6,.6D-5,.1D-4,.4D-4,.9D-4,
     & .2D-3,.3D-3,.4D-3,.7D-3,.1D-2,.2D-2,.25D-2,.28D-2,.3D-2,.3D-2,.1D-2/

      DATA BLI/-.1D-3,-.1D-3,-.1D-3,-.1D-3,-.1D-3,-.1D-3,-.1D-3,
     & -.1D-3,-.1D-3,
     & -.1D-3,-.1D-3,-.1D-3,-.1D-3,-.1D-3,-.1D-3,-.1D-3,-.1D-3,-.1D-3,
     & -.1D-3,-.0001,-.0001,-0.0001,.1,.1,.1,.1,.1,
     & .0001,.0001,.0001,.0001,.0001,.000001,.1D-10,.1D-10,
     & .1D-10,.1D-10,.1D-10,.1D-10,.1D-10,.1D-10,.1D-10,.1D-10,.1D-10,
     & .1D-10,.1D-10,.1D-10,.1D-10,.1D-10,.1D-10,.1D-10,.1D-10,.1D-10,.1D-10/

      DATA BUI/.1D-3,.1D-3,.1D-3,.1D-3,.1D-3,.1D-3,.1D-3,.1D-3,.1D-3,
     & .1D-3,
     & .1D-3,.1D-3,.1D-3,.1D-3,.1D-3,.1D-3,.1D-3,.1D-3,.1D-3,
     & .00001,0.0001,.6,.6,.6,.6,.6,
     & .6,.6,.6,.6,.6,1,.1,.1,.1,.1,.1,.1,.1,.1,.1,
     & .1,1.,1.,1.,1.,1.,1.,1.,1.,.2/


C
C z1 are the actual locations of the collocation points
C
      z1(1)  =0.3436D-02
      z1(2)  =0.1801D-01
      z1(3)  =0.4388D-01
      z1(4)  =0.8044D-01
      z1(5)  =0.1268D+00
      z1(6)  =0.1820D+00
      z1(7)  =0.2446D+00
      z1(8)  =0.3131D+00
      z1(9)  =0.3861D+00
      z1(10) =0.4617D+00
      z1(11) =0.5383D+00
      z1(12) =0.6139D+00
      z1(13) =0.6869D+00
      z1(14) =0.7554D+00
      z1(15) =0.8180D+00
      z1(16) =0.8732D+00
```

z1(17) =0.9195D+00
z1(18) =0.9562D+00
z1(19) =0.9819D+00
z1(20) =0.9966D+00

MUL1(1)=.2075E+01
MUL1(2)= -.5337E+01
MUL1(3)=.5964E+01
MUL1(4)=-.4122E+01
MUL1(5)=.1957E+01
MUL1(6)=.1000E+01
MUL2(1)=-.9509E-01
MUL2(2)=.3301E+00
MUL2(3)=.1000E+01
MUL3(1)=.4465E+00
MUL3(2)=.1000E+01
MUL4(1)=-.2251E+00
MUL4(2)=.7641E+00
MUL4(3)=.1000E+01
MUL5(1)=.8333E-03
MUL5(2)=-.9517E-02
MUL5(3)=.5145E-01
MUL5(4)=-.1791E+00
MUL5(5)=.4528E+00
MUL5(6)=.1000E+01

AIX1(0,1)=-.1984E+03
AIX1(1,1)=.1711E+03
AIX1(2,1)=-.1510E+03
AIX1(3,1)=.1383E+03
AIX1(4,1)=-.2516E+03
AIX1(5,1)=.8521E+03
AIX1(6,1)=-.6711E+04
AIX1(0,2)=.8330E+02
AIX1(1,2)=.3116E+02
AIX1(2,2)=.5414E+02
AIX1(3,2)=-.9823E+02
AIX1(4,2)=.1410E+03
AIX1(5,2)=-.4389E+03
AIX1(6,2)=.3319E+04
AIX1(0,3)=-.8690E+02
AIX1(1,3)=-.4419E+01
AIX1(2,3)=.1521E+02
AIX1(3,3)=.3952E+02
AIX1(4,3)=-.9473E+02
AIX1(5,3)=.2266E+03
AIX1(6,3)=-.1551E+04
AIX1(0,4)=.1642E+03
AIX1(1,4)=.6702E+00
AIX1(2,4)=-.1820E+01
AIX1(3,4)=.7898E+01
AIX1(4,4)=.3738E+02
AIX1(5,4)=-.1170E+03
AIX1(6,4)=.6091E+03
AIX1(0,5)=-.5651E+03
AIX1(1,5)=-.7707E-01
AIX1(2,5)=.1924E+00
AIX1(3,5)=-.6414E+00
AIX1(4,5)=.3972E+01
AIX1(5,5)=.4065E+02
AIX1(6,5)=-.2067E+03
AIX1(0,6)=.4488E+04
AIX1(1,6)=.4675E-02
AIX1(2,6)=-.1121E-01
AIX1(3,6)=.3381E-01
AIX1(4,6)=-.1593E+00

AIX1(5,6)=.1592E+01
AIX1(6,6)=.5242E+02

AIX2(0,1)=-.1034E+02
AIX2(1,1)=.7919E+00
AIX2(2,1)=-.1908E+02
AIX2(3,1)=.3139E+02
AIX2(0,2)=.5332E+01
AIX2(1,2)=.1114E+02
AIX2(2,2)=.9713E+01
AIX2(3,2)=-.4653E+02
AIX2(0,3)=-.1100E+02
AIX2(1,3)=-.1590E+01
AIX2(2,3)=.4038E+01
AIX2(3,3)=.2614E+02

AIX3(0,1)=-.8965E+01
AIX3(1,1)=.3130E+01
AIX3(2,1)=-.2927E+02
AIX3(0,2)=.8965E+01
AIX3(1,2)=.5835E+01
AIX3(2,2)=.2030E+02

AIX4(0,1)=-.5506E+02
AIX4(1,1)=.5121E+02
AIX4(2,1)=-.4152E+02
AIX4(3,1)=.7430E+02
AIX4(0,2)=.2668E+02
AIX4(1,2)=.4525E+01
AIX4(2,2)=.1064E+02
AIX4(3,2)=-.5062E+02
AIX4(0,3)=-.5176E+02
AIX4(1,3)=-.6718E+00
AIX4(2,3)=.4200E+01
AIX4(3,3)=.2808E+02

AIX5(0,1)=-.2572E+02
AIX5(1,1)=.8584E+01
AIX5(2,1)=-.9252E+01
AIX5(3,1)=.2393E+01
AIX5(4,1)=-.1212E+01
AIX5(5,1)=.1142E+01
AIX5(6,1)=-.2712E+01
AIX5(0,2)=.3232E+01
AIX5(1,2)=.3551E+02
AIX5(2,2)=-.1915E+02
AIX5(3,2)=-.1027E+02
AIX5(4,2)=.3953E+01
AIX5(5,2)=-.3372E+01
AIX5(6,2)=.7687E+01
AIX5(0,3)=-.9421E+00
AIX5(1,3)=-.4056E+02
AIX5(2,3)=.4537E+02
AIX5(3,3)=-.1646E+02
AIX5(4,3)=-.1880E+02
AIX5(5,3)=.1234E+02
AIX5(6,3)=-.2586E+02
AIX5(0,4)=.4970E+00
AIX5(1,4)=.4322E+02
AIX5(2,4)=-.3673E+02
AIX5(3,4)=.3956E+02
AIX5(4,4)=-.1061E+02
AIX5(5,4)=-.4340E+02
AIX5(6,4)=.7156E+02
AIX5(0,5)=-.4769E+00
AIX5(1,5)=-.3259E+02

```
AIX5(2,5)=.2508E+02
AIX5(3,5)=-.2079E+02
AIX5(4,5)=.3473E+02
AIX5(5,5)=.7365E+01
AIX5(6,5)=-.1766E+03
AIX5(0,6)=.1142E+01
AIX5(1,6)=.1157E+02
AIX5(2,6)=-.8544E+01
AIX5(3,6)=.6509E+01
AIX5(4,6)=-.8560E+01
AIX5(5,6)=.2639E+02
AIX5(6,6)=.1248E+03
C
C GK is the growth rate constant
C NC and NX are the number of equations and variables respectively
C
      GK=6.13D-4
      T=291.0
      HESSIN = 1D0
      PERT = 1D-5
      NX = 31
      NC = 23

      CALL COPYVEC(NX,XI,1,X,1)
      CALL COPYVEC(NC+NX,BLI,1,BL,1)
      CALL COPYVEC(NC+NX,BUI,1,BU,1)
      RETURN
      END
C
C F is the objective function
C
      REAL*8 FUNCTION F(X)
      REAL*8 X(*)
       F=0.0
       do 111 i=1,20
        if (i.le.6) then
           F = F-(X(i+10)*0.01)
        elseif (i.le.9) then
           F=F-(X(i+10)*X(6))
        elseif (i.le.11) then
           F=F-(X(i+10)*X(7))
        elseif (i.le.14) then
           F=F-(X(i+10)*X(8))
        elseif (i.lt.19) then
           F=F-(X(i+10)*X(9))
        else
           F=F-((X(i+10)*X(10))+X(31)*0.01)
        endif
111    continue
      RETURN
      END
C
C In the following subroutine the actual constraints are defined
C
      SUBROUTINE FUNC(X,B)
      REAL*8 X(*),B(*)
      REAL*8 z1,AIX1,AIX2,AIX3,AIX4,AIX5,BR1,CS1,GK,T,qj,C,phi,phi2
      REAL*8 CS2,CS3,CS4,CS5,grr,CL(20),CA(20),CM(20)
      REAL*8 phi3,phi4,phi5,Y1E,Y2E,Y3E,Y4E,Y5E,BR2,BR3,BR4,BR5
      REAL*8 MUL1,MUL2,MUL3,MUL4,MUL5,ff(20),tau(20),qq(20),bnt(20)
      COMMON /points/z1(20),MUL1(6),MUL2(3),MUL3(2),MUL4(3),MUL5(6)
      COMMON /mat/AIX1(0:6,6),AIX2(0:3,3),AIX3(0:2,2),AIX4(0:3,3),
     &          AIX5(0:6,6),GK

C
```

```
C BR's are the nucleation rates at the temperatures used
C
      BR1=0.1401D10
      BR2=0.1328D13
      BR3=0.7347D13
      BR4=0.7982D14
      BR5=0.3743D15
C
C CS's are the appropriate saturation concs
C

      CS1=0.8206
      CS2=0.80435
      CS3=0.7882
      CS4=0.7568
      CS5=0.7264

      C=1.0
C
C ff's are the f's of the theory, qq are the q's. Tau's are the
C corresponding residence times at point
C B is the mass lost due to crystallization
C

      ff(1)=0.0
      qq(1)=X(1)
      tau(1)=z1(1)*qq(1)
      bnt(1)=tau(1)*BR1*qq(1)
      grr=GK*((C-X(11))-CS1)
      CL(1)=bnt(1)*tau(1)*grr
      CA(1)=2*CL(1)*tau(1)*grr
      CM(1)=3*CA(1)*tau(1)*grr
      B(1)=0.0-(CM(1)*z1(1))
C
C Following are the twenty equations at the twenty collocation points
C Since the range is split into 5 finite elements, the equations are
C also split likewise.
C The number of points in each element is not same
C An extrapolation function is calculated at the end of each element
C this makes writing a general program rather difficult
C

      do 10 j=1,6
       B(1)=B(1)+(X(11+j)*AIX1(1,j)/X(1))
10     continue

      do 7999 k=2,20
       if (k.lt.6) then
        ff(k)=0.0
        qq(k)=qq(k-1)-ff(k)
        tau(k)=(z1(k)*qq(k))
        bni=((z1(k)-z1(k-1))*qq(k)*BR1)
        bnt(k)=bni+((1-(ff(k-1)/qq(k-1)))*bnt(k-1))
        grr=GK*((C-X(10+k))-CS1)
        CL(k)=(bnt(k)*tau(k)*grr)+((1-(ff(k-1)/qq(k-1)))*CL(k-1))
        CA(k)=(2*CL(k)*tau(k)*grr)+((1-(ff(k-1)/qq(k-1)))*CA(k-1))
        CM(k)=(3*CA(k)*tau(k)*grr)
        B(k)=0.0-(CM(k)*(z1(k)-z1(k-1)))
        do 11 j=1,6
         B(k)=B(k)+(X(10+j)*AIX1(k,j)/X(1))
11       continue

       elseif (k.eq.6) then
       ff(k)=X(6)
       qq(k)=X(2)+qq(k-1)-ff(k)
```

```
      tau(k)=(z1(k)*qq(k))
      bni=((z1(k)-z1(k-1))*qq(k)*BR1)
      bnt(k)=bni+((1-(ff(k-1)/qq(k-1)))*bnt(k-1))
      grr=GK*((1-X(10+k))-CS1)
      CL(k)=(bnt(k)*tau(k)*grr)+((1-(ff(k-1)/qq(k-1)))*CL(k-1))
      CA(k)=(2*CL(k)*tau(k)*grr)+((1-(ff(k-1)/qq(k-1)))*CA(k-1))
      CM(k)=(3*CA(k)*tau(k)*grr)
      B(k)=0.0-(CM(k)*(z1(k)-z1(k-1)))
      do 12 j=1,6
       B(k)=B(k)+(X(10+j)*AIX1(k,j)/X(1))
12     continue


      Y1E=0.0
        do 141 j=1,6
          Y1E=Y1E+(MUL1(j)*X(j+10))
141   CONTINUE

      qj=0.0
      do 142 jj=1,6
       qj=qj+(qq(jj)-ff(jj))
142     continue

      phi1=X(1)/qj
      C=((1-phi1)*(1-Y1E))+phi1

        elseif (k.lt.9) then
        ff(k)=0.0
        qq(k)=qq(k-1)-ff(k)
        tau(k)=(z1(k)*qq(k))
        bni=((z1(k)-z1(k-1))*qq(k)*BR2)
        bnt(k)=bni+((1-(ff(k-1)/qq(k-1)))*bnt(k-1))
        B(k)=0.0+Y1E*AIX2(0,k-6)
        grr=GK*((C-X(10+k))-CS2)
        CL(k)=(bnt(k)*tau(k)*grr)+((1-(ff(k-1)/qq(k-1)))*CL(k-1))
        CA(k)=(2*CL(k)*tau(k)*grr)+((1-(ff(k-1)/qq(k-1)))*CA(k-1))
        CM(k)=(3*CA(k)*tau(k)*grr)
         B(k)=B(k)-(CM(k)*(z1(k)-z1(k-1)))
          do 16 j=1,3
           B(k)=B(k)+(X(16+j)*AIX2(k-6,j)/X(2))
16    continue
        elseif (k.eq.9) then
        ff(k)=X(7)
        qq(k)=X(3)+qq(k-1)-ff(k)
        tau(k)=(z1(k)*qq(k))
        bni=((z1(k)-z1(k-1))*qq(k)*BR2)
        bnt(k)=bni+((1-(ff(k-1)/qq(k-1)))*bnt(k-1))
        B(k)=0.0+Y1E*AIX2(0,k-6)
        grr=GK*((C-X(k+10))-CS2)
        CL(k)=(bnt(k)*tau(k)*grr)+((1-(ff(k-1)/qq(k-1)))*CL(k-1))
        CA(k)=(2*CL(k)*tau(k)*grr)+((1-(ff(k-1)/qq(k-1)))*CA(k-1))
        CM(k)=(3*CA(k)*tau(k)*grr)
         B(k)=B(k)-(CM(k)*(z1(k)-z1(k-1)))
          do 17 j=1,3
           B(k)=B(k)+(X(16+j)*AIX2(k-6,j)/X(2))
17    continue


       Y2E=0.0
       do 171 j=1,3
         Y2E=Y2E+(MUL2(j)*X(j+16))
171   CONTINUE

       do 172 jj=7,9
            qj=qj+(qq(jj)-ff(jj))
172      continue
```

```
phi2=X(2)/qj
C=((1-phi2)*(1-Y2E))+phi2


elseif (k.lt.11) then
ff(k)=0.0
qq(k)=qq(k-1)-ff(k)
tau(k)=(z1(k)*qq(k))
bni=((z1(k)-z1(k-1))*qq(k)*BR3)
bnt(k)=bni+((1-(ff(k-1)/qq(k-1)))*bnt(k-1))
B(k)=0.0+Y2E*AIX3(0,k-9)
grr=GK*((C-X(k+10))-CS3)
CL(k)=(bnt(k)*tau(k)*grr)+((1-(ff(k-1)/qq(k-1)))*CL(k-1))
CA(k)=(2*CL(k)*tau(k)*grr)+((1-(ff(k-1)/qq(k-1)))*CA(k-1))
CM(k)=(3*CA(k)*tau(k)*grr)
B(k)=B(k)-(CM(k)*(z1(k)-z1(k-1)))
  do 18 j=1,2
   B(k)=B(k)+(X(19+j)*AIX3(k-9,j)/X(3))
18  continue
  elseif (k.eq.11) then
  ff(k)=X(8)
  qq(k)=X(4)+qq(k-1)-ff(k)
  tau(k)=(z1(k)*qq(k))
  bni=((z1(k)-z1(k-1))*qq(k)*BR3)
  bnt(k)=bni+((1-(ff(k-1)/qq(k-1)))*bnt(k-1))
  B(k)=0.0+Y2E*AIX3(0,k-9)
  grr=GK*((C-X(k+10))-CS3)
  CL(k)=(bnt(k)*tau(k)*grr)+((1-(ff(k-1)/qq(k-1)))*CL(k-1))
  CA(k)=(2*CL(k)*tau(k)*grr)+((1-(ff(k-1)/qq(k-1)))*CA(k-1))
  CM(k)=(3*CA(k)*tau(k)*grr)
  B(k)=B(k)-(CM(k)*(z1(k)-z1(k-1)))

    do 19 j=1,2
     B(k)=B(k)+(X(19+j)*AIX3(k-9,j)/X(3))
19  continue

   Y3E=0.0
   do 191 j=1,2
    Y3E=Y3E+(MUL3(j)*X(j+19))
191  CONTINUE

   do 192 jj=10,11
       qj=qj+(qq(jj)-ff(jj))
192    continue
   phi3=X(3)/qj
   C=((1-phi3)*(1-Y3E))+phi3

   elseif (k.lt.14) then
   ff(k)=0.0
   qq(k)=qq(k-1)-ff(k)
   tau(k)=(z1(k)*qq(k))
   bni=((z1(k)-z1(k-1))*qq(k)*BR4)
   bnt(k)=bni+((1-(ff(k-1)/qq(k-1)))*bnt(k-1))
   B(k)=0.0+Y3E*AIX4(0,k-11)
   grr=GK*((C-X(k+10))-CS4)
   CL(k)=(bnt(k)*tau(k)*grr)+((1-(ff(k-1)/qq(k-1)))*CL(k-1))
   CA(k)=(2*CL(k)*tau(k)*grr)+((1-(ff(k-1)/qq(k-1)))*CA(k-1))
   CM(k)=(3*CA(k)*tau(k)*grr)
    B(k)=B(k)-(CM(k)*(z1(k)-z1(k-1)))
     do 20 j=1,3
      B(k)=B(k)+(X(21+j)*AIX4(k-11,j)/X(4))
20  continue

   elseif (k.eq.14) then
   ff(k)=X(9)
   qq(k)=X(5)+qq(k-1)-ff(k)
```

```
        tau(k)=(z1(k)*qq(k))
        bni=((z1(k)-z1(k-1))*qq(k)*BR4)
        bnt(k)=bni+((1-(ff(k-1)/qq(k-1)))*bnt(k-1))
        B(k)=0.0+Y3E*AIX4(0,k-11)
        grr=GK*((C-X(k+10))-CS4)
        CL(k)=(bnt(k)*tau(k)*grr)+((1-(ff(k-1)/qq(k-1)))*CL(k-1))
        CA(k)=(2*CL(k)*tau(k)*grr)+((1-(ff(k-1)/qq(k-1)))*CA(k-1))
        CM(k)=(3*CA(k)*tau(k)*grr)
         B(k)=B(k)-(CM(k)*(z1(k)-z1(k-1)))
          do 21 j=1,3
           B(k)=B(k)+(X(21+j)*AIX4(k-11,j)/X(4))
21    continue

        Y4E=0.0
        do 221 j=1,3
          Y4E=Y4E+(MUL4(j)*X(j+21))
221   CONTINUE

        do 222 jj=12,14
             qj=qj+(qq(jj)-ff(jj))
222       continue
        phi4=X(4)/qj
        C=((1-phi4)*(1-Y4E))+phi4

        elseif (k.lt.20) then
        ff(k)=0.0
        qq(k)=qq(k-1)-ff(k)
        tau(k)=(z1(k)*qq(k))
        bni=((z1(k)-z1(k-1))*qq(k)*BR5)
        bnt(k)=bni+((1-(ff(k-1)/qq(k-1)))*bnt(k-1))
        B(k)=0.0+Y4E*AIX5(0,k-14)
        grr=GK*((C-X(k+10))-CS5)
        CL(k)=(bnt(k)*tau(k)*grr)+((1-(ff(k-1)/qq(k-1)))*CL(k-1))
        CA(k)=(2*CL(k)*tau(k)*grr)+((1-(ff(k-1)/qq(k-1)))*CA(k-1))
        CM(k)=(3*CA(k)*tau(k)*grr)
         B(k)=B(k)-(CM(k)*(z1(k)-z1(k-1)))
          do 23 j=1,6
           B(k)=B(k)+(X(24+j)*AIX5(k-14,j)/X(5))
23    continue

        elseif (k.eq.20) then
        ff(k)=X(10)
        qq(k)=qq(k-1)-ff(k)
        tau(k)=(z1(k)*qq(k))
        bni=((z1(k)-z1(k-1))*qq(k)*BR5)
        bnt(k)=bni+((1-(ff(k-1)/qq(k-1)))*bnt(k-1))
        B(k)=0.0+Y4E*AIX5(0,k-14)
        grr=GK*((C-X(k+10))-CS5)
        CL(k)=(bnt(k)*tau(k)*grr)+((1-(ff(k-1)/qq(k-1)))*CL(k-1))
        CA(k)=(2*CL(k)*tau(k)*grr)+((1-(ff(k-1)/qq(k-1)))*CA(k-1))
        CM(k)=(3*CA(k)*tau(k)*grr)
         B(k)=B(k)-(CM(k)*(z1(k)-z1(k-1)))
          do 26 j=1,6
           B(k)=B(k)+(X(24+j)*AIX5(k-14,j)/X(5))
26    continue

       endif
7999     continue



C
C The following two equations are the constraints on feed fract funct
C and prod removal function. Eq 23, calculates av. size
C
```

```
  B(21)=(X(1)+X(2)+X(3)+X(4)+X(5))-1.0
  B(22)=(X(6)+X(7)+X(8)+X(9)+X(10))-1.0
  AVL=(X(6)*CL(6))+(X(7)*CL(9))+(X(8)*CL(11))
  AVL=AVL+(X(9)*CL(14))+(X(10)*CL(20))
  AVN=(X(6)*bnt(6))+(X(7)*bnt(9))+(X(8)*bnt(11))
  AVN=AVN+(X(9)*bnt(14))+(X(10)*bnt(20))
  B(23)=X(31)-(AVL/AVN)

RETURN
END
```

(2) Listing of the FORTRAN program for detailed analysis

```
C in this program analytical solution to population balance
C is solved along with mass balance for detailed simulations of
C of the optimal network.
C The mass is conserved by defination, while the discretisation
C step is selected to make sure that moments from size match
C with those from growth rates. (The array dimensions reflect this)

      IMPLICIT DOUBLE PRECISION (A-H,O-Z)
      DOUBLE PRECISION L(240),NIN(240),N_IN(240)
      DOUBLE PRECISION NT
      DOUBLE PRECISION N_OUT1(240),LBAR_OUT,N_OUT2(240)
      double precision MOM(4), MO(4),LBAR2,MO1(4),MO2(4)
      double precision MO3(4),MO4(4),MO5(4),MOD(4)
      double precision N_OUT3(240),LBAR3,NO,N_OUTH(240)
      double precision N_OUT4(240),LBAR4,N_OUT(240)
      double precision N_OUT5(240),LBAR5,LBAR,LBAR_O
      INTEGER NEQ,N1,I,J,NM
      parameter (NEQ=240,N1=240,NM=4)
      COMMON /OPS/ VOL,L,NIN,KA,KV,MG
      COMMON /OP1/ RHO,FLOW,C_IN1,B

      open (unit=3,file='ms2.res',status='unknown')

      FLOW=0.23395636
      q1=0.58423041
      q2=0.14962904
      q3=0.12802904
      q4=0.10702904
      q5=0.03108239
      f1=1.28229e-5
      f2=1.28229e-5
      f3=0.18968067
      f4=0.45147736
      f5=0.35881692

      VOL=9.0775068
      FLOW11=q1*FLOW
      FLOW13=f1*FLOW
      FLOW1=FLOW11
      FLOW14=FLOW11-FLOW13
      FLOW21=q2*FLOW
      FLOW22=FLOW14
      FLOW2=FLOW21+FLOW22
      FLOW23=f2*FLOW
      FLOW24=(FLOW21+FLOW22)-FLOW23
      FLOW31=q3*FLOW
      FLOW32=FLOW24
      FLOW3=FLOW31+FLOW32
      FLOW33=f3*FLOW
      FLOW34=(FLOW31+FLOW32)-FLOW33
      FLOW41=0.12822904*FLOW
      FLOW42=FLOW34
```

```
FLOW4=FLOW41+FLOW42
FLOW43=f4*FLOW
FLOW44=(FLOW41+FLOW42)-FLOW43
FLOW51=q5*FLOW
FLOW52=FLOW44
FLOW5=FLOW51+FLOW52
FLOW53=FLOW51+FLOW52

TAU1=VOL/FLOW1
TAU2=VOL/FLOW2
TAU3=VOL/FLOW3
TAU4=VOL/FLOW4
TAU5=VOL/FLOW5
      B=3.e-4/6
      KA=1.
      KV=6.
      MG=101.0
      RHO=2110.D0

      L(1)=1.0e-4
      DO 20 I=2,NEQ
        L(I)=L(I-1)+B
20    CONTINUE

      NIN(1)=0.0
      DO 30 I=2,NEQ
       NIN(I)=0.0
30    CONTINUE

      DO 31 I=1,NEQ
       N_IN(I)=NIN(I)*(FLOW11/FLOW)
31    CONTINUE
      C_IN1=3.52
c
C N has the units of cm-1
c
1000   CONTINUE
      CS=2.888512
      C_IN1=C_IN1-1.E-4
      G0=2.207e-5*(C_IN1-CS)
      B0=1.8E16*EXP(-.5/(LOG(C_IN1/CS))**2)
      MO(1)=B0*VOL*1.e6
      MO(2)=MO(1)*(G0*TAU1)
      MO(3)=2*MO(2)*(G0*TAU1)
      MO(4)=6*MO(3)*(G0*TAU1)

     C_GRO=0.5*KA*MO(4)*(RHO/MG)/1.e6
     C_OUT=3.52-(C_GRO/FLOW11)

     DIFF=C_IN1-C_OUT

     IF (DIFF.GT.1.D-5) THEN
      GOTO 1000
     ELSE
      C_OUT1=C_OUT
     ENDIF

      DO 100 I=1,NEQ
       A=(VOL*1.E6*B0)/(G0*TAU1)
        DO 200 J=1,I
          A=A+((N_IN(J)*B/(G0*TAU1))*DEXP(L(J)/(G0*TAU1)))
200       CONTINUE
       N_OUT1(I)=A*DEXP(-L(I)/(G0*TAU1))
100    CONTINUE
```

```
      NT=0.0
      do 111 I=1,NEQ
       NT=NT+(N_OUT1(I)*B)
111    CONTINUE

      AA=(VOL*1.E6*B0)/(G0*TAU1)
      LBAR_OUT=MO(2)/MO(1)
      CV=SQRT((MO(1)*MO(3)/MO(2)**2)-1)

      Write(3,*) C_OUT1,CV,LBAR_OUT

      C_IN1=3.52
      CS2=2.837136
       cs3=2.774464
       CS4=2.663936
       CS5=2.556928

       CALL MS (N_OUT2,NEQ,C_OUT2,LBAR2,CV2,MO2,NM,N_OUT1,NEQ,
     +  C_OUT1,FLOW21,FLOW22,FLOW1,TAU2,CS2,MO,NM)

       CALL MS (N_OUT3,NEQ,C_OUT3,LBAR3,CV3,MO3,NM,N_OUT2,NEQ,
     + C_OUT2,FLOW31,FLOW32,FLOW2,TAU3,CS3,MO2,NM)

       CALL MS (N_OUT4,NEQ,C_OUT4,LBAR4,CV4,MO4,NM,N_OUT3,NEQ,
     + C_OUT3,FLOW41,FLOW42,FLOW3,TAU4,CS4,MO3,NM)

       CALL MS (N_OUT5,NEQ,C_OUT5,LBAR5,CV5,MO5,NM,N_OUT4,NEQ,
     + C_OUT4,FLOW51,FLOW52,FLOW4,TAU5,CS5,MO4,NM)

        c_oo=(C_OUT1*f1)+(C_OUT2*f2)
        c_oo=c_oo+(C_OUT3*f3)+(C_OUT4*f4)
        c_oo=c_oo+(C_OUT5*f5)

        write(3,*) N_OUT1
        write(3,*) N_OUT2
        write(3,*) N_OUT3
        write(3,*) N_OUT4
        Write(3,*) N_OUT5

        Write (3,999)  LBAR_OUT,LBAR2,LBAR3,LBAR4,LBAR5
999      FORMAT (1X,E10.4,/)
      END


      SUBROUTINE MS (N_OUT1,NEQ,C_OUT1,LBAR,CV,MO,N5,N_IN2,N1,
     +   C_IN2,FLOW_IN1,FLOW_IN2,FLOW1,TAU,CS,MOIN,N4)
      IMPLICIT DOUBLE PRECISION (A-H,O-Z)
      DOUBLE PRECISION L(240),NIN(240),N_IN(240),N_IN2(240),NO
      DOUBLE PRECISION N_OUT1(240),LBAR_OUT,MOM(4),MO(4),LBAR,NT
      DOUBLE PRECISION MOIN(4)
      INTEGER NEQ,N1,I,J,NM
      PARAMETER (NM=4)
      COMMON /OPS/ VOL,L,NIN,KA,KV,MG
      COMMON /OP1/ RHO,FLOW,C_IN1,B

      FLOW_IN=FLOW_IN1+FLOW_IN2
      DO 10 I=1,NEQ
      N_IN(I)=(NIN(I)*(FLOW_IN1/FLOW))+N_IN2(I)*(FLOW_IN2/FLOW1)
10     CONTINUE

      C_IN=((FLOW_IN1/FLOW_IN)*C_IN1)+C_IN2*(FLOW_IN2/FLOW_IN)
      C_IN1=C_IN

1000   CONTINUE
      C_IN1=C_IN1-1.E-4
```

```
G0=2.227e-5*(C_IN1-CS)
B0=1.8E16*DEXP(-.5/(LOG(C_IN1/CS))**2)
MO(1)=(B0*VOL*1e6)+(MOIN(1)*(FLOW_IN2/FLOW1))
MO(2)=(MO(1)*(G0*TAU))+(MOIN(2)*(FLOW_IN2/FLOW1))
MO(3)=(2*MO(2)*(G0*TAU))+(MOIN(3)*(FLOW_IN2/FLOW1))
MO(4)=(6*MO(3)*(G0*TAU))

C_GRO=0.5*KA*MO(4)*(RHO/MG)/1.e6
C_OUT=C_IN-(C_GRO/FLOW_IN)
DIFF=C_IN1-C_OUT
IF (DIFF.GT.1.D-5) THEN
 GOTO 1000
ELSE
 C_OUT1=C_OUT
ENDIF

 DO 100 I=1,240
  A=(VOL*1.E6*B0)/(G0*TAU)
   DO 200 J=1,I
     A=A+((N_IN(J)*B/(G0*TAU))*DEXP(L(J)/(G0*TAU)))
200    CONTINUE
 N_OUT1(I)=A*DEXP(-L(I)/(G0*TAU))
100  CONTINUE
 NT=0.0
 do 111 I=1,NEQ
 NT=NT+(N_OUT1(I)*B)
111  CONTINUE
 AA=(VOL*1.E6*B0)/(G0*TAU)
 LBAR=MO(2)/MO(1)
 CV=SQRT((MO(1)*MO(3)/MO(2)**2)-1)
 write(3,*) C_OUT,CV,LBAR

 RETURN

END
```

APPENDIX B: Listing of SPEEDUP file for the optimisation process flowsheet

```
OPTIONS

      ROUTINES
        SUPERDAE

      EXECUTION
        BOUNDCHECK = OFF
        TIME_STEP  = 5
        INTERVALS  = 200
#       RTE        = ON
        PRINTLEVEL = 2
        TARGET     = TERMINAL
        ITERATIONS = 400
        RESTOL     = 20.5

# IN THIS SECTION EXECUTION OPTIONS ARE DEFINED
****
DECLARE

# VARIABLE TYPES AND STREAM TYPES ARE DECLARED IN THIS SECTION

TYPE

      FLOWRATE       = 0.1    : 0.0      : 15          UNIT = "M3/SEC"
      DENSITY        = 1.0    : 0.0      : 1.0E5       UNIT = "KMOLM-3"
      HEAT           = 200    :-1.0E7    : 1.0E7       UNIT = "KJ"
      PRESS_DROP     = 0.0    : -1.0E-8  : 1.0E7       UNIT = "BAR"
      PRESSURE       = 1.0    : 0.5      : 5.0         UNIT = "BAR"
      CONCENTRATION  = 300    : 0.0      : 800         UNIT = "kg m3"
      VOLUME         = 5.0    : 1.0      : 100.0       UNIT = "M3"
      NUMBER         = 0.0    : -1.0E10  : 1.0E7       UNIT = "M-3"
      SIZES          = 14.5   : 0.0      : 1000        UNIT = "MICRON3"
      molweight      = 18.0   : 1.0      :500          UNIT = " AMU"
      NOTYPE         = 1.0    : -1.0E10  : 1.0E13      UNIT = "No units"
      PERCENTAGE     = 0.0    : 0.0      : 100         UNIT = " NOUNITS"
      FRACTION       = 0.1    : 0.0      : 1.0         UNIT = " NO UNITS"
      TIME           = 0.0    : 0.0      : 7.0E4       UNIT = "SEC"
      TEMPERATURE    = 298    : 273      : 700         UNIT = "K"
      MOLEFRACTION   = 0.1    : 0.0      : 1.0         UNIT = "---"
      CONTROL_SIGNAL = 1.0    : -1.0E2   : 1.0E3       UNIT = "---"
      FLOW_MOL_LIQ   = 0.5    : 0.00001  : 20          UNIT = "KMOL/SEC"
      ENTH_MOL_LIQ   = 0.02   : -1.0E6   : 1.0E10      UNIT = "GJ/KMOL"
      CONSTANT       = 1      : 1.0E-4   : 150         UNIT = "No units"
      MOL_HEAT_CAP   = 0.02   : -1.0E8   : 1.0E6       UNIT = "KJ/KMOL K"
      KERNAL         = 4.0E-1 : 1.0E-7   : 1.0E6       UNIT = "-----"
      RATE           = 0.0    :-1.0E7    : 1.0E7       UNIT = "M-3SEC-1"
      POSITIVE       = 0.0    : 0.0      : 1.0E30      UNIT = "---"


STREAM MAINSTREAM

SET
      NOSIZE = 20
TYPE
        FLOWRATE, NUMBER(NOSIZE),CONCENTRATION,TEMPERATURE

STREAM SOLIDS

SET
```

```
      NOSIZE = 20
      NOMOM  = 6
TYPE
        FLOWRATE, NUMBER(NOSIZE),CONCENTRATION,TEMPERATURE,
        NOTYPE(NOMOM),SIZES

STREAM   SOLID

SET
        NOSIZE = 20
        NOMOM  = 6
        NCOMP  =2

TYPE
        FLOWRATE, NUMBER(NOSIZE), NOTYPE (NOMOM), TEMPERATURE,
        MOLEFRACTION(NCOMP),MOL_HEAT_CAP,DENSITY,CONCENTRATION


STREAM LIQUID

SET
         NCOMP=2
TYPE
        FLOW_MOL_LIQ,TEMPERATURE,MOL_HEAT_CAP


****
PROCEDURE BETA
#
# this procedure calculates agglomeration kernal
# as a function of saturation and size
#
INPUT
      TEMPERATURE,CONCENTRATION

OUTPUT

      KERNAL

CODE
      SUBROUTINE BETA (T,CONC,BETO)
      implicit double precision (A-Z)
      PARAMETER (KV=1.0,KA=650.0,G2=0.9)


        A=-6106.8467
        B=98.896550
        C=-0.63677944
        D=0.0020375883
        E= -3.2426245E-6
        F= 2.0586348E-9
       CS=A+(B*T)+(C*T**2)+(D*T**3)+(E*T**4)+(F*T**5)
        S=CONC/CS
        BETAO=KV*KA*(S**G2)
        RETURN
        END

$ENDCODE



****
```

```
PROCEDURE BRE
#
# crystal breakage rate is caluclated as a function of volume
#
INPUT
      SIZES

OUTPUT
      NOTYPE(NOSIZE)

CODE

      SUBROUTINE BRE (SMIN,S,NEQ)
      implicit double precision (A-H,O-Z)
      INTEGER I,N1
      DIMENSION S(NEQ),V(20)
      PARAMETER (N1=20)

      BK=55.E-11
      S(1)=0.
      SV=1.0


      V(1)=SV*SMIN**3

      DO 200 I=2,N1
           V(I)=V(I-1)*2.

200    CONTINUE
      DO 150 I=2,NEQ
           S(I)=BK*(V(I)**2.)/10.
150    CONTINUE
      RETURN
      END
$ENDCODE

****
PROCEDURE BREH

INPUT
      SIZES

OUTPUT
      NOTYPE(NOSIZE)

CODE

      SUBROUTINE BREH (SMIN,S,NEQ)
      implicit double precision (A-H,O-Z)
      INTEGER I,N1
      DIMENSION S(NEQ),V(20)
      PARAMETER (N1=20)
      BK=.35E-11
      S(1)=0.
      SV=1.0


      V(1)=SV*SMIN**3

      DO 200 I=2,N1
           V(I)=V(I-1)*2.

200    CONTINUE
      DO 150 I=2,NEQ
           S(I)=BK*(V(I)**2.)/1000.
```

```
150    CONTINUE
       RETURN
       END
$ENDCODE

****
PROCEDURE DISR

INPUT
       SIZES(NOSIZE),CONCENTRATION,DENSITY,CONSTANT,
       DENSITY,NOTYPE,CONSTANT

OUTPUT
       RATE(NOSIZE)

CODE

       SUBROUTINE DISR (L,NEQ,ALPHA,RHO,MU,RHO_C,DIFF,
      + RMM_A,DIS_RATE,N1)
       INTEGER I,N1,NEQ
       DIMENSION L(NEQ),DIS_RATE(NEQ),L_M2(20),KD(20)
       DIMENSION SH(20),BRAC(20),BRAC2(20)
       implicit double precision (A-Z)


       SG=(RMM_A/RHO)*ALPHA
       DO 10 I=1,NEQ
        L_M2(I)=L(I)*1.E-6
10     CONTINUE

       DO 11 I=1,NEQ

       BRAC(I)=(L_M2(I)**3*RHO_C*(RHO_C-RHO)*9.8/MU**2)
       BRAC2(I)=(BRAC(I)*(MU/(RHO_C*DIFF)))**0.25
       SH(I)=2+(0.4*BRAC2(I))
       KD(I)=100*DIFF*1.E-6*SH(I)/L_M2(I)
11     CONTINUE

       DO 12 I=1,NEQ

       DIS_RATE(I)=KD(I)*SG
12     CONTINUE

       RETURN
       END
$ENDCODE

****
PROCEDURE HCOF
#
# Thermal properties are calculated here
#
INPUT
       MOL_HEAT_CAP,MOL_HEAT_CAP,CONSTANT,CONSTANT,DENSITY,
       DENSITY,CONSTANT,CONSTANT,CONSTANT,CONSTANT,CONSTANT,
       FLOW_MOL_LIQ,NOTYPE,TEMPERATURE
OUTPUT

       NOTYPE


CODE
```

```
   SUBROUTINE HCOF (CP,CP_J,MS,M_J,RHO,R_J,RMM,RMM_J,
+   D_C,D_J,N,F_J,KW,T,U)
   implicit double precision (A-Z)

  P=3.1415927
  K_MIX=4.325E-7 * (CP/RMM)*RHO*(RHO/RMM)**0.3333
  K_J=4.325E-7 * (CP_J/RMM_J)*R_J*(R_J/RMM_J)**0.3333

  Z=P*(D_J-D_C)**2*0.25
  Z2=F_J*1.0E-3/Z
  RE_J=R_J*Z2*(D_J-D_C)/M_J
  PR_J=(CP_J*M_J/(K_J*RMM_J))
  H_J=(4.2/(D_J-D_C))*(1.35+(0.02*(T-273)))*Z2**0.8
  RE=RHO*N*D_C*2/MS
  PR=CP*MS/(K_MIX*RMM)
  HC=(K_MIX*0.023/D_C)*(RE**0.8)*(PR**0.4)

  HW= 0.01*0.5/KW

  HJ_I=1/ H_J
  HC_I=1/HC
  U_IN=HJ_I+HC_I+HW
  U=1/U_IN
  RETURN
  END

$ENDCODE
****
PROCEDURE HCOF2:HCOFF

INPUT

    MOL_HEAT_CAP,MOL_HEAT_CAP,CONSTANT,CONSTANT,DENSITY,
    DENSITY,CONSTANT,CONSTANT,CONSTANT,CONSTANT,FLOWRATE,
    FLOW_MOL_LIQ,NOTYPE,TEMPERATURE
OUTPUT

    NOTYPE


CODE


    SUBROUTINE HCOFF (CP,CP_J,MS,M_J,RHO,R_J,RMM,RMM_J,
+   D_C,D_J,F_R,F_J,KW,T,U)
    implicit double precision (A-Z)

  P=3.1415927
  K_MIX=4.325E-7 * (CP/RMM)*RHO*(RHO/RMM)**0.3333
  K_J=4.325E-7 * (CP_J/RMM_J)*R_J*(R_J/RMM_J)**0.3333

  Z=P*(D_J-D_C)**2*0.25
  Z2=F_J*1.0E-3/Z
  RE_J=R_J*Z2*(D_J-D_C)/M_J
  PR_J=(CP_J*M_J/(K_J*RMM_J))
  H_J=(4.2/(D_J-D_C))*(1.35+(0.02*(T-273)))*Z2**0.8
  RE=RHO*F_R*1.E-3*D_C*4/(MS*P*D_C**2.)
  PR=CP*MS/(K_MIX*RMM)
  HC=(K_MIX*0.023/D_C)*(RE**0.8)*(PR**0.4)

  HW= 0.01*0.5/KW

  HJ_I=1/ H_J
  HC_I=1/HC
  U_IN=HJ_I+HC_I+HW
```

```
      U=1/U_IN
      RETURN
      END

$ENDCODE
****
PROCEDURE H_C :HC

# THIS PROCEDURE CALCULATES HEAT CAPACITY OF A STREAM FROM ITS #COMPOSITION AND
# TEMPERATURE

INPUT
      CONSTANT(NCOMP),CONSTANT(NCOMP),TEMPERATURE,MOLEFRACTION(NCOMP)
OUTPUT
      MOL_HEAT_CAP

CODE

            SUBROUTINE HC (A,NC,B,N1,T,X,N2,CP)
            INTEGER NC,I
            implicit double precision (A-Z)
            dimension A(NC),B(NC),X(NC)

            CP=0.
      DO 200 I=1,NC
            CP=CP+X(I)*(A(I)+(B(I)*T))
200      CONTINUE
      RETURN
      END

$ENDCODE

****

PROCEDURE KIN

# THIS PROCEDURE CALCULATES SOLUBILITY PRODUCT
# THROUGH THERMODYNAMIC CONSIDERATIONS

 INPUT
       VOLUME,CONCENTRATION,CONCENTRATION
       CONSTANT,CONSTANT,CONSTANT,
       DENSITY,NOTYPE (NMOM),
       CONSTANT,NOTYPE,SIZES,
       DENSITY,CONSTANT (NCOMP)

 OUTPUT
       RATE,RATE,RATE,KERNAL,NOTYPE


 CODE
      SUBROUTINE KIN (VOL,C,CS,N,P,Q,RHO,M,IM,MU,DIFF,L,
    + RHO_C,RMM,ICO,N_P,N_C,GRO,BETAO,A_RC)
      integer ICO,IM
      implicit double precision (A-Z)
      dimension M(IM),RMM(ICO)
      PARAMETER (PI=3.14159265359, R=8.314,D=0.13,KN=0.65E5)
      PARAMETER (DE=29700, NC=1.8,DC=0.18)
      PARAMETER (T=295,KV=1.0,KA=450.0,G2=0.9,PRE_N=0.85E26)
      PARAMETER (AV=6.02E26, K=1.38E-23)

C
C SIG THE INTERFACIAL ENERGY IS CALCULATED IN J/ m2,DG
C IS IN JOULES.
C
```

```
      SIG=0.414*K*T*((RHO_C*AV/RMM(2))**0.666)*(LOG(RHO_C/(RMM(2)*C)))
      S=C/CS
      SG=(((0.3*RMM(2))+(0.7*RMM(1)))/RHO)*(C-CS)
C
C P IS IN W kg-1 AND Q IN m3/ sec, PRE_N AND KN HAVE TO BE IN
C (MICRONS*sec)-1. VM IN m3.
C
C


      NP=P/(RHO*N**3*D**5)
      NQ=Q/(N*D**3)
      N_C=KN*(NQ/NP)*M(4)*1.E-12*S**1.7
      ZE=(1.049952E15/T**3)*(RMM(2)/RHO_C)**2
      IF (S.LT.1.35) THEN
       N_P=0.1E-4
      ELSE
       SN=(LOG(S))**2
       PN=DEXP(-16.*PI*ZE*SIG**3/(3*SN))
       N_P=PRE_N*PN
      ENDIF
C
C L IS CONVERTED IN METERS ANS KG TO MICRONS/sec
C
      X=((D/DC)**0.17)*((MU/(RHO*DIFF*1.E-6))**0.36)
      L_M2= L*1.E-6
      P_S=P/(RHO*VOL*1.E-3)
      SH=2.+0.47*X*((RHO*P_S**0.33*L_M2**1.33/MU)**0.62)
      KD=DIFF*1.E-6*SH/L_M2
      KR=2.0*EXP(-DE/(R*T))
      KG=((KD*KR)/(KD+KR))*100
      GRO=KG*SG
C
C KA IS IN sec-1
C
       BETAO=KV*KA*(S**G2)

C
C CRITICAL RADIUS OF THE NUCLEUS IN MICRONS
C

      S_A= LOG (S)
      A_S= SIG/(K*T)
      A_VM= RMM(2)/(RHO_C*AV)
      A_RC=2.E6*A_S*A_VM/S_A


      RETURN
      END
$ENDCODE

****
PROCEDURE MOMENT

# THIS PROCEDURE CALCULATES FIRST FOUR MOMENTS FROM N AND L

INPUT
     NUMBER(NOSIZE),SIZES(NOSIZE)

OUTPUT
     NOTYPE(NOMOM)

CODE
 SUBROUTINE MOMENT (N,NEQ,L,N1,MOM,NM)
 implicit double precision (A-H,O-Z)
 double precision N(NEQ),MOM(NM),L(NEQ)
 DOUBLE PRECISION NUM
```

```
      PARAMETER (R1=1.12996052494)

       DO 100 J=1,NM
          MOM(J)=0.
100     CONTINUE
       DO 200 I=1,NEQ
          X=R1*L(I)
          NUM=N(I)
       DO 250 J=1,NM
          MOM(J)=MOM(J)+NUM*X**(J-1)
250     CONTINUE
200     CONTINUE
       RETURN
       END
```

```
$ENDCODE
****
PROCEDURE PPROP


# THIS PROCEDURE CALCULATES HEAT CAPCACITY,DENSITY,VISCOSITY AND
# THERMAL CONDUCTIVITY OF THE SUSPENSION
# AS A FUNCTION OF COMPOSITION

INPUT
     DENSITY,DENSITY,FRACTION,CONSTANT

OUTPUT
     DENSITY, CONSTANT

CODE

          SUBROUTINE PPROP (RC,RL,V,M,RHO,MS)
          double precision RC,RL,V,M
          DOUBLE PRECISION MS,RHO

            RHO=(1-V)*(RL-RC)+RC
            MS=M*(1.+2.5*(V)+14.1*(V)**2)
            RETURN
            END

$ENDCODE

****
PROCEDURE PPROP3
#
# AGAIN A ROUTINE FOR PHYS. PROPS. THIS TIME FOR A DIFFERENT UNIT
# WHERE NOT ALL THE PROPERTIES ARE OF INTEREST
#
INPUT

     CONSTANT(NCOMP),CONSTANT(NCOMP),TEMPERATURE,MOLEFRACTION(NCOMP),
     DENSITY,DENSITY,FRACTION,CONSTANT,CONSTANT

OUTPUT
     MOL_HEAT_CAP,DENSITY,CONSTANT

CODE

          SUBROUTINE PPROP3 (A,NC,B,N1,T,X,N2,RC,RL,V,M,RMM,CP,RHO,MS)
          INTEGER I,NC,N1,N2
          implicit double precision (A-Z)
          dimension A(NC),B(NC),X(NC)
```

```
          CP=0.
      DO 200 I=1,NC
          CP=CP+X(I)*(A(I)+B(I)*T)
200       CONTINUE

          RHO=(1-VOID)*(RL-RC)+RC
          MS=M*(1.+2.5*(VOID)+14.1*(VOID)**2)
          RETURN
          END

$ENDCODE

****
PROCEDURE PVEL

#
# PARTICLE VELOCITES ARE CALCULATED HERE FOR THE HYDROCYCLON
#
INPUT

    SIZES(NOSIZE),DENSITY,DENSITY,CONSTANT,NOTYPE,
    NOTYPE,CONSTANT

OUTPUT

   NOTYPE(NOSIZE),NOTYPE(NOSIZE)

CODE


    SUBROUTINE PVEL (L,NEQ,RHO,R_C,MU,V_TV,V_TW,DH,UD_W,N1,UD_V,N2)
    integer I,NEQ
    IMPLICIT DOUBLE PRECISION (A-Z)
    DIMENSION L(NEQ),FC_V(20),FC_W(20),UV(20),UW(20)
    DIMENSION UD_V(NEQ),UD_W(NEQ),RE_W(20),RE_V(20)
    PARAMETER (PI=3.1415927)

     DO 20 I=1,NEQ

    FC_V(I)=(PI*(1.E-6*L(I))**3/6)*(R_C-RHO)*(5*V_TV**2/DH)
    FC_W(I)=(PI*(L(I)*1.E-6)**3/6)*(R_C-RHO)*(V_TW**2/DH)

20   CONTINUE

    DO 30 I=1,NEQ

      UD_V(I)=FC_V(I)/(3*PI*MU*L(I)*1.E-6)
      UD_W(I)=FC_W(I)/(3*PI*MU*L(I)*1.E-6)
30   CONTINUE

    DO 40 I=1,NEQ

       RE_V(I)=RHO*UD_V(I)*L(I)*1.E-6/MU
       RE_W(I)=RHO*UD_W(I)*L(I)*1.E-6/MU

40   CONTINUE

    TOL1=1.E-14

    DO 100 I=1,N
    IF (RE_W(I).LT.0.1) THEN
       UW(I)=UD_W(I)
    ELSE IF (RE_W(I).LT.1) THEN
    U1=0.0
115    CONTINUE
```

```
      U1=U1+1.E-5
       FW=(3*PI*MU*L(I)*1.E-6*U1)+(PI*(L(I)*1.E-6*U1)**2*(9/16)*RHO)
       DIFF=FC_W(I)-FW
          IF (DIFF.GT.TOL1) THEN
           GOTO 115
          ELSE
           UW(I)=U1
          ENDIF
       ELSE
       U1=0.0
135       CONTINUE
       U1=U1+0.0001
      FW=3*PI*MU*L(I)*1.E-6*U1*(1+((3/16)*RHO*U1*L(I)*1.E-6/MU))**0.5
       DIFF=FC_W(I)-FW
         IF (DIFF.GT.TOL1) THEN
          GOTO 135
         ELSE
          UW(I)=U1
         ENDIF
       ENDIF
100    CONTINUE

       TOL=1.E-12

       DO 200 I=1,N
       IF (RE_V(I).LT.0.1) THEN
          UV(I)=UD_V(I)
       ELSE IF (RE_V(I).LT.1) THEN
       U1=0.0
105    CONTINUE
       U1=U1+1.E-5
       FD=(3*PI*MU*L(I)*1.E-6*U1)+(PI*(L(I)*1.E-6*U1)**2*(9/16)*RHO)
       DIFF=FC_V(I)-FD
         IF (DIFF.GT.TOL) THEN
          GOTO 105
         ELSE
          UV(I)=U1
         ENDIF
       ELSE
       U1=0.0
110    CONTINUE
       U1=U1+0.001
      FD=3*PI*MU*L(I)*1.E-6*U1*(1+((3/16)*RHO*U1*L(I)*1.E-6/MU))**0.5
       DIFF=FC_V(I)-FD
         IF (DIFF.GT.TOL) THEN
          GOTO 110
         ELSE
          UV(I)=U1
         ENDIF

       ENDIF
200    CONTINUE
       RETURN
       END

$ENDCODE

****
PROCEDURE RA
#
# CONTRIBUTIONS TO POP BALANCE DUE TO DIFFERENT PHENOMENON
# ARE RETURNED
#
INPUT
       NUMBER(NOSIZE), SIZES,SIZES(NOSIZE),NOTYPE (NOSIZE),
       RATE,RATE,KERNAL
```

```
OUTPUT
     RATE (NOSIZE),RATE(NOSIZE),RATE(NOSIZE),RATE(NOSIZE),RATE(NOSIZE)

CODE
     SUBROUTINE RA(N,NEQ,SMIN,L,N1,S,N5,B,G,
    + BETAO,GR,N2,A,N4,D,N8,DIS,N3,PO,N9)
     implicit double precision (A-H,O-Z)
     double precision N(NEQ),L(NEQ),S(NEQ),DIS(NEQ)
     DOUBLE PRECISION GR(NEQ),A(NEQ),D(NEQ),V(20),PO(NEQ)
     PARAMETER(X=1.898214737,Y=0.884986671,Z=-1.898214737)
     PARAMETER (N10=20)

      DO 50 I=2,NEQ-1
       GR (I)=G*1.E4*(X*N(I-1)+Y*N(I)+Z*N(I+1))/L(I)
50    CONTINUE


     GR (1)  =B+G*1.E4/L(1)*(Y*N(1)+Z*N(2)+Z*N(1)*2.**(1./3.))
     GR (NEQ)=G*1.E4/(L(NEQ))*(X*N(NEQ-1)+Y*N(NEQ))


      DO 100 I=1,NEQ
       IF (I.EQ.1)THEN
        AGGLO =0.5*1.E-12*BETAO
       ELSE
        AGGLO =0.5*1.E-12*BETAO*(L(I-1)+L(I-1))**3*N(I-1)**2
       ENDIF
      DO 110 J=1,I-2
     AGGLO=AGGLO+2.**(J-I)*2.E-12*BETAO*(L(I-1)+L(J))**3*N(I-1)*N(J)
110     CONTINUE

      DEATH = 0.
      DO 120 J=1,NEQ
        IF (J.LT.I)THEN
           Q=2.**(J-I)
        ELSE
           Q=1.
           ENDIF
          DEATH=DEATH+BETAO*1.E-12*(L(I)+L(J))**3*N(I)*N(J)*Q
120    CONTINUE

     A(I)=AGGLO
     D(I)=DEATH

100    CONTINUE

     SV=1.0
     V(1)=SV*SMIN**3

     DO 222 I=2,N10
        V(I)=V(I-1)*2
222    CONTINUE


     DO 2000 I=1,NEQ
      PO(I)=0.5*S(I)*N(I)
2000    CONTINUE


     DO 5000 I=1,NEQ-1
       ENT=0.
     IF (I.EQ.1) THEN
      V_I=V(1)*2.
     ELSE
      V_I=V(I)
```

```
      ENDIF
      DO 6000 J=I+1,NEQ
       V_J=V(J)
       ENT=ENT+S(J)*N(J)*(V_I/V_J)
6000   CONTINUE

      DIS(I) = (ENT*3/2)

5000   CONTINUE
       DIS(NEQ)=0.0
      RETURN
      END

$ENDCODE
****
PROCEDURE RAD

INPUT
   NUMBER(NOSIZE)

OUTPUT
   NOTYPE(NOSIZE)


CODE
      SUBROUTINE RAD (N,NEQ,AB,N1)
      implicit double precision (A-H,O-Z)
      double precision N(NEQ)
      DIMENSION AB(NEQ)
       PARAMETER(A=-1.898214737,B=-0.884986671,C=1.898214737)
      AB(1)=0.0+((B+A)*N(1))+C*N(2)

      DO 11 I=2,NEQ-1
       AB(I)=A*N(I-1)+B*N(I)+C*N(I+1)
11     CONTINUE
       AB(NEQ)=A*N(NEQ-1)+B*N(NEQ)+C*N(1)*2.**(1/3)
       RETURN
       END
$ENDCODE
****
PROCEDURE RAH
#
# THIS ROUTINE IS FOR HC WERE AGGLOMERATION AND GROWTH ARE NOT
# MODELLED TO HAPPEN
#
INPUT
      NUMBER(NOSIZE), SIZES,SIZES(NOSIZE),NOTYPE (NOSIZE),
      KERNAL

OUTPUT
       RATE(NOSIZE),RATE(NOSIZE),RATE(NOSIZE),RATE(NOSIZE)

CODE
      SUBROUTINE RAH (N,NEQ,SMIN,L,N1,S,N5,
     + BETAO,A,N4,D,N8,DIS,N3,PO,N9)
      implicit double precision (A-H,O-Z)
      double precision N(NEQ),L(NEQ),S(NEQ),DIS(NEQ)
      DOUBLE PRECISION A(NEQ),D(NEQ),V(20),PO(NEQ)
      PARAMETER(X=1.898214737,Y=0.884986671,Z=-1.898214737)
      PARAMETER(N10=20)
```

```
      DO 100 I=1,NEQ
       IF (I.EQ.1)THEN
        AGGLO =0.5*1.E-12*BETAO
       ELSE
        AGGLO =0.5*1.E-12*BETAO*(L(I-1)+L(I-1))**3*N(I-1)**2
       ENDIF
       DO 110 J=1,I-2
     AGGLO=AGGLO+2.**(J-I)*2.E-12*BETAO*(L(I-1)+L(J))**3*N(I-1)*N(J)
110     CONTINUE

       DEATH = 0.
       DO 120 J=1,NEQ
         IF (J.LT.I)THEN
            Q=2.**(J-I)
          ELSE
            Q=1.
            ENDIF
          DEATH=DEATH+BETAO*1.E-12*(L(I)+L(J))**3*N(I)*N(J)*Q
120    CONTINUE

      A(I)=AGGLO
      D(I)=DEATH

100    CONTINUE

       SV=1.0
       V(1)=SV*SMIN**3

      DO 222 I=2,N10

        V(I)=V(I-1)*2
222    CONTINUE

      DO 2000 I=1,NEQ
       PO(I)=0.5*S(I)*N(I)
2000    CONTINUE


      DO 5000 I=1,NEQ-1
        ENT=0.
       IF (I.EQ.1) THEN
        V_I=V(1)*2.
       ELSE
        V_I=V(I)
       ENDIF
       DO 6000 J=I+1,NEQ
        V_J=V(J)
        ENT=ENT+S(J)*N(J)*(V_I/V_J)
6000   CONTINUE

       DIS(I) = (ENT*3/2)

5000   CONTINUE
        DIS(NEQ)=0.0
      RETURN
      END

$ENDCODE



****
PROCEDURE SAT

# SATURATION CONCENTRATION IS CALCULATED AS FUNCTION OF TEMP
#
```

```
INPUT
      TEMPERATURE

OUTPUT

      CONCENTRATION

CODE
      SUBROUTINE SAT (T,CS)
      implicit double precision (A-Z)

      A=-6106.8467
      B=98.896550
      C=-0.63677944
      D=0.0020375883
      E= -3.2426245E-6
      F= 2.0586348E-9

      CS=A+(B*T)+(C*T**2)+(D*T**3)+(E*T**4)+(F*T**5)

      RETURN
      END

$ENDCODE


****
PROCEDURE SIZES
#
# SIZE IS CALCULATED FROM THE GEOMETRIC PROG RATIO AND LMIN
#
INPUT
            SIZES,CONSTANT

OUTPUT
            SIZES(NOSIZE)


CODE
      SUBROUTINE SIZES (LMIN,R,L,NEQ)
      implicit double precision (A-H,O-Z)
      double precision L(NEQ),LMIN



       L(1)=LMIN
         DO 11 I=2,NEQ
            L(I)=L(I-1)*R
11       CONTINUE
      RETURN
      END

$ENDCODE


****
MODEL HYDRO

SET
      NOMOM
      NOSIZE
      PI=3.14159
TYPE
```

```
FLOW_IN,F_OUT1,F_OUT2       as FLOWRATE
N_IN,N_OUT1,N_OUT2,NUM      as ARRAY(NOSIZE) of NUMBER
MOM_P,MOM,MOM_R             as ARRAY(NOMOM) of NOTYPE
IN_OUT                      as ARRAY(NOSIZE) of NOTYPE
S_DAT                       as ARRAY(NOSIZE) of SIZES
G_A,GEN,G_DI,G_DO,G_D       as ARRAY(NOSIZE) OF RATE
D_R                         as ARRAY(NOSIZE) OF NOTYPE
S_1                         as SIZES
U_FL,V_RAD1,V_TW1           as NOTYPE
BETAO                       as KERNAL
CONC_IN,CONC_OUT1,CONC_OUT2 as CONCENTRATION
T_IN,T_OUT1,T_OUT2          as TEMPERATURE
EFFI                        as ARRAY (NOSIZE) of FRACTION
E_F,K_O,K_1,K_2             as ARRAY(NOSIZE) of NOTYPE
U_PW,U_PV                   as ARRAY(NOSIZE) of NOTYPE
L_P,L_R                     as SIZES
TA,TA_W,PSI,SIG,A_C,AF      as NOTYPE
PSI_1,V_TV1,F_M,HT_CONE     as NOTYPE
THE_F,C_AN                  as CONSTANT
W,V,V_TV,V_TW,V_RADV,V_THEV  as NOTYPE
V_THEW,V_RADW,W_SP          as NOTYPE
DH,D_VF,D_SP                as CONSTANT
D_ENG                       as NOTYPE
VOID                        as FRACTION
MU                          as CONSTANT
RHO_C,RHO,RHO_F             as DENSITY
MU_L,DC_R,KV                as CONSTANT
VOL                         as VOLUME

# COMPONENT 1 IS THE SOLVENT
# COMPONENT 2 IS THE DISSOLVED SOLUTE & CRYSTALS

STREAM
   INPUT  1 FLOW_IN,N_IN,CONC_IN,T_IN
   OUTPUT 1 F_OUT1,N_OUT1,CONC_OUT1,T_OUT1
   OUTPUT 2 F_OUT2,N_OUT2,CONC_OUT2,T_OUT2,MOM_P,L_P
#
# OUTPUT 1 AND OUTPUT 2 ARE OVERFLOW AND UNDERFLOW STREAMS
#

EQUATION

#
# FLUID FLOW EQUATIONS
# SPHERICAL POLAR CO ORDINATES ARE USED
# C_AN IS CONE SEMI - ANGLE IN RADIANS
# THE_F IS VORTEX ANGLE AND THE IS THE ANGLE IN THE
# ABOVE CO ORDINATE SYSTEM
# A_C IS INTEGRATION CONSTANT AND W IS VELOCITY COMPONENT
# DIRECTED INTO THE CYCLONE
# V,W ARE TANGENTIAL AND AXIAL COMPONENTS OF VELOCITY AT THE LEVEL
# WHERE FLOW BECOMES AXIALLY SYMETRIC
#
# Axial velocity is assumed not to be height dependent
#
 F_M=FLOW_IN/1000;
 D_VF=2*(HT_CONE-(DH/3))*(SIN(THE_F)/COS(THE_F));
 TA=0.5* TAN(THE_F);
 TA_W=0.5*TAN (C_AN);
 A_C=((1/SIN(C_AN))'2)+LOG(TA_W)-(1/SIN(C_AN))*(1/TAN(C_AN));
 AF=(A_C*(SIN(THE_F))'2)-((SIN(THE_F))'2*LOG(TA))+COS(THE_F)-1.0;
 HT_CONE=(0.5*DH*COS(C_AN)/SIN(C_AN))+(0.5*DH);
 SIG=1/(AF*(HT_CONE-(DH/3))'2);
 V=((SIG*F_M*W)'0.5)/(PI'0.5*HT_CONE);

# PSI IS STREAM FUNCTION
```

```
PSI_1=(A_C*(SIN(C_AN))'2)-((SIN(C_AN))'2*LOG(TA_W));
PSI=SIG*(HT_CONE-(DH/3))'2*(PSI_1+COS(C_AN)-1);

# V_LAMB,V_RAD,V_THE ARE TANGENTIAL, AXIAL AND RADIAL COMPONENTS
# OF FLUID VELOCITY

 V_TV1=V/((HT_CONE-(DH/3))*SIN(THE_F));
 V_TV=V_TV1*(1- (SIG*(F_M'2)/(PI*HT_CONE*V)'2)'0.5);
 V_TW1=V/((HT_CONE-(DH/3))*SIN(C_AN));
 V_TW=V_TW1*(1-(SIG*PSI*(F_M'2)/(PI*HT_CONE*V)'2))'0.5;
 V_RAD1=F_M/(2*PI*(HT_CONE)'2);
 V_RADV=V_RAD1*((2*A_C*COS(THE_F))-(2*SIG*COS(THE_F)*LOG(TA)));
 V_RADW=V_RAD1*((2*A_C*COS(C_AN))-(2*SIG*COS(C_AN)*LOG(TA_W)));
 V_THEV=(F_M/(2*PI*HT_CONE'2))*(2*PSI/SIN(2*THE_F));
 V_THEW=(F_M/(2*PI*HT_CONE'2))*(2*PSI/SIN(2*C_AN));

# IN CYLINDERICAL CO ORDINATES V_RADV & V_THEV ARE EXPRESSED AS W_FL,U_FL

 W_SP=(V_RADW*COS(C_AN))+(V_THEW*SIN(C_AN));
 U_FL=(V_RADV*SIN(THE_F))-(V_THEV*COS(THE_F));


#
# EFFI IS THE FRACTION OF PARTICLE OF SIZE L REPORTING TO
# THE UNDERFLOW
#

# CENTRIFUGAL FORCE ON PARTICLES OF ALL SIZES ARE CALCULATED AT
# THE TWO BOUNDARIES; VORTEX FINDER AND MAIN CYCLONE WALLS

 D_ENG=(DH/2)-((DH/7)/2);
 E_F=EXP(-2*PI*(DH/2)*U_PW*D_ENG/F_M);
 K_O=((DH/2)*U_PW+(D_VF/2)*U_FL+(D_VF/2)*U_PV)/(2*(D_VF/2)*U_PV);
 K_1=((D_VF/2)*U_PV-(D_VF/2)*U_FL-(DH/2)*U_PW)/(2*(D_VF/2)*U_PV);
 K_2=(DH/2)*U_PW/((D_VF/2)*U_PV);
 EFFI=1-((K_O-(K_1'2+K_2'2)'0.5)*E_F);

# POPULATION BALANCE
VOL=((1/3)*PI*(DH/2)'2*(HT_CONE-(0.5*DH)))+(0.5*DH*PI*(DH/2)'2);
T_IN=T_OUT1;
T_OUT1=T_OUT2;
F_OUT2=1000*W_SP*PI*(D_SP/2)'2;
CONC_OUT1=CONC_IN;
CONC_OUT2=CONC_IN;
FLOW_IN=F_OUT1+F_OUT2;
GEN  = G_A+G_DI-(G_D+G_DO);
$NUM  = GEN-IN_OUT;
IN_OUT=((N_OUT1+N_OUT2)*(F_OUT1+F_OUT2)-(N_IN*FLOW_IN))/(VOL*1000);
NUM*EFFI=N_OUT2;
NUM*(1-EFFI)=N_OUT1;
#
  VOID=KV*MOM(4)*1.0E-12;
  L_P=MOM_P(2)/MOM_P(1);
  L_R=MOM_R(2)/MOM_R(1);
#
# REQUIRED PROCEDURES ARE CALLED
#

PROCEDURE
  (S_DAT) SIZES (S_1,DC_R)
  (D_R) BREH (S_1)
  (BETAO) BETA (T_OUT1,CONC_IN)
  (MOM_P) MOMENT (N_OUT2,S_DAT)
  (MOM_R) MOMENT (N_OUT1,S_DAT)
  (MOM) MOMENT (NUM,S_DAT)
```

```
  (G_A,G_D,G_DI,G_DO) RAH (NUM,S_1,S_DAT,D_R,BETAO)
  (RHO,MU) PPROP (RHO_C,RHO_F,VOID,MU_L)
  (U_PW,U_PV) PVEL (S_DAT,RHO,RHO_C,MU,V_TV,V_TW,DH)
****
MODEL JFEED

# THIS MODEL DEFINES THE PHYSICAL PROPERTIES OF THE HEATING/COOLING
# STREAM TO THE JACKET

 SET
  ncomp
 TYPE
#  Output:
   F_out    AS              flow_mol_liq
   T_out    AS              TEMPERATURE
   x_out    as array  (ncomp) OF MOLEFRACTION
   Cp_OUT   AS              MOL_HEAT_CAP
   cp_a,cp_b as array (ncomp)  OF  CONSTANT

 STREAM
  OUTPUT 1    F_out, T_out,CP_OUT

 EQUATION

#  Material balance - complete the mole fraction array
   SIGMA (X_OUT)=1.0;

 PROCEDURE
  ( CP_OUT) h_C (cp_a,cp_b,T_out,x_out)



****
MODEL MSMPR


SET
      NOSIZE
      NCOMP
      NOMOM
      PI=3.14
      R=8.314  # KJ /KMOL K #
TYPE
   FLOW_IN,FLOW_OUT          as FLOWRATE
   MOM_IN,MOM_OUT            as ARRAY(NOMOM) of NOTYPE
   N_IN,N_OUT,NUM            as ARRAY(NOSIZE) of NUMBER
   D_R                  as ARRAY(NOSIZE) of NOTYPE
   S_DAT                 as ARRAY(NOSIZE) of SIZES
   L,S_1,DEL_R              as SIZES
   GEN,G_G,G_A,G_D,G_DI,G_DO   as ARRAY(NOSIZE) of RATE
   P,Q1,N                 as CONSTANT
   Q                    as HEAT
   B,N_C,GRO,N_P             as RATE
   B_Delay                as RATE
   C_OUT,IN_OUT,C_IN,C_D,CS    as CONCENTRATION
   MB_ERROR,MB_AN            as CONCENTRATION
   BAL,CR_N                as NOTYPE
   BETAO                  as KERNAL
   DIF                   as NOTYPE
   TD                    as NOTYPE
   C_N                    as NOTYPE
   VOL                    as VOLUME
   RHO,RHO_C,RHO_F           as DENSITY
   VOID                   as FRACTION
   TIME,F                  as NOTYPE
   K_WALL                   as NOTYPE
```

```
TD_C                    as NOTYPE
MU,KV,KS,MU_J           as CONSTANT
MU_L,DC_R               as CONSTANT
RMM                     as ARRAY(NCOMP) of CONSTANT
JF_IN,JF_OUT            as FLOW_MOL_LIQ
HFIN_OUT,DH_C           as HEAT
U,HJ_IN,HEAT_CR,D_HEAT  as NOTYPE
TJ_IN,TJ_OUT,TJ         as TEMPERATURE
T_IN,T_OUT,TV           as TEMPERATURE
RHO_J                   as DENSITY
VOL_J,A_J,J_HEAT        as NOTYPE
CP_A,CP_B               as ARRAY(NCOMP) of CONSTANT
D_J,D_CS,SS             as CONSTANT
L_CS,RMM_J,RMM_1,L_J,RMM_A  as CONSTANT  # RMM_S IS for the solvent
   CP,CP_IN,CP_J,CP_JI      as MOL_HEAT_CAP
   X_IN                     as ARRAY(NCOMP) of MOLEFRACTION
   XJ_OUT                   as ARRAY(NCOMP) OF MOLEFRACTION

# COMPONENT 1 IS THE SOLVENT
# COMPONENT 2 IS THE DISSOLVED SOLUTE

STREAM
   INPUT 2 FLOW_IN,N_IN,MOM_IN,T_IN,X_IN,CP_IN,RHO_F,C_IN
   OUTPUT 2 FLOW_OUT,N_OUT,C_OUT,T_OUT
   INPUT 1 JF_IN,TJ_IN,CP_JI
   OUTPUT 1 JF_OUT,TJ_OUT,CP_J

EQUATION

 #  POPULATION BALANCE

     FLOW_IN=FLOW_OUT;
     GEN  = G_G+G_A+G_DI-(G_D+G_DO);
     $NUM  = GEN-((N_OUT*FLOW_OUT-N_IN*FLOW_IN)/VOL);
     N_OUT= NUM;

# MASS BALANCE

    VOL=1000*L_CS*PI*(D_CS/2)'2;
    $C_D=IN_OUT-C_N-0.5*KS*(RHO_C/RMM(2))*GRO*MOM_OUT(3)*1.0E-8;
    C_N=(RHO_C/RMM(2))*KV*B*(S_DAT(1)'3)*1.0E-12 ;
    IN_OUT=(FLOW_IN*C_IN-FLOW_OUT*C_OUT)/VOL;
    C_OUT=C_D;
    SS=C_OUT/CS;

    RMM_A=(RMM(1)*X_IN(1))+(RMM(2)*X_IN(2));

# HEAT BALANCE
#
 VOL*1.0E-3*CP*(RHO/RMM_A)*$TV=D_HEAT;
 D_HEAT=P+HEAT_CR+HFIN_OUT+Q;
 HFIN_OUT=(FLOW_IN*RHO_F*CP_IN*T_IN-FLOW_OUT*RHO*CP*T_OUT)*(1.0E-3/RMM_A);
 HEAT_CR=DH_C*C_OUT*FLOW_OUT*1.0E-3;
 T_OUT=TV;
#
# JACKET MASS AND ENERGY BALANCE
#
 JF_OUT=JF_IN;
 VOL_J = (((L_J-L_CS)*PI*D_J'2)/4)+((D_J-D_CS)/2)'2*PI*L_J;
 (RHO_J/RMM_J)* CP_J*VOL_J*$TJ = J_HEAT;
 HJ_IN=((JF_IN*TJ_IN*CP_JI)-(JF_OUT*TJ_OUT*CP_J))*(1.0E-3*RHO_J/RMM_J);
 J_HEAT=HJ_IN-Q;
 TJ_OUT=TJ;

 Q=U*A_J*(TJ_IN-T_OUT);
 XJ_OUT(1)=1.0;
```

```
 XJ_OUT(2)=0.0;
#
# NUCLEATION RATE
#
    B=N_C+N_P;

#
# VOIDAGE RELATIONSHIP NOTE MOM(4) IS ACTUALLY MOM(3) BECAUSE
# COUNTER STARTS AT 1
#

    VOID=KV*MOM_OUT(4)*1.0E-12;
    L=MOM_OUT(2)/MOM_OUT(1);
     A_J=(PI*D_CS*L_CS)+(PI*D_CS'2/4);
#
# TIME DELAY EXPRESSION FOR NUCLEI TO GROW TO THE SIZE AT
# FIRST INTERVAL
#

  DEL_R=S_DAT(1)-(2*CR_N);
  TD=DEL_R*1.0E-4/GRO;

   IF N_P < 5.0
    THEN
     TD_C=14.0
    ELSE
     TD_C=TD
    ENDIF;

   B_Delay=DELAY F BY TD_C;

   IF TIME  < TD_C
     THEN
       F = 0.0
    ELSE
       F=B
   ENDIF;


#
# SOLUTE MASS BALANCE CHECK
#

  BAL=KV*(MOM_OUT(4)-MOM_IN(4))*1.0E-12*(RHO_C/RMM(2));
  MB_ERROR=BAL-(C_IN-C_OUT);
  RMM(1)=RMM_1;
  MB_AN=KS*TAU*(MOM_OUT(1)-MOM_IN(1))*(RHO_C/RMM(2))*(GRO*TAU)'3;
#
# REQUIRED PROCEDURES ARE CALLED
#

PROCEDURE
  (S_DAT) SIZES (S_1,DC_R)
  (D_R) BRE (S_1)
  (G_G,G_A,G_D,G_DI,G_DO) RA (NUM,S_1,S_DAT,D_R,F,GRO,BETAO)
  (MOM_OUT) MOMENT (NUM,S_DAT)
  (N_P,N_C,GRO,BETAO,CR_N) KIN (VOL,C_OUT,CS,N,P,Q1,RHO,
     MOM_OUT,MU,DIF,L,RHO_C,RMM)
  (CS)    SAT (T_OUT)
  (CP,RHO,MU) PPROP3 (CP_A,CP_B,T_OUT,X_IN,RHO_C,RHO_F,VOID,MU_L,RMM_1)
  (CP_J) H_C (CP_A,CP_B,TJ_OUT,XJ_OUT)
  (U) HCOF ( CP,CP_J,MU,MU_J,RHO,RHO_J,RMM_A,RMM_J,
          D_CS,D_J,N,JF_OUT,K_WALL,TJ_OUT)

****
```

```
MODEL SF

# This model defines the inlet stream to the MSMPR and calculates its moments
# if particles exist #
# THE FINES DISSOLVER IS AMALGUMATED HERE
#
SET
      NOSIZE
      NCOMP
      PI=3.14
      NOMOM
# Variable declaration is done in Type section

TYPE
FLOW_IN,FLOW,FLOW_R  as FLOWRATE
RHO_F,RC,R_SOL,R_SV  as DENSITY
C_IN,C_OUT          as CONCENTRATION
CS,C_RECYCLE,SS      as CONCENTRATION
N_IN,N_R,N_OUT,N_OUT1 as ARRAY(NOSIZE) of NUMBER
N_DIS,N_TOT          as ARRAY(NOSIZE) of NUMBER
MOM,MOM_O,MOM_01     as ARRAY(NOMOM) of NOTYPE
DIS_RATE             as ARRAY(NOSIZE) of RATE
DIFF_N,AB            as ARRAY(NOSIZE) of NOTYPE
MU_L,MU,L_CS,D_CS    as CONSTANT
VOL,KS               as CONSTANT
LEN                  as ARRAY(NOSIZE) of SIZES
T_OUT,T_IN,T_RECYCLE as TEMPERATURE
TEMP                 as TEMPERATURE
CP_OUT               as MOL_HEAT_CAP
TM                   as NOTYPE
CP_A,CP_B,RMM        as ARRAY(NCOMP) of CONSTANT
X_OUT                as ARRAY(NCOMP) of MOLEFRACTION
L1,L_DIS,L_IN        as SIZES
      DIS_EF,DIF,DIS_RV    as NOTYPE
      M_DIS,K_WALL         as NOTYPE
      KV,D_R,RT,RMM_A      as CONSTANT
      VOID                 as FRACTION
      JF_IN,JF_OUT         as FLOW_MOL_LIQ
      HFIN_OUT,DH_C        as HEAT
      U,HJ_IN,HEAT_CR,D_HEAT      as NOTYPE
      TJ_IN,TJ_OUT,TJ      as TEMPERATURE
      TV,T_DIS             as TEMPERATURE
      RHO_J                as DENSITY
      VOL_J,A_J,J_HEAT,Q   as NOTYPE
      D_J,MU_J             as CONSTANT
      RMM_J,L_J            as CONSTANT   # RMM_S IS for the solvent
      CP_J,CP_JI           as MOL_HEAT_CAP
      XJ_OUT               as ARRAY(NCOMP) OF MOLEFRACTION
STREAM
      INPUT  1      FLOW_IN,N_IN,C_IN,T_IN
      INPUT  2      FLOW_R,N_R,C_RECYCLE,T_RECYCLE
      INPUT  3      JF_IN,TJ_IN,CP_JI
      OUTPUT 1      FLOW,N_OUT,MOM_O,T_OUT,X_OUT,CP_OUT,RHO_F,C_OUT
      OUTPUT 2      JF_OUT,TJ_OUT,CP_J

# VOID=0 MEANS NO SOLVENT

EQUATION

# Mass Balance

      FLOW=FLOW_IN+FLOW_R;

      IF TM < 1.0
       THEN
```

```
 T_OUT=((FLOW_IN/FLOW)*T_IN)+((FLOW_R/FLOW)*T_RECYCLE)
ELSE
 T_OUT=((FLOW_IN/FLOW)*T_IN)+((FLOW_R/FLOW)*T_DIS)
ENDIF;

IF TM < 1.0
 THEN
 C_OUT=((FLOW_IN*C_IN)+(FLOW_R*C_RECYCLE))/FLOW
ELSE
 C_OUT=(((FLOW_IN*C_IN)+(FLOW_R*C_RECYCLE))/FLOW)+(M_DIS*RT)
ENDIF;

IF TM < 1.0
 THEN
 N_OUT=N_TOT
ELSE
 N_OUT=N_OUT1+N_IN
ENDIF;

IF TM < 1.0
 THEN
 MOM_O=MOM
ELSE
 MOM_O=MOM_01
ENDIF;

N_R+N_IN=N_TOT;
VOID=KV*MOM(4)*1.0E-12;
RHO_F=(X_OUT(1)*R_SV)+((1-X_OUT(1))*RC);
X_OUT(2)=1-X_OUT(1);


RT=VOL/FLOW;
    (AB*1.E4*DIS_RATE/LEN)=(N_DIS-N_R)/RT;
    DIS_EF=MOM(1)-MOM_O(1);
    DIFF_N=N_TOT-N_OUT1;
    L_DIS=MOM_O(2)/MOM_O(1);
    L_IN = MOM(2)/MOM(1);
    VOL=1000*L_CS*PI*(D_CS/2)'2;
    DIS_RV=SIGMA (DIS_RATE)/20;
    M_DIS=0.5*KS*(RC/RMM(2))*DIS_RV*(MOM_O(3)-MOM(3))*1.0E-8;
    SS=CS-C_OUT;
    RMM_A=(RMM(1)*X_OUT(1))+(RMM(2)*X_OUT(2));

    VOL*1.0E-3*CP_OUT*(RHO_F/RMM_A)*$TV=D_HEAT;
    D_HEAT=HEAT_CR+HFIN_OUT+Q;
    HFIN_OUT=FLOW_R*RHO_F*CP_OUT*(T_RECYCLE-T_DIS)*(1.0E-3/RMM_A);
    HEAT_CR=-DH_C*C_OUT*FLOW_R*1.0E-3;
    T_DIS=TV;
#
# JACKET MASS AND ENERGY BALANCE
#
   JF_OUT=JF_IN;
   VOL_J = (((L_J-L_CS)*PI*D_J'2)/4)+((D_J-D_CS)/2)'2*PI*L_J;
   (RHO_J/RMM_J)* CP_J*VOL_J*$TJ = J_HEAT;
HJ_IN=((JF_IN*TJ_IN*CP_JI)-(JF_OUT*TJ_OUT*CP_J))*(1.0E-3*RHO_J/RMM_J);
   J_HEAT=HJ_IN-Q;
   TJ_OUT=TJ;

   Q=U*A_J*(TJ_IN-T_DIS);

   XJ_OUT(1)=1.0;
   XJ_OUT(2)=0.0;

  N_OUT1 =N_DIS;
  A_J=(PI*D_CS*L_CS)+(PI*D_CS'2/4);
```

```
PROCEDURE
     (MOM) MOMENT (N_TOT,LEN)
     (MOM_01) MOMENT (N_OUT,LEN)
     (RHO_F,MU) PPROP (RC,R_SOL,VOID,MU_L)
     (LEN) SIZES (L1,D_R)
     (CP_OUT) H_C (CP_A,CP_B,T_OUT,X_OUT)
     (AB) RAD (N_DIS)
     (DIS_RATE) DISR (LEN,SS,RHO_F,MU,RC,DIF,RMM_A)
     (CS) SAT (TEMP)
     (CP_J) H_C (CP_A,CP_B,TJ_OUT,XJ_OUT)
     (U) HCOF2 ( CP_OUT,CP_J,MU,MU_J,RHO_F,RHO_J,RMM_A,RMM_J,
          D_CS,D_J,FLOW_R,JF_OUT,K_WALL,TJ_OUT)
****
FLOWSHEET
STREAM S_FD INPUT 1 of F_MIXER is FEED 1
STREAM HY_FD OUTPUT 1 of CLASSIFIER is INPUT 2 of F_MIXER
STREAM JF_CS INPUT 1 of CSTR is OUTPUT of JF  TYPE LIQUID
STREAM FM_CS INPUT 2 of CSTR is OUTPUT 1 of F_MIXER TYPE SOLID
STREAM JC_JF OUTPUT 1 of CSTR is INPUT 3 of F_MIXER  TYPE LIQUID
STREAM CS_HY OUTPUT 2 of CSTR is INPUT of CLASSIFIER
STREAM JF_JC OUTPUT 2 of F_MIXER is PRODUCT 1 TYPE LIQUID
STREAM HY_P2 OUTPUT 2 OF CLASSIFIER IS PRODUCT 2 TYPE SOLIDS

****
UNIT CLASSIFIER IS A HYDRO

****
UNIT CSTR IS A MSMPR
****
UNIT F_MIXER IS A SF

****
UNIT JF  IS A JFEED
****
OPERATION
#
# IN THIS SECTION INPUTS TO DIFFERENT UNITS ARE ASSIGNED
#

 SET


 WITHIN F_MIXER

 FLOW_IN       = 0.1
 N_IN(1)       = 1.0
 L1            = 5.0         # first size class
 D_R           = 1.259921     # length discretization ratio
 MU_L          = 0.87E-3      # KG(MS)-1
 N_IN(2:5)     = 1.0
 N_IN (6 :10)   = 1.0
 N_IN (11:15)   = 0.0
 N_IN (16:20)   = 0.0
 KV            = 1.0
 TM            = T
 TEMP          = IF T < 400.0 THEN 296.45 ELSE
               IF T < 750.0 THEN 296.75 ELSE 297.5
               ENDIF ENDIF
 DIF           = 2.5E-3
 RMM(1)        = 18.0
 RMM(2)        = 101.0
 D_CS          = 0.0267
 L_CS          = 1.445
 KS            = 6.0
 C_IN          = 3.52    # feed concentration
```

```
RC          = 2110          # density of crystal
R_SOL        = 1170          # density of solution
R_SV        = 1000.0        # density of pure solvent
CP_A        = <75.243,26.964>
CP_B        = <1.923E-3,0.265>
T_IN        = 295.0      # feed temperature
MU_J        = 0.8E-3
D_J         = 0.05
L_J         = 1.65       # LENGTH OF JACKET
RMM_J        = 18.0         # RMM of the jacket fluid
K_WALL        = 300.875E-3     # THERMAL COND. OF WALL KW (mK)-1
RHO_J       = 1000.0
DH_C        = 36085.94
#
 WITHIN JF

  T_OUT         = IF T < 150 THEN 281.25 ELSE
                  IF T < 220 THEN 283.0 ELSE 282.0
                  ENDIF ENDIF
  F_OUT          = 0.150
  CP_A          = <75.243,26.964>
  CP_B          = <1.923E-3,0.265>
  x_out(2)      =  0.0


  WITHIN CSTR
   KS       = 6.0          # shape factor
   RHO_C     = F_MIXER.RC  # density of crystal
   KV        = F_MIXER.KV  # volume factor
   MU_L      = F_MIXER.MU_L
   S_1       = F_MIXER.L1
   DC_R      = F_MIXER.D_R
   P         = 0.8775       # power of stirrer W
   Q1         = 0.002        # pumping capacity of the stirrer
   N         = 5           # revs of the stirrer in Hz
   DIF        = 2.5e-3       # diffusivity (MS)-1
   RMM(1)     = 18           # RMM of the solvent
   RMM(2)     = 101          # RMM of the solute
   RHO_J      = F_MIXER.RHO_J
   DH_C       = F_MIXER.DH_C  # kj/kmol heat of crystallization
   TIME       = T
   CP_A       = <75.243,26.964>      # heat cap. cons
   CP_B       = <1.923E-3,0.265>     # heat cap. constant
   K_WALL     = F_MIXER.K_WALL
   D_CS       = 0.229         # diameter of the MSMPR
   L_CS       = 0.25         # length of the REACTOR
   MU_J       = F_MIXER.MU_J
   D_J        = 0.247
   L_J        = 0.26         # LENGTH OF JACKET
   RMM_J      = F_MIXER.RMM_J        # RMM of the jacket fluid

WITHIN CLASSIFIER

C_AN    = 0.0987
THE_F   = 0.02094
DH      = 0.13
D_SP    = 0.0095
KV      = F_MIXER.KV
RHO_C   = F_MIXER.RC
MU_L    = F_MIXER.MU_L
S_1     = F_MIXER.L1
DC_R    = F_MIXER.D_R
W       = 0.01257
RHO_F   = F_MIXER.R_SOL
```

```
  PRESET

     WITHIN F_MIXER
          MU          = 0.9E-3 : 0.8E-3 : 1.0E-1
#         T_DUM       = 296.5  : 295.0  : 350.0

     WITHIN CSTR
          U           = 23.0   : 0.0   :40
#         TD_C        = 12.05  : 0.0   : 200
          MU          = 0.9E-3 : 0.8E-3 : 1.0E-1
   INITIAL

     WITHIN F_MIXER
          TV          = F_MIXER.T_IN
          TJ          = JF.T_OUT
     WITHIN CSTR
          NUM (1)     = 1.0
          NUM (2 : 5)  = 1.0
          NUM (6 :10)  = 0.0
          NUM (11:15)  = 0.0
          TV          = F_MIXER.T_IN
          NUM (16:20)  = 0.0
          C_D         = F_MIXER.C_IN
          TJ          = JF.T_OUT

      WITHIN CLASSIFIER
          NUM (1)     = 1.0
          NUM (2 : 5)  = 1.0
          NUM (6 :10)  = 0.0
          NUM (11:15)  = 0.0
          NUM (16:20)  = 0.0
****
```

APPENDIX C: The data used for first generation of decision trees

Tot. Crys	Crys/vol	Av. Size	F Flowrate	W for HC	T diss	T cool	T Feed	C Feed
Cut Point Value			**0.10471**	**0.012961**	**296.6253**	**281.6037**	**295.3791**	**3.53191**
Information Entropy			0.285389	0.349194	0.350304	0.355776	0.357343	0.372917
Test Selection Criterion at the Root			**0.184655**	**0.12085**	**0.11974**	**0.114268**	**0.112701**	**0.097127**
No. of exemplers at s < T			*0/36/29*	*6/34/36*	*7/35/28*	*8/28/28*	*3/25/20*	*5/35/23*
No. of exemplers at s > T			*29/06/00*	*23/08/03*	*22/07/01*	*21/14/01*	*26/17/9*	*24/07/06*
127.6808	1120.754	48.018	0.113924	0.014192	297.0408	282.8724	297.7039	3.51085
127.6998	941.454	46.293	0.135641	0.015243	297.391	279.9231	299.4552	3.609103
164.4728	1299.215	49.121	0.126594	0.014565	297.1648	280.2445	296.3242	3.526484
177.8544	1462.234	50.612	0.121632	0.014633	296.2738	281.0029	296.4384	3.574079
179.8919	1572.083	50.68	0.114429	0.013652	296.8607	282.3321	296.8036	3.556072
188.0673	1671.397	51.835	0.112521	0.013509	296.813	282.1891	296.5651	3.551302
197.9313	1775.678	52.519	0.111468	0.01343	296.7867	282.1101	296.4335	3.548669
186.471	1677.788	52.732	0.111141	0.013406	296.7785	282.0856	296.3927	3.547853
187.1142	1613.137	52.761	0.115994	0.012829	296.5862	281.5086	295.4311	3.520762
199.2449	1794.676	52.812	0.11102	0.013396	296.7755	282.0765	296.3775	3.547549
203.3035	1834.075	52.923	0.110848	0.013384	296.7712	282.0636	296.356	3.54712
193.7863	1848.859	53.308	0.104814	0.01377	296.8999	282.4496	296.9993	3.532034
206.1305	1869.885	53.324	0.110237	0.013338	296.7559	282.0178	296.2796	3.545592
214.4997	1954.261	53.42	0.10976	0.013302	296.744	281.982	296.22	3.5344
214.1798	1945.992	53.439	0.110062	0.013325	296.7516	282.0047	296.2578	3.545156
226.7462	1923.273	53.539	0.117896	0.011891	296.2738	281.2943	296.8689	3.509224
216.0543	1968.138	53.628	0.109776	0.013303	296.7444	281.9832	296.2221	3.544441
227.206	2069.045	53.64	0.109812	0.013306	296.7453	281.9859	296.2265	3.544531
219.0029	2000.063	53.811	0.109498	0.013282	296.7375	281.9624	296.1873	3.543745
226.3873	2004.705	53.878	0.112928	0.012972	296.8999	281.6522	295.6704	3.552321
214.0622	1956.836	53.881	0.109392	0.013274	296.7348	281.9544	296.174	3.543479
228.2201	2040.649	53.936	0.111837	0.012817	296.5824	281.295	295.4121	3.481295
218.3312	2054.476	54.089	0.106271	0.01373	296.4644	282.0493	296.9335	3.535676
207.0407	1952.054	54.099	0.106063	0.011992	296.5893	283.3131	294.0372	3.535157
229.0157	2100.214	54.111	0.109044	0.013248	296.7261	281.9283	296.1305	3.542611
257.2789	2231.503	54.552	0.115294	0.012451	296.4603	281.5558	294.8016	3.558235
223.2197	2069.57	54.899	0.107858	0.013159	296.6965	281.8394	295.9823	3.539645
243.2242	2260.973	55.088	0.107575	0.013138	296.6894	281.8181	295.9468	3.538936
265.6279	2300.446	55.41	0.115468	0.012247	296.6267	281.295	294.4612	3.558669
252.8847	2553.024	55.682	0.099053	0.013369	296.7664	282.3875	296.3322	3.486554
261.0501	2450.599	55.792	0.106525	0.013059	296.6631	281.7394	295.8157	3.536314
268.9202	2538.731	56.194	0.105927	0.013015	296.6482	281.6946	295.7409	3.534818
234.2066	2348.313	56.672	0.099734	0.01354	296.1861	282.2196	296.616	3.519336
281.9091	2685.974	56.852	0.104956	0.012942	296.6239	281.6217	295.6195	3.53239
284.254	2728.751	56.884	0.10417	0.013025	296.4085	281.7047	295.7579	3.530425
285.1842	2723.458	57.017	0.104714	0.012924	296.6178	281.6035	295.5892	3.531785
285.293	2724.705	57.022	0.104706	0.012923	296.6177	281.603	295.5883	3.531766
299.6767	2862.816	57.041	0.104679	0.012921	296.617	281.6009	295.5848	3.531696
283.7737	2728.934	57.111	0.103987	0.01295	296.6267	281.6325	295.6334	3.528241
320.16	2760.143	57.114	0.115994	0.011924	296.2847	280.808	293.9235	3.559985
323.2324	3377.912	57.257	0.09569	0.013755	296.1948	282.435	296.975	3.509224
327.0485	3112.761	57.847	0.105067	0.012637	296.5223	281.4033	295.1116	3.528926
294.0781	2839.414	58.153	0.10357	0.012778	296.5692	281.4576	295.346	3.532667
308.2981	2979.215	58.91	0.103483	0.012593	296.5076	281.2729	295.0381	3.528707
272.9374	3108.981	58.914	0.08779	0.012876	296.6019	283.3131	297.5097	3.509475
317.2075	3116.691	59.043	0.101777	0.012703	296.5444	281.3833	295.2221	3.524442
324.6515	3206.181	59.161	0.101258	0.012664	296.5314	281.3443	295.1572	3.523145
327.9793	3230.05	59.213	0.10154	0.012685	296.5385	281.3655	295.1925	3.523849
326.0613	3185.904	59.248	0.102345	0.01255	296.5459	281.2301	294.9668	3.525862
289.7202	3202.744	59.37	0.09046	0.013617	296.849	282.2969	296.7448	3.49615
332.5391	3248.721	59.372	0.10236	0.012673	296.5344	281.0033	296.1721	3.516032
373.4535	3276.425	59.57	0.113982	0.01257	296.5893	279.75	293.5787	3.54985
381.5159	3712.4	59.8	0.102768	0.012128	296.8481	281.317	294.2633	3.526921
343.5613	3412.205	59.851	0.100686	0.012621	296.5171	281.3014	295.0857	3.521715
346.5402	3447.818	59.987	0.10051	0.012608	296.5128	281.2883	295.0638	3.521275
394.3689	3817.816	60.052	0.103297	0.011482	296.4763	281.5558	293.1869	3.528241
353.8733	3535.798	60.317	0.100083	0.012576	296.5021	281.2562	295.0103	3.520207
355.3074	3553.074	60.384	0.1	0.01257	296.5	281.25	295	3.52
320.472	3506.719	60.746	0.091388	0.012723	296.1105	282.2969	295.2554	3.498471
317.0086	3215.848	61.547	0.098577	0.01304	296.6568	280.575	295.5838	3.497379
432.2246	4263.537	61.571	0.101377	0.0117	296.2101	280.6723	295.5507	3.481048
389.5058	3971.591	61.868	0.098073	0.012425	296.4518	281.1055	294.7591	3.515182
381.1819	3956.632	61.922	0.09634	0.012323	296.4176	281.6522	296.5881	3.554811
397.3161	4037.232	61.958	0.098413	0.012746	296.5344	280.808	295.2931	3.516032
360.4675	4113.517	62.075	0.08763	0.012728	296.5859	282.3878	294.2296	3.491014

APPENDIX D: Listing of the MATLAB program for LQG/LTR design

```
% System Dynamics

clear all
% The four transfer function between inputs and outputs
% Dead time has been approximated through 2nd order Pade
%
[num1,den1]=pade(30,2);
[num2,den2]=pade(60,2);
N1=0.66/70;
D1=[1 1/70];
N2=(-0.25/100)*num1;
D2=conv([1 1/100],den1);
N21=(1/D2(:,1))*N2;
D21=(1/D2(:,1))*D2;
N3=-5/230;
D3=[1 1/230];

N4=(11.1/168)*num2;
D4=conv([1 1/168],den2);
N41=(1/D4(:,1))*N4;
D41=(1/D4(:,1))*D4;
 roots(D1)
 roots(D2)
 roots(D21)
 roots(D3)
 roots(D4)
 roots(D41)
 printsys(N1,D1,'s')
 printsys(N2,D2,'s')
 printsys(N21,D21,'s')
 printsys(N3,D3,'s')
 printsys(N4,D4,'s')
 printsys(N41,D41,'s')
%
% Convolution of the system to put it under common denomentors
%
 com_den=conv(D41,conv(D3,conv(D1,D21)));
 com_num1=conv(N1,conv(D21,conv(D3,D41)));
 com_num2=conv(N21,conv(D1,conv(D3,D41)));
 com_num3=conv(N3,conv(D1,conv(D21,D41)));
 com_num4=conv(N41,conv(D1,conv(D21,D3)));


% State-space realisation of transfer function matrix

A0=[0 1 0 0 0 0 0 0;
   0 0 1 0 0 0 0 0;
   0 0 0 1 0 0 0 0;
   0 0 0 0 1 0 0 0;
   0 0 0 0 0 1 0 0;
   0 0 0 0 0 0 1 0;
   0 0 0 0 0 0 0 1;
   -com_den(:,9)   -com_den(:,8) -com_den(:,7) -com_den(:,6) -com_den(:,5) -com_den(:,4) -com_den(:,3) -
com_den(:,2)];


A=[A0 zeros(size(A0));
  zeros(size(A0)) A0];
```

```
eigx(A);



B0=[zeros(7,1);1];
B=[B0 zeros(size(B0));
  zeros(size(B0)) B0];

c11=[com_num1(1,8)  com_num1(1,7) com_num1(1,6) com_num1(1,5)  com_num1(1,4)  com_num1(1,3)
com_num1(1,2) com_num1(1,1)];
c21=[com_num3(1,8)  com_num3(1,7) com_num3(1,6) com_num3(1,5)  com_num3(1,4)  com_num3(1,3)
com_num3(1,2) com_num3(1,1)];
c12=[com_num2(1,8)  com_num2(1,7) com_num2(1,6) com_num2(1,5)  com_num2(1,4)  com_num2(1,3)
com_num2(1,2) com_num2(1,1)];
c22=[com_num4(1,8)  com_num4(1,7) com_num4(1,6) com_num4(1,5)  com_num4(1,4)  com_num4(1,3)
com_num4(1,2) com_num4(1,1)];

C=[c11 c12;
  c21 c22];
D=zeros(2,2);

ccc=ctrb(A,B);
rank (ccc);
rank (A);
ooo=obsv(A,C);
rank (ooo)
gama=zeros(16,2);
omega=-eye(2);

% Dist. Dynamics
n_dist1=0.05/120;
d_dist1=[1 1/120];
n_dist2=-2/140;
d_dist2=[1 1/140];

% state-space realisation of the individual disturbance models

[Ad1,Bd1,Cd1,Dd1]=tf2ss(n_dist1,d_dist1);
[Ad2,Bd2,Cd2,Dd2]=tf2ss(n_dist2,d_dist2);

% Augmentation of the disturbance models

Ad=[Ad1, 0;
    0,Ad2];
Bd=[Bd1, 0;
    0,Bd2];
Cd=[Cd1, 0;
    0,Cd2];
Dd=[Dd1, 0;
    0,Dd2];

% Act. Dynamics

n_act1=1/25;
d_act1=[1 1/25];
n_act2=1/5;
d_act2=[1 1/5];

% State space relaisation of the actuator models

[Act1,Bct1,Cct1,Dct1]=tf2ss(n_act1,d_act1);
[Act2,Bct2,Cct2,Dct2]=tf2ss(n_act2,d_act2);
Act=[Act1, 0;
    0,Act2];
```

```
Bct=[Bct1, 0;
    0,Bct2];
Cct=[Cct1, 0;
    0,Cct2];
Dct=[Dct1, 0;
    0,Dct2];


% Creating Synthesis (Augmented) model of chemical process
% The whole C matrix appears in the last row becasue integral states depend on the states

Aaug=[A B*Cct gama*Cd zeros(16,2);
    zeros(2,16) Act zeros(2,4);
    zeros(2,18) Ad zeros(2,2);
    C zeros(2,6)];

% Open loop analysis of augmented sysytem

eigx(Aaug);

Baug=[zeros(16,2);Bct;zeros(4,2)];
gamaug=[zeros(18,4);Bd zeros(2,2);zeros(2,2) [-1 0;0 -1]];

% Outputs:{temp(K),conductivity(mS),delta_TJ(k),RR(%),dist_T(k)
% dist_cond(mS),x1,x2,x3,x4,x5,x6,x7,x8,x9,x10,x11,x12,x13,x14,x15,x16
% int_T,int_cond}

Caug=[C D*Cct omega(:,1)*Cd(1,1) omega(:,2)*Cd(2,2) zeros(2,2);
    zeros(1,16) 1/3 zeros(1,5);
    zeros(1,17) 1/3 zeros(1,4);
    zeros(2,18) Cd zeros(2,2);
    eye(18) zeros(18,4);
    zeros(2,20) eye(2)];

Daug=zeros(26,2);
omegaug=zeros(26,4);

% Regulator Design
% Creating target zeros using shaping filter on T-Tcmd and C-Ccmd to shape the close loop
% i.e. to have closed loop eigen-values at the desired location

zeta=1; omega1=0.02;
ktdot=1.0;kt=2.0*omega1*zeta;kintt=omega1*omega1;
ccrit1=[ktdot,kt,kintt]*[Caug(1,:);Caug(1,:);Caug(25,:)];
dcrit1=[ktdot,kt,kintt]*[Baug(1,:);Daug(1,:);Daug(25,:)];

zeta=1;omega1=0.02;
kcdot=1.0;kc=2.0*omega1*zeta;kintc=omega1*omega1;
ccrit2=[kcdot,kc,kintc]*[Caug(2,:);Caug(2,:);Caug(26,:)];
dcrit2=[kcdot,kc,kintc]*[Baug(2,:);Daug(2,:);Daug(26,:)];
ccrit3=Caug(4,:);dcrit3=Daug(4,:);

ccrit=[ccrit1;ccrit2;ccrit3];dcrit=[dcrit1;dcrit2;dcrit3];

% Weighting matrcies of the objective function

Q=[10000000000  0  0;
  0 10000000  0
  0  0  0] ;

R=[1000  0;
    0 10000];

% Optimal gain matrix (solvig steady-state Riccati equation)
```

```
g=lqrcross((Aaug+0.0045*eye(size(Aaug))),Baug,ccrit,dcrit,Q,R);


% Closed-loop analysis

eigx(Aaug-Baug*g)
Acl=Aaug-Baug*g;

% RMS responses to white noise disturbance

X_open=lyap(Aaug,gamaug(:,1:2)*[1,0;0,1]*gamaug(:,1:2)');
Y_open=Caug*X_open*Caug';
sigY_open=sqrt(diag(Y_open))'
X=lyap(Acl,gamaug(:,1:2)*[1,0;0,1]*gamaug(:,1:2)');
Y=Caug*X*Caug';
sigY=sqrt(diag(Y))'



% Frequency responses of close loop transfer function from T to Tcmd and
% C to Ccmd

figure(1)
bode(Acl,gamaug(:,3),Caug(1,:),0)
subplot(2,1,1),title('T / Tcmd')

figure(2)
bode(Acl,gamaug(:,4),Caug(2,:),0)
subplot(2,1,1),title('C / Ccmd')


%Step command responses (Close loop)

t=0:1:1000;
Tcmd=0.5*(1-exp(-0.05*t));
[y,x]=lsim(Acl,gamaug(:,3),-Caug(1,:),0,Tcmd,t);
figure(3)
subplot(2,1,1),plot(t,y,'-');%axis([0,100,0,1500])
title('Temperature Command responses: 1 deg')
ylabel('Temperature (deg)'),xlabel('Time (sec)');
hold on
subplot(2,1,1),plot(t,Tcmd,'g.');%axis([0,100,0,1500]);
hold off
[y,x]=lsim(Acl,gamaug(:,3),Caug(2,:),0,Tcmd,t);
subplot(2,1,2),plot(t,y,'-'),ylabel('Conductivity (mS)'),xlabel('Time (sec)')

[y,x]=lsim(Acl,gamaug(:,3),Caug(3,:),0,Tcmd,t);
figure(4)
subplot(2,1,1),plot(t,y,'-');%axis([0,100,0,1500])
title('Temperature Command responses: 1 deg')
ylabel('delta_Temp (deg)'),xlabel('Time (sec)');subplot(2,1,1),plot(t,Tcmd,'g.');%axis([0,100,0,1500]);
hold off
[y,x]=lsim(Acl,gamaug(:,3),Caug(4,:),0,Tcmd,t);
subplot(2,1,2),plot(t,y,'-'),ylabel('RR (%)'),xlabel('Time (sec)')


Ccmd=4.0*(1-exp(-0.05*t));
[y,x]=lsim(Acl,gamaug(:,4),-Caug(1,:),0,Ccmd,t);
figure(5)
subplot(2,1,1),plot(t,y,'-');%axis([0,100,0,1500])

title('Temperature Command responses: 1 deg')
```

```
ylabel('Temperature (deg)'),xlabel('Time (sec)');

[y,x]=lsim(Acl,gamaug(:,4),Caug(2,:),0,Ccmd,t);
subplot(2,1,2),plot(t,y,'-'),ylabel('Conductivity (mS)'),xlabel('Time (sec)')
hold on
subplot(2,1,2),plot(t,Ccmd,'g.');
hold off
[y,x]=lsim(Acl,gamaug(:,4),Caug(3,:),0,Ccmd,t);
figure(6)
subplot(2,1,1),plot(t,y,'-');%axis([0,100,0,1500])
title('Temperature Command responses: 1 deg')
ylabel('delta_Temp (deg)'),xlabel('Time (sec)');subplot(2,1,1),plot(t,Tcmd,'g.');%axis([0,100,0,1500]);

[y,x]=lsim(Acl,gamaug(:,4),Caug(4,:),0,Ccmd,t);
subplot(2,1,2),plot(t,y,'-'),ylabel('RR (%)'),xlabel('Time (sec)')



% Single loop robustness Analysis

% Delta TJ loop
aloop=Aaug-Baug*[0,0;0,1]*g;
bloop=Baug(:,1);
cloop=g(1,:);
dloop=0;
figure(7)
pbode(aloop,bloop,cloop,dloop,1,1,.01,100)
subplot(2,1,1),title('')

% Delta RR loop
aloop=Aaug-Baug*[1,0;0,0]*g;
bloop=Baug(:,2);
cloop=g(2,:);
dloop=0;
figure(8)
pbode(aloop,bloop,cloop,dloop,1,1,.01,100)
subplot(2,1,1),title('')



% Estimater design

Aest=Aaug(1:20,1:20);
Best=Baug(1:20,:);
Gest=gamaug(1:20,1:2);
%Sensors:{T,C}
Cest=[C D*Cct omega(:,1)*Cd(1,1) omega(:,2)*Cd(2,2)];

Dest=zeros(2,2);
Gest1=[Best,Gest];

% Process noise and sensor noise covariance matrices
Wo=eye(2);
Vo=0.1*diag([sigY(1,1),sigY(1,2)]);

% Optimal estimator gain matrix (Solving Steady-state Riccati equation)

k=lqrcross(Aest',Cest',Gest',Dest,Wo,Vo);k=k';

% Estimator eigen-values

eigx(Aest-k*Cest)


%Controller formulation
```

```
gest=g(:,1:20);
gi=g(:,21:22);
Acont=[Aest-Best*gest-k*Cest,-Best*gi;
      zeros(2,22)];

Bcont=[k;[1,0;0,1]];
% Bccont is B command of the controller

Bccont=[zeros(20,2);-eye(2)];
Ccont=-g;
Dcont=zeros(2,2);

%Closed-loop analysis with optimal estimator

ACL=[Aest,Best*Ccont;Bcont*Cest,Acont];

eigx(ACL)
BCL=[zeros(40,2);[-1,0;0,-1]];
CCL=[Caug(:,1:20),zeros(26,22)];
CCL(1,41)=1.0;CCL(2,42)=1.0;
GCL=[Gest;zeros(22,2)];
XCL=lyap(ACL,GCL*GCL');
YCL=CCL*XCL*CCL';
sigYCL=sqrt(diag(YCL));sigYCL=sigYCL'

% Single loop robustness analysis with estimator
% Break one loop at a time at the input. Tfr. func. with input=input and
%output=controller output

%Delta TJ control Loop
aloop1=[Aest,Best*[0,0;0,1]*Ccont;Bcont*Cest,Acont];
bloop1=[Best(:,1);zeros(22,1)];
cloop1=[zeros(1,20),Ccont(1,:)];
dloop1=0;
figure(9)
pbode(aloop1,bloop1,cloop1,dloop1,1,1,.01,100)



%Delta RR control Loop
aloop2=[Aest,Best*[1,0;0,0]*Ccont;Bcont*Cest,Acont];
bloop2=[Best(:,2);zeros(22,1)];
cloop2=[zeros(1,20),Ccont(2,:)];
dloop2=0;
figure(10)
pbode(aloop2,bloop2,cloop2,dloop2,1,1,.01,100)



%
%Loop Transfer Recovery

Gest2=[Gest1];
Wox=diag([1.0,1,10.0,10.0]);
Vox=Vo;
Destx=zeros(4,2);
kx=lqrcross(Aest',Cest',Gest2',Destx,Wox,Vox);kx=kx';
eigx(Aest-kx*Cest)

%Controller formulation
gestx=g(:,1:20);
gix=g(:,21:22);
Acontx=[Aest-Best*gestx-kx*Cest,-Best*gix;
      zeros(2,22)];
```

```
Bcontx=[kx;[1,0;0,1]];
Bccontx=[zeros(20,2);-eye(2)];
Dcontxx=zeros(2,4);
Bcontxx=[Bcontx,Bccontx];

Ccontx=-g;
Dcontx=zeros(2,2);

%Closed Loop analysis
ACLx=[Aest,Best*Ccontx;Bcontx*Cest,Acontx];

eigx(ACLx);
BCLx=[zeros(40,2);[-1,0;0,-1]];
CCLx=[Caug(:,1:20),zeros(26,22)];
CCLx(1,41)=1.0;CCLx(2,42)=1.0;
GCLx=[Gest;zeros(22,2)];
XCLx=lyap(ACLx,GCLx*GCLx');
YCLx=CCLx*XCLx*CCLx';
sigYCLx=sqrt(diag(YCLx));sigYCLx=sigYCLx'

%Delta TJ Loop
aloop1x=[Aest,Best*[0,0;0,1]*Ccontx;Bcontx*Cest,Acontx];
bloop1x=[Best(:,1);zeros(22,1)];
cloop1x=[zeros(1,20),Ccontx(1,:)];
dloop1x=0;
figure(11)
pbode(aloop1x,bloop1x,cloop1x,dloop1x,1,1,.01,100)

%Delta RR Loop
aloop2x=[Aest,Best*[1,0;0,0]*Ccontx;Bcontx*Cest,Acontx];
bloop2x=[Best(:,2);zeros(22,1)];
cloop2x=[zeros(1,20),Ccontx(2,:)];
dloop2x=0;
figure(12)
pbode(aloop2x,bloop2x,cloop2x,dloop2x,1,1,.01,100)


%Step command responses (open loop)

t=0:1:1000;
Tcmd=0.5*(1-exp(-0.05*t));
[y,x]=lsim(Aaug,Baug(:,1),Caug(1,:),0,Tcmd,t);
figure(13)
subplot(2,1,1),plot(t,y,'-');%axis([0,100,0,1500])
title('Temperature Command responses: 1 deg')
ylabel('Temperature (deg)'),xlabel('Time (sec)');
hold on
subplot(2,1,1),plot(t,Tcmd,'g.');%axis([0,100,0,1500]);
hold off
[y,x]=lsim(Aaug,Baug(:,1),Caug(2,:),0,Tcmd,t);
subplot(2,1,2),plot(t,y,'-'),ylabel('Conductivity (mS)'),xlabel('Time (sec)')
Ccmd=4.0*(1-exp(-0.05*t));
[y,x]=lsim(Aaug,Baug(:,2),Caug(1,:),0,Ccmd,t);
figure(14)
subplot(2,1,1),plot(t,y,'-');%axis([0,100,0,1500])

title('Temperature Command responses: 1 deg')
ylabel('Temperature (deg)'),xlabel('Time (sec)');

[y,x]=lsim(Aaug,Baug(:,2),Caug(2,:),0,Ccmd,t);
subplot(2,1,2),plot(t,y,'-'),ylabel('Conductivity (mS)'),xlabel('Time (sec)')
hold on
subplot(2,1,2),plot(t,Ccmd,'g.');
hold off
```

APPENDIX E: Listing of the run file of the MATLAB program

```
% This the run file from the matlab control program, these comments have been added after the
% execution
ans =

  -0.0143


ans =

  -0.1000 + 0.0577i
  -0.1000 - 0.0577i
  -0.0100


ans =

  -0.1000 + 0.0577i
  -0.1000 - 0.0577i
  -0.0100


ans =

   -0.0043


ans =

  -0.0500 + 0.0289i
  -0.0500 - 0.0289i
  -0.0060


ans =

  -0.0500 + 0.0289i
  -0.0500 - 0.0289i
  -0.0060

 % Please refer to chapter six to find what the number of TRF means in the real process
 % The first transfer function
num/den =

     0.009429
   -----------
   s + 0.01429
num/den =

       0.002451 s^2 - 0.0004902 s + 3.268e-05
   ----------------------------------------------
   -0.9805 s^3 - 0.2059 s^2 - 0.01503 s - 0.0001307
% The second transfer function

num/den =

     -0.0025 s^2 + 0.0005 s - 3.333e-05
   ---------------------------------------
   s^3 + 0.21 s^2 + 0.01533 s + 0.0001333
% Third TFR function
num/den =
```

```
    -0.02174
  -----------
  s + 0.004348
% Fourth TFR function

num/den =

       -0.06574 s^2 + 0.006574 s - 0.0002191
  ----------------------------------------------
  -0.995 s^3 - 0.1054 s^2 - 0.003909 s - 1.974e-05

num/den =

    0.06607 s^2 - 0.006607 s + 0.0002202
  ----------------------------------------
  s^3 + 0.106 s^2 + 0.003929 s + 1.984e-05

% open loop eigen-values of the system
      Eigenvalues          Damping   Frequency(rad/sec)
-4.34783e-03  0.00000e+00i    1.000    4.34783e-03
-4.34783e-03  0.00000e+00i    1.000    4.34783e-03
-5.95238e-03  0.00000e+00i    1.000    5.95238e-03
-5.95238e-03  0.00000e+00i    1.000    5.95238e-03
-1.00000e-02  0.00000e+00i    1.000    1.00000e-02
-1.00000e-02  0.00000e+00i    1.000    1.00000e-02
-1.42857e-02  0.00000e+00i    1.000    1.42857e-02
-1.42857e-02  0.00000e+00i    1.000    1.42857e-02
-5.00000e-02  2.88675e-02i    0.866    5.77350e-02
-5.00000e-02 -2.88675e-02i    0.866    5.77350e-02
-5.00000e-02  2.88675e-02i    0.866    5.77350e-02
-5.00000e-02 -2.88675e-02i    0.866    5.77350e-02
-1.00000e-01  5.77350e-02i    0.866    1.15470e-01
-1.00000e-01 -5.77350e-02i    0.866    1.15470e-01
-1.00000e-01  5.77350e-02i    0.866    1.15470e-01
-1.00000e-01 -5.77350e-02i    0.866    1.15470e-01

% Rank of controllability matrix
ans
16
% Rank of the A matrix
ans
16
% Rank of the observability matrix
ans
8

% Eigen-values of the augmented system
      Eigenvalues          Damping   Frequency(rad/sec)
 0.00000e+00  0.00000e+00i    1.000    0.00000e+00
 0.00000e+00  0.00000e+00i    1.000    0.00000e+00
-4.34783e-03  0.00000e+00i    1.000    4.34783e-03
-4.34783e-03  0.00000e+00i    1.000    4.34783e-03
-5.95238e-03  0.00000e+00i    1.000    5.95238e-03
-5.95238e-03  0.00000e+00i    1.000    5.95238e-03
-7.14286e-03  0.00000e+00i    1.000    7.14286e-03
-8.33333e-03  0.00000e+00i    1.000    8.33333e-03
-1.00000e-02  0.00000e+00i    1.000    1.00000e-02
-1.00000e-02  0.00000e+00i    1.000    1.00000e-02
-1.42857e-02  0.00000e+00i    1.000    1.42857e-02
-1.42857e-02  0.00000e+00i    1.000    1.42857e-02
-4.00000e-02  0.00000e+00i    1.000    4.00000e-02
-5.00000e-02  2.88675e-02i    0.866    5.77350e-02
-5.00000e-02 -2.88675e-02i    0.866    5.77350e-02
-5.00000e-02  2.88675e-02i    0.866    5.77350e-02
-5.00000e-02 -2.88675e-02i    0.866    5.77350e-02
```

```
-1.00000e-01  5.77350e-02i     0.866     1.15470e-01
-1.00000e-01 -5.77350e-02i     0.866     1.15470e-01
-1.00000e-01  5.77350e-02i     0.866     1.15470e-01
-1.00000e-01 -5.77350e-02i     0.866     1.15470e-01
-2.00000e-01  0.00000e+00i      1.000     2.00000e-01

% Eigen-values of the closed loop system with LQR design
 -4.65217e-03  0.00000e+00i     1.000     4.65217e-03
 -4.89872e-03  0.00000e+00i     1.000     4.89872e-03
 -5.95238e-03  0.00000e+00i     1.000     5.95238e-03
 -7.14286e-03  0.00000e+00i     1.000     7.14286e-03
 -8.33333e-03  0.00000e+00i     1.000     8.33333e-03
 -8.61538e-03  0.00000e+00i     1.000     8.61538e-03
 -8.61538e-03  0.00000e+00i     1.000     8.61538e-03
 -9.79394e-03  0.00000e+00i     1.000     9.79394e-03
 -1.00000e-02  0.00000e+00i     1.000     1.00000e-02
 -1.42857e-02  0.00000e+00i     1.000     1.42857e-02
 -5.00000e-02  2.88675e-02i     0.866     5.77350e-02
 -5.00000e-02 -2.88675e-02i     0.866     5.77350e-02
 -5.75124e-02  2.46042e-02i     0.919     6.25543e-02
 -5.75124e-02 -2.46042e-02i     0.919     6.25543e-02
 -1.00000e-01  5.77350e-02i     0.866     1.15470e-01
 -1.00000e-01 -5.77350e-02i     0.866     1.15470e-01
 -1.08034e-01  5.57743e-02i     0.889     1.21581e-01
 -1.08034e-01 -5.57743e-02i     0.889     1.21581e-01
 -4.35753e-01  4.15894e-01i     0.723     6.02370e-01
 -4.35753e-01 -4.15894e-01i     0.723     6.02370e-01
 -8.33329e-01  8.26417e-01i     0.710     1.17363e+00
 -8.33329e-01 -8.26417e-01i     0.710     1.17363e+00
ans =
 -8.3333e-01+  8.2642e-01i
 -8.3333e-01-  8.2642e-01i
 -4.3575e-01+  4.1589e-01i
 -4.3575e-01-  4.1589e-01i
 -1.0803e-01+  5.5774e-02i
 -1.0803e-01-  5.5774e-02i
 -1.0000e-01+  5.7735e-02i
 -1.0000e-01-  5.7735e-02i
 -5.7512e-02+  2.4604e-02i
 -5.7512e-02-  2.4604e-02i
 -5.0000e-02+  2.8868e-02i
 -5.0000e-02-  2.8868e-02i
 -1.4286e-02
 -4.6522e-03
 -4.8987e-03
 -5.9524e-03
 -9.7939e-03
 -1.0000e-02
 -8.6154e-03
 -8.6154e-03
 -8.3333e-03
 -7.1429e-03
% The open loop covariance of process outputs to moderate disturbances

sigY_open =
  Columns 1 through 6
   3.2275e-03   1.1952e-01            0            0   3.2275e-03   1
.1952e-01
  Columns 7 through 12
         0            0            0            0            0
      0
  Columns 13 through 18
         0            0            0            0            0
      0
  Columns 19 through 24
         0            0            0            0            0
```

```
     0
 Columns 25 through 26
         0         0

% close loop covariance of process outputs to moderate disturbances
sigY =
 Columns 1 through 6
  3.2716e-03   1.2421e-01   3.2898e-02   2.7636e-02   3.2275e-03   1
.1952e-01
 Columns 7 through 12
  4.1196e+08   2.5212e+06   2.5706e+04   4.5535e+02   1.5139e+01   8
.9308e-01
 Columns 13 through 18
  8.3511e-02   1.2211e-02   1.5898e+09   9.8043e+06   1.0170e+05   1
.7754e+03
 Columns 19 through 24
  5.4541e+01   2.9389e+00   2.7005e-01   4.4231e-02   9.8694e-02   8
.2908e-02
 Columns 25 through 26
  1.3355e-02   1.2654e+00

% Eigen values of the system with the estimator

      Eigenvalues          Damping   Frequency(rad/sec)
-4.34783e-03  0.00000e+00i     1.000    4.34783e-03
-4.34783e-03  0.00000e+00i     1.000    4.34783e-03
-5.95238e-03  0.00000e+00i     1.000    5.95238e-03
-5.95238e-03  0.00000e+00i     1.000    5.95238e-03
-1.00000e-02  0.00000e+00i     1.000    1.00000e-02
-1.00000e-02  0.00000e+00i     1.000    1.00000e-02
-1.42857e-02  0.00000e+00i     1.000    1.42857e-02
-1.42857e-02  0.00000e+00i     1.000    1.42857e-02
-2.44971e-02  0.00000e+00i     1.000    2.44971e-02
-4.00000e-02  0.00000e+00i     1.000    4.00000e-02
-5.00000e-02  2.88675e-02i     0.866    5.77350e-02
-5.00000e-02 -2.88675e-02i     0.866    5.77350e-02
-5.00000e-02  2.88675e-02i     0.866    5.77350e-02
-5.00000e-02 -2.88675e-02i     0.866    5.77350e-02
-1.00000e-01  5.77350e-02i     0.866    1.15470e-01
-1.00000e-01 -5.77350e-02i     0.866    1.15470e-01
-1.00000e-01  5.77350e-02i     0.866    1.15470e-01
-1.00000e-01 -5.77350e-02i     0.866    1.15470e-01
-1.28382e-01  0.00000e+00i     1.000    1.28382e-01
-2.00000e-01  0.00000e+00i     1.000    2.00000e-01
ans =
 -1.2838e-01
 -2.4497e-02
 -1.0000e-01+  5.7735e-02i
 -1.0000e-01-  5.7735e-02i
 -1.0000e-01+  5.7735e-02i
 -1.0000e-01-  5.7735e-02i
 -5.0000e-02+  2.8868e-02i
 -5.0000e-02-  2.8868e-02i
 -5.0000e-02+  2.8868e-02i
 -5.0000e-02-  2.8868e-02i
 -1.4286e-02
 -1.0000e-02
 -1.4286e-02
 -1.0000e-02
 -5.9524e-03
 -5.9524e-03
 -4.3478e-03
 -4.3478e-03
 -4.0000e-02
 -2.0000e-01
% Closed loop eigen-values with the estimator
```

Eigenvalues		Damping	Frequency(rad/sec)
-4.34783e-03	0.00000e+00i	1.000	4.34783e-03
-4.34783e-03	0.00000e+00i	1.000	4.34783e-03
-4.65217e-03	0.00000e+00i	1.000	4.65217e-03
-4.89872e-03	0.00000e+00i	1.000	4.89872e-03
-5.95238e-03	1.96776e-07i	1.000	5.95238e-03
-5.95238e-03	-1.96776e-07i	1.000	5.95238e-03
-5.95238e-03	0.00000e+00i	1.000	5.95238e-03
-7.14286e-03	0.00000e+00i	1.000	7.14286e-03
-8.33333e-03	0.00000e+00i	1.000	8.33333e-03
-8.61538e-03	0.00000e+00i	1.000	8.61538e-03
-8.61538e-03	0.00000e+00i	1.000	8.61538e-03
-9.79394e-03	0.00000e+00i	1.000	9.79394e-03
-9.99957e-03	0.00000e+00i	1.000	9.99957e-03
-1.00000e-02	0.00000e+00i	1.000	1.00000e-02
-1.00004e-02	0.00000e+00i	1.000	1.00004e-02
-1.42855e-02	0.00000e+00i	1.000	1.42855e-02
-1.42857e-02	0.00000e+00i	1.000	1.42857e-02
-1.42859e-02	0.00000e+00i	1.000	1.42859e-02
-2.44971e-02	0.00000e+00i	1.000	2.44971e-02
-4.00000e-02	0.00000e+00i	1.000	4.00000e-02
-5.00000e-02	2.88674e-02i	0.866	5.77350e-02
-5.00000e-02	-2.88674e-02i	0.866	5.77350e-02
-5.00000e-02	2.88675e-02i	0.866	5.77350e-02
-5.00000e-02	-2.88675e-02i	0.866	5.77350e-02
-5.00000e-02	2.88676e-02i	0.866	5.77351e-02
-5.00000e-02	-2.88676e-02i	0.866	5.77351e-02
-5.75124e-02	2.46042e-02i	0.919	6.25543e-02
-5.75124e-02	-2.46042e-02i	0.919	6.25543e-02
-1.00000e-01	5.77351e-02i	0.866	1.15470e-01
-1.00000e-01	-5.77351e-02i	0.866	1.15470e-01
-1.00000e-01	5.77350e-02i	0.866	1.15470e-01
-1.00000e-01	-5.77350e-02i	0.866	1.15470e-01
-1.00000e-01	5.77350e-02i	0.866	1.15470e-01
-1.00000e-01	-5.77350e-02i	0.866	1.15470e-01
-1.08034e-01	5.57743e-02i	0.889	1.21581e-01
-1.08034e-01	-5.57743e-02i	0.889	1.21581e-01
-1.28382e-01	0.00000e+00i	1.000	1.28382e-01
-2.00000e-01	0.00000e+00i	1.000	2.00000e-01
-4.35753e-01	4.15894e-01i	0.723	6.02370e-01
-4.35753e-01	-4.15894e-01i	0.723	6.02370e-01
-8.33329e-01	8.26417e-01i	0.710	1.17363e+00
-8.33329e-01	-8.26417e-01i	0.710	1.17363e+00

ans =

-8.3333e-01+ 8.2642e-01i
-8.3333e-01- 8.2642e-01i
-4.3575e-01+ 4.1589e-01i
-4.3575e-01- 4.1589e-01i
-2.0000e-01
-1.2838e-01
-1.0803e-01+ 5.5774e-02i
-1.0803e-01- 5.5774e-02i
-1.0000e-01+ 5.7735e-02i
-1.0000e-01- 5.7735e-02i
-1.0000e-01+ 5.7735e-02i
-1.0000e-01- 5.7735e-02i
-1.0000e-01+ 5.7735e-02i
-1.0000e-01- 5.7735e-02i
-5.7512e-02+ 2.4604e-02i
-5.7512e-02- 2.4604e-02i
-5.0000e-02+ 2.8868e-02i
-5.0000e-02- 2.8868e-02i
-5.0000e-02+ 2.8868e-02i
-5.0000e-02- 2.8868e-02i
-5.0000e-02+ 2.8867e-02i
-5.0000e-02- 2.8867e-02i

```
-2.4497e-02
-4.0000e-02
-1.4286e-02
-1.4285e-02
-1.4286e-02
-4.8987e-03
-4.6522e-03
-9.7939e-03
-1.0000e-02
-1.0000e-02
-9.9996e-03
-8.6154e-03
-4.3478e-03
-4.3478e-03
-8.6154e-03
-5.9524e-03
-5.9524e-03+  1.9678e-07i
-5.9524e-03-  1.9678e-07i
-8.3333e-03
-7.1429e-03

% Output co-variance with the LQG design
sigYCL =
  Columns 1 through 6
   2.2871e-01   1.6306e+01   6.2322e-02   2.6442e-02   3.2275e-03   1
.1952e-01
  Columns 7 through 12
   2.3520e+10   6.5009e+07   3.7214e+05   3.4812e+03   5.3111e+01   1
.3985e+00
  Columns 13 through 18
   6.7448e-02   6.0802e-03   4.2674e+10   1.2284e+08   7.5385e+05   7
.7749e+03
  Columns 19 through 24
   1.3422e+02   4.0203e+00   2.0649e-01   1.7561e-02   1.8697e-01   7
.9326e-02
  Columns 25 through 26
         0         0
Warning: Gain margin undefined; phase does not cross -180
Freq(Rad/Sec)   Gain Margin(dB)
Freq(Rad/Sec)   Phase Margin(Deg)
  0.01155        -259.6
ans =
     []
Freq(Rad/Sec)   Gain Margin(dB)
  0.07604         14.65
Freq(Rad/Sec)   Phase Margin(Deg)
ans =
   1.4652e+01

% Eigen-values with LTR
       Eigenvalues          Damping   Frequency(rad/sec)
-4.34783e-03  0.00000e+00i     1.000    4.34783e-03
-4.34783e-03  0.00000e+00i     1.000    4.34783e-03
-5.95238e-03  0.00000e+00i     1.000    5.95238e-03
-5.95238e-03  0.00000e+00i     1.000    5.95238e-03
-1.00000e-02  0.00000e+00i     1.000    1.00000e-02
-1.00000e-02  0.00000e+00i     1.000    1.00000e-02
-1.42857e-02  0.00000e+00i     1.000    1.42857e-02
-1.42857e-02  0.00000e+00i     1.000    1.42857e-02
-4.00000e-02  0.00000e+00i     1.000    4.00000e-02
-5.00000e-02  2.88675e-02i     0.866    5.77350e-02
-5.00000e-02 -2.88675e-02i     0.866    5.77350e-02
-5.00000e-02  2.88675e-02i     0.866    5.77350e-02
-5.00000e-02 -2.88675e-02i     0.866    5.77350e-02
-7.33216e-02  0.00000e+00i     1.000    7.33216e-02
-1.00000e-01  5.77350e-02i     0.866    1.15470e-01
```

```
-1.00000e-01 -5.77350e-02i     0.866    1.15470e-01
-1.00000e-01  5.77350e-02i     0.866    1.15470e-01
-1.00000e-01 -5.77350e-02i     0.866    1.15470e-01
-2.00000e-01  0.00000e+00i     1.000    2.00000e-01
-4.05414e-01  0.00000e+00i     1.000    4.05414e-01
ans =
 -4.0541e-01
 -1.0000e-01+  5.7735e-02i
 -1.0000e-01-  5.7735e-02i
 -1.0000e-01+  5.7735e-02i
 -1.0000e-01-  5.7735e-02i
 -7.3322e-02
 -5.0000e-02+  2.8868e-02i
 -5.0000e-02-  2.8868e-02i
 -5.0000e-02+  2.8868e-02i
 -5.0000e-02-  2.8868e-02i
 -1.4286e-02
 -1.4286e-02
 -5.9524e-03
 -5.9524e-03
 -1.0000e-02
 -4.3478e-03
 -1.0000e-02
 -4.3478e-03
 -4.0000e-02
 -2.0000e-01

% Closed loop eigen-vales with LQG/LTR
      Eigenvalues          Damping   Frequency(rad/sec)
-4.34783e-03  0.00000e+00i     1.000    4.34783e-03
-4.34783e-03  0.00000e+00i     1.000    4.34783e-03
-4.65217e-03  0.00000e+00i     1.000    4.65217e-03
-4.89872e-03  0.00000e+00i     1.000    4.89872e-03
-5.95238e-03  0.00000e+00i     1.000    5.95238e-03
-5.95238e-03  7.41146e-08i     1.000    5.95238e-03
-5.95238e-03 -7.41146e-08i     1.000    5.95238e-03
-7.14286e-03  0.00000e+00i     1.000    7.14286e-03
-8.33333e-03  0.00000e+00i     1.000    8.33333e-03
-8.61538e-03  0.00000e+00i     1.000    8.61538e-03
-8.61538e-03  0.00000e+00i     1.000    8.61538e-03
-9.79394e-03  0.00000e+00i     1.000    9.79394e-03
-9.99952e-03  0.00000e+00i     1.000    9.99952e-03
-1.00000e-02  0.00000e+00i     1.000    1.00000e-02
-1.00005e-02  0.00000e+00i     1.000    1.00005e-02
-1.42857e-02  0.00000e+00i     1.000    1.42857e-02
-1.42857e-02  4.80418e-07i     1.000    1.42857e-02
-1.42857e-02 -4.80418e-07i     1.000    1.42857e-02
-4.00000e-02  0.00000e+00i     1.000    4.00000e-02
-5.00000e-02  2.88675e-02i     0.866    5.77350e-02
-5.00000e-02 -2.88675e-02i     0.866    5.77350e-02
-5.00000e-02  2.88675e-02i     0.866    5.77350e-02
-5.00000e-02 -2.88675e-02i     0.866    5.77350e-02
-5.00000e-02  2.88676e-02i     0.866    5.77351e-02
-5.00000e-02 -2.88676e-02i     0.866    5.77351e-02
-5.75124e-02  2.46042e-02i     0.919    6.25543e-02
-5.75124e-02 -2.46042e-02i     0.919    6.25543e-02
-7.33216e-02  0.00000e+00i     1.000    7.33216e-02
-9.99999e-02  5.77351e-02i     0.866    1.15470e-01
-9.99999e-02 -5.77351e-02i     0.866    1.15470e-01
-1.00000e-01  5.77350e-02i     0.866    1.15470e-01
-1.00000e-01 -5.77350e-02i     0.866    1.15470e-01
-1.00000e-01  5.77349e-02i     0.866    1.15470e-01
-1.00000e-01 -5.77349e-02i     0.866    1.15470e-01
-1.08034e-01  5.57743e-02i     0.889    1.21581e-01
-1.08034e-01 -5.57743e-02i     0.889    1.21581e-01
-2.00000e-01  0.00000e+00i     1.000    2.00000e-01
```

```
-4.05414e-01  0.00000e+00i     1.000    4.05414e-01
-4.35753e-01  4.15894e-01i     0.723    6.02370e-01
-4.35753e-01 -4.15894e-01i     0.723    6.02370e-01
-8.33329e-01  8.26417e-01i     0.710    1.17363e+00
-8.33329e-01 -8.26417e-01i     0.710    1.17363e+00

% Output co-variance with the LQG/LTR design
sigYCLx =
  Columns 1 through 6
   2.3059e-01   1.6366e+01   6.6082e-02   3.1325e-02   3.2275e-03   1
.1952e-01
  Columns 7 through 12
   2.3528e+10   6.5089e+07   3.7337e+05   3.5121e+03   5.4696e+01   1
.5657e+00
  Columns 13 through 18
   9.3091e-02   1.0792e-02   4.2697e+10   1.2316e+08   7.5944e+05   7
.9364e+03
  Columns 19 through 24
   1.4261e+02   4.7429e+00   2.9971e-01   3.5726e-02   1.9825e-01   9
.3974e-02
  Columns 25 through 26
         0         0
Warning: Gain margin undefined; phase does not cross -180
Freq(Rad/Sec)   Gain Margin(dB)
Freq(Rad/Sec)   Phase Margin(Deg)
  0.01148         -259
ans =
     []
Freq(Rad/Sec)   Gain Margin(dB)
  0.07739        11.88
Freq(Rad/Sec)   Phase Margin(Deg)
ans =
   1.1882e+01
```